Iowa State University
Digital Repository

2011

Behavior of composite pavement foundation materials subjected to cyclic loading

Alexander James Wolfe
Iowa State University

Follow this and additional works at: https://lib.dr.iastate.edu/etd

 Part of the Civil and Environmental Engineering Commons

Behavior of composite pavement foundation materials subjected to cyclic loading

by

Alexander James Wolfe

A thesis submitted to the graduate faculty

In partial fulfillment of the requirements for the degree of

MASTER OF SCIENCE

Major: Civil Engineering (Geotechnical Engineering)

Program of Study Committee:
David J. White, Major Professor
Vernon R. Schaefer
Neal R. Iverson

Iowa State University

Ames, Iowa

2011

TABLE OF CONTENTS

LIST OF TABLES

LIST OF FIGURES

LIST OF SYMBOLS

Symbol	Description	Units
a	Radius of loading plate	mm
A	Sample cross-section area	m^2
B	Width of footing	m
c_c	Coefficient of curvature	—
c_u	Coefficient of uniformity	—
DCP	Dynamic cone penetrometer	mm/blow
d_o	Measured deflection	mm
$d_{o(ri)}$	Deflection measured at the ith sensor	mm
D_{10}	Particle diameter corresponding to 10% finer	mm
D_{30}	Particle diameter corresponding to 30% finer	mm
D_{60}	Particle diameter corresponding to 60% finer	mm
D_i	Radial distance from the center of the plate to i^{th} sensor	mm
E_{FWD}	Elastic modulus determined from FWD data	MPa
E_{LWD}	Elastic modulus determined from LWD data	MPa
$E_{LWD\text{-}P3(XX)}$	Elastic modulus determined using 300 mm diameter plate Prima LWD with drop height XX cm	MPa
$E_{LWD\text{-}Z3(XX)}$	Elastic modulus determined using 300 mm diameter plate Zorn LWD with drop height XX cm	MPa
$E_{LWD\text{-}Z2(XX)}$	Elastic modulus determined using 200 mm diameter plate Zorn LWD with drop height XX cm	MPa
E_{v1}	Initial elastic modulus from plate load test	MPa
E_{v2}	Reloading elastic modulus from plate load test	MPa
$E_{s(T307)}$	Dynamic secant modulus determined from resilient modulus tests	MPa
$E^*_{s(T307)}$	Cyclic secant modulus determined from resilient modulus tests	MPa
f	Shape factor for LWD and FWD	—
G_s	Specific gravity	—
I_z	Influence factor at z depth	—
k_s	Modulus of subgrade reaction	MPa/mm

k	Stiffness estimated from a static plate load test	MPa/mm
k_1, k_2, k_3	Regression coefficients	—
LWD	Light weight deflectometer	MPa
M_r	Resilient modulus	MPa
$M_{r(T307)}$	AASHTO T307 average resilient modulus	MPa
$M_{r(T307)-X}$	AASHTO T307 resilient modulus determined from sequence X	MPa
$M_{r(DCPI)}$	Resilient modulus determined from DCP data	MPa
$M_{r(LWD)}$	Resilient modulus determined from LWD data	MPa
P	Applied load at surface	N
P_a	Atmospheric pressure	kPa
P_4	Percent of material passing the No. 4 sieve	%
P_{200}	Percent of material passing the No. 200 sieve	%
S	Degree of saturation	%
s_u	Undrained shear strength	kPa
z	Depth from the surface	mm
$\sigma_1, \sigma_2, \sigma_3$	Principal stresses	kPa
σ_B	Bulk stress	kPa
σ_d	Deviator stress	kPa
σ_o	Applied stress	kPa
σ_z	Stress at depth of z	kPa
ν	Poisson's ratio	—
τ_{oct}	Octahedral shear stress	MPa
ε_p	Permanent strain	—
ε_r	Resilient strain	—
ε_v	Vertical strain	—
u	Pore water pressure	kPa
γ_{dmax}	Maximum dry unit weight	kN/m^3
w_{opt}	Optimum moisture content	%

UNIT CONVERSIONS

Measurement	From Metric Units	Conversion Factor	To English Units
Length	millimeter (mm)	0.03937	inches (in)
Length	millimeter (mm)	0.00328	feet (ft)
Length	centimeter (cm)	0.39370	inches (in)
Length	centimeter (cm)	0.03281	feet (ft)
Length	meter (m)	39.37	inches (in)
Length	meter(m)	3.281	feet (ft)
Weight	gram (g)	0.0022	pound (lb)
Weight	kilogram (kg)	2.205	pound (lb)
Force	newton (N)	0.2248	pound-force (lbf)
Force	kilo Newton (kN)	224.81	pound-force (lbf)
Density	kilo gram per cubic meter (kg/m^3)	0.0624	pound per cubic feet (pcf)
Unit Weight	kilo Newton per cubic meter (kN/m^3)	6.3659	pound per cubic feet (pcf)
Pressure	kilo pascal (kPa)	0.145	pounds per square inch (psi)
Pressure	kilo pascal (kPa)	20.89	pounds per square feet (psf)
Pressure	mega pascal (MPa)	145.04	pounds per square in. (psi)
Pressure	mega pascal (MPa)	20885.4	pounds per square feet (psf)

ABSTRACT

This study investigated relationships between field and laboratory moduli in relation to the pavement thickness design values and how individual foundation layers affect the composite moduli of pavement foundation systems.

Currently, common practice is to determine pavement foundation layer construction quality from unit weight and moisture values, which do not necessarily relate to pavement thickness design input values (e.g. modulus). Moduli, however, provide direct, quantifiable values that describe the physical characteristics of foundation materials and can be related to pavement system performance. Resilient moduli are used in AASHTO 1993 pavement design manual and the current MEPDG.

Laboratory prepared specimens were studied to compare the effects of different conditions found in situ (e.g., moisture and dry unit weight variances). To simulate layered condition in the field, a method was developed to prepare and test layered composite samples. Previous laboratory tests have focused on single layer moduli, whereas in situ tests encompass several layers of pavement foundation systems. Composite samples better simulated the layering effects found in situ. In situ test results were also compared to composite sample laboratory test results to evaluate the relationships between the test methods.

Key results from this investigation demonstrated that 1) composite behavior differs significantly from single sample behavior (i.e., weak lower layers significantly affect the composite moduli); 2) laboratory composite resilient moduli can be estimated from single material resilient moduli; 3) undrained shear strength properties were significantly correlated to laboratory resilient moduli; and 4) laboratory, in situ, and design moduli are poorly related (i.e., between measured laboratory and empirically calculated resilient moduli, as well as between measured elastic and resilient moduli).

CHAPTER 1. INTRODUCTION

This chapter is organized into sections that present the industry and technical problems addressed in this project, the research goals and objectives, and a discussion of the significance of this research. The final section describes the chapter organization of this thesis.

INDUSTRY PROBLEM

A currently aging transportation infrastructure, increasing traffic loads, and ever present economic constraints have made designing quality foundation layers critical to pavement performance.

Moduli provide direct stiffness values to quantify pavement foundation support conditions. In situ and laboratory determined moduli typically do not correlate well with each other. Differences in stress and boundary conditions between in situ and laboratory tests make it difficult to correlate the values with great confidence.

Additionally, often due to time and economic constraints, design and quality control/quality assurance (QC/QA) parameters are derived from few test sites and used to characterize large portions of the construction project despite enormous nonuniform subsurface conditions.

Tests that simulate traffic loading conditions can measure resilient and permanent deformations which can then be linked to the selection of foundation materials and long term pavement performance. Additionally, some in situ devices can quickly and easily provide data about the in situ moduli of pavement foundations as a way to check construction quality and link engineering properties (beyond density and moisture) to the pavement foundation behavior. In practice, there needs to be systematic analyses to evaluate pavement foundation moduli in relation to the expected design values.

TECHNICAL PROBLEM

Currently there is a weak understanding of how individual foundation layers affect the composite moduli of pavement systems. For design and QC/QA, in situ test values are used to characterize the composite response of all foundation layers.

In situ values provide composite moduli because the tests do not isolate single foundation layers. However, laboratory tests tend to investigate the moduli of single layers, neglecting the effects of the surrounding layers. Empirical equations are then used to convert data from single material samples into values that characterize the behavior of multilayered pavement structures. Von Quintus and Killingsworth (1997) developed an equation to relate in situ individual material layers to layered systems, but few other researchers have attempted to directly investigate layered laboratory samples. This study aims to investigate the effects of individual layers in relation to the composite foundation system

RESEARCH GOALS

The research goals of this project are to (1) evaluate the moduli of single and composite laboratory specimens as a step toward in situ measurement and analysis of layered pavement foundation systems and (2) better understand the relationships between in situ and laboratory moduli.

RESEARCH OBJECTIVES

This project has four main objectives.

1. Determine stiffness properties as functions of moisture content (e.g., saturation) and density (e.g., relative compaction, relative density, etc.).
2. Compare moduli derived from empirical equations to moduli that were measured in the laboratory.
3. Determine the resilient behavior of composite pavement foundation samples through
    a. developing a standard procedure for constructing a composite sample;
    b. relating composite material sample behavior to single material sample behavior;
    c. analyzing fines migration, stiffness, and strain properties with and without geosynthetic separation material; and
    d. comparing measurements relative to field data and design assumptions.
4. Compare the resilient properties of pavement foundation stabilization techniques.

SIGNIFICANCE OF THE RESEARCH

Advancing the understanding and application of soil moduli are necessary for economical designs and the development of high performance pavement systems. Unlike resilient moduli, other moduli (e.g., elastic, modulus of subgrade reaction) are not well correlated to

long term performance (e.g., permanent deformation from cyclic loading). Current pavement foundation design practices are based on mechanistic and empirical approaches and regional experience. Mechanistic approaches include resilient moduli regressions, but analysis techniques are not advanced enough to incorporate resilient moduli data and predict long-term pavement performance in practice (NCHRP 2004b). Some empirical correlations are drawn from small, specific datasets, and these correlations, although applied in current practice, should be used with caution because the relationships apply only to a limited range of in situ conditions. Regional experience provides a range of values or certain construction methods to use based on elementary soil classifications.

Laboratory resilient modulus tests correspond to actual roadway conditions because standard methods simulate roadway use by subjecting samples obtained in situ to repeated loads and controlled stresses. Laboratory tests in this study will evaluate stiffness responses for a number of pavement foundation materials from locations in several states and compare the broad range of data to form a more complete idea of design parameter derivations and effects on pavement performance.

Overall, this research provides the groundwork toward developing better methods for pavement foundation design and quality control/quality assurance (QC/QA). These priorities are the first step toward the design and construction of long lasting pavement systems.

ORGANIZATION OF THE DOCUMENT

Following this introductory chapter, the thesis is organized into five additional chapters. Chapter 2 reviews previous literature and provides background information for this study. Chapter 3 describes the laboratory and field test methods. Chapter 4 summarizes the laboratory and in situ properties that characterize the tested materials. Chapter 5 presents the results and analyses for the laboratory and in situ tests performed on the materials from each of the six tests sites. Chapter 6 summarizes the conclusions and outcomes derived from this research. Chapter 6 also discusses how the conclusions can be practically applied and offers suggestions for future research. A list of referenced works and appendices are located at the end.

CHAPTER 2. LITERATURE REVIEW AND BACKGROUND

This chapter reviews the literature about the cyclic behavior of pavement foundation materials and describes the context of this project.

This literature review consists of four main parts: history and definition of resilient modulus testing, typical resilient responses of pavement foundation materials, pavement design using resilient moduli, and correlations to other test methods.

RESILIENT MODULUS

This section presents a definition of resilient modulus and a history of resilient modulus testing.

History of resilient moduli testing

Prior to World War II, pavement thickness and foundation design were based on regional experience, soil classification, and static load techniques (Vinson 1989). After World War II, researchers began to investigate the effects of repeated stress applications on deformation. Hveem (1955) was one of the first to compare the effects of standing wheel loads (i.e., static loading) and moving wheel loads (i.e., repeated loading) on pavement deformation. Seed et al. (1955) concluded that modulus values for subgrades, obtained from stress-strain diagrams of statically loaded specimens, were significantly lower than the moduli of resilient deformation—that is, resilient modulus values. Early work on resilient moduli was a product of researchers attempting to determine fatigue failures in asphalt pavements. This early work indicated the importance of modeling traffic loading conditions with repeated load tests.

Groeger et al. (2003) provide the history of the developments that led to the current AASHTO T307 sample preparation and testing procedures. The Long Term Pavement Performance (LTPP) Protocol P46 is the basis for the current AASHTO T307 "Standard Method of Test for Determining the Resilient Modulus of soils and Aggregate Materials."

Studies involving vehicle speed, deflections, and how vertical stress pulses are affected by depth lead to the creation of the first modern standard for testing resilient modulus, AASHTO T274, in 1982. An assessment in 1988 recognized some areas of the method were unclear. The revised procedure, LTPP Protocol P46, "Resilient Modulus of Unbound Granular Base/Subbase Materials and Subgrade Soils," was then developed. The final

procedure was implemented in 1996. The sample preparation and testing procedures for Protocol P46 were chosen to study the goals of the LTPP program, and in 1999, Protocol P46 was modified and adopted as AASHTO T307, "Determining the Resilient Modulus of Soils and Aggregate Materials." Differences from Protocol P46 and AASHTO T307 include the types of loading systems allowed, cycle durations, number of points per cycle, and compaction methods allowed. These differences allow more testing agencies to adopt the AASHTO standard (Groeger et al. 2003).

In the AASHTO T307 standard, load repetitions are applied to the sample for 15 different sequences of cyclic deviator and confining stress. The stress values are different for base/subbase materials and subgrade soils. Stress values used in the resilient modulus test can be found in Chapter 3, Methods. The stresses for base and subbase materials are generally higher than subgrade soils to simulate the higher loads experienced by the upper layers of pavement foundations under traffic loading conditions.

As long as the permanent deformation do not reach 5% strain—considered failure, and after all of the stress sequences have been applied, a quick shear test is performed on the sample to collect strength data as part of the resilient modulus testing procedure.

Definition

Resilient modulus (M_r) is the ratio of the cyclic deviator stress versus the resilient strain. After a number of loading cycles, the modulus reaches a steady value. Resilient modulus is calculated from this value as:

$$M_r = \frac{\sigma_d}{\varepsilon_r} \tag{1}$$

where: M_r = resilient modulus,

σ_d = deviator stress (the difference in principal stresses), and

ε_r = resilient strain.

Two types of strain occur during resilient modulus load cycles—permanent strain (ε_p) and resilient strain (ε_r). Permanent strain is accumulated over many short load pulses and leads to the permanent deformation of the sample. Resilient, or recoverable, strain occurs when the sample rebounds after the load is applied and released cyclically. The elements of a resilient modulus stress-strain curve are illustrated in Figure 1. Resilient modulus values

provide a stress-strain relationship for pavement foundation materials to be used in the structural analysis of layered pavement systems (FHWA 1996). Because resilient modulus tests simulate conditions of pavement foundation systems subjected to wheel loads, the current MEPDG method uses resilient modulus as a key parameter for both flexible and rigid pavement foundation design (NCHRP 2004b). The MEPDG method is summarized in the section entitled, "Overview of the MEPDG Method."
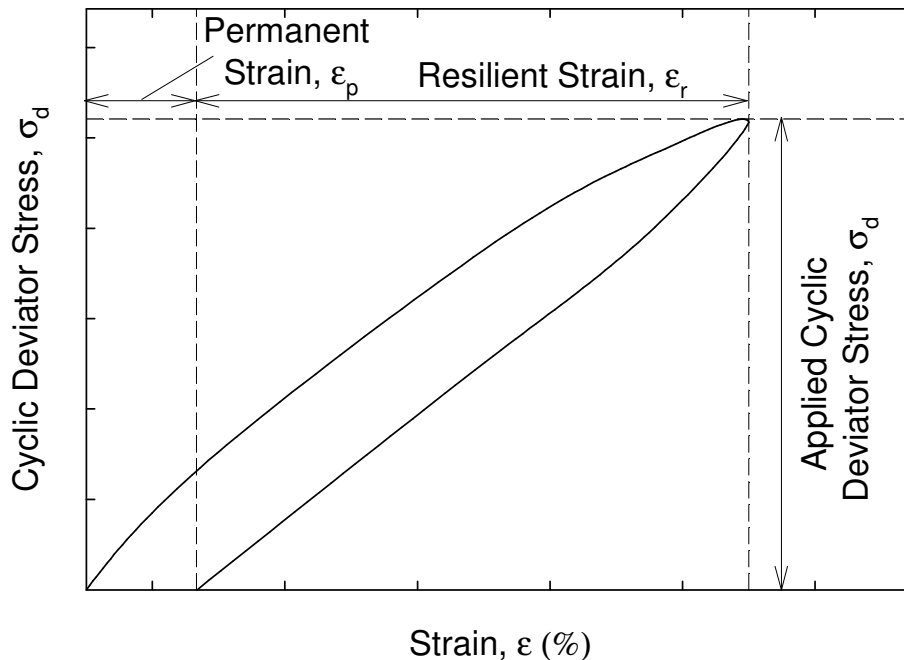
Figure 1. Elements of a resilient modulus stress-strain curve

A series of confining stresses and deviator stresses are incrementally adjusted to evaluate ranges of stress conditions for a given specimen. Laboratory test standards involve several hundred short load pulses applied vertically to the sample under increasing deviator stresses to simulate the cyclic loading from vehicles on the pavement structure. Resilient modulus tests have been studied over a range of variables including moisture content and degree of compaction (Seed et al. 1962; Southgate and Mahboub 1994). The amount of stress applied to a sample depends on whether the foundation layer is a base/subbase material or a subgrade material.

RESILIENT RESPONSES OF PAVEMENT FOUNDATION MATERIALS

Both flexible and rigid pavement structures are typically designed in three layers: the wearing surface and two foundation layers—the base and subbase—and the subgrade. The deformation response of foundation materials needs accurate classification to design the correct pavement thickness. Some of the deformation is recoverable—that is, it is resilient—but some of the deformation is permanent (Zaman et al. 1994). The primary geotechnical factors that affect pavement surface distresses and failures are the stiffness and strength of the foundation materials. Both the stiffness and strength are influenced by many variables that occur during and after construction including initial density, initial moisture content, changes in saturation over time, particle size distribution, particle shape, and soil classification. Most soils exhibit the effects of increasing stiffness with increasing confinement and decreasing stiffness with increasing shear stress (Andrei et al. 2004).

Huang (1993) illustrated the effects of pavement modulus ratio (the modulus of the upper layer divided by the modulus of the lower layer) on the stress at foundation layer interfaces. In a simplified two-layer example with stiff surface conditions—that is rigid pavements—over a soft subgrade (i.e., high modulus ratio), the applied stress at the surface reduces to about 8% at the pavement-subgrade interface. An example with soft surface conditions—that is flexible pavements—over a soft subgrade (i.e., low modulus ratio), the applied stress at the surface reduces to 68% of stress at the pavement-subgrade interface. Additional layers between the surface pavement and the subgrade further decrease the stresses occurring at the layer interfaces and lead to applied stresses that are much lower than the ultimate strength of the layers.

The materials used to construct pavement foundations include the following:

- granular and cohesive soils;
- geosynthetics for separation, drainage, and mechanical stabilization; and
- chemically stabilized soils.

These materials are placed in layers and can be designed to achieve certain resilient properties under the cyclic loading conditions of traffic.

Granular

Granular materials used in pavement foundations typically include gravels, sands, and crushed recycled pavements such as concrete and asphalt. These materials make up the base and subbase layers of pavement foundations. Resilient moduli of granular materials have been shown to be dependent on several factors such as stress state, density, physical properties, gradation, moisture content, and material type.

The resilient modulus of a material increases as the stress state—the sum of principal stresses—increases. Increasing the confining stress increases the resilient modulus (Hicks 1971; Brown 1974). For a single confining stress, Brown (1974) also showed that the deviator stress is proportional to the permanent strain after 10,000 cycles. Hicks (1971) illustrated that for a given confining stress with non-saturated specimens resilient modulus was found to increase with any of the following: increased density; increased particle angularity and surface roughness; decreased fines content (material passing No. 200 sieve); or decreased degree of saturation. Saturated pavement foundations occur when the base and subbase layers are not well drained and water is held within the layers. Hicks (1971) indicated saturated specimens experienced a generally constant static pore water pressure, but the transient pore water pressure dropped instantly and was much lower than the repeated load. High pore water pressures decrease the effective strength of granular material.

A considerable cause of damage and failure for rigid pavements is pumping. Water infiltrates pavement foundation layers and accumulates in voids within the pavement layers. Under traffic loading, the accumulated water is expelled and may also eject subgrade soil particles (Bhatti et al. 1996).

Unbound granular materials experience critical stress levels—shakedown limits—under repeated pavement loads that occur as foundation systems transition from stable to unstable conditions. Werkmeister et al. (2004) found that stable conditions correspond to resilient behavior, while the unstable conditions correspond to significant permanent deformation. Werkmeister et al. (2004) described four idealized types of shakedown behavior: purely elastic, elastic shakedown, plastic shakedown, and incremental collapse; however, repeated load triaxial tests did not indicate purely elastic behavior for granular material. When loaded, pavement materials always exhibit some permanent and resilient deformations. Three types

of permanent strain accumulation were observed: plastic shakedown, plastic creep, and incremental collapse. The plastic shakedown response involves small permanent strains for a finite number of load applications (i.e., post compaction period). After these load applications, the response becomes resilient and no additional permanent strain occurs. Plastic creep is intermediate to the plastic shakedown and incremental collapse. The initial load cycles respond in a manner similar to plastic shakedown (decreasing permanent strains), but after many load cycles, the permanent strains begin to increase at a constant rate. Failure (i.e., unacceptably high permanent strains) may occur if enough load cycles are applied to the material. The incremental collapse response is always plastic. Permanent strain increases with each successive load application.

Each shakedown response is dependant on the type of material, load level, and number of application cycles. For relatively low load levels, a material will experience plastic shakedown; for relatively high load levels, a material will experience incremental collapse.

Recycled portland cement concrete (RPCC) material is made from crushed and processed pavement on the construction site. RPCC is typically crushed to meet specified gradation requirements for natural materials used as bases or subbases. Overall, RPCC material has similar resilient behavior to other granular materials. Studies (Nataatmadja and Tan 2001; Mayrberger and Hodek 2007) have shown that samples may be affected by the hydration of residual concrete. Although the resilient modulus of a granular material typically decreases with an increase in moisture content, RPCC specimens showed an increase in resilient modulus with the addition of water and mellowing time. The properties that can significantly affect mechanistic behavior of RPCC include concrete compressive strength, material gradation, and flakiness index. The flakiness index is the percentage of flat particles (thickness of less than one half the nominal size) in an aggregate gradation (TxDOT 2004).

Recycled asphalt pavement (RAP) is a material made from excavated and crushed asphalt concrete pavement. Alam et al. (2010) reviewed previous literature stating that an increase in RAP content increases resilient moduli. Increases in resilient moduli are also common in blends of RAP with virgin granular material. The study by Alam et al. (2010) indicates resilient moduli increase for both high- and low-bulk stress levels. Statistical analyses show dry density to have a significant positive effect on resilient moduli. However, moisture

content has an inverse relationship to resilient moduli. Additionally, in situ tests show increasing RAP content decreases distresses at the pavement surface.

Even in granular materials, soil suction can affect the stiffness. Soil suction consists of two parts—matric suction and osmotic suction. Matric suction is developed from the particle–particle attraction due to capillary and surface adsorptive forces; osmotic suction is developed from the attraction of water due to dissolved salts in the pore fluid (Liang et al. 2008). Osmotic suction has negligible effects, especially on coarse to fine grained soils; therefore, matric suction is the major factor of total suction for these soils (Liang et al. 2008, Terzaghi et al. 1996). Soil suction is related to degree of saturation. Low matric suction correlates to a high degree of saturation, and high matric suction correlates to a low degree of saturation. Yang et al. (2008) found that soil had larger deformations at low initial matric suction levels, and the resilient modulus decreased with increasing deviator stress. Increases in matric suction reduced the resilient strain, which indicated that high matric suction increased the effective stress and decreased deformation (Yang et al. 2008).

For flexible pavement design, the National Cooperative Highway Research Program Project 1-28A (NCHRP 2004a) recommended determining resilient moduli at specific stress states using Equation 2. The stress states for granular materials correspond to base and subbase materials—$\sigma_3 = 35$ kPa (5 psi) and $\sigma_{cyclic} = 103$ kPa (15 psi).

$$M_r = k_1 P_a \left(\frac{\sigma_B - 3k_6}{P_a} \right)^{k_2} \left(\frac{\tau_{oct}}{P_a} + k_7 \right)^{k_3} \tag{2}$$

where: P_a = atmospheric pressure (MPa);

σ_B = bulk stress (MPa) = $\sigma_1 + \sigma_2 + \sigma_3$;

τ_{oct} = octahedral shear stress (MPa) = $\dfrac{\sqrt{(\sigma_1 - \sigma_2)^2 + (\sigma_2 - \sigma_3)^2 + (\sigma_3 - \sigma_1)^2}}{3}$;

$\sigma_1, \sigma_2, \sigma_3$ = principal stresses; and

k_1, k_2, k_3, k_6, k_7 = regression coefficients.

Cohesive

Cohesive soils are typically found in the lowest layers of pavement foundations (i.e., the subgrade). These soils are made up of fine grained materials such as silts and clays but can include some gravels or sands. Resilient moduli of cohesive soils are affected by several factors including the number of stress applications, magnitude of repeated stresses, thixotropy, compaction method, compaction density, compaction water content, and changes in density and water content after compaction. Many factors can be accounted for in the laboratory through sample preparation and conditioning sequences. Once these factors are accounted for, it is possible to closely simulate the field conditions in the laboratory (Seed et al. 1962).

When all other factors are constant, Seed et al. (1962) found resilient moduli of cohesive subgrade soils are stress dependent. At low stress levels, resilient moduli decrease as applied stress increases. These low stress levels simulate what the subgrade will be subjected to during its lifetime. However, stress on a soil element decreases with depth, so the deviator stress applied at the pavement surface decreases in magnitude with depth, and resilient modulus values increase with depth.

Frost et al. (2004) found that at the threshold stress, resilient moduli tend to approach a constant value at which the resilient strain is directly proportional to applied stress. The threshold stress for subgrade soils is defined as the point when permanent strain becomes unstable (i.e., the rate of permanent deformation increases exponentially). Therefore, permanent strain of the subgrade can be controlled by transmitting the applied vertical stress through overlying layers and limiting the stress applied to the subgrade.

Thixotropy is the apparent increase in strength due to age and occurs both in the laboratory when samples are allowed to rest before testing and in the field. In both test settings, thixotropy results in a noticeable decrease in permanent deformation. Seed et al. (1962) concluded that for low numbers of stress applications (as seen in the lab), the thixotropic effects can be significant, but for high numbers of stress applications (as seen in the field), the effects would be negligible.

Compaction techniques affect the resilient behavior of cohesive soils. The 2009 version of the AASHTO T307 resilient modulus procedure incorporates standard methods for

kneading and static compaction of cohesive soils in the laboratory. Preparation of laboratory specimens with kneading compaction produces soil properties that correspond to the effects of in situ compaction equipment. In a comparison study between static and kneading compaction, Kouassi et al. (2000) found that statically compacted samples had higher initial tangent moduli, independent of water content. Static compaction techniques produce a flocculated soil particle structure at all locations along the moisture-density curve. Kneading compaction techniques produce a flocculated soil structure at less than optimum moisture contents and a dispersed soil structure at above optimum moisture contents because of the development of high shearing strains during compaction. A flocculated soil structure results in higher resilient moduli when compared to a dispersed structure (Robnett and Thompson 1973; Seed et al. 1962). In a comparison study between the resilient properties of laboratory compacted specimens (i.e., compaction by kneading and static techniques) and undisturbed in situ samples, Seed et al. (1962) found that the resilient moduli of undisturbed in situ samples strongly agree with the specimens compacted by kneading compaction. Laboratory static compaction resulted in resilient modulus values that were much larger than in situ samples.

For subgrade materials, Drumm et al. (1997) reported that an increase in either moisture content or degree of saturation leads to a decrease in resilient modulus. Degree of saturation is a better parameter than moisture content to relate resilient modulus values because it incorporates both soil moisture and density. High pore water pressures in saturated subgrades can develop from traffic loads. These high pore water pressures decrease the effective strength of the material. The loss of strength and dynamic loading can cause fine material (material passing No. 200 sieve) to be pumped into the subbase or base layers leading to permanent deformation of the subgrade (Christopher et al. 2006).

A study by Khoury and Zaman (2004) investigated the effect of moisture content changes in cohesive soils after compaction. Clayey soils retain cohesion after wetting and drying cycles, unlike silty soils that lose plasticity when they dry. In general, an increase in saturation after compaction decreases resilient moduli, while drying the soil increases resilient moduli. During both laboratory wetting and drying processes, the initial moisture content is an important factor that influences resilient modulus values. Lower initial moisture contents have higher M_r values after wetting. Khoury and Zaman (2004) show there are

larger increases in resilient moduli when samples are initially compacted at higher moisture contents and then dried.

Several studies have reported the effects of suction on resilient moduli values for cohesive materials (Yang et al. 2008; Liang et al. 2008). For very fine grained materials (i.e., clays), osmotic suction becomes a more important factor to the total suction (Terzaghi et al. 1996) because of the ability of fine grained materials to adsorb water with dissolved salts onto the particle surfaces and in pore spaces. Just as with granular materials, increased suction relates to lower degrees of saturation and therefore higher resilient moduli (Yang et al. 2008).

For flexible pavement design, the NCHRP Project 1-28A (NCHRP 2004a) recommended determining resilient moduli at specific stress states using Equation 2. The stress states for cohesive materials correspond to subgrade materials—$\sigma_3 = 14$ kPa (2 psi) and $\sigma_{cyclic} = 41$ kPa (6 psi).

Geosynthetics

Geosynthetics have five major functions in geotechnical engineering: separation, reinforcement, filtration, drainage, and use as a barrier. Separation involves keeping unlike materials apart. Reinforcement increases the overall in situ soil strength by adding tensile strength or shear resistance to weak soils. Filtration allows liquids to pass, but keeps other particles from moving with the liquid. Drainage transmits liquids through the geosynthetic structure. As barriers, geosynthetics keep solids, liquids, and gasses from coming in contact with each other (Koerner and Soong 1995). Several types of geosynthetics, including geotextiles, geogrids, geonets, geomembranes, and geocomposites, have been developed to fulfill these major functions. However, because this study concerns the strength and stiffness characteristics of pavement foundations, information about materials whose primary functions are filtration, drainage, or use as a barrier will not be provided in this review.

Geotextiles are porous and flexible materials, typically made from polypropylene or polyester. The primary uses for geotextiles include separation and reinforcement. Geogrids are netlike polymer materials primarily used for reinforcement or separation of large aggregates (Koerner 1991). For reinforcement, geosynthetic materials are placed either at interfaces between strong and weak layers or at several depths to intercept potential failure

surfaces. For separation, geosynthetic materials are placed at the interface between two materials that should not contaminate each other.

Tingle and Jersey (2005) demonstrated that pavement foundations stabilized with geotextiles had less permanent deformation than foundations with no reinforcement, and that, for soft subgrades, the dominant geotextile function was separation, rather than reinforcement. Loulizi et al. (1999) compared geotextile and geogrid stabilized road sections with non-stabilized sections and determined that geosynthetic stabilization increased the service life of pavements. Specifically, geotextile (which was less expensive than geogrid) carries more equivalent single axel loads (ESALs) before failure than geogrid reinforced sections. The separation function of the geotextile decreased the percentage of subgrade fines that contaminated the base layer, leading to increased pavement performance. The authors also state that a reduction in base layer contamination would lead to a lower resilient modulus for the base course layer.

Chemical stabilization

Chemicals are commonly used to stabilize inadequate pavement foundation layers. Chemical stabilization increases the strength or used as a treatment to reduce the volume change of heave-susceptible soils. Chemical soil stabilization techniques facilitate compaction (i.e., drying very wet soils) and treat weak or highly plastic soils. Stabilization involves thoroughly mixing pulverized soil with binders (e.g., cement, fly ash, lime, asphalt, etc.) to obtain the desired properties. Different soils require different binders depending on gradation, soil type, moisture content, and desired specifications. Chemical stabilization is used on base and subgrade soils to attain one or more of the following properties (Papagiannakis and Masad 2008):

- reduce the plasticity index (PI),
- reduce the volume change,
- reduce the clay and silt sized particles,
- increase the shrinkage limit,
- improve the strength, and
- increase the resilient modulus.

Portland cement, which is the most commonly used cement for soil stabilization, is a fine powdered hydraulic cement that reacts with water or water and lime to form strong, stable bonds of hydrated silicates and aluminates (Winterkorn 1991).

Fly ash is a coal power plant by-product. In the presence of water, it reacts with lime, setting and hardening much like other hydraulic binders. Type F and type C fly ash are the principal fly ash products used in soil stabilization. Type F fly ash requires the addition of lime to set, while type C fly ash is self-cementing when used with water. Fly ash mixtures are principally pozzolanic reactions involving silica and alumina compounds in the fly ash reacting with free lime (ACAA 2008).

Both cement and fly ash should be used with caution when mixing with clay soils because the rapid set times may not allow thorough mixing, resulting in an inhomogeneous material.

Lime stabilization refers to the chemicals quicklime (calcium oxide) or hydrated lime (calcium hydroxide). Both of these chemicals are burned forms of limestone (calcium carbonate). Lime stabilization is most effective for plastic clays. The basic chemical reactions that occur when lime, clay, and water are mixed include cation exchange and flocculation-agglomeration, cementation, and carbonation (Winterkorn 1991). Cation exchange and flocculation-agglomeration reduces the plasticity of the clay. Cementation increases the soil strength with both time and the presence of pozzolanic clays. Carbonation is an unwanted reaction that occurs when there is too much lime added or too little pozzolanic clays.

Solanki et al. (2010) demonstrated that lime, class C fly ash and cement kiln dust increase the design resilient moduli (determined at a confining stress of 13.8 kPa (2 psi) and a deviator stress of 41.3 kPa (6 psi)) of subgrade clay soils. At low application rates (3–6%), lime treatment increased M_r values by 140–810%, depending on soil type. Greater applications of lime decreased the strength values of the soil. High application rates (10–15%) of class C fly ash and cement kiln dust also increased M_r values by 130–1100% and 400–2000%, respectively, depending on soil type.

GEOTECHNICAL PAVEMENT DESIGN PARAMETERS

Pavement design history

Pavement design guides became standardized after the AASHO road tests during the late 1950's. The first guide was developed in 1961 and included empirical correlations from the AASHO road tests. These correlations were only applicable for the small set of environmental conditions and soil properties from the road tests. Often empirical correlations are modified based on regional experience (Christopher et al. 2006).

Each successive design guide has incorporated increasingly sophisticated geotechnical parameters into the pavement design process. The current procedure proposed in the *Guide for Mechanistic-Empirical Design of New and Rehabilitated Pavement Structures* (NCHRP 2004b) involves incorporating parameters from both empirical and mechanistic methods into the design of pavement systems. Empirical design methods are based on regional experience of how pavements perform in relation to traffic volumes, material properties, and thickness of the pavement system. Mechanistic design methods use mathematics to analyze the relationship between environment, traffic volume, and material characteristics of pavement systems. Table 1 summarizes the geotechnical inputs used in previous and current pavement design guides.

Table 1. Summary of geotechnical inputs for AASHTO pavement design guides Part I

(Christopher et al. 2006)

Property	Description	Flexible Pavement Inputs	Rigid Pavement Inputs	Comments
SN	Structural number	A, B		A: only soil used in AASHO Road Test
a_i	Structural layer coefficients (to determine SN)	A, B, C, D		A: only soil used in AASHO Road Test; All: for granular base and subbase layers
S_i	Soil support value	B		
R	Empirical regional factor to adjust SN	B		B: each state agency determine value from own experience
k_s	Modulus of subgrade reaction		B, C, E	C: seasonally adjusted, E: elastic value on top of subgrade (i.e., only the recoverable deformation used to compute k_s)
D_2	Thickness of base layer	B, C, D, E		
D_3	Thickness of subbase layer	B, C, D, E	C, D, E	C: k_s is a function of M_r, E_{SB}, D_{SB}, D_{SG}, and LS
F	Friction factor (reinforcement design in JRCP)		B, C, D, E	
M_r	Resilient modulus of subgrade	C, D, E	C, D, E	C: seasonally adjusted. For rigid pavements, C: k_s is a function of M_r, E_{SB}, D_{SB}, D_{SG}, and LS
E_{SB}	Resilient modulus of subbase (for layer coefficient)	C, D, E	C, D, E	C: k_s is a function of M_r, E_{SB}, D_{SB}, D_{SG}, and LS
E_{BS}	Resilient modulus of base (for layer coefficient)	C, D, E		
m_2	Moisture coefficient for base layer	C, D, E		
m_3	Moisture coefficient for subbase layer	C, D, E		
D_{SG}	Depth from top of subgrade to rigid foundation		C, D, E	C: k_s is a function of M_r, E_{SB}, D_{SB}, D_{SG}, and LS
LS	Loss of support factor		C, D	C: k_s is a function of M_r, E_{SB}, D_{SB}, D_{SG}, and LS
C_d	Drainage factor		C, D	

A = AASHO 1961 and 1962 Interim Guide for the Design of Rigid and Flexible Pavements;
B = AASHO 1972 Interim Guide for the Design of Pavements;
C = AASHTO 1986 Guide for the Design of Pavement Structures;
D = AASHTO 1993 Guide for the Design of Pavement Structures; and
E = 1998 supplement to the 1993 AASHTO Pavement Design Guide;

Table 2. Summary of geotechnical inputs for AASHTO pavement design guides Part II

(Christopher et al. 2006)

θ	Swell rate	D, E	D, E	
V_r	Maximum potential swell	D, E	D, E	
P_s	Probability of swelling	D, E	D, E	
φ	Frost heave rate	D, E	D, E	
ΔPSI_{Max}	Maximum potential serviceability loss from frost heave	D, E	D, E	
P_F	Probability of frost heave	D, E	D, E	
k_1, k_2, k_3	Nonlinear resilient modulus parameters	F_1		
M_r	Back calculated resilient modulus	F_1		
$k_{dynamic}$	Back calculated modulus of subgrade reaction		F_1	
v	Poisson's ratio	F_1, F_2, F_3	F_1, F_2, F_3	
	Interface friction	F_1, F_2, F_3	F_1, F_2, F_3	
CBR	California Bearing Ratio	F_2	F_2	
R	R-value	F_2	F_2	
DCP	Dynamic cone penetration index	F_2	F_2	
PI	Plasticity Index	F_2	F_2	
P200	Percent passing 0.075 mm (No. 200 sieve)	F_2	F_2	
M_r	Estimated resilient modulus	F_2, F_3	F_2	
	AASHTO soil classification	F_3	F_3	
	USCS soil classification	F_3	F_3	

D = AASHTO 1993 Guide for the Design of Pavement Structures;
E = 1998 supplement to the 1993 AASHTO Pavement Design Guide;
F_1 = Mechanistic Empirical Pavement Design Guide, Level 1 input;
F_2 = Mechanistic Empirical Pavement Design Guide, Level 2 input; and
F_3 = Mechanistic Empirical Pavement Design Guide, Level 3 input.

Overview of the MEPDG method

The current methodology for pavement design is prescribed by the Mechanistic-Empirical Pavement Design Guide (MEPDG) (NCHRP 2004b) which combines mechanics-based determination of pavement responses with empirical distress models to predict pavement performance (Christopher et al. 2006).

The MEPDG design approach for pavement systems is iterative, as seen in Figure 2. Distresses at the end of the design life are compared against design limits. The pavement design is adjusted and the MEPDG method is repeated until all predicted distresses are within the design limits.
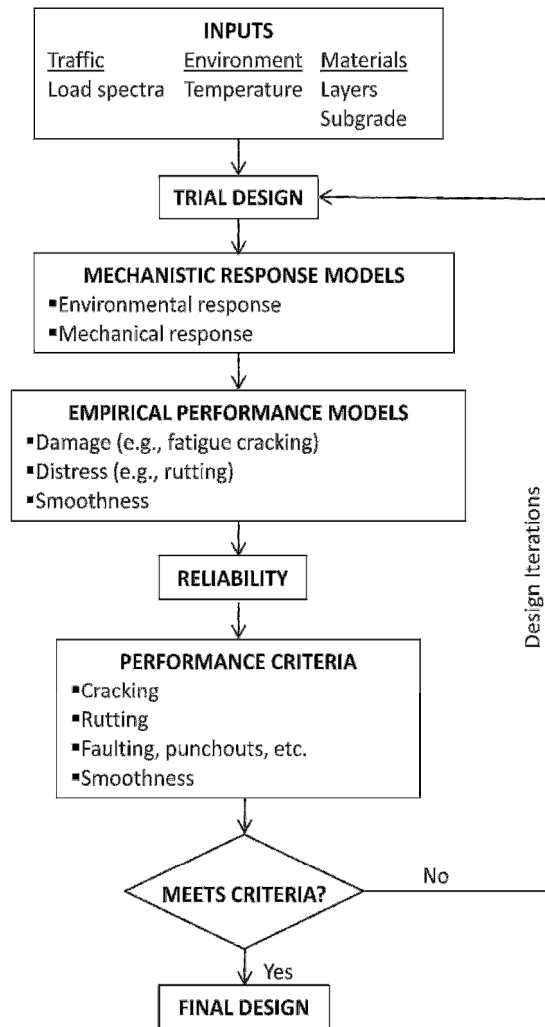
Figure 2. Pavement system design process for M-EPDG (adapted from

Christopher et al. 2006)

The MEPDG uses a hierarchical approach for specifying design inputs. The idea for using a hierarchical approach is that the level of engineering effort used to determine the design inputs should correlate with the importance, size, and cost of the project. MEPDG (NCHRP 2004b) characterizes three levels for rating the quality of design inputs used for pavement foundations. Level 1 inputs give the highest accuracy and lowest uncertainty and typically require direct determination from in situ or laboratory tests (e.g., FWD testing or laboratory triaxial testing). Laboratory test methods for modulus testing include AASHTO T307, Determining the Resilient Modulus of Soil and Aggregate Materials" and

NCHRP Project 1-28A, "Harmonized Test Methods for Laboratory Determination of Resilient Modulus for Flexible Pavement Design" (NCHRP 2004a). Level 2 inputs provide intermediate accuracy and are derived from limited tests or through correlations with other determined properties (e.g., estimating resilient moduli through CBR correlations). Level 3 inputs are the least accurate and are the default values based on regional experience. Level 3 inputs should be used when the consequences for early failure are minimal (e.g., low volume roads).

The current design method characterizes subgrades and unbound pavement foundation layers using resilient modulus values under both rigid and flexible pavements. Resilient modulus values are used in pavement design as a measure of unbound material stiffness. The M_r parameter is highly dependent on the state of stress, water content, and soil structure (George 2004). Many non-linear constitutive models have been proposed that incorporate the effects of stress levels and predict M_r values, as seen in Table 6. The pavement foundation material property design inputs vary for flexible pavements versus rigid pavements. The general differences between flexible and rigid pavement geotechnical inputs for MEPDG are summarized in Table 2 using the symbols F_1, F_2, or F_3.

The MEPDG (NCHRP 2004b) recommends two types of models to characterize the behavior of pavement foundation systems, elastic layer theory and finite element method (FEM). Elastic layer theory uses one resilient modulus value to characterize the entire soil layer, demonstrated in rigid pavement design. FEM uses the k_1, k_2, and k_3 regression coefficients from Equation 3 in laboratory resilient modulus tests as inputs for flexible pavement design.

Geotechnical design parameters

Rigid pavements

The current MEPDG (NCHRP 2004b) method does not incorporate Level 1 inputs applicable for rigid pavement design. Level 2 inputs use relationships between soil strength or index properties to correlate with resilient modulus values. MEPDG software calculates the modulus of subgrade reaction (k_s) from the subgrade resilient modulus value. Several relationships recommended by the design guide (NCHRP 2004b) include California bearing ratio (CBR), plasticity index, gradation, and dynamic cone penetrometer (DCP). The design

software provides a system to incorporate seasonal changes to resilient modulus values. Designers can either input a single representative resilient modulus value and use the Enhanced Integrated Climactic Model (EICM) to adjust the value for seasonal changes or input a representative resilient modulus value for each month of the year. Level 3 inputs include typical values, experience, or historical records as resilient modulus values (NCHRP 2004b).

For rigid pavements, the modulus of subgrade reaction, k_s, is the parameter used to determine the stiffness of pavement foundation layers. Modulus of subgrade reaction is characterized by the elastic constant of springs and is an input for the analysis of rigid pavements (Papagiannakis and Masad 2008). This value is dependant on the soil stiffness as well as the slab size and stiffness.

The modulus of subgrade reaction was first introduced in the 1972 AASHO Interim Guide for the Design of Pavements, and plate load tests were the recommended method to determine k_s. Through the years, other tests were included to determine moduli of subgrade reaction. The 1986 AASHTO Guide for the Design of Pavement Structures included correlations with resilient moduli (adjusted for base thickness and stiffness, shallow rock layers, loss of slab support, and seasonal variations) for new road construction and falling weight deflectometer back calculation for pavement rehabilitation. The 1993 AASHTO Guide for the Design of Pavement Structures included determining composite k_s values that represents the combined stiffness of subbase and subgrade layers.

The current MEPDG recommends all subgrade and unbound layers for all pavement types are characterized using resilient modulus. A conversion from subgrade resilient moduli to the moduli of subgrade reaction alters the pavement structure into a simplified version consisting of the concrete slab, base, and effective dynamic ks value (Figure 3). The MEPDG software internally performs the conversion from resilient moduli to moduli of subgrade reaction. The $k_{dynamic}$ value is then be adjusted for the depth to a rigid foundation, seasonal changes, and loss of support under the slab to become the effective modulus of subgrade reaction, k_{eff} (Christopher et al. 2006). The rigid pavement response model is based on a spring foundation (i.e., Winkler foundation) model that requires the modulus of subgrade reaction $k_{dynamic}$ value. The assumption of a Winkler foundation is that the subgrade does not

transfer shear stresses. The k_s value is a constant that, when multiplied by the deflection, determines the reaction of the base on the slab (Ullidtz 1987).
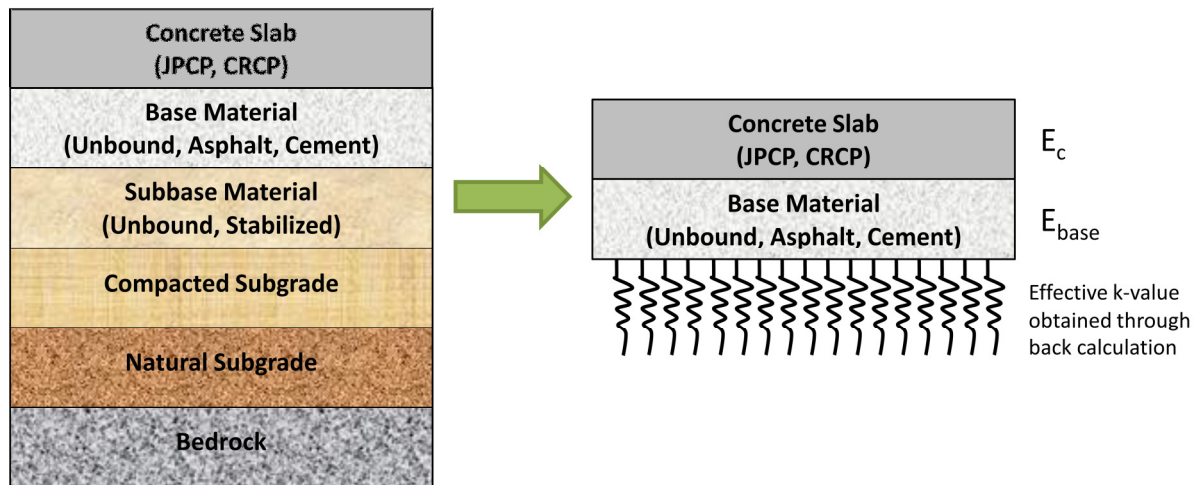
Figure 3. Conversion model of resilient moduli to moduli of subgrade reaction for rigid pavements (adapted from NCHRP 2004b)

Flexible pavements

For flexible pavements, Level 1 inputs are the k_1, k_2, and k_3 regression coefficients from Equation 3. The design software does not use actual resilient moduli test data; it incorporates the regression coefficients to determine the resilient moduli at different depths (i.e., different vertical and confining stresses).These regression coefficients are directly applicable only with the use of finite element analyses (FEM). A computer program uses FEM technology to determine the pavement response from nonlinear resilient moduli in the foundation layers. The MEPDG (NCHRP 2004b) does not recommend using the nonlinear method to determine resilient moduli from Equation 3 because of the lack of calibration between pavement distress and FEM. Level 2 and Level 3 foundation layer resilient moduli are the same inputs as rigid pavements. Equation 3 can be used to input Level 2 values for flexible pavements by determining a single resilient modulus value using an iterative method (Crisman and Facchin 2009).

MEPDG (NCHRP 2004b) recommends the universal constitutive model developed by Witczak and Uzan (1988):

$$M_r = k_1 P_a \left(\frac{\sigma_B}{P_a}\right)^{k_2} \left(\frac{\tau_{oct}}{P_a}+1\right)^{k_3} \qquad (3)$$

where: P_a = atmospheric pressure (MPa);

σ_B = bulk stress (MPa) = $\sigma_1 + \sigma_2 + \sigma_3$;

τ_{oct} = octahedral shear stress (MPa) $= \dfrac{\sqrt{(\sigma_1-\sigma_2)^2 + (\sigma_2-\sigma_3)^2 + (\sigma_3-\sigma_1)^2}}{3}$;

$\sigma_1, \sigma_2, \sigma_3$ = principal stresses; and

k_1, k_2, k_3 = regression coefficients.

Regression coefficient k_1 is proportional to Young's modulus. It should be positive because M_r values will never be negative in real application. An increase in the bulk stress should result in higher M_r values. Larger M_r values indicate a stiffening response, so regression coefficient k_2 should be positive. An increase in the shear stress should result in a softening response and lower M_r values. Therefore, regression coefficient k_3 should be negative (NCHRP 2004b).

Typical values

Depending on the layer thickness and soil classification, typical resilient modulus values for unbound granular and subgrade materials can range from 34.5 MPa to 289.6 MPa (8,000 psi to 42,000 psi) at optimum moisture content (NCHRP 2004b). Typical resilient modulus values at optimum moisture content and dry density according to the material classification can be seen in Table 3. The resilient modulus values will need to be adjusted if the constructed materials are not at optimum moisture content and dry density (AASHTO 2008).

Table 3. Typical resilient modulus values according to material classification

(NCHRP 2004b)

Material Classification	Resilient Modulus Range				Typical Resilient Modulus	
	Low (psi)	High (psi)	Low (MPa)	High (MPa)	psi	MPa
A-1-a	38500	42000	265.4	289.6	40000	275.8
A-1-b	35500	40000	244.8	275.8	38000	262.0
A-2-4	28000	37500	193.1	258.6	32000	220.6
A-2-5	24000	33000	165.5	227.5	28000	193.1
A-2-6	21500	31000	148.2	213.7	26000	179.3
A-2-7	21500	28000	148.2	193.1	24000	165.5
A-3	24500	35500	168.9	244.8	29000	199.9
A-4	21500	29000	148.2	199.9	24000	165.5
A-5	17000	25500	117.2	175.8	20000	137.9
A-6	13500	24000	93.1	165.5	17000	117.2
A-7-5	8000	17500	55.2	120.7	12000	82.7
A-7-6	5000	13500	34.5	93.1	8000	55.2
CH	5000	13500	34.5	93.1	8000	55.2
MH	8000	17500	55.2	120.7	11500	79.3
CL	13500	24000	93.1	165.5	17000	117.2
ML	17000	25500	117.2	175.8	20000	137.9
SW	28000	37500	193.1	258.6	32000	220.6
SP	24000	33000	165.5	227.5	28000	193.1
SW-SC	21500	31000	148.2	213.7	25,500	175.8
SW-SM	24000	33000	165.5	227.5	28000	193.1
SP-SC	21500	31000	148.2	213.7	25500	175.8
SP-SM	24000	33000	165.5	227.5	28000	193.1
SC	21500	28000	148.2	193.1	24000	165.5
SM	28000	37500	193.1	258.6	32000	220.6
GW	39500	42000	272.3	289.6	41000	282.7
GP	35500	40000	244.8	275.8	38000	262.0
GW-GC	28000	40000	193.1	275.8	34500	237.9
GW-GM	35500	40500	244.8	279.2	38500	265.4
GP-GC	28000	39000	193.1	268.9	34000	234.4
GP-GM	31000	40000	213.7	275.8	36000	248.2
GC	24000	37500	165.5	258.6	31000	213.7
GM	33000	42000	227.5	289.6	38500	265.4

CORRELATIONS TO OTHER TEST METHODS

Several methods have been studied to find various ways to correlate easily determined soil properties to resilient modulus values. Correlations involve both laboratory tests (e.g., index properties and soil strength) as well as in situ tests (e.g., falling weight deflectometer, California bearing ratio, dynamic cone penetrometer, and plate load test). A summary of the correlations used in the MEPDG method can be found in Table 4. The models in Table 4 satisfy MEPDG Level 2 parameters (i.e., correlations with other material properties).

George (2003) discusses two concerns with comparing laboratory results to in situ results. The first concern deals with residual stress. In the field, vertical compaction with a roller increases the lateral stress, but only some of that stress is recovered once the roller "walks out". The stress remaining in the soil structure is termed residual stress. In situ deflection tests are significantly influenced by residual stress. The effect of residual stress on Shelby tube samples is minimal because the lateral stresses are somewhat relieved when the sample is removed from the in situ condition. Larger residual stress in situ could cause the resilient modulus to be larger than the sampled material tested in the laboratory. The second concern is the stress-dependant nonlinearity of subgrade soils. The laboratory specimen stress state is nearly uniform because of the small and finite size of the sample. However, in situ stress states are almost always nonuniform in vertical and horizontal directions.

Table 4. Models relating material index and strength properties to resilient

modulus (NCHRP 2004b and Shukla and Sivakugan 2011)

Strength/Index Property	Model	Comments
CBR	$M_r = 10(CBR), CBR \le 5$ [a] $M_r = 17.6(CBR)^{0.64}, CBR > 5$ [b] $CBR_{Unsat} = (S_r)^{2.3} \times CBR_{Sat}$ [a] $CBR_{Lab} = 1.35 \times CBR_{Field}$ [a]	M_r = resilient modulus (MPa); CBR = California bearing ratio (%); S_r = Degree of saturation (%); CBR_{Unsat} = Unsaturated CBR; CBR_{Sat} = Saturated CBR
PI and gradation	$CBR = \dfrac{75}{1 + 0.728(wPI)}$ [b]	CBR = California bearing ratio (%); wPI = P200*PI; P200 = percent passing No. 200 sieve size; PI = plasticity index (%)
Gradation	$CBR = 28.09(D_{60})^{0.358}$ [b]	Used for coarse, clean soils (wPI = 0); CBR = California bearing ratio (%); D_{60} = diameter at 60% passing from the grain size distribution (mm)
DCP	$CBR = \dfrac{292}{DCPI^{1.12}}$ [b]	CBR = California bearing ratio (%); DCP = DCP index (mm/blow)

[a] = Shukla and Sivakugan 2011
[b] = NCHRP 2004b

Index properties

Many of the published resilient modulus correlations to soil index properties are specific to a certain soil classification, soil type, or geographic region. Equations compiled by George (2004) and Puppula (2008) show the broad range of variables researchers use to correlate resilient modulus to soil index properties including moisture content, degree of saturation, percent clay content, percent silt content, AASHTO classification, plasticity index, and liquid limit. MEPDG (NCHRP 2004b) suggests a single equation to correlate index properties to resilient moduli, as seen in Table 4.

Soil strength

Compressive strength tests are common and economical laboratory procedures for determining soil strength. Both confined and unconfined variations are used to measure soil strength. Some tests apply a confining stress to the sample to simulate the lateral stress on a

soil element under the ground surface. The soil sample is then compressed at a given strain rate until it fails. An unconfined compressive strength test is performed without any confining stress applied to the soil sample.

For fine-grained soils, Thompson and Robnett (1979) found strong positive correlations between M_r and static stress-strain data—through unconfined compressive strength and static modulus. Lee et al. (1997) derived an empirical correlation between laboratory tested M_r values and stress at 1% axial strain ($S_{u1.0\%}$) in an unconfined compression test. The correlation showed a similar relationship between M_r and $S_{u1.0\%}$ for three different soils used in the study. The MEPDG method does not describe a correlation between compressive strength and resilient moduli.

Falling weight deflectometer

A falling weight deflectometer is an in situ, nondestructive testing device that drops a weight from a series of heights to determine the elastic modulus of the pavement and pavement foundation layers. The pavement foundation elastic modulus values are back calculated using assumptions about layer thicknesses. Several sensors detect surface deflection from distances ranging from directly under the dropped weight to approximately 1.8 m (5 ft) away from the center.

Depending on the stiffness and homogeneity of the layered soils, different moduli could be determined from the FWD data by using different deflections along the measurement array. George (2003) determined that deflections directly under the dropped weight reflect the moduli of the entire subgrade for stiff soils; deflections farther away from the dropped weight reflect moduli from only the lower reaches of the soil layers. The best correlations of FWD moduli and laboratory resilient moduli, therefore, occur when deflections directly under the dropped weight and deflections 457.2 cm to 914.4 cm (1.5 ft to 3 ft) from the dropped weight are used together. Table 5 summarizes the laboratory M_r versus FWD moduli used in the AASHTO 1993 and current MEPDG (NCHRP 2004b) design guides.

Table 5. Summary of average values to convert in situ calculated layer moduli

to equivalent laboratory resilient moduli (AASHTO 2008)

Layer Type	Location	C-Value (M_r/E_{FWD} Ratio)
Aggregate Base/Subbase	Between stabilized and HMA layer	1.43
	Below PCC layer	1.32
	Below HMA layer	0.62
Subgrade-Embankment	Below stabilized subgrade/embankment	0.75
	Below HMA or PCC layer	0.52
	Below unbound aggregate base	0.35

George (2003) discusses several discrepancies with comparing laboratory resilient modulus test results with in situ FWD test results. Laboratory tests that determine resilient moduli, only measure resilient deformation. The FWD analysis measures total deflections. Additionally, the nonhomogeneous and nonlinear properties of in situ soil layers and conditions can affect the deflections of each sensor and could lead to lower elastic moduli determined by FWD analyses. Finally, use of static load theory to determine dynamic deflection is inconsistent and tends to underestimate actual moduli. These discrepancies illustrate the reasons resilient moduli and FWD elastic moduli do not lead to a one to one relationship.

Light weight deflectometer

Much like the FWD, the light weight deflectometer (LWD) is an in situ, non-destructive testing device that drops a known weight from a known height to calculate the elastic modulus of pavement foundation layers (E_{LWD}). The main differences between the FWD and the LWD are that the dropped weight is less for the LWD and only the deflection under the load plate is measured with the LWD (instead of the series of deflection sensors in an FWD that measure the deflection basin away from the load plate). Depending on the type of device used, other authors (e.g., Fleming et al. 2000, Nazzal 2003) reported LWD/FWD ratios of approximately 0.4–1.3. Factors that affect the E_{LWD} values include size of loading plate, plate contact stress, plate rigidity, loading rate, buffer stiffness, measured versus assumed load and

drop height, and differences in the type and location of deflection transducers (White et al. 2009).

California bearing ratio

The California bearing ratio (CBR) test assesses the strength of roadway base courses and subgrades. CBR tests measure the resistance to penetration of a piston into soil compared to the penetration resistance into a standard well graded crushed stone (Papagiannakis and Masad 2008). It does not apply the impulse-type loads applied by traffic. Resilient modulus tests produce data that represent the dynamic response and properties of pavement foundation layers under traffic loading better than other static laboratory tests such as the CBR (Zehgal 2004). CBR measures the shear strength of a soil, and it is therefore not expected to correlate well with stiffness values. Thompson and Robnett (1979) determined that for soils at optimum and wet of optimum moisture conditions, the CBR value did not correlate well to resilient modulus values. Many CBR relationships are limited in their ability to correlate to resilient modulus because they do not account for stress dependency (Drumm et al. 1990). The CBR of intact, stiff clays reflects the undrained strength, and the CBR of low stiffness clays reflects both stiffness and undrained strength (Shukla and Sivakugan 2011).

Dynamic cone penetrometer

A dynamic cone penetrometer (DCP) is a device that measures the in situ strength of soil (Figure 4). The device works by dropping an eight kilogram (17.6 lb) hammer onto a rod with a cone tip from a height of 575 mm (22.6 in.) and measuring the penetration distance for a given number of blows (ASTM D6951). The penetration rate is then correlated to estimate CBR, thickness of soil layers, shear strength of soil layers, and other material properties. Direct correlations between DCP and resilient modulus values are available, but additional laboratory and field studies must be performed to validate the results. Typical correlations relate the penetration rate (PR) to resilient modulus with constants using a power law. According to Roy (2007), it is possible to obtain resilient modulus values from DCP data comparable to back-calculated FWD values by concerting PR to CBR and CBR to M_r.

Figure 4. A dynamic cone penetrometer (DCP) in use

Plate load test

The static plate load test (PLT) device involves a hydraulic jack pressing a steel bearing plate onto a soil surface and measuring the resulting load and deflection (Figure 5). The test determines the in situ modulus of subgrade reaction (k_s). As discussed above, k_s indicates the level of support the soil can provide to overlying structures. Additionally, elastic moduli can be determined from plate load test data as seen from equations in Table 8.

Figure 5. Plate load test (PLT) performed on subgrade

DETERMINING MODULI FOR PAVEMENT FOUNDATIONS

Current test and design methods for pavement foundations use three principal types of moduli to characterize the soil properties, resilient, elastic, and modulus of subgrade reaction. Whereas resilient moduli are determined from the recoverable strains, elastic moduli and moduli of subgrade reaction are determined using total strains or deflections. Depending on the test method used to determine the modulus value and the pavement surface type, certain moduli are design inputs for specific layers.

Resilient modulus numerical models

Several resilient moduli models have been developed to characterize the nonlinearity of a soil layer. The accuracy of the resulting model depends on the type of material (i.e., fine grained or cohesive vs. granular) and accurate measurements of the parameters used in the equations. Puppala (2008) compiled a list of resilient moduli equations that model the nonlinear behavior of the parameter. The equations are summarized in Table 6.

Table 6. Summary of two and three parameter resilient modulus models (Puppala 2008)

Model	Original Reference	Parameters
$M_r = k_1 P_a \left(\dfrac{\sigma_3}{P_a}\right)^{k_2}$	Dunlap (1963)	$k_1, k_2, k_3, k_4, k_6, k_7$ = model constants;
$M_r = k_1 P_a \left(\dfrac{\sigma_B}{P_a}\right)^{k_2}$	Seed et al. (1967)	P_a = atmospheric pressure;
$M_r = k_2 + k_3(k_1 - \sigma_d) \quad k_1 > \sigma_d$ $M_r = k_2 + k_4(\sigma_d - k_1) \quad k_1 < \sigma_d$	Thompson and Elliott (1985)	$\sigma_1, \sigma_2, \sigma_3$ = principal stresses; σ_B = bulk stress = $\sigma_1 + \sigma_2 + \sigma_3$;
$M_r = k_1 P_a \left(\dfrac{\sigma_B}{P_a}\right)^{k_2} \left(\dfrac{\sigma_d}{P_a}\right)^{k_3}$	Uzan (1985)	σ_d = deviator stress; τ_{oct} = octahedral shear stress =
$M_r = k_1 P_a \left(\dfrac{\sigma_B}{P_a}\right)^{k_2} \left(\dfrac{\sigma_d}{P_a}\right)^{k_3}$	Pezo (1993)	$\dfrac{\sqrt{(\sigma_1-\sigma_2)^2+(\sigma_2-\sigma_3)^2+(\sigma_3-\sigma_1)^2}}{3}$;
$M_r = k_1 P_a \left(1 + \dfrac{\sigma_B}{P_a}\right)^{k_2} \left(1 + \dfrac{\sigma_d}{P_a}\right)^{k_3}$ $M_r = k_1 P_a \left(1 + \dfrac{\sigma_B}{P_a}\right)^{k_2} \left(1 + \dfrac{\tau_{oct}}{P_a}\right)^{k_3}$	Ooi et al. (2004)	$(\mu_a - \mu_w)$ = matric suction; and α_1, β_1 = regression constants
$M_r = k_1 P_a \left(\dfrac{\sigma_B}{P_a}\right)^{k_2} \left(1 + \dfrac{\tau_{oct}}{P_a}\right)^{k_3}$	Witczak and Uzan (1988) *MEPDG recommended	
$M_r = k_1 P_a \left(\dfrac{\sigma_B - 3k_6}{P_a}\right)^{k_2} \times$ $\left(k_7 + \dfrac{\tau_{oct}}{P_a}\right)^{k_3} + \alpha_1(\mu_a - \mu_w)^{\beta_1}$	Gupta et al. (2007)	

Von Quintus and Killingsworth (1997) calculate a single equivalent resilient modulus value for an entire multilayer pavement system using Equation 4 when the resilient modulus is larger for the upper layer. When the upper layer resilient modulus is smaller than the underlying layer, the design input is the smaller value.

$$M_{r(EquivComposite)} = \frac{D_{s1}^3 M_{r1} + D_{s2}^3 M_{r2}}{\left(D_{S1}\right)^3 + \left(D_{S2}\right)^3} \tag{4}$$

where: M_{r1} = resilient modulus of the upper layer;

M_{r2} = resilient modulus of the lower layer;

D_{S1} = thickness of the upper layer; and

D_{S2} = thickness of the lower layer.

Elastic moduli

Elastic modulus is the ratio of stress to strain of a material and, for soils, is measured directly from compression tests. Elastic moduli are a measure of how well a material returns to the original size and shape when stressed within the elastic range. Past the elastic range, a material will deform permanently. Figure 6 shows the differences of two moduli, secant and tangent. In the elastic range, secant moduli and tangent moduli are equal, but at strains higher than the elastic range, the values differ. This study will involve secant modulus values for comparison with determined resilient modulus values.
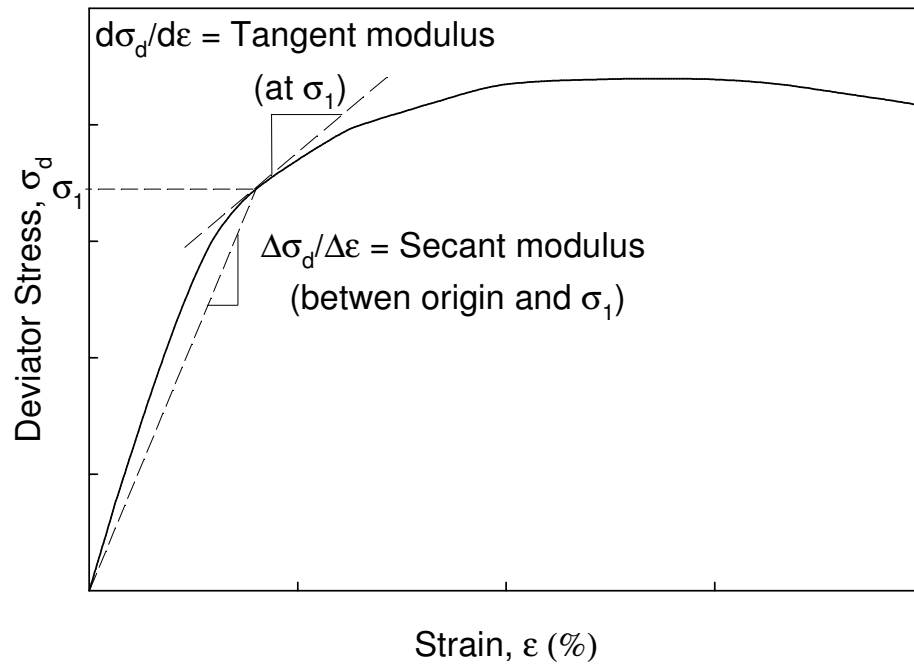
Figure 6. Determination of tangent and secant moduli

Vennapusa and White (2009) discuss the theoretical determination of elastic modulus based on the Bousinnesq elastic solution. The relationship between applied stress and soil

displacement for a base resting on an elastic half-space is derived in Equation 5. Elastic moduli are derived from FWD data using Equation 5.

$$E = \frac{(1-v^2)\sigma_0 a}{d_0} f \qquad (5)$$

where: E = elastic modulus (MPa);

d_0 = measured displacement (mm);

υ = Poisson's ratio;

σ_0 = applied stress (MPa);

a = radius of the loading plate (mm); and

f = shape factor depending on stress distribution (for this study, F = 8/3 for granular materials and F = π/2 for non-granular materials).

Elastic moduli from Figure 6 are determined from deviator stress and total strain, while elastic moduli from Equation 5 are determined from applied stress and total deformation. Typical values of elastic moduli are seen in Table 7.

Table 7. Typical elastic modulus values for road construction materials (Huang 1993

and Maheshwari 2011)

Material	Elastic Modulus Range				Typical Elastic Modulus	
	Low (psi)	High (psi)	Low (MPa)	High (MPa)	psi	MPa
Portland cement concrete	3×10^6	6×10^6	20700	41400	4×10^6	27600
Cement-treated bases	1×10^6	3×10^6	6700	20700	2×10^6	13800
Soil cement materials	5×10^4	2×10^6	350	13800	1×10^6	6700
Lime-fly ash materials	5×10^5	2.5×10^6	3450	17200	1×10^6	6700
Sand and gravel	1×10^4	2.5×10^4	69	173	121	17500
Dense Sand	5100	8000	35	55	6550	45
Medium-dense sand	2500	4100	17	28	3300	23
Loose sand	1450	3500	10	24	2500	17
Silty sand	1450	2500	10	17	2000	14
Stiff clay	7600	17000	52	117	12000	83
Medium clay	4700	12300	32	85	8000	55
Soft clay	1800	7700	12	53	5000	34
Very soft clay	1000	5700	7	39	3000	21

Christopher et al. (2006) illustrated how to back calculate resilient moduli from FWD test data using Equation 6. The subgrade resilient modulus design values are typically less than the back calculated resilient modulus values from FWD data. The AASHTO design guide recommends reducing the back calculated resilient moduli to 33% for flexible pavements and 25% for rigid pavements (Christopher et al. 2006).

$$M_r = \frac{0.24P}{d_r r} \qquad (6)$$

$$R \geq 0.7a_e$$

$$a_e = \sqrt{a^2 + \left(D^3 \sqrt{\frac{E_p}{M_r}} \right)^2}$$

where: Mr = back calculated subgrade resilient modulus (psi);

P = applied load (lbs);

d_r = deflection at a distance r from the center of the load (in.);

r = distance from the center of the load (in.);

a_e = radius of the stress bulb at the subgrade-pavement interface (in.);

a = load plate radius (in.);

D = total pavement thickness above the subgrade (in.);

E_p = effective pavement modulus by the following equation:

$$d_0 = 1.5pa \left\{ \frac{1}{M_r \left[\sqrt{1 + \frac{D^3}{a} \sqrt{\frac{E_p}{M_r}}} \right]^2} + \frac{1 - \frac{1}{\sqrt{1 + \left(\frac{D}{a} \right)^2}}}{E_p} \right\}$$

d_0 = deflection measured at the center of the load plate, adjusted to a standard temperature of 68°F (in.); and

p = load plate pressure (psi).

Moduli of subgrade reaction

The MEPDG method derives the modulus of subgrade reaction from resilient modulus tests. The modulus of subgrade reaction is defined as the ratio of the pressure applied to a surface through a loading area divided by the displacement of the loading area. Plate load tests (PLT) are a typical in situ method to determine the moduli of subgrade reaction. Equation 7 describes how to calculate the modulus of subgrade reaction from PLT data.

$$k = \frac{p}{\Delta} \tag{7}$$

where: k = modulus of subgrade reaction;

p = pressure on the plate; and

Δ = deflection of the plate.

Ullidtz (1987) describes two equations to determine the modulus of subgrade reaction from elastic modulus values, seen in Table 8.

Table 8. Equations to determine modulus of subgrade reaction (Ullidtz 1987; Shukla

and Sivakugan 2011)

Equation	Parameters
$k = \dfrac{E}{f(1-\upsilon^2)a}$	E = elastic layer modulus; f = stress distribution factor; υ = Poisson's ratio; and a = plate radius from plate load test. Only valid for tests directly on the subgrade
$k = \dfrac{0.54 \times E_m}{h_e}$	E_m = subgrade modulus; and h_e = equivalent thickness of the concrete slab. Valid for loads on a concrete slab
$k = \dfrac{E}{H(1+\upsilon)(1-2\upsilon)}$	E = elastic layer modulus; υ = Poisson's ratio; and H = thickness of the soil layer

Equation 5 also relates elastic modulus to modulus of subgrade reaction through the use

of applied stress and measured plate displacement. Seen in the Table 8 equation, the

parameters are reorganized to show the relationship between elastic modulus and modulus of

subgrade reaction. Typical ranges of moduli of subgrade reaction are summarized in Table 9.

Table 9. Ranges of moduli of subgrade reaction (Shukla and Sivakugan 2011)

Soil Type		k_s (MPa/mm)
Sand (dry or moist)	Dense	0.125–0.375
	Medium	0.025–0.125
	Loose	0.008–0.025
Sand (saturated)	Dense	0.130–0.150
	Medium	0.035–0.040
	Loose	0.010–0.015
Clay	Hard	>0.050
	Very stiff	0.025–0.030
	Stiff	0.012–0.025

CHAPTER 3. METHODS

This chapter summarizes the test methods and standards employed in the field and the laboratory to compare the resilient moduli of pavement foundations with soil index properties, gradation, and other in situ testing procedures (e.g., falling weight deflectometer and plate load tests). Resilient properties that were the result of different foundation construction materials collected from six sites in four states were studied (Table 10).

Table 10. Summary of investigated sites and materials

State	Site location	Materials
Michigan	I-94	Existing subbase, base, subgrade*
Michigan	I-96	Subbase, subgrade*
Pennsylvania	US-22	Cement-treated base (CTB), asphalt-treated base (ATB), subbase, subgrade
Pennsylvania	US-422	Base, injected stabilization foam
Iowa	I-29	Existing subbase, base, subbase, subgrade
Wisconsin	US-10	Subbase, subgrade

* = Samples obtained by Shelby tube also tested

RESEARCH DESIGN

Laboratory soil tests provided index properties and data to classify the materials and correlate properties to resilient behavior. Because laboratory resilient modulus testing equipment can be very expensive and labor intensive, finding correlations to easily determine soil properties could result in widespread use of resilient modulus as a valuable design parameter.

In situ soil tests provided data used to fabricate laboratory samples that match the constructed conditions. In situ tests also provide methods to determine resilient soil properties without using expensive laboratory resilient modulus equipment.

Information about the laboratory tests is presented first, followed by information about the in situ tests.

LABORATORY TEST METHODS

Laboratory tests were performed on sampled materials to determine the intrinsic material properties, classifications, and mechanical properties. The laboratory tests and test methods are summarized in Table 11. The laboratory tests were divided into four sections: soil index

properties, laboratory compaction, sample preparation, and determination of resilient moduli. The laboratory data was compared to the in situ material properties.

Table 11. Summary of methods used for laboratory soil tests

Laboratory test	Test method
Standard Test Method for Particle-Size Analysis of Soils	ASTM D422-63
Standard Test Methods for Liquid Limit, Plastic Limit, and Plasticity Index of Soils	ASTM D4318-10
Standard Test Method for Density, Relative Density (Specific Gravity), and Absorption of Coarse Aggregate	ASTM C127-07
Standard Test Method for Specific Gravity of Soil Solids by Water Pycnometer	ASTM D854-10
Standard Test Method for Laboratory Compaction Characteristics of Soil Using Standard Effort (12,400 ft-lbf/ft^3 (600 kN-m/m^3))	ASTM D698-07
Standard Test Method for Laboratory Compaction Characteristics of Soil Using Modified Effort (56,000 ft-lbf/ft^3 (2,700 kN-m/m^3))	ASTM D1557-09
Standard Test Methods for Maximum Index Density and Unit Weight of Soils Using a Vibratory Table	ASTM D4253-00
Standard Test Methods for Minimum Index Density and Unit Weight of Soils and Calculation of Relative Density	ASTM D4254-00
Iowa Modified Relative Density Test for Determination of Bulking Moisture Contents of Cohesionless Soils	White et al. 2002
Standard method of test for determining the resilient modulus of soils and aggregate materials	AASHTO T307

Soil index properties

Soil index properties were determined from grain size analyses, Atterberg limits tests, and specific gravity tests.

Grain size analyses were performed according to ASTM D422-63. Samples were divided into two parts by the No. 10 sieve. Mechanical sieve analyses were performed on material

washed and retained on the No. 10 sieve. Hydrometer analyses, using a 152H hydrometer, were performed on material passing the No. 10 sieve. After the hydrometer tests, the material was washed over the No. 200 sieve, oven dried, and mechanically sieved through the No. 20, No. 40, No. 100, and No. 200 sieves.

Atterberg limit tests (i.e., liquid limit—LL, plastic limit—PL, and plasticity index—PI) were performed according to ASTM D4318-10 using the dry preparation method. AASHTO and Unified Soil Classification System (USCS) methods classified the soils using particle size analysis and Atterberg limits.

Two methods were used to determine the specific gravities of the materials, ASTM D854-10 and ASTM C127-07. ASTM D854-10 followed Method B, the procedure for oven-dried specimens. ASTM C127-07 was performed on materials retained on the No. 4 sieve. For materials that contained particles both greater and less than the No. 4 sieve, Equation 8 (ASTM D854-10) was used to calculate the average specific gravity for all material, corrected to 20^oC.

$$G_{ave@20^o C} = \frac{1}{\dfrac{R}{100 \cdot G_{1@20^o C}} + \dfrac{P}{100 \cdot G_{2@20^o C}}} \qquad (8)$$

where: R = percent of soil retained on the No. 4 sieve;

P = percent of soil passing the No. 4 sieve;

$G_{1@20C}$ = apparent specific gravity of soils retained on the No. 4 sieve as determined by ASTM C127, corrected to 20^oC; and

$G_{2@20C}$ = apparent specific gravity of soils passing the No. 4 sieve as determined by ASTM D854, corrected to 20^oC.

Laboratory compaction

Three laboratory compaction tests were used to determine the relationship between dry density and moisture content for the investigated materials. Test methods were determined on the basis of gradation requirements. Proctor compaction methods ASTM D698-07 and D1557-07 were used on materials meeting the gradation requirements set by the test standards. Maximum and minimum relative density tests were performed on granular materials according to ASTM D4253-00 and D4254-00 using a vibratory table. Additionally,

moisture-density relationships for granular materials were performed using the variable moisture relative density tests from White et al. (2002). Varying the moisture of samples in small increments illustrates the bulking moisture content (where small capillary stresses in partially saturated materials resist compaction forces, leading to low dry unit weights) as well as a range of moisture contents to obtain maximum compaction.

Sample preparation

Several materials investigated in this study had specific preparation methods to accurately simulate in situ conditions. AASHTO T307 describes two principal types of soil. Type I materials are defined as untreated base, subbase, or subgrade soils with gradations that include less than 70% passing No. 10 sieve, less than 20% passing No. 200 sieve, and a plasticity index less than or equal to ten. Type II materials include all untreated granular bases or subbases and untreated subgrade soils that do not meet the requirements for Type I. Subgrade soils obtained from thin-walled tube samples are included as Type II materials (AASHTO T307).

Material type and sieve analysis test results determine the sample preparation method. Undisturbed subgrade soil samples were obtained from thin walled tube samples. Reconstituted cohesive and granular materials were also tested. AASHTO T307 test standard recommends the use of kneading, static, or vibratory compaction to reconstitute the materials.

Kneading and static compaction techniques are applicable to Type II materials. Vibratory compaction is applicable to both Type I and Type II materials. The kneading compaction technique is better than static compaction at arranging the laboratory soil particle structure to best represent the in situ soil conditions (Seed et al. 1962). The kneading compactor used in this study was a Cox and Sons model CS 1000-C Electronic-Hydraulic Kneading Compactor. AASHTO T307 test standard states the maximum particle size must be less than 25% of the inner mold diameter for all compaction methods. Particles larger than this value are removed—that is scalped. Cohesive soils use kneading and static compaction, while non-cohesive materials use vibratory compaction.

The following sections present the preparation techniques used for the cohesive, granular, composite, back saturated, treated subgrade, and Pennsylvania US-422 samples.

Cohesive materials

Both undisturbed and disturbed cohesive materials were sampled and tested. Undisturbed samples provide the best representation of in situ soil conditions and properties. Disturbed soils were reconstituted in a laboratory to attempt to match the in situ conditions.

Undisturbed samples of subgrade materials were collected in general accordance with ASTM D1587 using a hydraulic tube attachment on the Iowa State University Geotechnical Mobile Laboratory truck (White et al. 2008). The hydraulic cylinder pushed a thin-walled, 71.1 mm (2.8 in.) diameter Shelby tube into the compacted subgrade using the truck weight as a reaction force. The hydraulic cylinder was then converted into a horizontal position to extrude the soil (Figure 7). Intact specimens with a minimum length of 142.2 mm (5.6 in.) were trimmed from the extruded tube sample. The trimmed specimens were then mounted to the triaxial base, and resilient modulus and unconsolidated-undrained (UU) compression tests were performed.

Figure 7. Shelby tube sampling; subgrade sample retrieval (left),

sample extrusion (right)

Disturbed cohesive samples were collected and later reconstituted. Cohesive samples were reconstituted using two compaction methods outlined in AASHTO T307, kneading and

static compaction. Cyclic properties of cohesive samples change with different compaction techniques. Before compaction, cohesive materials were conditioned to target moisture contents matching in situ values and allowed to mellow for at least 16 hours.

Kneading compactors reconstitute soil samples using set numbers of tamps at specific pressures. Figure 8 shows the Cox and Sons model CS 1000-C kneading compactor used in this study. Soil was placed in a steel split mold and compacted in five lifts of equal mass. An additional 3-5% soil mass was added to each layer to account for loss of material during compaction. AASHTO T307 states that during kneading compaction the applied pressure should be adjusted so the tamper foot only penetrates the soil 5–10 mm (0.2–0.4 in.). After each tamp (Figure 9), the base is mechanically rotated to provide an even distribution of compaction energy to the lift. An aluminum funnel collar placed at the top of the split mold allows the final lift to be compacted approximately 6.4 mm (0.25 in.) above the mold and trimmed. After kneading compaction, the aluminum funnel collar was removed, the sample height was trimmed to 203.2 mm (8 in.), and the sample was removed from the split mold (Figure 10).

Figure 8. Cox and Sons kneading compactor used for cohesive soils

Figure 9. Soil compacted by kneading tamper foot

Figure 10. Compacted sample being removed from a 4 in. diameter split mold

Static compaction involves a hydraulic press, steel mold, and six steel spacers (Figure 11) to form the soil into a 101.6 mm diameter by 203.2 mm tall (4 in. diameter by 8 in. tall) cylinder. The compaction process is described in AASHTO T307 and seen in Figure 12. When making the single material samples, the soil was compacted in five lifts of equal mass and thickness. Each lift of soil was pressed between the steel spacers to a uniform thickness. After compaction, the soil specimens were extruded (Figure 13).

Figure 11. Aluminum spacers (4 in. diameter) used during static compaction

Figure 12. Static compaction of a cohesive specimen

Figure 13. Extruding a statically compacted specimen

Granular materials

Granular materials have almost no cohesion, so vibratory compaction is the most efficient procedure for compacting them.

AASHTO T307 procedure requires that the maximum particle size of the material should be less than 20% of the sample diameter, which is about 20.3 mm (0.8 in.) for a 101.6 mm (4 in.) diameter sample. Several materials investigated in this study contained maximum particle sizes of 25.4 mm (1 in.) or slightly greater. Oversize particle size correction equations in ASTM D4718-87 "Standard Practice for Correction of Unit Weight and Water Content for Soils Containing Oversize Particles" change the theoretical density of the sample but do not change the corresponding modulus values. Additionally, using only material passing the 19.1 mm (0.75 in.) sieve did not represent the in situ pavement foundation materials. Therefore, a scalp and replace method was chosen to give the most accurate laboratory representation of the investigated materials.

To meet AASHTO T307 specifications, the particle size distribution of the material was modified by scalping particles retained on the 19.1 mm (0.75 in.) sieve and replacing them

with the same percentage by weight of the material that was retained on the No. 4 sieve and passing the 19.1 mm (0.75 in.) sieve. The material was oven dried before it was separated so the weight of moisture did not affect the percent of material scalped and replaced. This scalp and replace procedure also was performed to correct the resilient moduli for density.

Before compaction, materials were conditioned to target moisture contents and allowed to mellow for at least 3–6 hours. A 101.6 mm (4 in.) diameter split mold restrained the material during vibratory compaction (Figure 14). Vibratory compaction was achieved in five lifts of equal mass and thickness using an electric rotary hammer drill and a circular steel platen placed against the material (Figure 15) according to AASHTO T307. Calipers were used to verify consistent compaction layer thicknesses (Figure 16).

Figure 14. Split mold, steel platen (4 in. diameter), and vibratory hammer for compaction of granular materials

Figure 15. Compaction of granular materials in split mold

Figure 16. Verifying the thickness of each compacted layer with calipers

Stabilized subgrade samples

Cement- and fly ash-treated samples were made for soils from Pennsylvania US-22 and Iowa I-29, respectively. When preparing the cement- and fly ash-treated subgrades, the moisture content was first determined. The laboratory target moisture content for the cement-treated Pennsylvania US-22 subgrade was approximately 2% above the optimum moisture content (determined by standard Proctor tests) with additional water to bring the water-cement (w/c) ratio to 0.28. The target moisture content for the fly ash-treated Iowa I-29 subgrade was approximately 2% above the optimum moisture content. Water was added to the soils, and the materials mellowed overnight. 10% cement by dry weight was added to the Pennsylvania US-22 subgrade, and 15% fly ash by dry weight was added to the Iowa I-29 subgrade. The cement and fly-ash treated subgrades were kneading compacted using five layers, 12 tamps per layer, and 1034 kPa (150 psi) per tamp. Compaction delay is the time between first adding the cement or fly ash to the moist soil to the end of compaction. The resilient properties, density, and strength of the samples were sensitive to very short or large compaction delays, so all samples had compaction delays of 10–25 minutes. To simulate a 28 day curing time, the cement- and fly ash-treated specimens were placed in an oven at 38.8°C (100°F) for seven days.

Composite samples

AASHTO T307 does not describe the procedure for fabricating composite samples. Composite samples that were studied include base over subbase, base over geosynthetic over subbase, subbase over subgrade, and subbase over geosynthetic over subgrade. Figure 17 shows idealized composite samples.
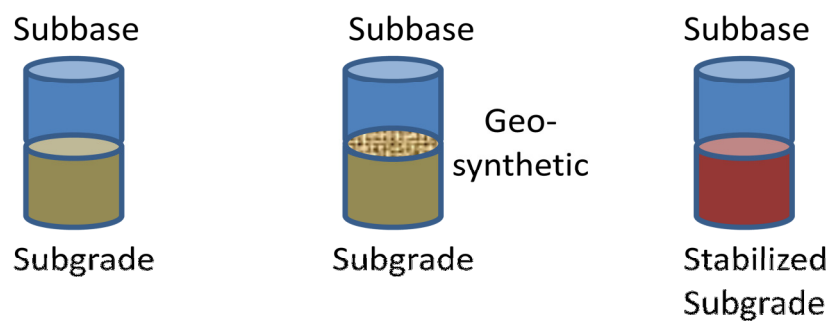
Figure 17. Elements of idealized fabricated composite samples

If both layers were non-cohesive, all materials were compacted using an electric rotary hammer drill and three lifts per layer in the split mold as discussed above for granular materials. The bottom material was compacted first. If any geosynthetic material was to be tested, it was placed at the top of the bottom layer before the upper layer was compacted. Each layer was compacted using three lifts of equal mass, resulting in six total lifts for each specimen.

For composite samples of a granular layer over subgrade, the bottom subgrade layer was compacted first using the static compaction technique described above, in three lifts. The first two lifts were about 40.6 mm (1.6 in.) thick, and the third lift was about 20.3 mm (0.8 in.) thick. A pre-determined amount of material was placed in each lift keeping the unit weight constant. After compaction of the subgrade, the sample was extruded and placed on the triaxial chamber base. The split mold used for granular materials was then placed around the sample, and the base layer was compacted in three equal lifts of 33.9 mm (1.3 in.) using the vibratory compaction procedure described above.

Using kneading compaction, cohesive composite samples were compacted in three lifts, but the mass was constant for each lift. The applied pressure was adjusted to allow the tamper foot to only penetrate approximately 5–10 mm (0.2–0.4 in.) into the lift. After compaction, the sample was placed on the triaxial chamber base. The split mold used for granular materials was then placed around the sample, and the upper granular layer was compacted on top of the cohesive layer.

Back saturation samples

Back saturation involved incrementally increasing both confining stresses and water pressure into the bottom of samples (back pressure) until the specimens were saturated. It required the use of a triaxial cell and an ELE International Tri-Flex 2 Master Control Panel to regulate the water pressures. Samples were first compacted to moisture and density values that match data collected in situ. Samples were placed in the triaxial cell and the back saturation procedure began.

Water applied a confining lateral stress to the sample. Then, water was forced into the bottom of a specimen at a slightly lower pressure than the confining stress. The difference in pressure depended on the material type and how fast the sequence was completed. Generally,

a low pressure difference worked best for course, granular material that becomes saturated quickly. Dense, cohesive soils took several days or weeks to fully saturate. Vertical paper filter strips were placed on the outside of cohesive samples to expedite the saturation process.

Measurements of pore water pressure were taken after each increase in confining stress. The pore water pressure transducer was placed at the center height of the sample (Figure 18). The confining stress was increased first; then the back pressure was increased. After the pressures were increased, samples sat until the pore water pressure stabilized, and the sequence was repeated. The back saturation equipment is shown in Figure 18 and Figure 19.
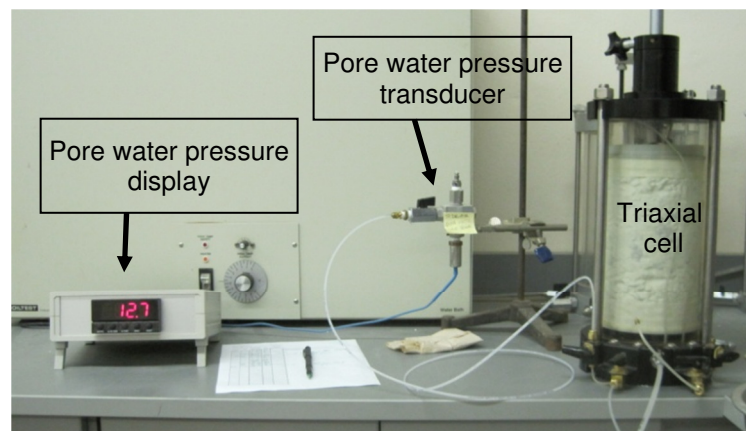
Figure 18. Pore water pressure display, pore water pressure transducer, and triaxial cell used in back saturation prior to M_r tests
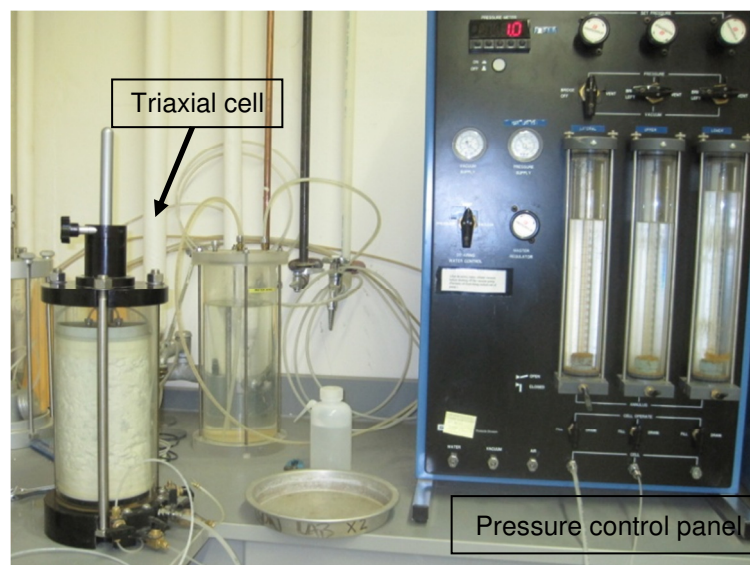
Figure 19. Sample in a triaxial cell and pressure control wall used in back saturation

prior to M$_r$ tests

A sample was considered to be fully saturated when the ratio of the difference in pore water pressures (Δu) over the difference in confining stresses ($\Delta\sigma_3$) was greater than or equal to 0.95, shown in Equation 9 (ASTM D4767-04).

$$\frac{\Delta u}{\Delta\sigma_3} \geq 0.95 \tag{9}$$

where: Δu is the difference in porewater pressure from the previous stress increase and

$\Delta\sigma_3$ is the difference in confining stress from the previous stress increase.

After the saturation process was complete, all samples were allowed to drain for six minutes. During this time, all of the drains on the triaxial chamber were opened to atmospheric pressure. This draining period simulated wet pavement foundation systems that are still able to drain. One sample was back saturated but not allowed to drain. This undrained sample simulated worst-case, ponded foundation systems. Once the draining was complete, each sample was immediately tested in the resilient modulus test apparatus using drained conditions.

Pennsylvania US-422 samples

Preparation of Pennsylvania US-422 samples included an injected foam stabilizer and therefore required a different preparation approach. Open graded stone (OGS), OGS injected with light-weight, high-density polyurethane (HDP) foam (OGS+HDP), and HDP foam samples were tested in this study. The OGS was a granular material and was compacted using the same vibratory method described above. The OGS+HDP sample was compacted in the field similar to the procedure followed for OGS sample but in a 101.6 mm (4 in.) diameter plastic mold (Figure 20). Following compaction, the plastic mold was capped and HDP foam was injected into the mold. After injecting the HDP foam, pressure was applied on top of the specimen cap until the foam hardened, simulating the confinement effect under pavement. HDP foam specimens were injected into an empty plastic mold and capped. The plastic molds were sealed and transported to the laboratory for further tests. Prior to testing, samples in plastic molds were trimmed to a constant height, 203.2 mm (8 in.), at the edges to remove any irregular end surfaces. Trimmed HDP foam and OGS+HDP samples are shown

in Figure 21. The molds were cut open and the samples were removed and tested in the resilient modulus test apparatus.

Figure 20. Compaction of OGS+HDP sample in the field
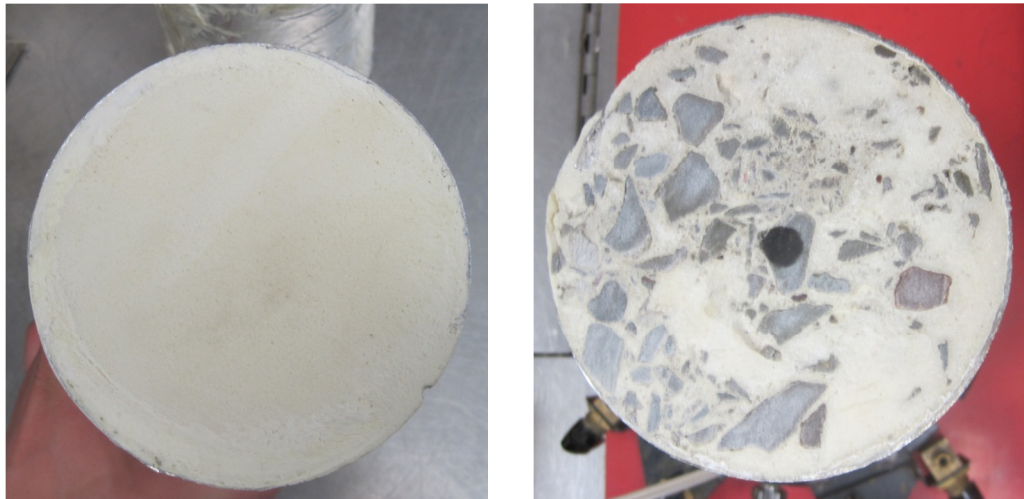
Figure 21. End view of trimmed HDP foam (left) and OGS+HDP (right) samples

Determination of resilient moduli

This section discusses the testing and data analysis procedures used to determine the resilient moduli of samples.

Resilient modulus testing

Resilient modulus (M_r) tests were performed in accordance with AASHTO T307. Resilient modulus tests were performed using the Geocomp automated M_r test system. The system consisted of a Load Trac-II load frame, an electrically controlled servo valve, an external signal conditioning unit, and a computer with a network card for data acquisition. System parameters were input using software version 1.09.289. A proportional-integral-derivative (PID) controller adjusted the system parameters in real-time to apply the correct target loads, as the stiffness of the specimen changed during the test. Figure 22 shows a triaxial test chamber and the computer equipment used in this study. The chamber can hold 71.1 mm (2.8 in.) or 101.6 mm (4 in.) diameter samples. The load was measured using an externally mounted load cell with a capacity of 11.1 kN (2500 lbf). Two linear voltage displacement transducers (LVDTs) were mounted to opposite sides of and equidistant from the piston rod outside the test chamber.

Figure 22. Triaxial chamber, load frame, and computer equipment for performing resilient modulus tests

For this study, M_r tests were performed on 101.6 mm (4 in.) diameter by 203.2 mm (8 in.) tall samples following the AASHTO T307 loading sequences. Different loading sequences were used for different layers in pavement foundations to simulate the stresses each layer encounters in traffic loading. Base, subbase, and composite specimens were subjected to

higher stresses (Table 12), and subgrade specimens were subjected to lower stresses (Table 13). Prior to the actual load sequences, a conditioning sequence with a minimum of 500 load repetitions was first performed on the sample. This sequence minimized the effects of imperfect contacts between the sample cap and the test sample. Each load cycle consisted of a 0.1 second haversine-shaped load pulse followed by a 0.9 second rest period. Resilient modulus was calculated as the ratio of the applied cyclic deviator stress (σ_d) and resilient strain (ε_r). The average σ_d and ε_r values of the last five cycles in a loading sequence were used in M_r calculations. The resilient modulus test was completed when either all cycles have been or if the sample experiences greater than 5% permanent strain (ε_p).

Table 12. Resilient modulus test sequences and stress values for base

and subbase materials (AASHTO T307)

Sequence No.	Confining stress		Max. axial stress		No. of cycles
	kPa	psi	kPa	psi	
0	103.4	15	103.4	15	500-1000
1	20.7	3	20.7	3	100
2	20.7	3	41.4	6	100
3	20.7	3	62.1	9	100
4	34.5	5	34.5	5	100
5	34.5	5	68.9	10	100
6	34.5	5	103.4	15	100
7	68.9	10	68.9	10	100
8	68.9	10	137.9	20	100
9	68.9	10	206.8	30	100
10	103.4	15	68.9	10	100
11	103.4	15	103.4	15	100
12	103.4	15	206.8	30	100
13	137.9	20	103.4	15	100
14	137.9	20	137.9	20	100
15	137.9	20	275.8	40	100

Table 13. Resilient modulus test sequences and stress values for subgrade materials

(AASHTO T307)

Sequence No.	Confining stress		Max. axial stress		No. of cycles
	kPa	psi	kPa	psi	
0	41.4	6	27.6	4	500-1000
1	41.4	6	13.8	2	100
2	41.4	6	27.6	4	100
3	41.4	6	41.4	6	100
4	41.4	6	55.2	8	100
5	41.4	6	68.9	10	100
6	27.6	4	13.8	2	100
7	27.6	4	27.6	4	100
8	27.6	4	41.4	6	100
9	27.6	4	55.2	8	100
10	27.6	4	68.9	10	100
11	13.8	2	13.8	2	100
12	13.8	2	27.6	4	100
13	13.8	2	41.4	6	100
14	13.8	2	55.2	8	100
15	13.8	2	68.9	10	100

Following the M_r tests, UU strength tests, also known as quick-shear tests, were performed on each sample in accordance with AASHTO T307. UU tests were only performed on samples that experienced less than 5% ε_p during resilient modulus tests. During UU tests, a confining pressure of 27.6 kPa (4 psi) for subgrade samples or 34.5 kPa (5 psi) to base, subbase, or composite samples was applied while samples were compressed at 1% axial strain per minute. Undrained shear strengths (s_u) were determined at the peak values (i.e., the point before the load values decrease with increasing strain) or at 5% ε_p, whichever came first.

Data analysis

In this study, pavement foundation design values were developed from regression coefficients (k_1, k_2, and k_3 values) and average resilient modulus values ($M_{r(T307)}$) , both determined from resilient modulus test data.

The test data was consolidated to the final five load cycles in each sequence. Bulk stress, octahedral shear stress, and measured resilient modulus values from the last five load cycles in each sequence were input into the statistical analysis program, JMP (version 8.0.2). The program inputs these values into the MEPDG equation (Equation 10) developed by Witczak and Uzan (1988)—herein described as the universal model—to determine k_1, k_2, and k_3 values that fit the calculated resilient modulus values to the measured resilient modulus values. The equation used in this study was a nonlinear model that combines both the effects of increasing stiffness with increasing confinement and decreasing stiffness with increasing shear stress into a single constitutive model.

$$M_r = k_1 P_a \left(\frac{\sigma_B}{P_a} \right)^{k_2} \left(\frac{\tau_{oct}}{P_a} + 1 \right)^{k_3} \tag{10}$$

where: P_a = atmospheric pressure (MPa);

σ_B = bulk stress (MPa) = $\sigma_1 + \sigma_2 + \sigma_3$;

τ_{oct} = octahedral shear stress (MPa) $= \dfrac{\sqrt{(\sigma_1 - \sigma_2)^2 + (\sigma_2 - \sigma_3)^2 + (\sigma_3 - \sigma_1)^2}}{3}$;

σ_1, σ_2, σ_3 = principal stresses; and

k_1, k_2, k_3 = regression coefficients.

The k_1 coefficient is proportional to M_r and therefore is always > 0. The k_2 coefficient explains the behavior of the material with changes in the volumetric stresses. Increasing volumetric stresses increases the M_r value and therefore the k_2 coefficient should be ≥ 0. The k_3 coefficient explains the behavior of the material with changes in shear stresses. Increasing shear stress softens the material and yields a lower M_r value. Therefore the k_3 coefficient should be ≤ 0.

When performing multiple regression analyses, the R^2 values were adjusted for the number of regression parameters according to Equation 11. The adjusted R^2 value for multiple regression analyses can then be compared to R^2 from simple regression analyses to determine which model best describes the data.

$$R_{adj}^2 = 1 - \left[\frac{(1 - R^2)(n-1)}{(n-p-1)} \right] \tag{11}$$

where: n = the number of data points and

p = the number of regression parameters.

Internal repeatability tests

Geocomp, the manufacturer of the resilient modulus test equipment, provided a reference sample to verify that the results are reproducible. The polyurethane reference sample properties were determined by Geocomp and are provided in Table 14.

Table 14. Polyurethane resilient modulus reference sample properties

Property	Value
Diameter	101.6 mm (4.0 in.)
Height	151.13 mm (5.95 in.)
CBR	2.54 mm (0.1 in.) : 4% 5.08 mm (0.2 in.) : 5%
Resilient Modulus (no confining pressure)	4.83 MPa (700 psi)

Seven resilient modulus tests were performed. The sample was subjected to the subgrade resilient modulus test sequences, as described in Table 13.The data was analyzed and the regression coefficients (k-values), adjusted linear regression (R^2 adj) analyses, and resilient moduli values are summarized in Table 15. The low average resilient moduli coefficient of variation suggests that the apparatus produces repeatable results.

Table 15. Summary of polyurethane regression coefficients and resilient modulus values

	k_1	k_2	k_3	R^2 (adj)	Average M_r (MPa)
Minimum	55.45	-0.01	0.28	0.47	6.3
Maximum	60.15	0.06	0.68	0.90	6.5
Average	58.10	0.02	0.46	0.72	6.4
Standard Deviation	1.43	0.02	0.13	—	0.08
Coefficient of Variation				—	1.2%

External comparison tests

Two external companies were chosen to validate a resilient modulus test performed using the Iowa State University (ISU) Geotechnical Mobile Laboratory equipment. A dry sample of base gravel obtained from a test site in West Virginia was sent to GeoTesting Express and Boudreau Engineering, Inc. Each company was instructed to compact and moisture condition the material to 21.81 kN/m^3 and 4.3%, respectively, to match the conditions tested using the

ISU equipment. The ISU test was performed according to the methods described in Chapter 3 for granular material. The results from the ISU testing are summarized in Table 16. The permanent strain at the end of testing was about 0.2%, and the average resilient modulus ($M_{r(T307)}$) was 271.7 MPa.

Table 16. Summary of resilient modulus test performed using ISU equipment

for comparison to external data

Sequence No.	Confining Pressure, σ_c (kPa)	Max Deviator Stress, σ_d (kPa)	Mean Bulk Stress, σ_B (kPa)	Average M_r (MPa)	Permanent Strain, ε_p (%)
0	41.4	27.6	151.7	289.5	0.1
1	21.1	20.3	83.5	87.4	0.1
2	20.9	44.0	106.8	114.5	0.1
3	20.7	59.0	121.2	119.5	0.1
4	34.5	37.2	140.6	149.1	0.1
5	34.3	65.8	168.6	156.1	0.1
6	34.5	98.2	201.6	180.7	0.1
7	69.2	69.9	277.6	261.1	0.2
8	69.1	133.6	340.8	388.0	0.2
9	69.4	203.0	411.0	335.8	0.2
10	103.8	72.4	383.9	322.1	0.2
11	103.7	100.2	411.3	336.7	0.2
12	103.6	205.2	515.9	356.2	0.2
13	137.3	100.6	512.4	392.0	0.2
14	137.3	134.2	546.1	390.6	0.2
15	137.1	268.8	680.2	486.4	0.2
			$M_{r(T307)}$	**271.7**	

The independent engineering company, Boudreau Engineering, Inc., also performed a resilient modulus test on the base gravel material. The specimen was compacted to 21.82 kN/m^3 at 4.3% moisture content in six equal lifts using a modified Proctor hammer, and a 152.4 mm (6 in.) diameter by 304.8 mm (12 in.) tall mold. The resilient modulus test was performed according to AASHTO T307 using an Instron test frame and closed-loop, servo-hydraulic resilient modulus equipment (Figure 23). The data is summarized in Table

17. The permanent strain at the end of the test was not reported, and the $M_{r(T307)}$ value was 314.2 MPa.

Figure 23. Boudreau Engineering, Inc. resilient modulus test equipment (photo courtesy of Rick Boudreau)

Table 17. Summary of resilient modulus test performed by Boudreau Engineering, Inc.

for comparison to ISU data

Sequence No.	Confining Pressure, σ_c (kPa)	Max Deviator Stress, σ_d (kPa)	Mean Bulk Stress, σ_B (kPa)	Average M_r (MPa)	Permanent Strain, ε_p (%)*
0	—	—	—	—	—
1	20.7	20.8	82.9	151.9	—
2	20.7	40.7	102.8	172.4	—
3	20.7	61.5	123.5	191.9	—
4	34.5	33.9	137.4	196.8	—
5	34.5	68.6	172.0	232.0	—
6	34.5	103.2	206.6	256.1	—
7	68.9	68.4	275.2	299.6	—
8	68.9	137.9	344.8	351.0	—
9	68.9	207.0	413.8	376.2	—
10	103.4	68.8	379.1	332.9	—
11	103.4	103.5	413.8	364.3	—
12	103.4	207.5	517.8	431.3	—
13	137.9	103.7	517.4	409.9	—
14	137.9	138.3	552.0	438.8	—
15	137.9	276.8	690.4	508.4	—
			$M_{r(T307)}$	**314.2**	

* = ε_p not provided

The materials testing division of Geocomp Corporation, GeoTesting Express, performed a resilient modulus test on the base gravel material. GeoTesting Express compacted the specimen to 21.86 kN/m^3 at 4.2% moisture content in five equal lifts using a wooden dowel, rubber mallet, and a 101.6 mm (4 in.) diameter by 203.2 mm (8 in.) tall split mold (Figure 24). GeoTesting Express performed the resilient modulus test according to AASHTO T307 using a Load Trac-II load frame and a hydraulic load application unit (Figure 25). The data is summarized in Table 18. The permanent strain at the end of the test was 0.5%, and the $M_{r(T307)}$ value was 104.0 MPa.

Figure 24. GeoTesting Express compaction process using a wooden dowel, rubber mallet, and split mold (photo courtesy of Nancy Hubbard)
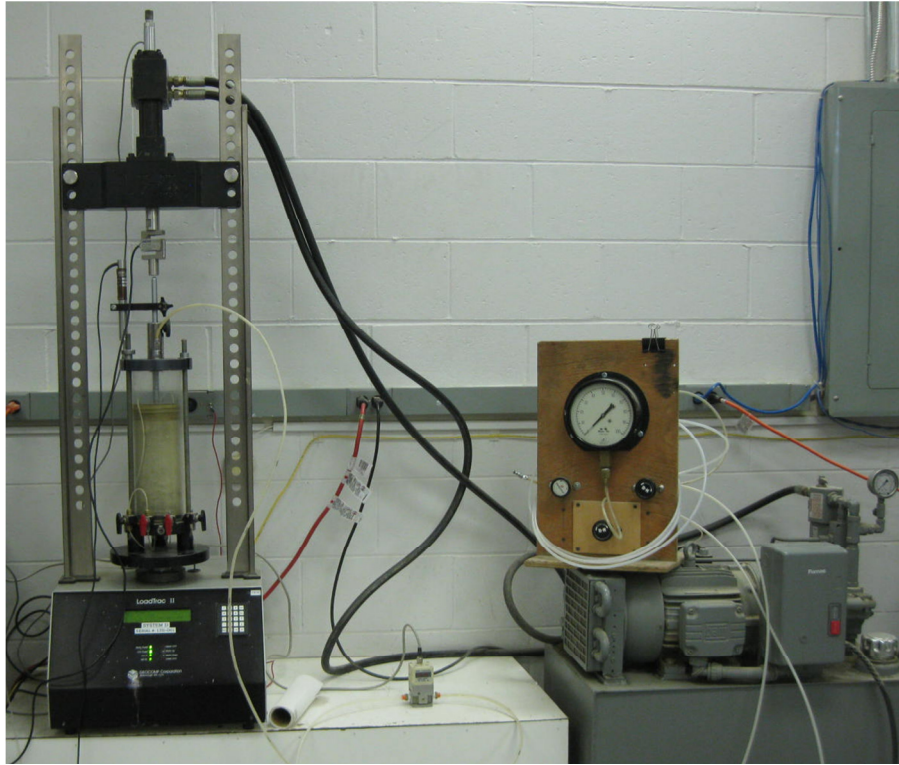
Figure 25. GeoTesting Express resilient modulus test equipment (photo courtesy of Nancy Hubbard)

Table 18. Summary of resilient modulus test performed by GeoTesting Express for

comparison to ISU data

Sequence No.	Confining Pressure, σ_c (kPa)	Max Deviator Stress, σ_d (kPa)	Mean Bulk Stress, σ_B (kPa)	Average M_r (MPa)	Permanent Strain, ε_p (%)
0	—	—	—	—	—
1	22.3	22.6	89.3	47.2	—
2	22.3	45.4	112.1	60.7	—
3	22.1	66.2	132.4	69.3	—
4	36.0	38.4	146.3	62.0	—
5	36.1	72.8	181.1	78.6	—
6	35.9	109.8	217.5	90.9	—
7	70.3	72.8	283.8	93.4	—
8	70.3	140.7	351.4	116.2	—
9	70.4	231.9	443.1	135.0	—
10	105.1	73.8	389.0	103.5	—
11	105.0	105.9	420.9	117.5	—
12	105.0	224.6	539.6	147.9	—
13	138.4	106.8	522.1	127.2	—
14	138.7	140.1	556.3	138.7	—
15	138.8	290.8	707.2	172.0	0.5
			$M_{r(T307)}$	**104.0**	

Overall, the ISU data was most comparable to the Boudreau Engineering, Inc. data. The $M_{r(T307)}$ value for Boudreau Engineering was about 16% greater than the ISU value. The GeoTesting Express $M_{r(T307)}$ value was about 60% less than the ISU value. According to the MEPDG (NCHRP 2004b), coefficients of variation greater than 25% for resilient moduli measured at the same stress states are not uncommon. Therefore, the coefficient of variation between the ISU data and Boudreau Engineering data is well within the range of accuracy, but the GeoTesting Express data is much less. The main difference between the ISU and Boudreau Engineering procedures was the specimen size, and the main difference between the ISU and GeoTesting Express procedures was the compaction method. The stresses and resilient modulus values for each sequence are summarized in Figure 26.
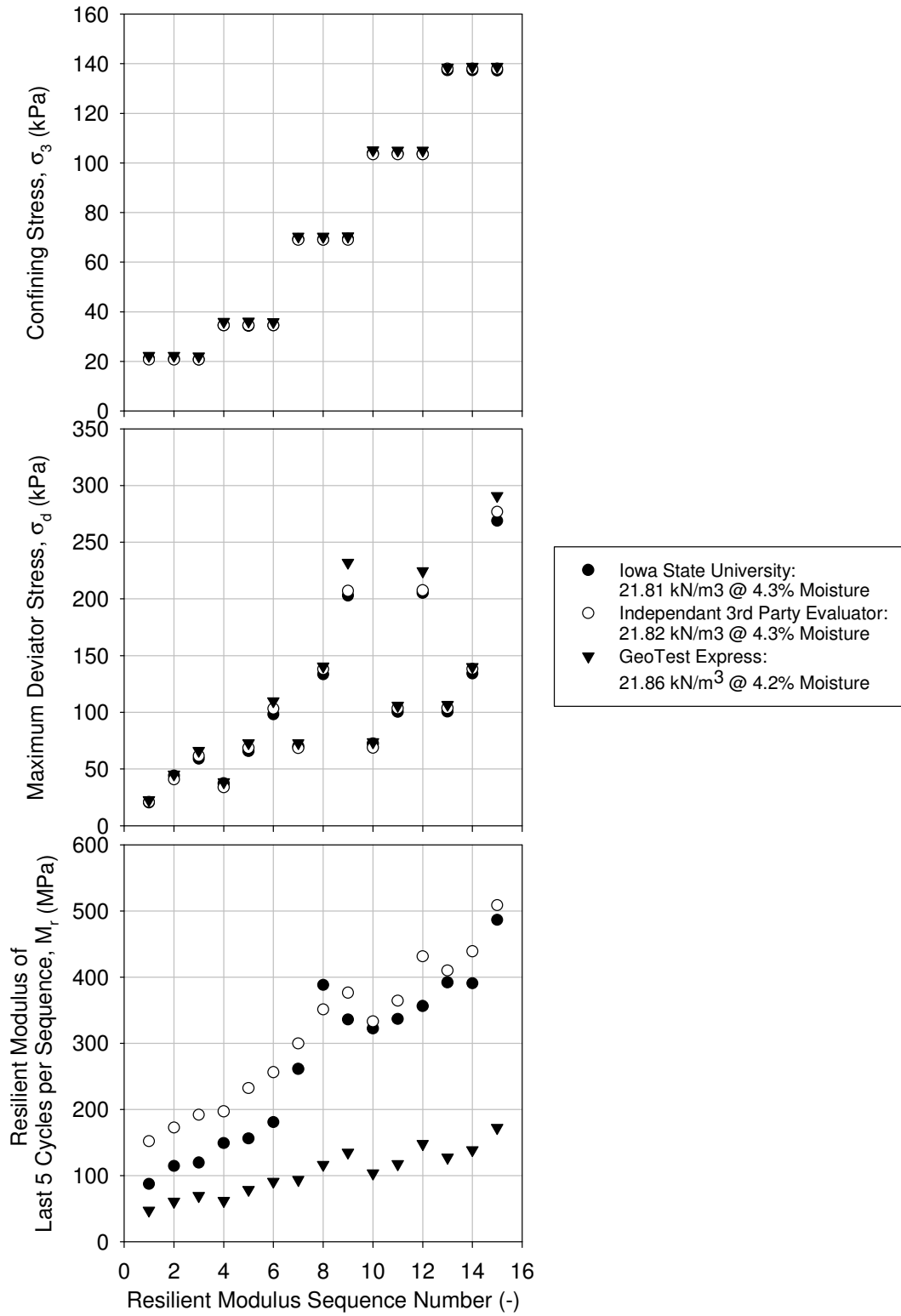
Figure 26. Comparison of stress and resilient modulus values for external laboratory comparisons

IN SITU TEST METHODS

In situ tests were performed on all materials to determine the mechanical properties of the materials. The in situ tests and testing methods are summarized in Table 19. The in situ tests are divided into four sections: falling weight deflectometer, plate load test, nuclear moisture-density gauge, and dynamic cone penetrometer.

Table 19. Summary of devices and methods used for in situ soil testing

Test device	Method followed
Falling weight deflectometer (FWD)	FHWA 2000
Plate load test (PLT)	ASTM D1196
Nuclear moisture-density gauge (NG)	ASTM D6938-10
Dynamic cone penetrometer (DCP)	ASTM D6951/D6951M-09

Falling weight deflectometer

Falling weight deflectometer (FWD) tests were performed using a KUAB 2m-FWD 150 (Figure 27) in general accordance with the LTPP Manual for Falling Weight Deflectometer Measurements, Operational Field Guidelines (FHWA 2000). Different materials required different load sequences to capture the stress and strain variation. FWD tests were performed on concrete pavements as well as base and subgrade layers. Deflections were measured by sensors placed at the center of the plate, and at 0.2 m, 0.3 m, 0.5 m, 0.6 m, 0.8 m, 0.9 m, 1.2 m, 1.52 m, and 1.8 m offsets from the center of the plate.

Figure 27. Falling weight deflectometer (FWD) in use on a concrete pavement surface

Elastic moduli were calculated from FWD data (E_{FWD}) using Equation 12 and the deflection reading at the center of the load plate. This method determined composite elastic moduli of pavement layers directly under the FWD plate, which should relate to laboratory resilient and dynamic moduli from composite material samples.

$$E = \frac{(1 - v^2)\sigma_0 a}{d_0} f \tag{12}$$

where: d_o = measured settlement (mm);

υ = Poisson's ratio;

σ_o = applied stress (MPa);

a = radius of the plate (mm);

E = Young's modulus (MPa); and

f = shape factor dependant on assumed contact stress distribution (for this study, f = 8/3 for granular materials, f = π/2 for non-granular materials, and f = 2 for the segmented plate FWD).

Light weight deflectometer

Light weight deflectometer (LWD) tests were performed using the Light Drop Weight Tester ZFG2000 by Gerhard Zorn. The LWD device used a 300 mm diameter plate and 720 mm drop height.

Prior to performing the LWD test, a flat area on the material surface was prepared. Three seating drops were performed, and three test drops were recorded. Deflections for each test drop were recorded and averaged at each point. The applied stress was assumed constant for the known plate diameter, drop weight, drop height, and spring constant.

Elastic moduli were calculated from LWD data ($E_{LWD-Z3(72)}$) using the average deflection reading and Equation 12. The $E_{LWD-Z3(72)}$ values were representative of layers beneath the plate to a distance of 1–2 times the plate diameter. Therefore, for most test locations, the $E_{LWD-Z3(72)}$ represented composite pavement foundation samples.

Plate load test

Static plate load tests (PLT) were conducted in general accordance with ASTM D1196. The tests were performed using a custom apparatus on the Freightliner for the Geotechnical

Mobile Laboratory (White and Gieselman 2009). A static load was applied to a 300 mm diameter bearing plate using the weight of the truck as the reaction force. The bearing plate was placed directly on the subgrade or base layers. Bearing plate displacement was measured using three linear voltage displacement transducers (LVDTs). The average value from the three LVDTs was used in calculations. A data logger continuously recorded the load and deformation readings during the test. Initial (E_{v1}) and reload (E_{v2}) elastic moduli readings were determined by Equation 12. Stress and deformation readings were taken from 0.2 to 0.4 MPa (29 to 58 psi) for granular materials and 0.1 to 0.2 MPa (14.5 to 29 psi) for non-granular subgrade soils (White et al. 2009).

Moduli of subgrade reaction, k, is the ratio of applied load to displacement of a bearing plate. The modulus of subgrade reaction is the support stiffness of the layers under a rigid slab and is determined in situ by PLT (Packard 1973). In addition to E_{v1} and E_{v2}, k values were determined by dividing the applied load by the deflection determined over the E_{v1} reading.

Nuclear moisture-density gauge

A calibrated nuclear moisture-density gauge (NG) device (Figure 28) measured the dry unit weight ($\square_d$) and moisture content (*w*) of base and subgrade materials. Tests were performed in accordance with ASTM D6938-10. Generally, two moisture and dry unit weight measurements were obtained at each point and the average value was reported. Penetration depths were determined based on which material layers needed to be assessed.

Figure 28. Nuclear moisture-density gauge with auxiliary equipment

Dynamic cone penetrometer

Dynamic cone penetrometer (DCP) tests were performed in accordance with ASTM D6951-03. The DCP works by dropping an 8 kg (17.6 lb) hammer onto a rod with a cone tip from a height of 575 mm (22.6 in.) and measuring the penetration distance for a given number of blows. Tests were performed to a depth of 1 m with the typical DCP apparatus and extended to 2 m using extension rods. Dynamic cone penetration index (DCPI) was calculated for each test. Weighted average DCPIs were calculated for each foundation layer using Equation 13 (White et al. 2009).

$$DCPI_z = \frac{DCPI_i \cdot z_i + DCPI_{i+1} \cdot z_{i+1} + ... + DCPI_n \cdot z_n}{\sum z_n} \tag{13}$$

where: $DCPI_z$ = DCPI for the foundation layer of thickness z (mm/blow) and $DCPI_{i,i+1,...n}$ = DCPI of blows i to n (mm/blow).

The soil strength was assessed through correlations with California bearing ratio (CBR) and DCPI values. Resilient moduli were calculated from the $DCPI_{Ave}$ for each layer using Equations 14, 15, 16, and 17 (ASTM D6951) and Equations 18 and 19 from Mohammad et al. (2008). Equations 18 and 19 are specific to cohesive and granular materials, respectively, whereas Equation 17 is used for all soil types.

$$CBR = \frac{292}{DCPI^{1.12}} \quad \text{; for all soils except for CH and CL soils with CBR} < 10 \tag{14}$$

$$CBR = \frac{1}{(0.017019 \cdot DCPI)^2} \quad \text{; CL soils with CBR} < 10 \tag{15}$$

$$CBR = \frac{1}{(0.002871 \cdot DCPI)} \quad \text{; CH soils} \tag{16}$$

$$M_{r(DCPI)} = 17.6(CBR)^{0.64} \quad \text{; for all materials} \tag{17}$$

$$M_{r(DCPI))} = \frac{1046.6}{DCPI^{1.096}} \quad \text{; for cohesive materials} \tag{18}$$

$$M_{r(DCPI)} = \frac{391.1}{DCPI^{0.23}} \quad \text{; for granular materials} \tag{19}$$

where: DCPI = dynamic cone penetrometer index (mm/blow);

CBR = California bearing ratio (%); and

M_r = resilient modulus (MPa).

CHAPTER 4. MATERIALS

This chapter summarizes the index properties of materials collected from investigations at six field sites as seen in Table 10. Materials were obtained from each of the pavement foundation layers. When possible, materials were obtained from the original pavement foundations as well as the new or reconstructed pavement foundations. The laboratory characteristic properties (i.e., classification, Atterberg limits, specific gravity, Proctor compaction, and relative density) are summarized in a table for each location.

Table 20. Summary of investigated sites and materials

State	Site location	Materials
Michigan	I-94	Existing subbase, base, subgrade*
Michigan	I-96	Subbase, subgrade*
Pennsylvania	US-22	Cement-treated base (CTB), asphalt-treated base (ATB), subbase, subgrade
Pennsylvania	US-422	Base, injected stabilization foam
Iowa	I-29	Existing subbase, base, subbase, subgrade
Wisconsin	US-10	Subbase, subgrade

* = Samples obtained by Shelby tube also tested

MICHIGAN I-94

The pavement foundation materials from Michigan I-94 were sampled from St. Clair and Macomb Counties in Michigan. The laboratory tests performed include: particle size distribution analysis, Atterberg limits tests, standard and modified Proctor tests, relative density tests, specific gravity determinations, and x-ray analysis. The results for each of the materials are summarized in Table 21.

Table 21. Summary of Michigan I-94 soil properties

Laboratory Property	Slag Base	Existing Sand Subbase	Subgrade
USCS classification	GP	SP-SM	ML
AASHTO classification	A-1-a	A-2-4(0)	A-4(0)
Coefficient of uniformity (c_u)	2.0	3.5	—
Coefficient of curvature (c_c)	1.1	1.3	—
Liquid limit (LL)	NP	NP	32
Plastic limit (PL)	NP	NP	17
Plasticity index (PI)	NP	NP	17
Specific gravity (G_s)	—	2.67	2.66–2.72
Optimum moisture content, w_{opt} (%) standard Proctor	—	—	13.8
Dry unit weight (kN/m^3) standard Proctor	—	—	18.58
Optimum moisture content, w_{opt} (%) modified Proctor	—	—	9.6
Dry unit weight (kN/m^3) modified Proctor	—	—	19.84
Min dry unit weight (kN/m^3) relative density	14.05	15.65	—
Max dry unit weight (kN/m^3) relative density	16.23	19.09	—
Gravel size (%) (>4.75mm)	98	2	2
Sand size (%) (4.75 to 0.075mm)	0	87	47
Silt size (%) (0.075 to 0.002mm)	2	8	25
Clay size (%) ($\leq$0.002mm)		4	26

NP = not plastic

Shelby tube samples of the subgrade were obtained from the site. At each test point, one tube was obtained from approximately 0.4 to 1.0 m (1.5 to 3.5 ft) and one tube was obtained from 1.0 to 1.7 m (1.5 to 5.5 ft) below ground surface. The tubes were 0.6 m (2 ft) long and had an interior diameter of 71.1 mm (2.8 in.). From each tube, approximately 153 mm (6 in.) of intact and relatively undisturbed material was trimmed and prepared for testing.

Particle size distributions provided the data for classification (Figure 29, Figure 30, and Figure 31). Resilient modulus tests performed on slag base material samples had particle size distributions that were scalped and replaced to meet AASHTO T307 specifications, as described in the Methods chapter. The scalped and replaced particle size distribution for the

base slag is included in Figure 29. Relative density tests provided moisture-dry unit weight relationship for the slag base and existing sand base (Figure 32 and Figure 33). Standard and modified Proctor tests provided the moisture-dry unit weight relationship for the subgrade (Figure 34).

The moisture-dry unit weight figures for the slag base and subgrade materials include in situ values, in addition to the laboratory values. The slag base had larger in situ dry unit weight values than the laboratory determined relative density, seen in Figure 32. The in situ base slag relative densities ranged from 128–380% with an average of about 260%. The maximum relative density of the resilient modulus samples was about 178%. It is likely that the higher dry unit weights observed in situ were due to possible segregation and gradation variations in the base slag material. The slag base at Test Bed 1 also typically had lower moisture contents than the slag base at Test Bed 3. The in situ data indicates the slag base material has highly variable moisture and unit weight values.

Shelby tube samples also had larger moisture contents than laboratory samples. Shelby tube samples were 2.8–8.4% wet of standard proctor optimum moisture content and relative compaction ranged from 89–93% of maximum standard Proctor dry unit weight, seen in Figure 34. The large range of Shelby tube moisture and relative compaction values indicates variable subgrade support conditions.

Figure 29. Michigan I-94 slag base particle size distribution

Figure 30. Michigan I-94 existing sand subbase particle size distribution
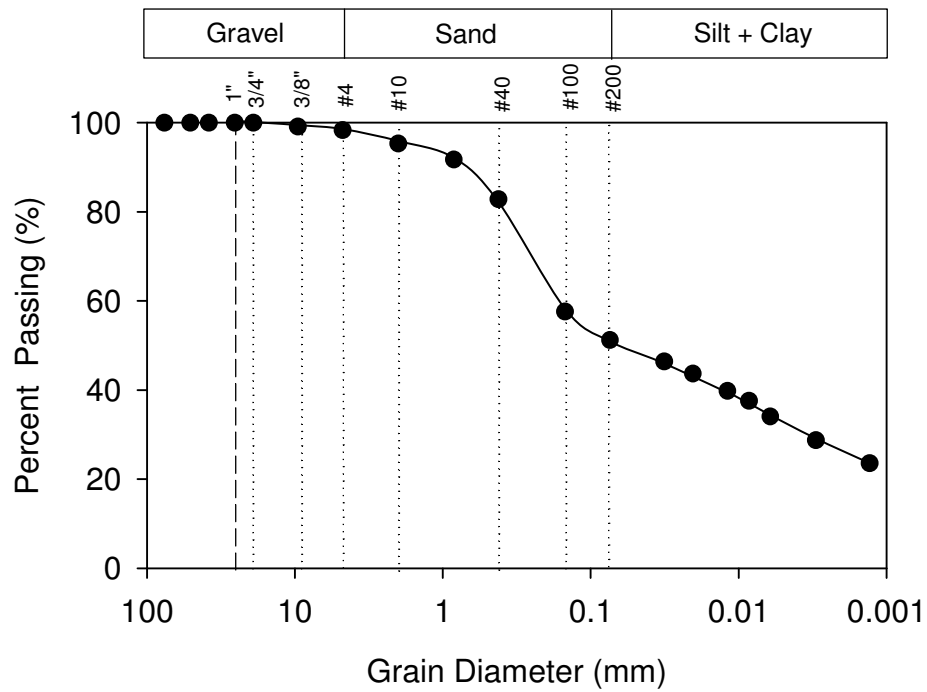
Figure 31. Michigan I-94 subgrade particle size distribution
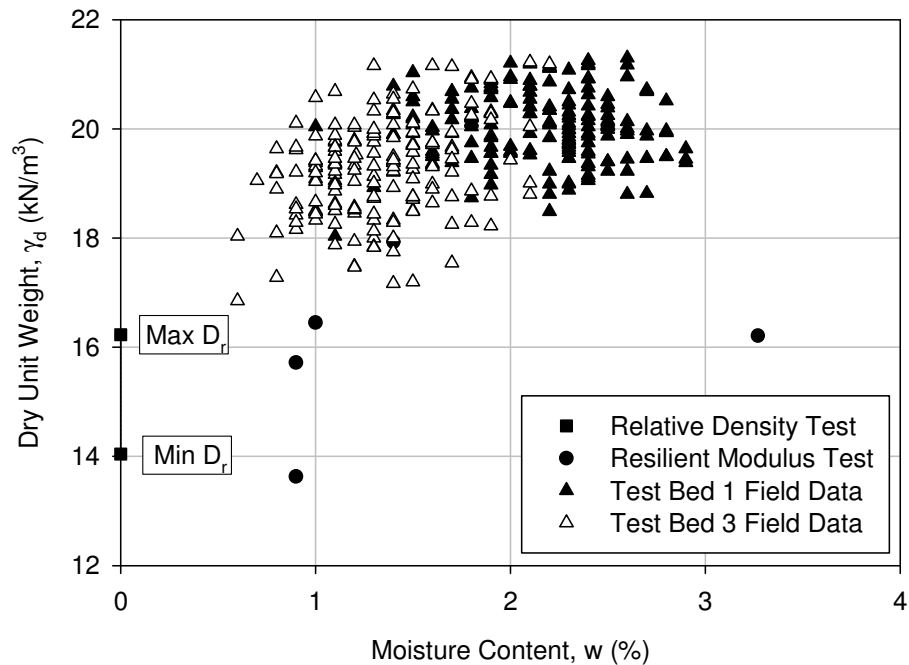
Figure 32. Michigan I-94 slag base moisture-dry unit weight relationships
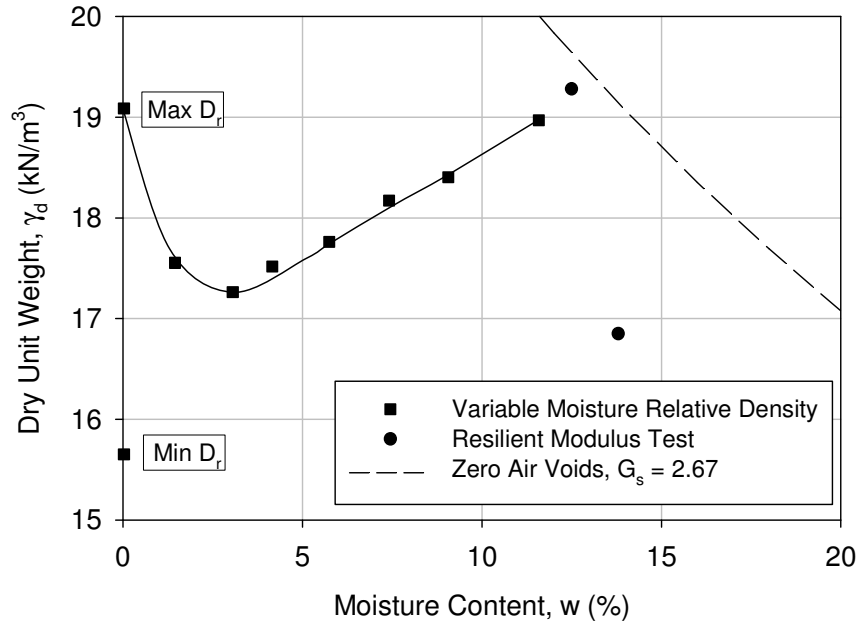
Figure 33. Michigan I-94 existing sand base moisture-dry unit weight relationships
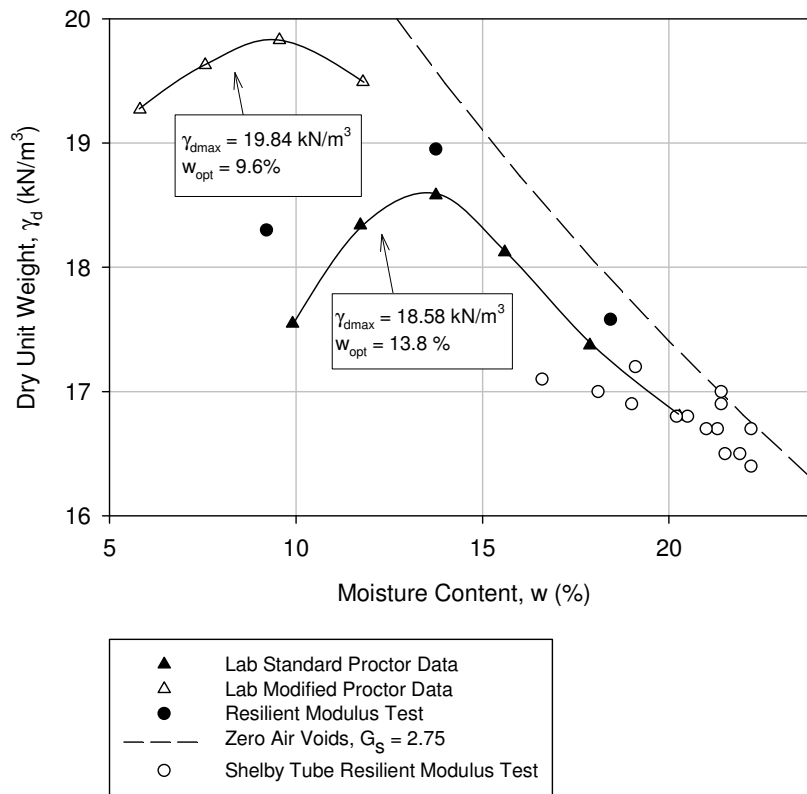
Figure 34. Michigan I-94 existing subgrade moisture-dry unit weight relationships

Scanning electron microscopy (SEM) analyses were performed on several slag base samples. The SEM images provide detailed morphology of samples. Morphology down to a sub-micron scale can be obtained from rough and polished samples. Rough samples were particles analyzed without any modification. Rough samples show surface morphology. Polished samples were made from particles placed in epoxy and ground down to view the internal structure. Polished sections show grain size and intergrowth.

The rough base slag samples illustrated a vesicular surface texture, seen in Figure 35. The polished base slag samples illustrated light and dark gray intrusions that indicate different cooling phases during formation of the slag (Figure 36). Additionally, the polished samples showed vesicles that extended from the surface to the interior. An x-ray map indicated most of the material to be made from silicon, magnesium, calcium, and oxygen with sulfur dispersed throughout and a grain of iron (Figure 37).

Energy-dispersive spectroscopy (EDS), performed together with SEM, provide elemental information about a localized image area. The EDS results provided similar conclusions as the x-ray map. Energy-dispersive x-ray spectra of two slag base samples are provided in Figure 38.
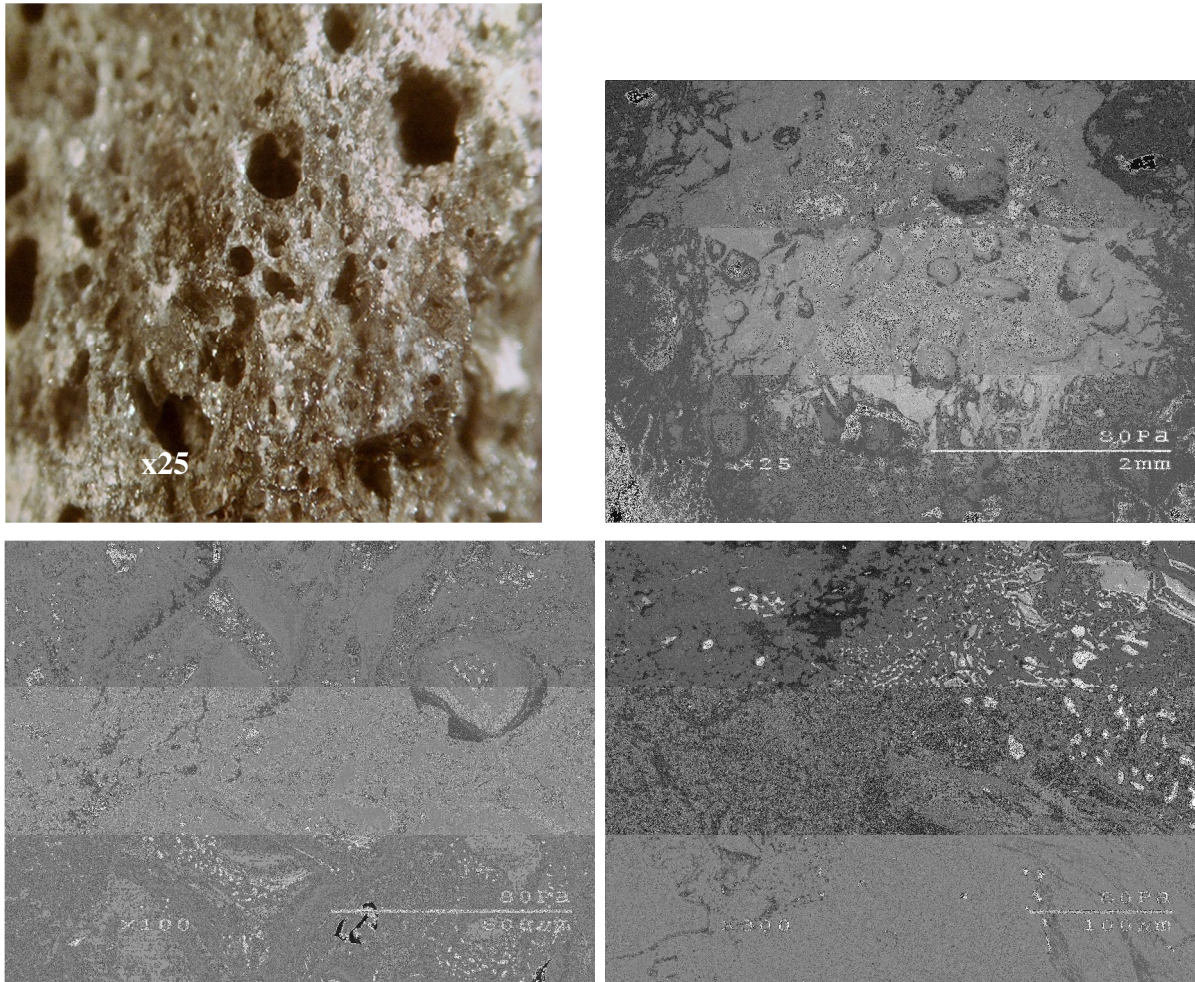
Figure 35. SEM images of a Michigan I-94 rough base slag sample at different magnifications
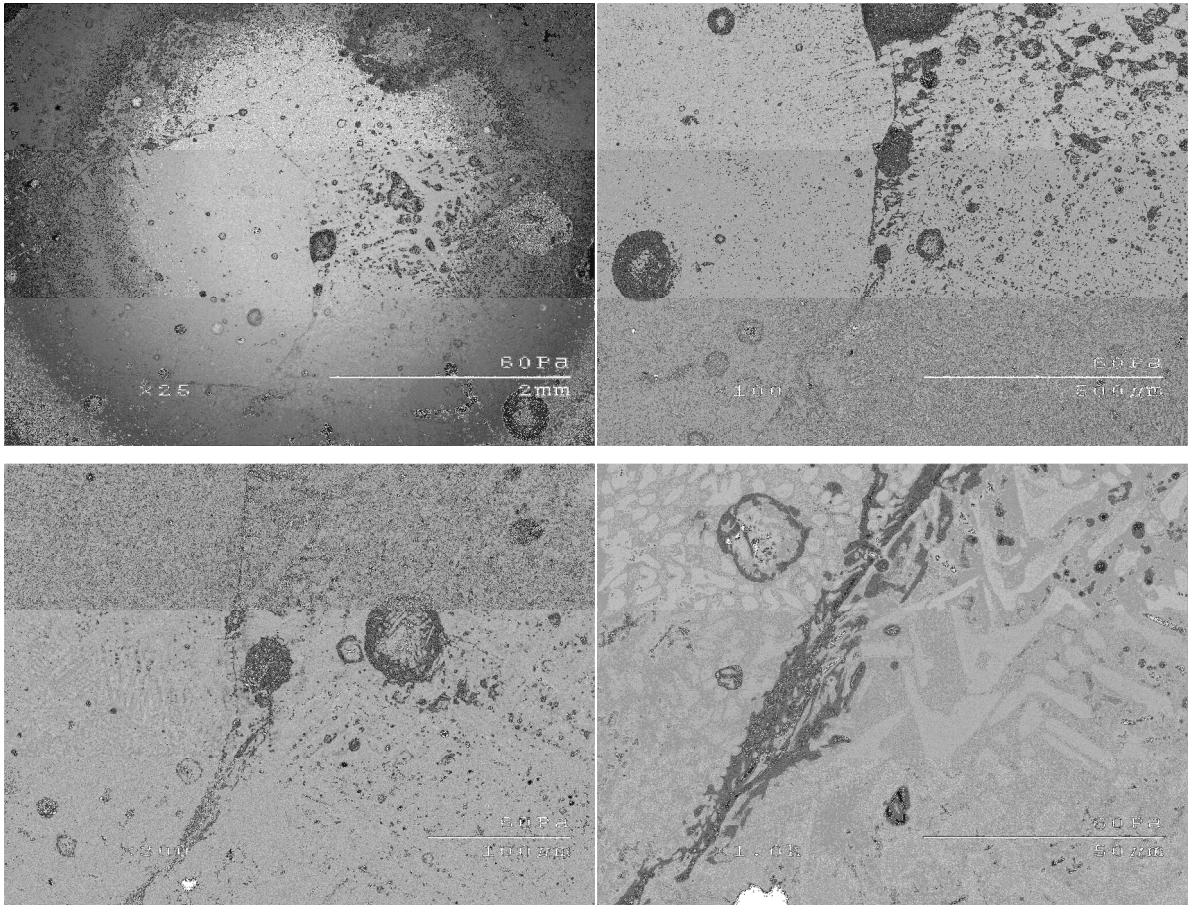
Figure 36. SEM images of a Michigan I-94 polished base slag sample at different magnifications
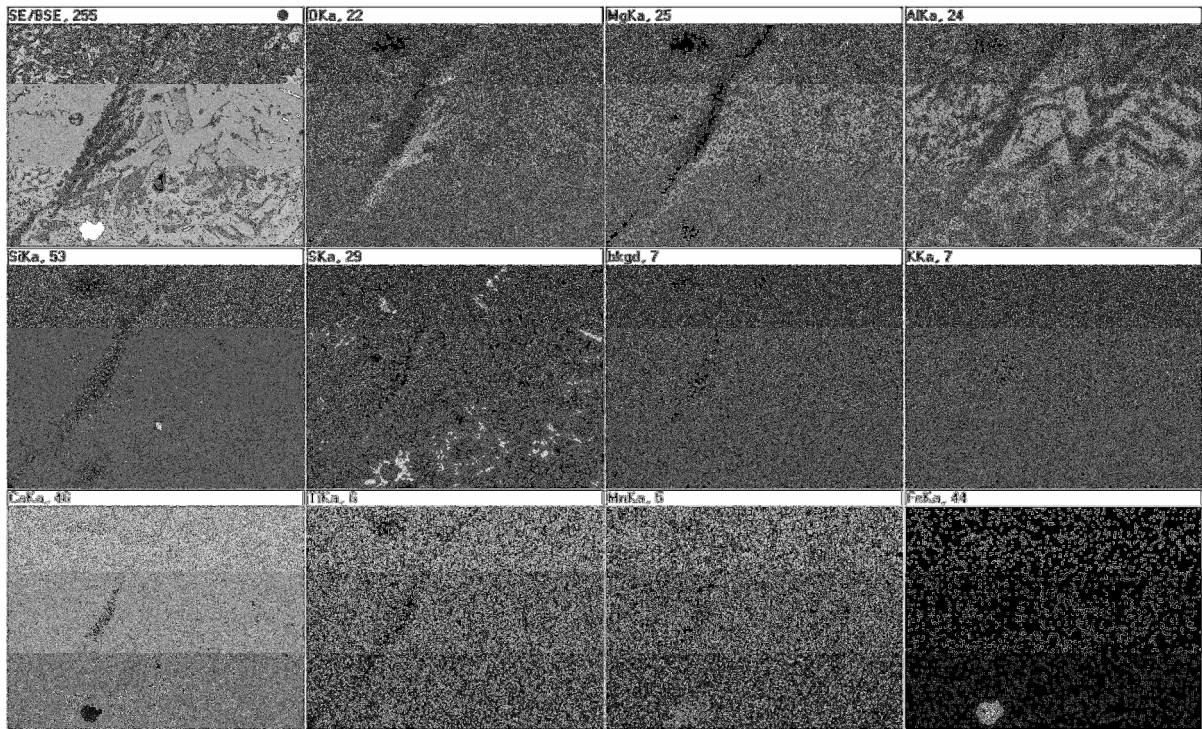
Figure 37. X-ray map of the Michigan I-94 polished base slag sample from Figure 36
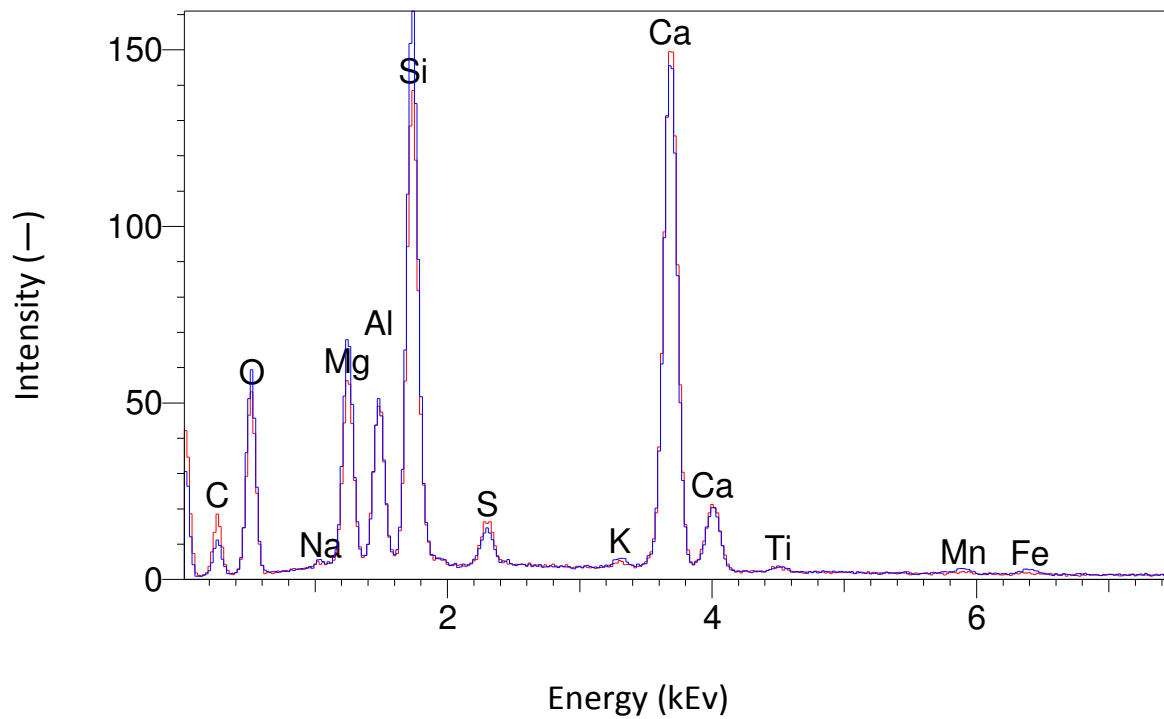
Figure 38. Energy-dispersive x-ray spectra from two Michigan I-94 slag base samples

MICHIGAN I-96

The pavement foundation materials from Michigan I-96 were sampled from Clinton and Eaton Counties in Michigan. The laboratory tests performed include: particle size distribution analysis, Atterberg limits tests, standard and modified Proctor tests, and relative density tests. The results for each of the materials are summarized in Table 22.

Table 22. Summary of Michigan I-96 soil properties

Laboratory Property	Existing Sandy Subbase	Subgrade
USCS classification	SP-SM	SM
AASHTO classification	A-1-b	A-4(0)
Coefficient of uniformity (c_u)	13.3	41.0
Coefficient of curvature (c_c)	0.8	2.9
Liquid limit (LL)	NP	20
Plastic limit (PL)	NP	12
Plasticity index (PI)	NP	8
Specific gravity (G_s) (*Assumed)	2.60*	2.70*
Optimum moisture content, w_{opt} (%) standard Proctor	8.1	9.6
Dry unit weight (kN/m^3) standard Proctor	19.95	20.06
Optimum moisture content, w_{opt} (%) modified Proctor	6.3	8.5
Dry unit weight (kN/m^3) modified Proctor	20.38	20.58
Min dry unit weight (kN/m^3) relative density	14.97	—
Max dry unit weight (kN/m^3) relative density	20.06	—
Gravel size (%) (>4.75mm)	24	4
Sand size (%) (4.75 to 0.075mm)	68	52
Silt size (%) (0.075 to 0.002mm)	9	38
Clay size (%) ($\leq$0.002mm)		5

NP = not plastic

Shelby tube samples of the subgrade were obtained from the site. The samples were obtained approximately 0.4 to 1.0 m (1.5 to 3.5 ft) below ground surface. The tubes were 0.6 m (2 ft) long and had an interior diameter of 71.1 mm (2.8 in.). Two 153 mm (6 in.) long, intact, and relatively undisturbed material were obtained from the Shelby tube samples for testing.

Particle size distributions provided the data for classification (Figure 39 and Figure 40). Standard and modified Proctor tests provided the moisture-density relationships for the existing sandy subbase and subgrade material (Figure 41 and Figure 42).

The moisture-dry unit weight figures for the existing sandy subbase material included both in situ and laboratory values. In situ existing sand subbase moisture values ranged from 3.4% below to 2.1% above optimum standard Proctor moisture content. In situ sand subbase relative compaction values ranged from 94–107% of the maximum standard Proctor dry unit weight. Resilient modulus tests were performed at moisture values from 0.3–3.7% below standard Proctor optimum moisture content and at relative compaction values ranging from 96–105% of the maximum standard Proctor dry unit weight. The moisture-dry unit weight relationships for sand subbase are shown in Figure 41.

In situ moisture and dry unit weight values were not determined for the subgrade material. Resilient modulus tests were performed at moisture values from 2.8% below to 3.1% above optimum standard Proctor moisture content. Relative compaction values ranged from 97–103% of the maximum standard Proctor dry unit weight. The moisture-dry unit weight relationships for subgrade are shown in Figure 42.
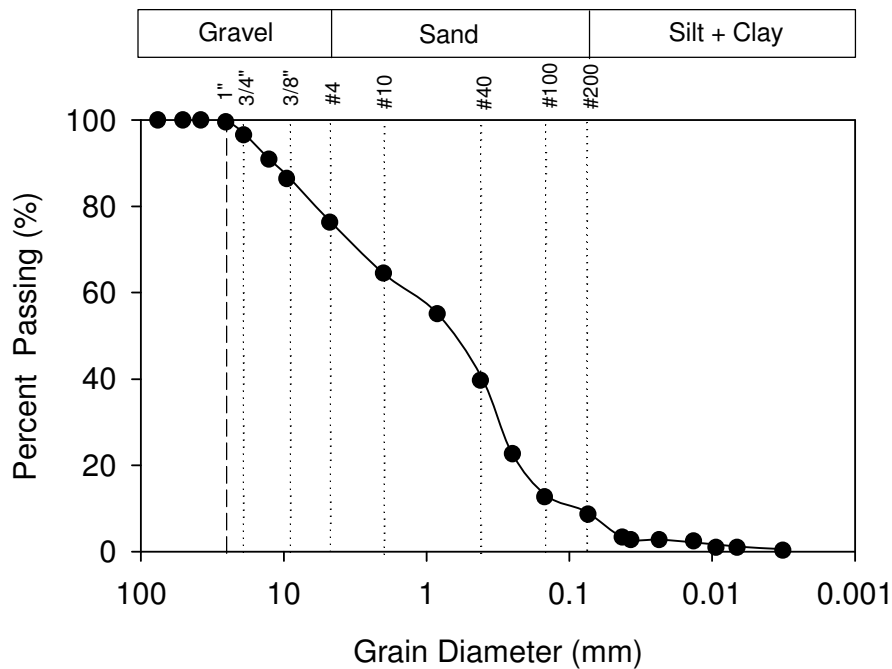
Figure 39. Michigan I-96 existing sand subbase particle size distribution
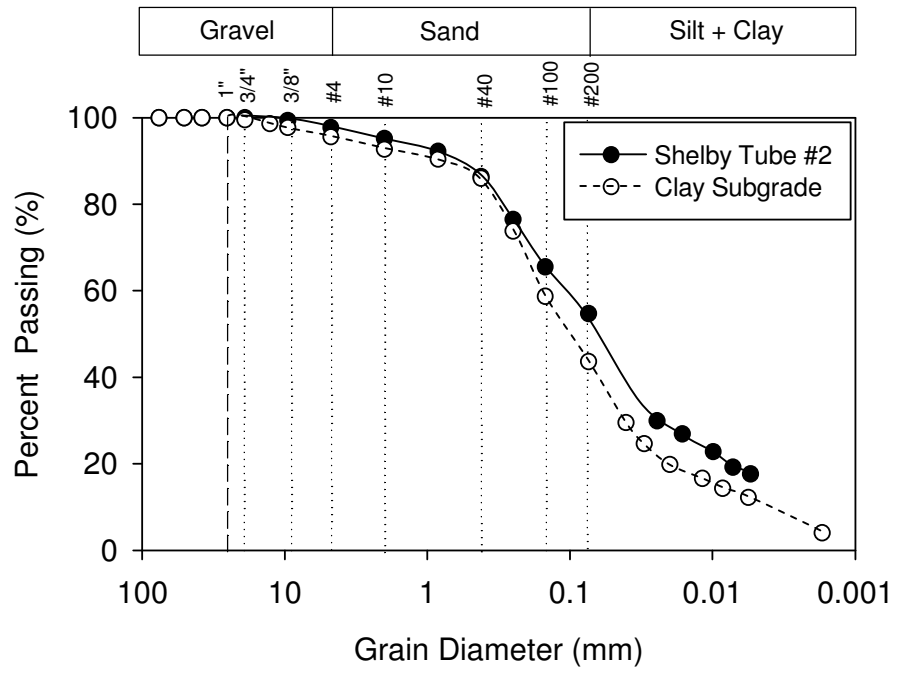
Figure 40. Michigan I-96 Shelby tube and subgrade particle size distribution
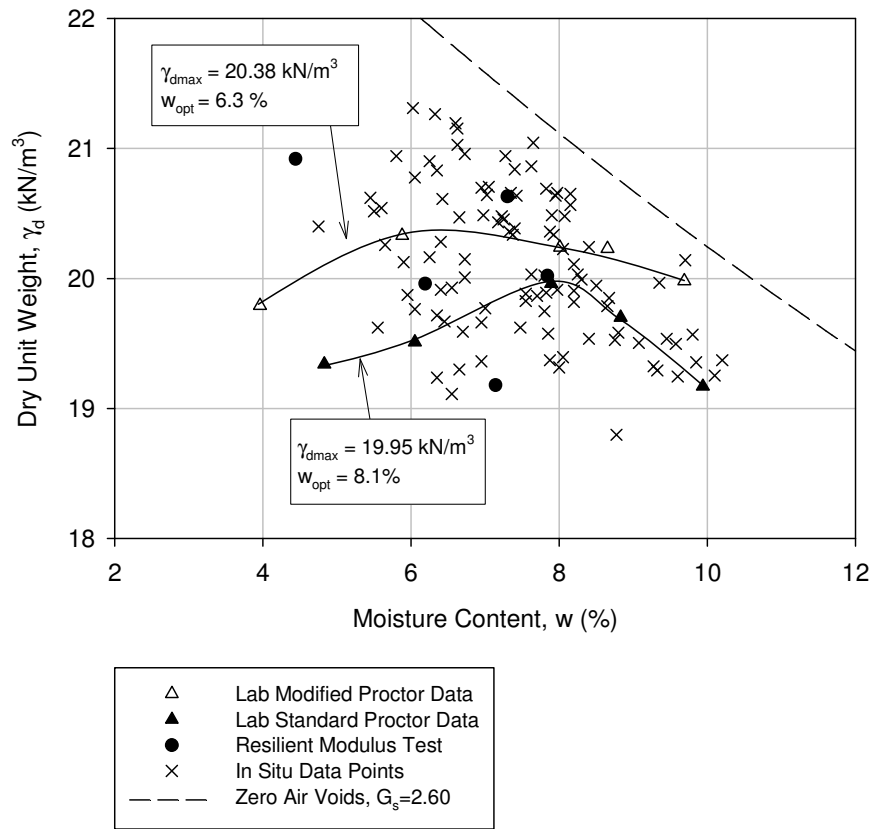
**Figure 41. Michigan I-96 existing sand subbase moisture-dry unit weight relationship**
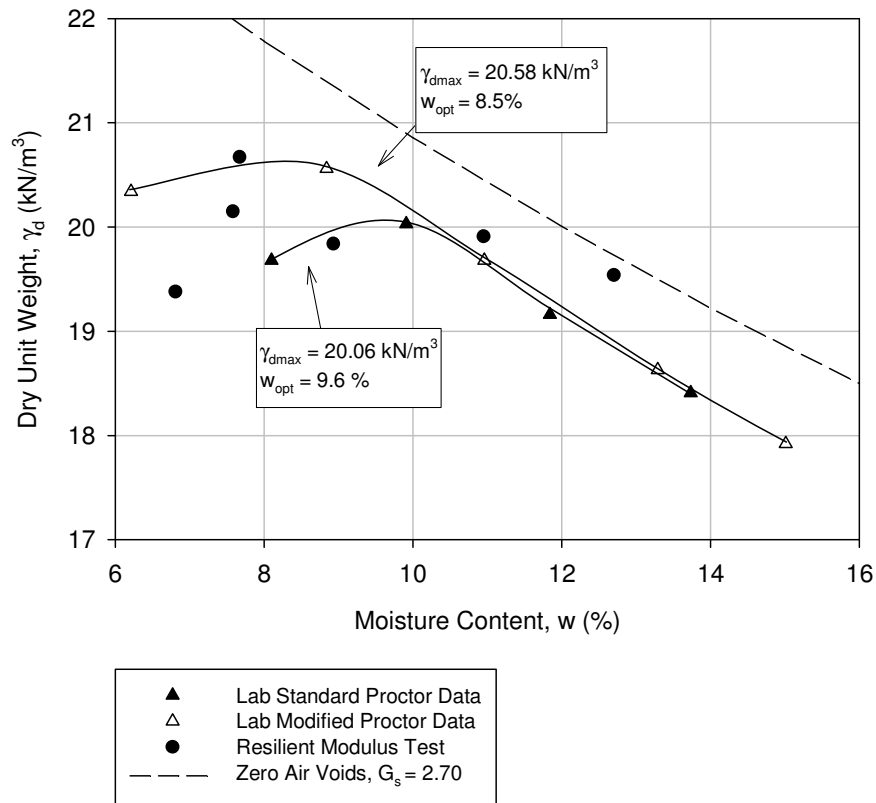
Figure 42. Michigan I-96 subgrade moisture-dry unit weight relationship

PENNSYLVANIA US-22

The pavement foundation materials from Pennsylvania US-22 were sampled from Blairsville, Pennsylvania. The laboratory tests performed include: particle size distribution analysis, Atterberg limits tests, standard and modified Proctor tests, relative density tests, and specific gravity determinations. The results for each of the materials are summarized in Table 23.

Table 23. Summary of Pennsylvania US-22 soil properties

Laboratory Property	TB-2 Class 2A Subbase	TB-6 Subgrade
USCS classification	GP-GM	ML
AASHTO classification	A-1-a	A-4(0)
Coefficient of uniformity (c_u)	—	—
Coefficient of curvature (c_c)	—	—
Liquid limit (LL)	NP	37
Plastic limit (PL)	NP	22
Plasticity index (PI)	NP	15
Specific gravity (G_s) (*Assumed)	2.82	2.78*
Optimum moisture content, w_{opt} (%) standard Proctor	—	16.3
Dry unit weight (kN/m^3) standard Proctor	—	17.70
Optimum moisture content, w_{opt} (%) modified Proctor	—	12.1
Dry unit weight (kN/m^3) modified Proctor	—	19.10
Min dry unit weight (kN/m^3) relative density	14.94	—
Max dry unit weight (kN/m^3) relative density	18.14	—
Gravel size (%) (>4.75mm)	55	11
Sand size (%) (4.75 to 0.075mm)	34	31
Silt size (%) (0.075 to 0.002mm)	12	36
Clay size (%) ($\leq$0.002mm)		22

NP = not plastic

Particle size distributions provided the data for classification (Figure 43 and Figure 44). Resilient modulus tests performed on the class 2A subbase crushed limestone samples had a particle size distribution that was scalped and replaced to meet AASHTO T307 specifications, as described in the Methods Chapter. The scalped and replaced particle size distribution is included in Figure 43 for the class 2A subbase material.

Relative density tests provided moisture-dry unit weight relationships for the Class 2A subbase material (Figure 45). Standard and modified Proctor tests provided the moisture-dry unit weight relationships for the TB-6 subgrade material (Figure 46).

The moisture-dry unit weight figures for the class 2A subbase material included both in situ and laboratory values. In situ dry unit weights for the class 2A subbase were larger than

the laboratory values. In situ class 2A relative density values ranged from 168–235%. In situ moisture contents ranged from 3.4–9.1%. Resilient modulus class 2A relative density values ranged from 203–206%. Resilient modulus class 2A moisture contents ranged from 5.6–7.3%. Possible reasons for the higher in situ dry unit weight values include segregation and gradation variations. High in situ dry unit weight values should provide a stiff subbase layer, even with variable moisture content values. The moisture-dry unit weight relationships for the class 2A subbase are shown in Figure 45.

The moisture-dry unit weight relationships for the TB-6 subgrade material included both in situ and laboratory values. In situ TB-6 subgrade relative compaction values ranged from 91–105% of the maximum standard Proctor dry unit weight. In situ TB-6 subgrade moisture values ranged from 3.7% below to 5.6% above optimum standard Proctor moisture content. Resilient modulus TB-6 subgrade relative compaction values ranged from 101–112% of the maximum standard Proctor dry unit weight. Resilient modulus TB-6 subgrade moisture values ranged from 1.1% below to 2.3% above optimum standard Proctor moisture content. The large range of moisture content and dry unit weight values would lead to high variability in subgrade support values (i.e. modulus values). The moisture-dry unit weight relationships for the TB-6 subgrade are shown in Figure 46.
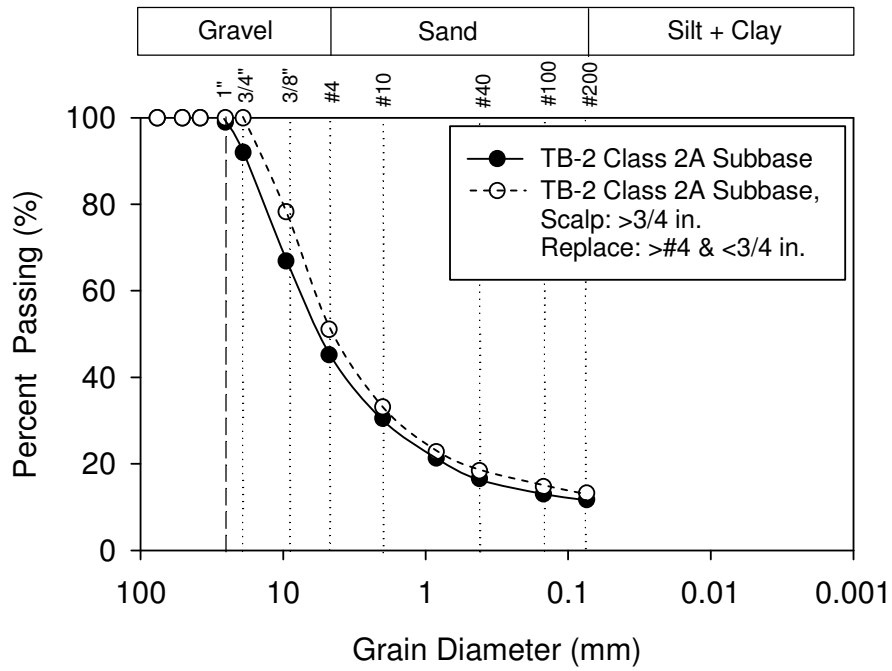
Figure 43. Pennsylvania US-22 class 2A subbase material particle size distribution
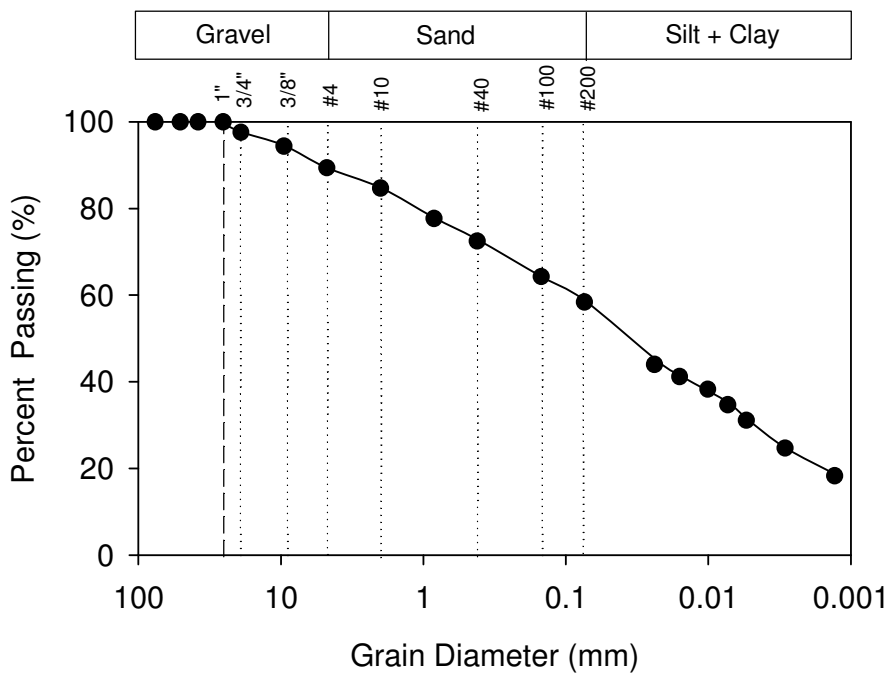
Figure 44. Pennsylvania US-22 clay subgrade particle size distribution
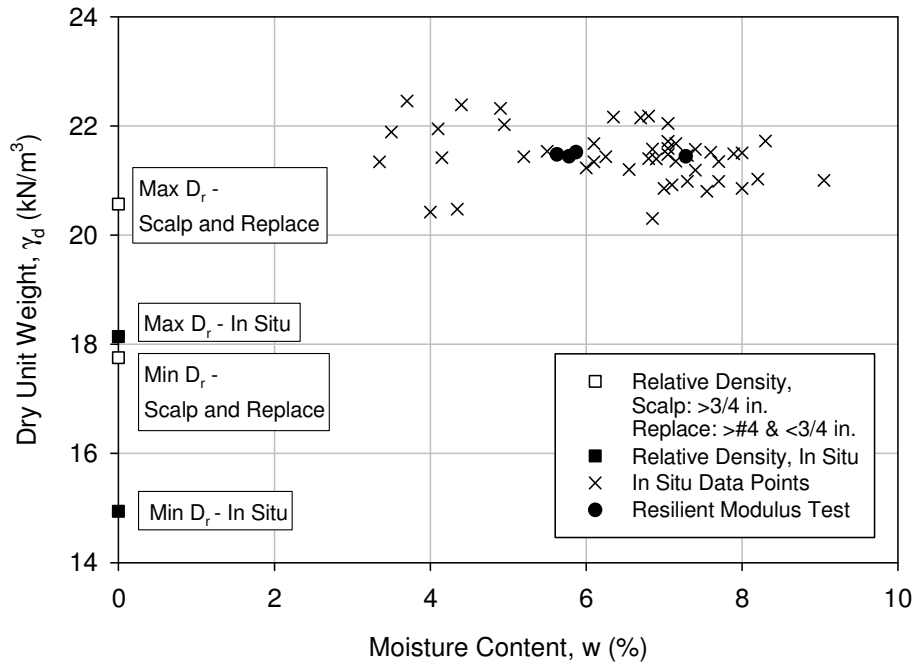
Figure 45. Pennsylvania US-22 Class 2A subbase moisture-density relationship
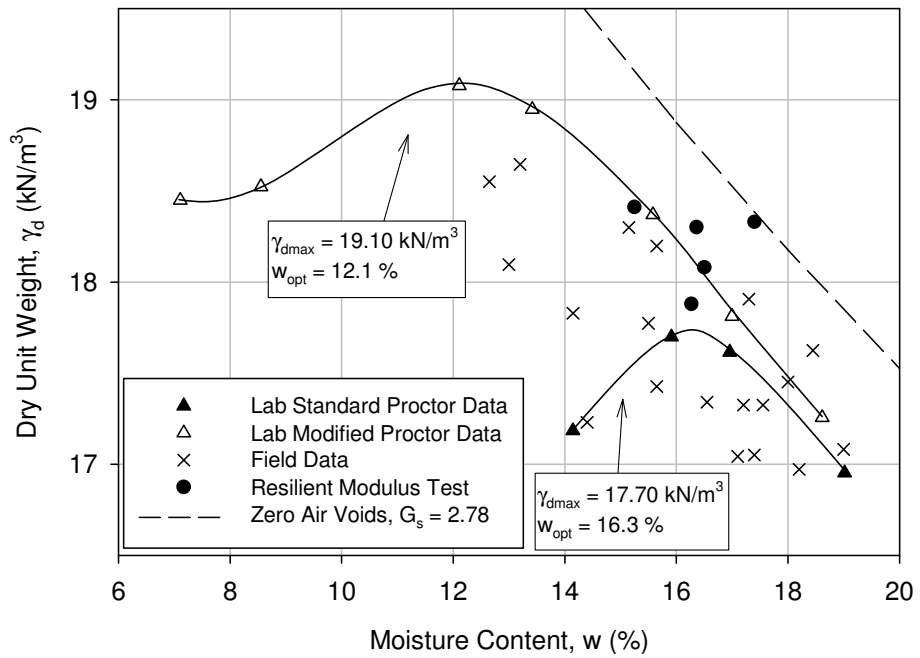
Figure 46. Pennsylvania US-22 TB-6 subgrade moisture-density relationship

PENNSYLVANIA US-422

The pavement foundation materials from Pennsylvania US-422 were sampled near
Indiana, Pennsylvania. The laboratory tests performed include: particle size distribution
analysis, Atterberg limits tests, relative density tests, and specific gravity determinations. The
results for each of the materials are summarized in Table 24.

Table 24. Summary of Pennsylvania US-422 soil properties

Laboratory Property	OGS Base 0-4"
USCS classification	GW
AASHTO classification	A-1-a
Coefficient of uniformity (c_u)	4.0
Coefficient of curvature (c_c)	1.6
Liquid limit (LL)	NP
Plastic limit (PL)	NP
Plasticity index (PI)	NP
Specific gravity (G_s) (*Assumed)	2.70*
Optimum moisture content, w_{opt} (%) standard Proctor	—
Dry unit weight (kN/m^3) standard Proctor	—
Optimum moisture content, w_{opt} (%) modified Proctor	—
Dry unit weight (kN/m^3) modified Proctor	—
Min dry unit weight (kN/m^3) relative density	15.59
Max dry unit weight (kN/m^3) relative density	19.88
Gravel size (%) (>4.75mm)	90
Sand size (%) (4.75 to 0.075mm)	7
Silt size (%) (0.075 to 0.002mm)	4
Clay size (%) (≤0.002mm)	

NP = not plastic

Particle size distributions provided the data for classification (Figure 47). Resilient
modulus tests performed on the OGS base material samples had a particle size distribution
that was scalped and replaced to meet AASHTO T307 specifications, as described in the
Methods Chapter. The scalped and replaced particle size distribution is included in Figure 47
for the OGS base material.

A high density polyurethane (HDP) foam material was injected in situ and into test specimens (as described in the Methods Chapter). The HDP foam is made of two liquid chemicals that combine under heat to form the stabilizing material.

Figure 47. Pennsylvania US-422 OGS base particle size distribution

IOWA I-29

The pavement foundation materials from Iowa I-29 were sampled from Monona County in Iowa. The laboratory tests performed include: particle size distribution analysis, Atterberg limits tests, standard and modified Proctor tests, relative density tests, and specific gravity determinations. The results for each of the materials are summarized in Table 25.

Table 25. Summary of Iowa I-29 soil properties

Laboratory Property	Recycled Concrete (RPCC) Base	Recycled Asphalt (RAP) Subbase	Select Backfill Subbase	Existing Sand Subbase	TB-1 Subgrade	TB-2 Subgrade
USCS classification	GW	GW	SP	SW-SM	ML	ML
AASHTO classification	A-1-a	A-1-a	A-1-b	A-1-b	A-4(2)	A-4(0)
Coefficient of uniformity (c_u)	13.8	13.7	9.6	20.5	—	—
Coefficient of curvature (c_c)	2.0	1.4	0.5	1.3	—	—
Liquid limit (LL)	NP	NP	NP	NP	27	31
Plastic limit (PL)	NP	NP	NP	NP	23	20
Plasticity index (PI)	NP	NP	NP	NP	4	11
Specific gravity (G_s) (*Assumed)	2.64	2.55	2.70	2.70	2.65	2.69
Optimum moisture content, w_{opt} (%) standard Proctor	—	—	—	—	14.4	17.8
Dry unit weight (kN/m^3) standard Proctor	—	—	—	—	17.63	16.38
Optimum moisture content, w_{opt} (%) modified Proctor	—	—	—	—	11.1	13.5
Dry unit weight (kN/m^3) modified Proctor	—	—	—	—	18.99	18.00
Min dry unit weight (kN/m^3) relative density	14.75	14.82	16.38	14.20	—	—
Max dry unit weight (kN/m^3) relative density	19.30	18.86	20.67	20.80	—	—
Gravel size (%) (>4.75mm)	59	51	37	25	6	3
Sand size (%) (4.75 to 0.075mm)	41	49	63	6	21	5
Silt size (%) (0.075 to 0.002mm)	0.4	0.2	0.2	7	59	65
Clay size (%) (≤0.002mm)	0.4	0.2	0.2	3	15	27

NP = not plastic

Particle size distributions provided the data for classification (Figure 48, Figure 49, Figure 50, Figure 51, and Figure 52). Resilient modulus tests performed on RPCC base and select backfill subbase material samples had particle size distributions that were scalped and

replaced to meet AASHTO T307 specifications, as described in the Methods Chapter. The scalped and replaced particle size distributions are included in Figure 48 and Figure 50 for RPCC base and select backfill subbase, respectively.

Relative density tests provided moisture-density relationship for the RPCC base, RAP subbase, select backfill subbase, and existing sand subbase (Figure 53, Figure 54, Figure 55, and Figure 56). Standard and modified Proctor tests provided the moisture-density relationship for the TB-1 and TB-2 subgrade materials (Figure 57).

The moisture-dry unit weight figures for the RPCC base material included both in situ and laboratory values. In situ dry unit weights for the RPCC base were less than the laboratory values. In situ RPCC base relative density values ranged from 12–58%. In situ moisture contents ranged from 6.4–8.9%. Resilient modulus RPCC base relative density values ranged from 42–49%. Resilient modulus RPCC base moisture contents ranged from 5.0–10.2%. The zero air voids (ZAV) curve for RPCC base was located off the chart. The moisture-dry unit weight relationships for RPCC base are shown in Figure 53.

The moisture-dry unit weight figures for the RAP subbase material included both in situ and laboratory values. In situ dry unit weights for the RAP subbase were less than the laboratory values. In situ RAP subbase relative density values ranged from 76–106%. In situ moisture contents ranged from 6.9–9.3%. Resilient modulus RAP subbase relative density values ranged from 62–130%. Resilient modulus RAP subbase moisture contents ranged from 0.6–9.9%. The moisture-dry unit weight relationships for RAP subbase are shown in Figure 54.

The moisture-dry unit weight figures for the select backfill subbase material included both in situ and laboratory values. In situ dry unit weights for the select backfill subbase were scattered around the laboratory values. In situ select backfill subbase relative density values ranged from 90–129%. In situ moisture contents ranged from 4.2–7.1%. Resilient modulus select backfill subbase relative density values ranged from 99–132%. Resilient modulus select backfill subbase moisture contents ranged from 3.6–7.1%. The moisture-dry unit weight relationships for select backfill subbase are shown in Figure 55.

The moisture-dry unit weight figures for the existing sand subbase material included only laboratory values. Laboratory moisture and dry unit weight values for the existing sand

subbase were selected to evaluate the effects of unit weight and moisture on resilient modulus. Resilient modulus existing sand subbase relative density values ranged from 55–111%. Resilient modulus existing sand subbase moisture contents ranged from 0.0–9.4%. The moisture-dry unit weight relationships for existing sand subbase are shown in Figure 56.

The moisture-dry unit weight relationships for the two subgrade materials included both in situ and laboratory values. The subgrade material from TB-2 will be used to compare the in situ and laboratory data because of the similarities between the field data and standard Proctor results. In situ subgrade relative compaction values ranged from 95–100% of the maximum standard Proctor dry unit weight. In situ subgrade moisture values ranged from 0.2% below to 4.5% above optimum standard Proctor moisture content. Resilient modulus subgrade relative compaction value ranged was 109% of the maximum standard Proctor dry unit weight. Resilient modulus subgrade moisture value was 2.9% below optimum standard Proctor moisture content. Moisture content values for the subgrade materials tended to be wet of optimum, seen in Figure 57. This led to low dry unit weights and would indicate low subgrade stiffness values.
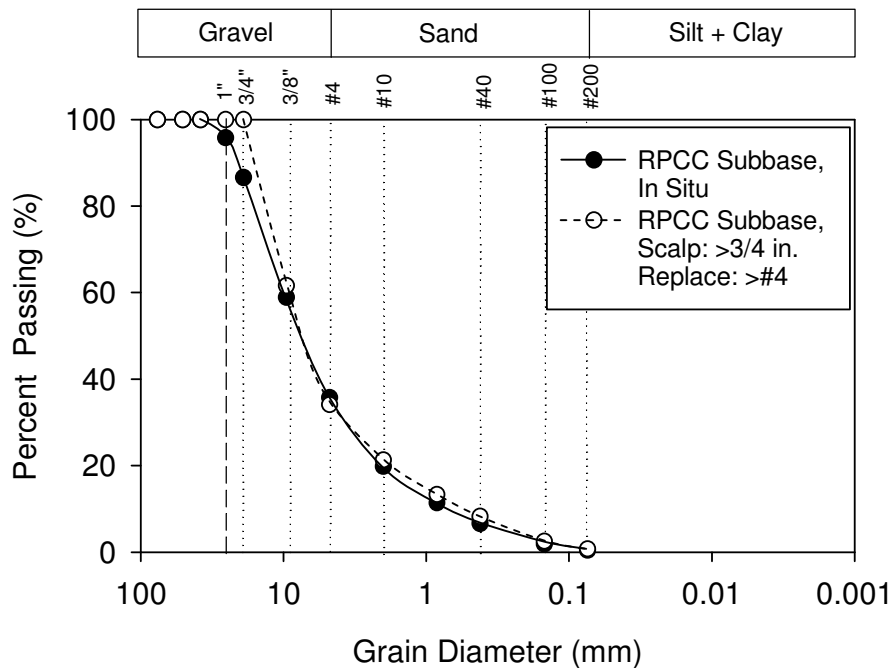
Figure 48. Iowa I-29 RPCC particle size distribution for in situ and scalp and replace materials
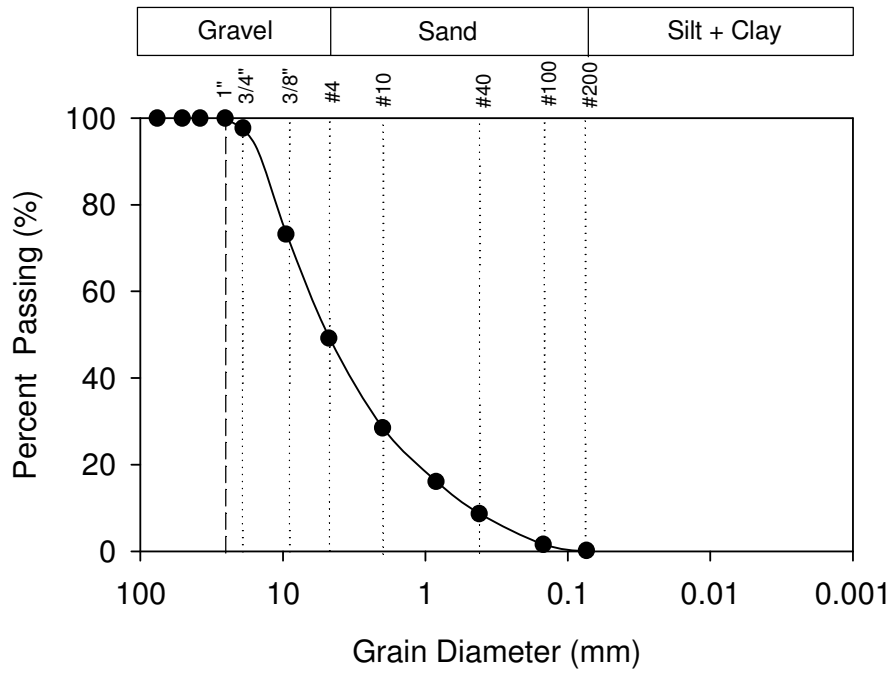
Figure 49. Iowa I-29 RAP subbase particle size distribution
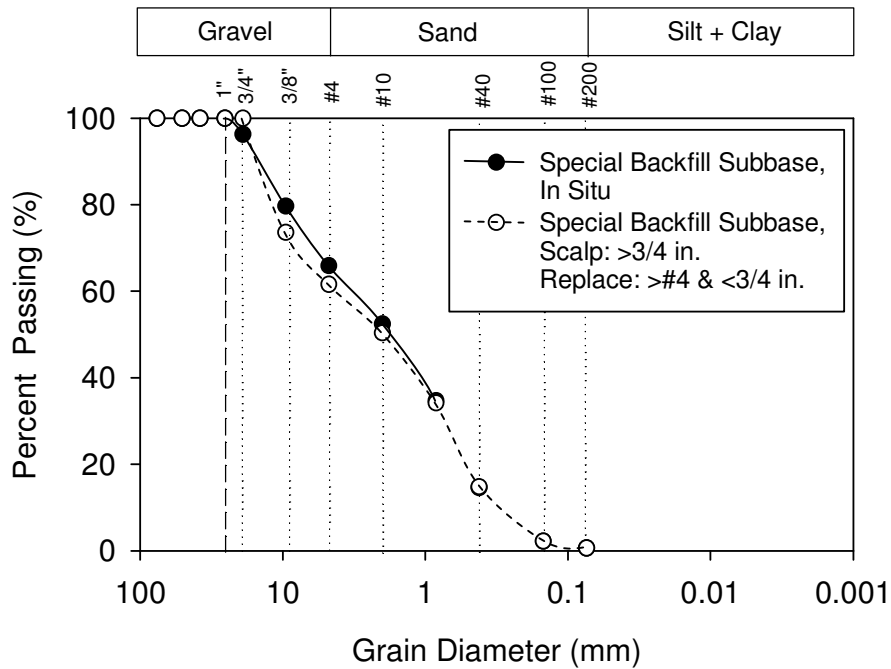
Figure 50. Iowa I-29 select backfill subbase particle size distribution for in situ

and scalp and replace materials
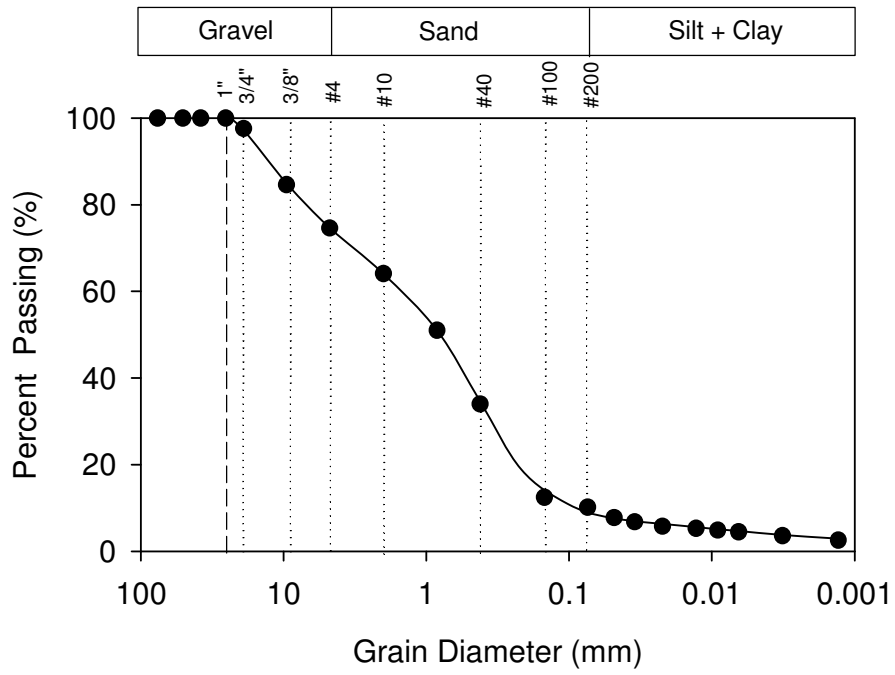
Figure 51. Iowa I-29 existing sand subbase particle size distribution
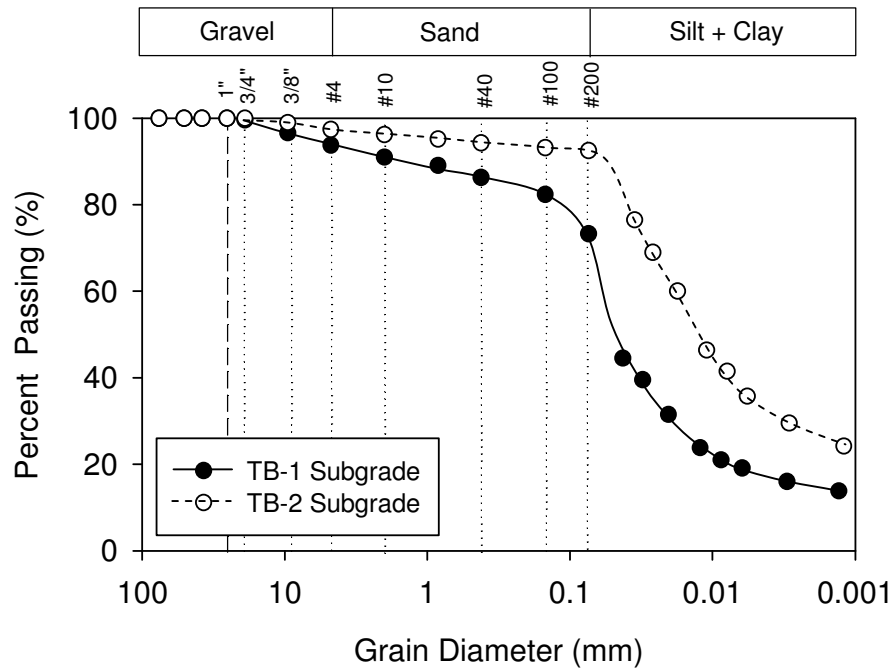
Figure 52. Iowa I-29 TB-1 and TB-2 subgrade particle size distribution
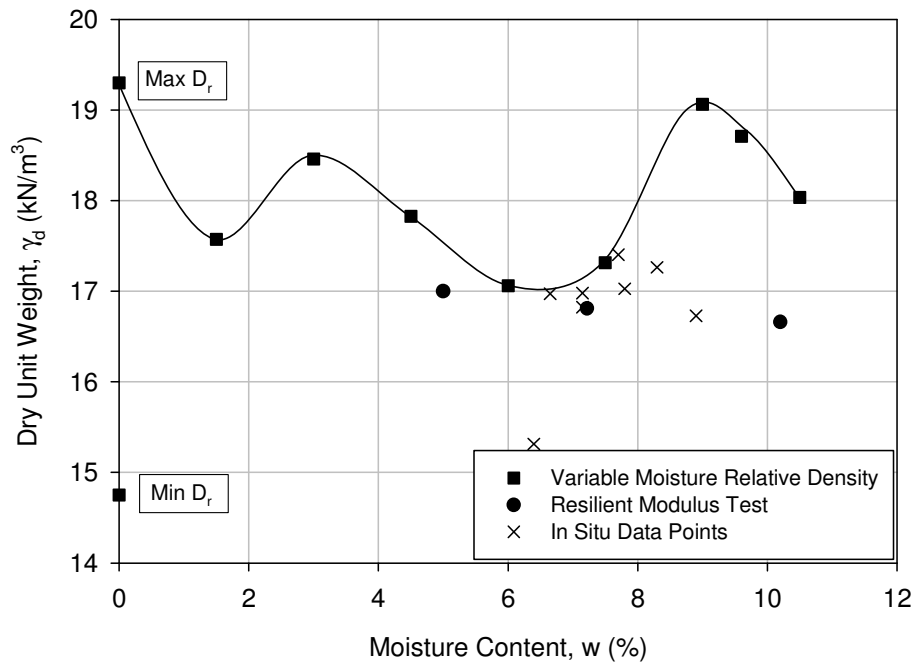
Figure 53. Iowa I-29 RPCC base moisture-unit weight relationship
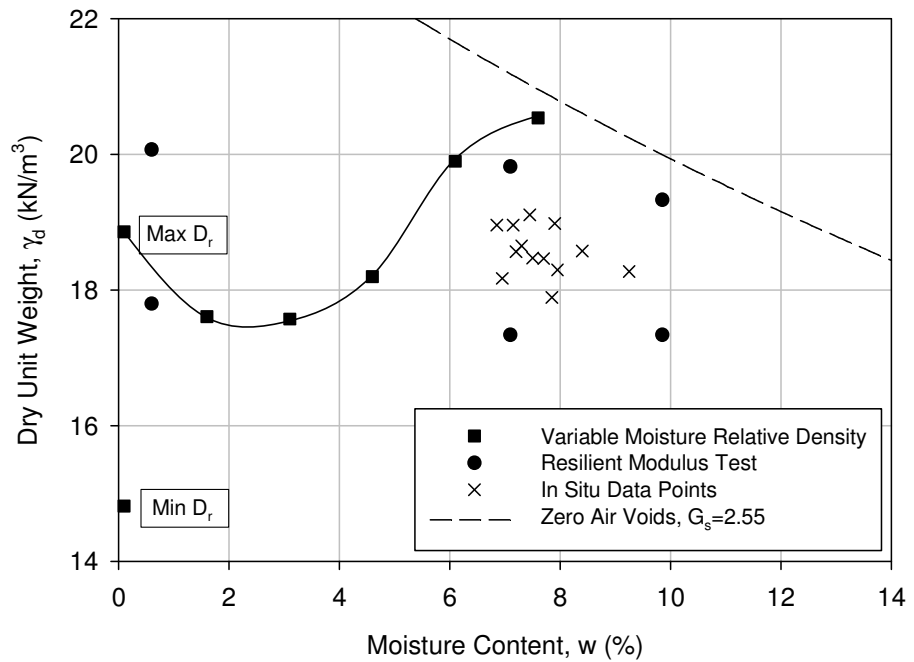
Figure 54. Iowa I-29 RAP subbase moisture-unit weight relationship
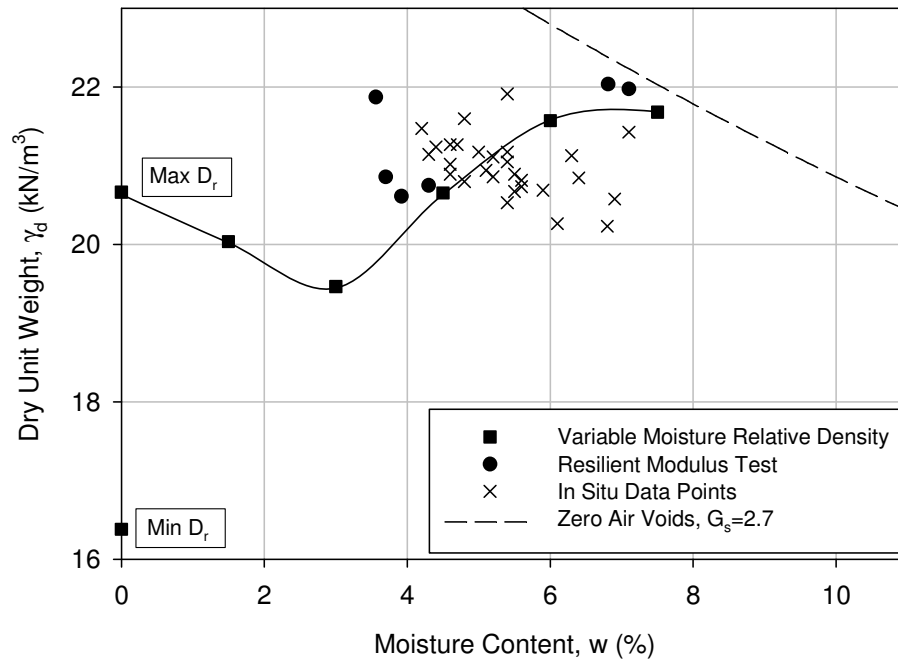
Figure 55. Iowa I-29 select backfill subbase moisture-unit weight relationship
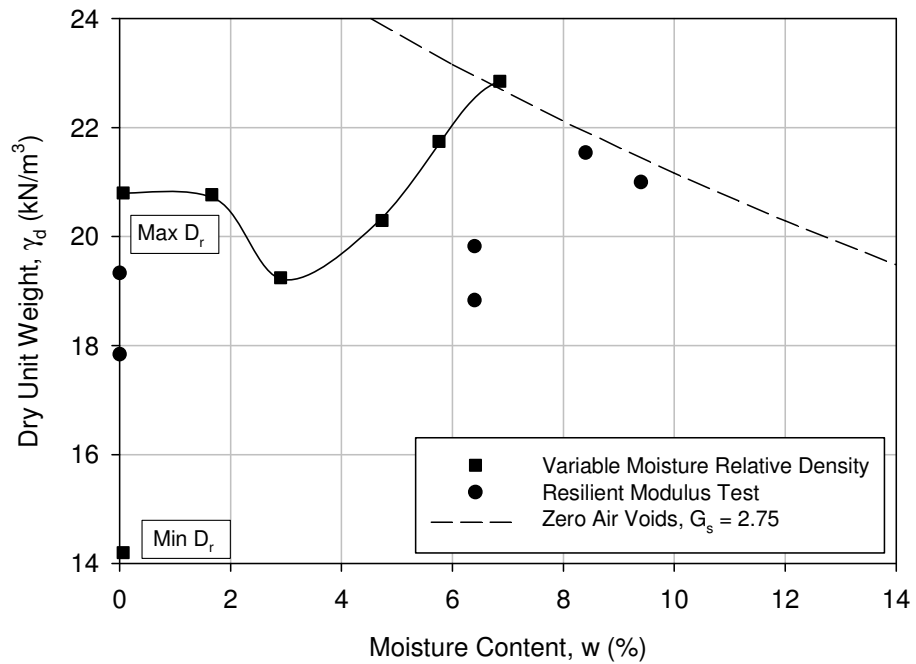
Figure 56. Iowa I-29 existing sand subbase moisture-unit weight relationship
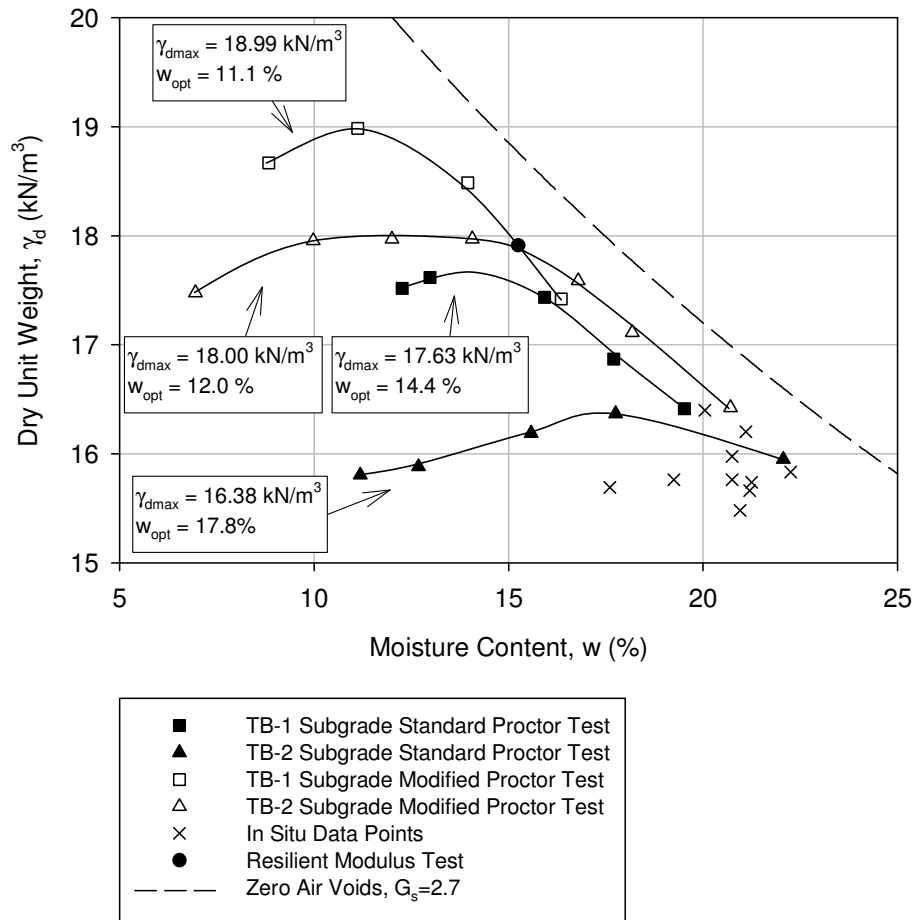
Figure 57. Iowa I-29 subgrade materials moisture-unit weight relationships

WISCONSIN US-10

The pavement foundation materials from Wisconsin US-10 were sampled near Steven's Point, Wisconsin. The laboratory tests performed include: particle size distribution analysis, Atterberg limits tests, standard and modified Proctor tests, and relative density tests. The results for each of the materials are summarized in Table 26.

Table 26. Summary of Wisconsin US-10 soil properties

Laboratory Property	Existing Sandy Subbase	Subgrade
USCS classification	SP	CL
AASHTO classification	A-3	A-6(8)
Coefficient of uniformity (c_u)	1.9	NA
Coefficient of curvature (c_c)	1.0	NA
Liquid limit (LL)	NP	38
Plastic limit (PL)	NP	20
Plasticity index (PI)	NP	18
Specific gravity (G_s) (*Assumed)	2.75*	2.78*
Optimum moisture content, w_{opt} (%) standard Proctor	12.0	12.4
Dry unit weight (kN/m^3) standard Proctor	17.37	18.70
Optimum moisture content, w_{opt} (%) modified Proctor	11.6	10.5
Dry unit weight (kN/m^3) modified Proctor	17.72	20.30
Min dry unit weight (kN/m^3) relative density	15.07	—
Max dry unit weight (kN/m^3) relative density	18.19	—
Gravel size (%) (>4.75mm)	3	13
Sand size (%) (4.75 to 0.075mm)	97	28
Silt size (%) (0.075 to 0.002mm)	0.2	46
Clay size (%) ($\leq$0.002mm)	0.2	13

NP = not plastic

Particle size distributions provided the data for classification (Figure 58 and Figure 59). Moisture-unit weight relationships for the existing sandy subbase were obtained from both relative density tests as well as standard and modified Proctor tests (Figure 60). Moisture-unit weight relationships for the subgrade were obtained by standard and modified Proctor tests (Figure 61).

The moisture-dry unit weight figures for the existing sandy subbase material included both in situ and laboratory values. In situ existing sand subbase moisture values ranged from 7.8–9.7% below optimum standard Proctor moisture content. In situ sand subbase relative

compaction values ranged from 90–95% of the maximum standard Proctor dry unit weight, while the relative density values ranged from 16–48%. Resilient modulus tests were performed at moisture values from 0.4–9.3% below standard Proctor optimum moisture content. Resilient modulus samples were also tested at relative compaction values ranging from 91–103% of the maximum standard Proctor dry unit weight and relative density values of 21–88%. The two groups of values indicate variability at different locations over the site. The moisture-dry unit weight relationships for sand subbase are shown in Figure 60.

The moisture-dry unit weight figures for the subgrade material included both in situ and laboratory values. In situ subgrade moisture values ranged from 1.1–6.4% below optimum standard Proctor moisture content. In situ subgrade relative compaction values ranged from 101–111% of the maximum standard Proctor dry unit weight. The subgrade material in situ moisture content and dry unit weight values tended to be on the dry side of optimum but corresponded with the modified Proctor curve. The low moisture contents and high dry unit weights would also suggest that the subgrade stiffness values would be large. Resilient modulus tests were performed at moisture values from 5.5% below to 3.1% above optimum standard Proctor moisture content. Relative compaction values ranged from 102–110% of the maximum standard Proctor dry unit weight. The moisture-dry unit weight relationships for subgrade are shown in Figure 61.
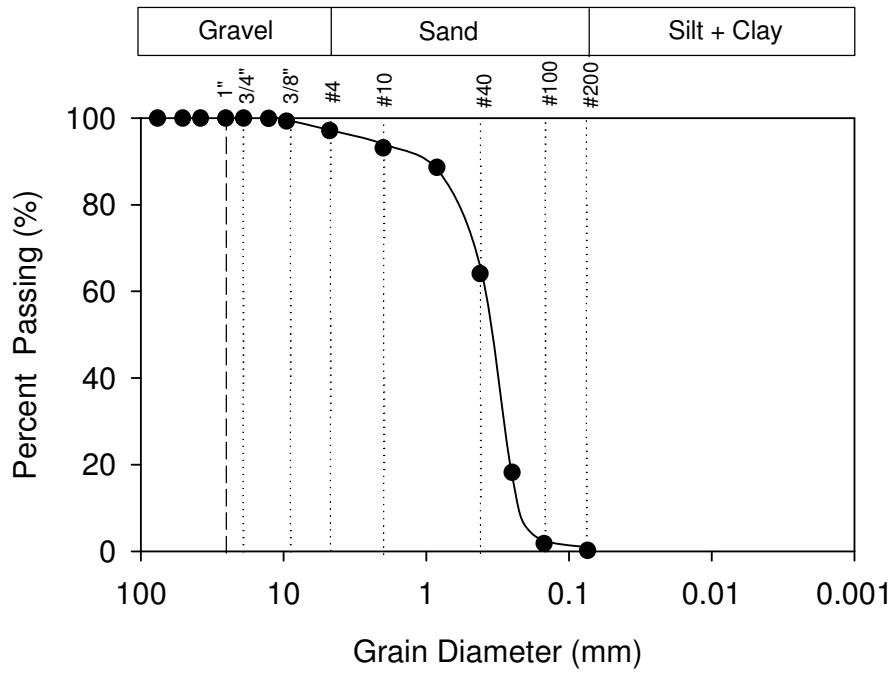
Figure 58. Wisconsin US-10 existing sandy subbase particle size distribution
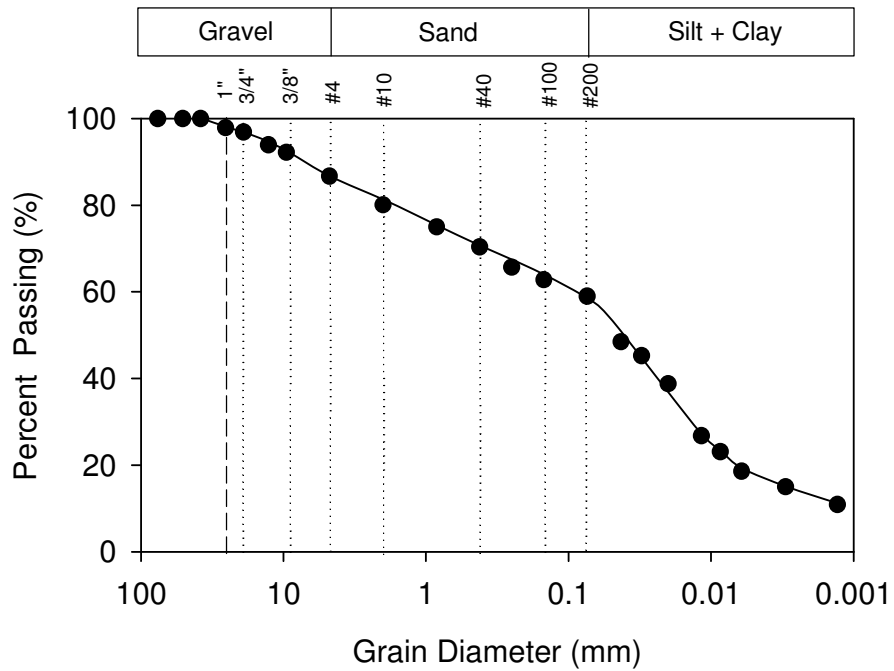
Figure 59. Wisconsin US-10 subgrade particle size distribution
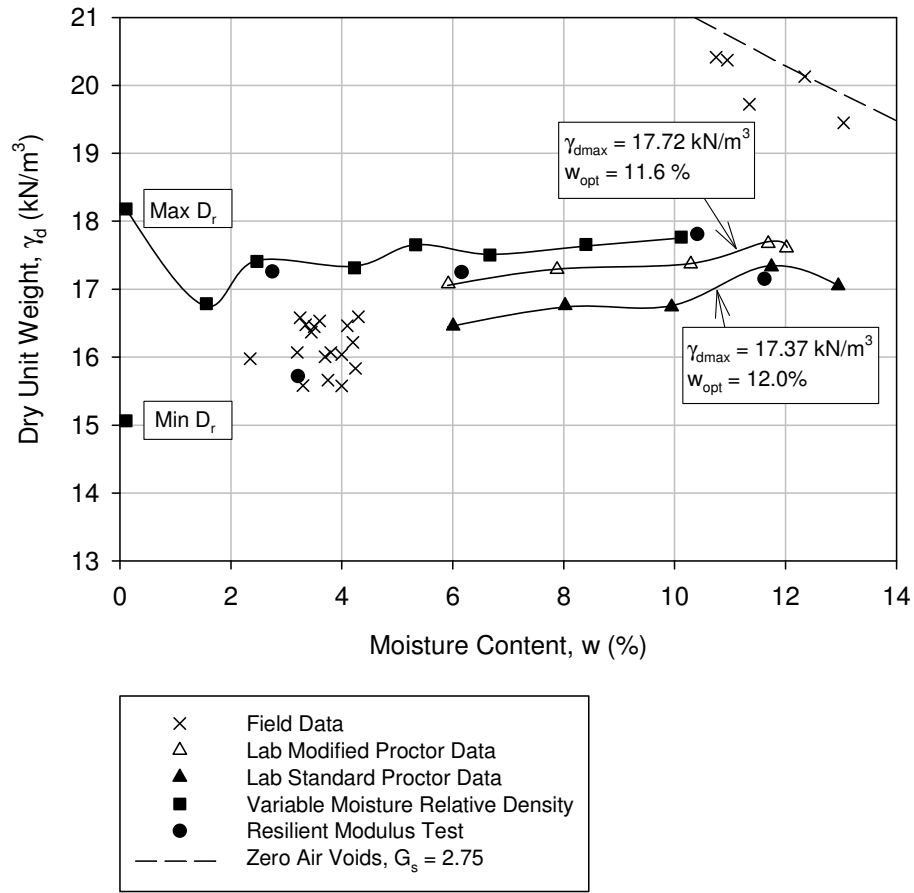
Figure 60. Wisconsin US-10 sand subbase moisture-density relationship
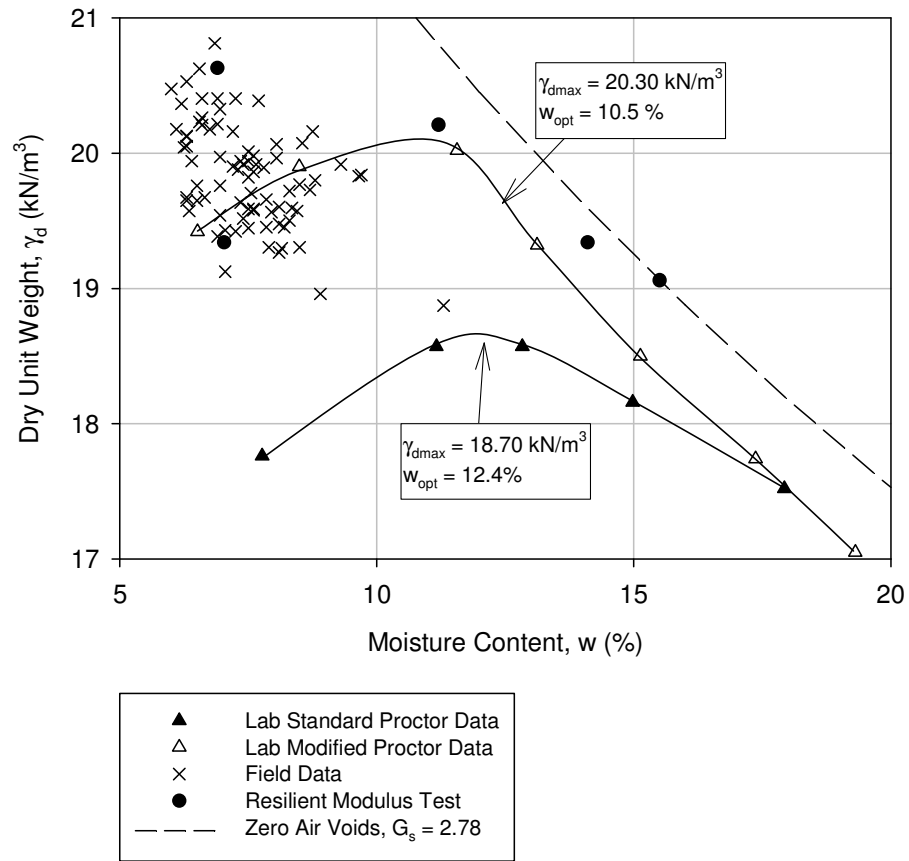
Figure 61. Wisconsin US-10 subgrade moisture-density relationship

CHAPTER 5. RESULTS AND DISCUSSION

This chapter presents and discusses the test results from laboratory and in situ studies collected from six field sites—Michigan I-94, Michigan I-96, Pennsylvania US-22, Pennsylvania US-422, Iowa I-29, and Wisconsin US-10. Laboratory studies include moduli and index property determination. Two ranges of moisture and dry unit weight values were investigated to observe the effects on resilient moduli. In situ studies include moduli determination through plate load (PLT), light weight deflectometer (LWD), falling weight deflectometer (FWD), and dynamic cone penetrometer (DCP) tests. Data from each site was studied to determine relationships for laboratory and field parameters. Additionally, assumed design values are compared to the values determined in the laboratory. Different stabilization techniques (i.e., fly ash-treated subgrade, cement-treated subgrade, and high-density polyurethane foam injection) were also investigated in relation to changes in stiffness with different treatments. The movement of fine particles within laboratory specimens due to cyclic loading was also studied.

In the following discussions, materials were classified into groups—cohesive, granular, base, subbase, and subgrade. The distinction between the cohesive and granular materials was determined using Hilf's (1991) description from the Bureau of Reclamation's 1968 *Earth Manual*. Soils that were classified as the Unified Soil Classification System (USCS) symbols CH, CL, MH, ML, SC, SM, GC, CM, or any combination of any two of these symbols were considered to be cohesive. All other symbols were considered granular materials.

Base, subbase, and subgrade materials were classified according to the location in the foundation system the material was obtained. Base materials made up the granular layer directly under the pavement layer. Subbase materials made up the granular layers under the base layer. Subgrade materials made up the cohesive materials under the subbase layers.

LABORATORY STUDIES

Laboratory studies include moduli and material index property determination. Laboratory modulus tests were performed on single and composite material samples. Material index properties were performed on each material.

Three moduli types were computed using data from resilient modulus tests—resilient (M_r), dynamic secant (E_s), and cyclic secant (E^*_s) moduli. Single sample resilient modulus tests were compared to the stress states, dry unit weight, moisture content, and degree of saturation. AASHTO T307 recommends testing one material per specimen, but in this study, composite material samples were also studied to investigate how layering different materials affected the overall modulus. Finally, statistical analyses were performed between specimens with different variables (i.e., moisture content, dry unit weight, layering, and disturbance) to quantify which variables significantly affected the resilient modulus values.

The secant moduli were calculated from the resilient moduli data but include the permanent strain instead of resilient strain. The secant moduli are measures of the elastic characteristics of pavement foundation materials.

Material index properties were compared to single sample resilient moduli. The materials were simplified into granular and cohesive materials. The tested properties were percent passing No. 200 sieve, percent passing No. 4 sieve, coefficient of uniformity (c_u), coefficient of curvature (c_c), liquid limit (LL), plasticity limit (PL), undrained shear strength (s_u), and dry unit weight-moisture content ratio.

Single material sample resilient moduli

Resilient modulus values were directly calculated from the data by averaging the last five cycles from each sequence. Test sequences and stress values for granular and composite samples are summarized in Table 27. Test sequences and stress values for cohesive samples are summarized in Table 28. Appendix A provides resilient modulus sample calculations. The following sections present the variances in stress state, dry unit weight, moisture content, and degree of saturation as functions of resilient moduli values.

Stress states

The AASHTO T307 resilient modulus method requires the application of several confining and deviator stresses to samples. These stresses were chosen to model the values that occur in situ. According to stress distribution theory, high stresses are expected for materials closer to the point of application (i.e., pavement surface), and low stresses are expected with increasing depth (i.e., subgrades). For this study, granular materials were found near the pavement surface and cohesive materials were found at depth. The resilient

modulus test uses a range of stress states that represent stresses likely to be experienced beneath pavements. Table 27 and Table 28 report the stress values used in the resilient moduli test sequences.

For each sample type, boundaries were developed from the maximum and minimum resilient modulus values. Granular and composite samples had linear boundaries of resilient modulus values; cohesive samples had curvilinear boundaries of resilient modulus values. The curvilinear boundaries developed from the low scatter of resilient moduli at $M_{r(T307)}$ values less than 100 MPa. The linear boundaries for granular and composite samples were extrapolated to a $M_{r(T307)} = 0$ intercept, while the curvilinear boundaries had a slightly positive intercept for cohesive samples. Equal numbers of sequences were applied to both granular and cohesive samples. However the range of measured resilient moduli is much greater for granular and composite samples, which illustrates the confining stress dependence of the granular materials.

Current pavement design uses resilient moduli data to either determine regression coefficients (k-values) for finite element analyses or to determine a single resilient modulus value to represent the foundation support conditions. The National Highway Cooperative Research Program (NCPRP) Project 1-28A (2004a) suggested that a resilient modulus value be determined by interpolating the resilient moduli values using Equation 20 with $\sigma_{cyclic} = 103$ kPa (15 psi) and $\sigma_3 = 35$ kPa (5 psi) for granular materials and $\sigma_{cyclic} = 41$ kPa (6 psi) and $\sigma_3 = 14$ kPa (2 psi) for cohesive materials, where σ_{cyclic} is defined as $\sigma_{maximum}$ minus $\sigma_{contact}$. The NCHRP stress states align close to Sequence 6 and Sequence 13 in AASHTO T307 for granular and cohesive soils, respectively.

$$M_r = k_1 P_a \left(\frac{\sigma_B - 3k_6}{P_a} \right)^{k_2} \left(\frac{\tau_{oct}}{P_a} + k_7 \right)^{k_3}$$

(20)

where: P_a = atmospheric pressure (MPa);

σ_B = bulk stress (MPa) = $\sigma_1 + \sigma_2 + \sigma_3$;

τ_{oct} = octahedral shear stress (MPa) $= \dfrac{\sqrt{(\sigma_1 - \sigma_2)^2 + (\sigma_2 - \sigma_3)^2 + (\sigma_3 - \sigma_1)^2}}{3}$;

$\sigma_1, \sigma_2, \sigma_3$ = principal stresses; and

k_1, k_2, k_3 = regression coefficients.

For many comparisons, this study investigated the effects of all the stress states by averaging all of the individual sequence resilient moduli into one value, $M_{r(T307)}$. However, different stress states have a very large effect on the resilient moduli for all sample types. The difficulty lies in predicting the exact stress conditions the soil will experience in situ. It is important to use the stress state (or possibly the range of stress states) that correlates to the anticipated in situ conditions to determine the design value.

Resilient moduli values for each sequence were compared as functions of the $M_{r(T307)}$ values for granular, cohesive, and composite samples in Figure 62. The dashed lines illustrate the range of resilient moduli from each sample. The solid lines illustrate where the average resilient moduli and the resilient moduli measured for each sequence are equal.

Resilient moduli of granular samples increased with each sequence. Increasing sequences for granular samples had increasing confining stresses. The results indicate confining stress dependency for granular samples. Cohesive samples had a weaker relationship between sequences and lower $M_{r(T307)}$ values than granular samples. Part of the issue may be that increasing sequences did not have a trend of increasing stresses.

Composite samples had two behaviors, depending on the sample stiffness. At higher $M_{r(T307)}$ values (above about 100 MPa), the results were similar to granular samples— increased sequences led to increased M_r values at each sequence. At lower $M_{r(T307)}$ values (below about 100 MPa), higher sequences did not correspond to larger M_r values at each sequence. The behavior of these soft samples appeared more similar to cohesive samples.

Table 27. M$_r$ test sequences and stress values for granular and composite samples

(AASHTO T307)

Sequence No.	Confining stress, σ$_c$ kPa	psi	Max. axial stress, σ$_d$ kPa	psi	No. of cycles
0	103.4	15	103.4	15	500-1000
1	20.7	3	20.7	3	100
2	20.7	3	41.4	6	100
3	20.7	3	62.1	9	100
4	34.5	5	34.5	5	100
5	34.5	5	68.9	10	100
6	34.5	5	103.4	15	100
7	68.9	10	68.9	10	100
8	68.9	10	137.9	20	100
9	68.9	10	206.8	30	100
10	103.4	15	68.9	10	100
11	103.4	15	103.4	15	100
12	103.4	15	206.8	30	100
13	137.9	20	103.4	15	100
14	137.9	20	137.9	20	100
15	137.9	20	275.8	40	100

Table 28. M$_r$ test sequences and stress values for cohesive samples (AASHTO T307)

Sequence No.	Confining stress, σ$_c$ kPa	psi	Max. axial stress, σ$_d$ kPa	psi	No. of cycles
0	41.4	6	27.6	4	500-1000
1	41.4	6	13.8	2	100
2	41.4	6	27.6	4	100
3	41.4	6	41.4	6	100
4	41.4	6	55.2	8	100
5	41.4	6	68.9	10	100
6	27.6	4	13.8	2	100
7	27.6	4	27.6	4	100
8	27.6	4	41.4	6	100
9	27.6	4	55.2	8	100
10	27.6	4	68.9	10	100
11	13.8	2	13.8	2	100
12	13.8	2	27.6	4	100
13	13.8	2	41.4	6	100
14	13.8	2	55.2	8	100
15	13.8	2	68.9	10	100

Figure 62. Comparison of $M_{r(T307)}$ and the M_r value measured from each sequence for granular samples (top), cohesive samples (middle), and composite samples (bottom)

The degree of saturation also affects the resilient moduli at different stress states. With the exception of one stiff cohesive sample at approximately 90% saturation, resilient moduli values decreased from 60% to about 95%. The increase in stiffness at about 60% saturation could be the result of increased suction. Yang et al. (2008) determined that resilient strain and soil suction from the attraction of capillary and surface adsorptive forces are inversely related. Increasing degree of saturation reduces the suction and effective stresses in the soil, which lead to reduced soil stiffness. Figure 63 compares the resilient modulus values measured from each sequence and the degree of saturation for cohesive samples. Additional analyses of the effects of degree of saturation on resilient moduli are located under the Degree of Saturation section.
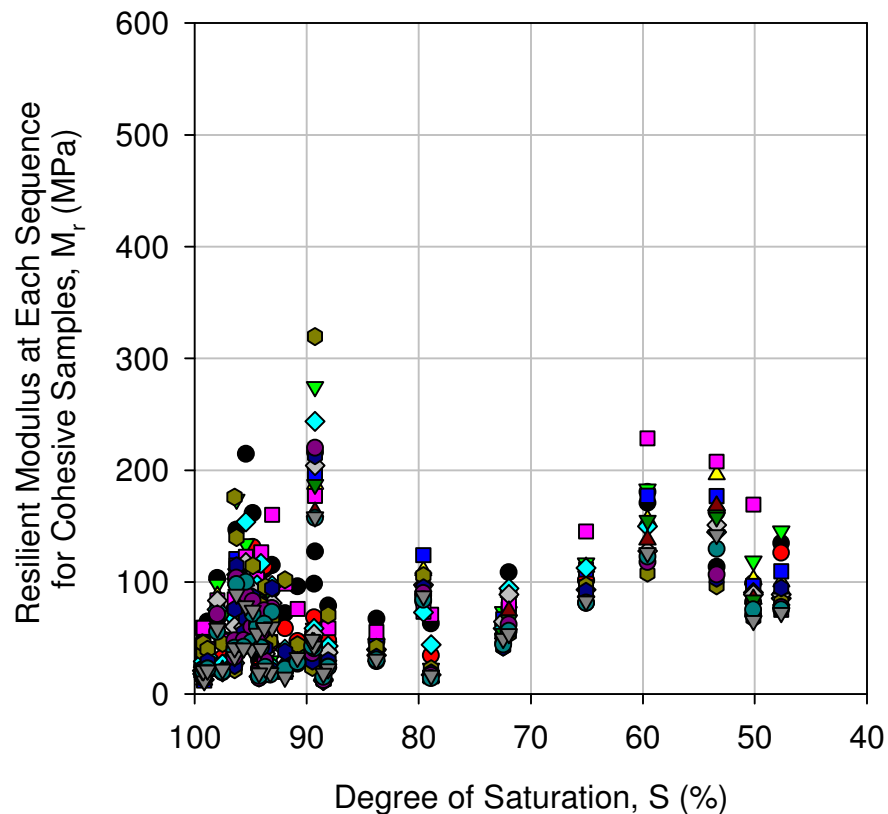
Figure 63. Comparison of the M_r value measured from each sequence and the degree of saturation for cohesive samples

Dry unit weight

Unit weight is known to be one of the parameters that affect resilient modulus values (Alam et al. 2010; Seed et al. 1962; Southgate and Mahboub 1994). With all other parameter equal, denser materials will have higher resilient than less dense materials. The dry unit weight (γ_d) was determined using the moisture content of the material and the measured volume of the sample before performing the resilient modulus test. Maximum and minimum relative density tests were performed on granular materials with a vibratory table according to ASTM 4253 and ASTM 4254, respectively. The maximum and minimum relative density values were used with the measured dry unit weight to determine relative density. Relative compaction used maximum dry unit weight standard Proctor values (ASTM D698) and the measured dry unit weight to determine the percent compaction for cohesive soils.

Overall, the relationship between $M_{r(T307)}$ and γ_d did not have a clear trend in this study. The densities were selected to mimic the conditions found at the test sites. This indicates that for the tested range of densities the resilient moduli are not clearly influenced by the dry unit weight alone. Dry unit weight, in conjunction with additional factors (e.g., confining stress, moisture content, degree of saturation, etc.), may provide a clearer relationship with $M_{r(T307)}$ values than only dry unit weight values. Figure 64 summarizes the relationship of dry unit weight, relative density, and relative compaction as functions of $M_{r(T307)}$ for single material samples.
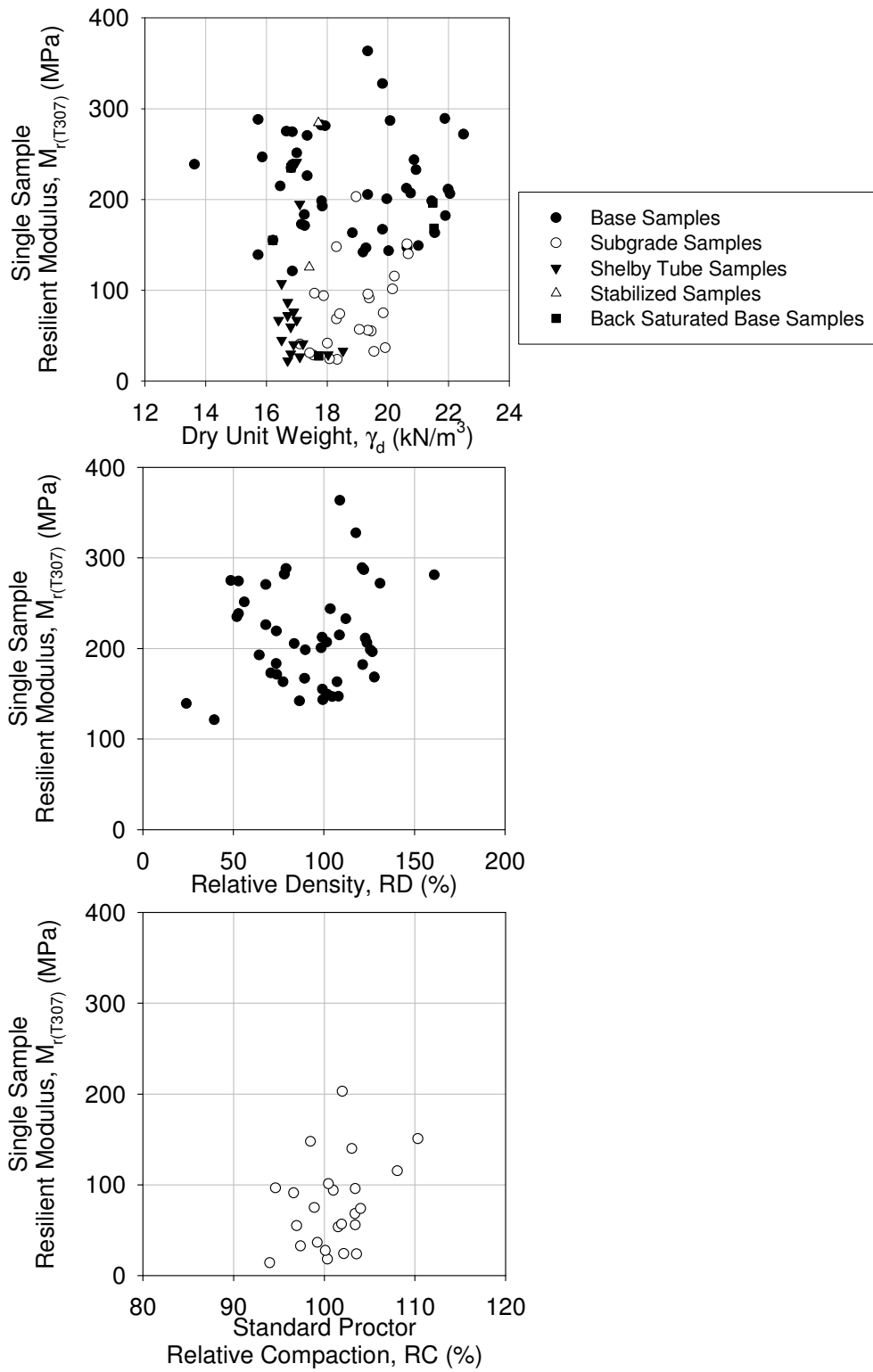
Figure 64. Summary of dry unit weight (γ_d), relative density (RD), and

relative compaction (RC) as functions of $M_{r(T307)}$ for single material samples

Moisture content

Moisture content (w) was determined by oven drying excess material used to fabricate the sample. Moisture content is a parameter that tends to reduce the resilient modulus values (Alam et al. 2010; Seed et al. 1962; Southgate and Mahboub 1994). The low permeability of subgrade and cohesive materials cause the samples to hold water during resilient modulus testing, whereas base, subbase, and granular materials have higher permeabilities and tend to drain the water quickly.

As expected, the general trend of this study indicates increasing resilient moduli with decreasing moisture content. This trend is more apparent with the subgrade samples than the base samples. For the range of moisture contents tested, the base materials had a weak inverse trend for M_r values and moisture content. Base samples with high moisture contents during testing are difficult to obtain because they tend to drain rapidly. The high moisture contents seen in subgrade and Shelby tube samples illustrate the results of effective stress on resilient moduli. Even though, the drainage valves are open during resilient modulus testing, the one second load cycles do not allow the pore water pressures to dissipate fast enough in fine grained soils. When water becomes trapped in the pore spaces of the soil, the effective stress decreases and the resilient moduli is seen to decrease. Dotted lines link back saturated samples to corresponding partially saturated samples. The effects of saturation are discussed in the next section. Figure 65 summarizes the relationship of the moisture content as a function of resilient moduli for single material samples.
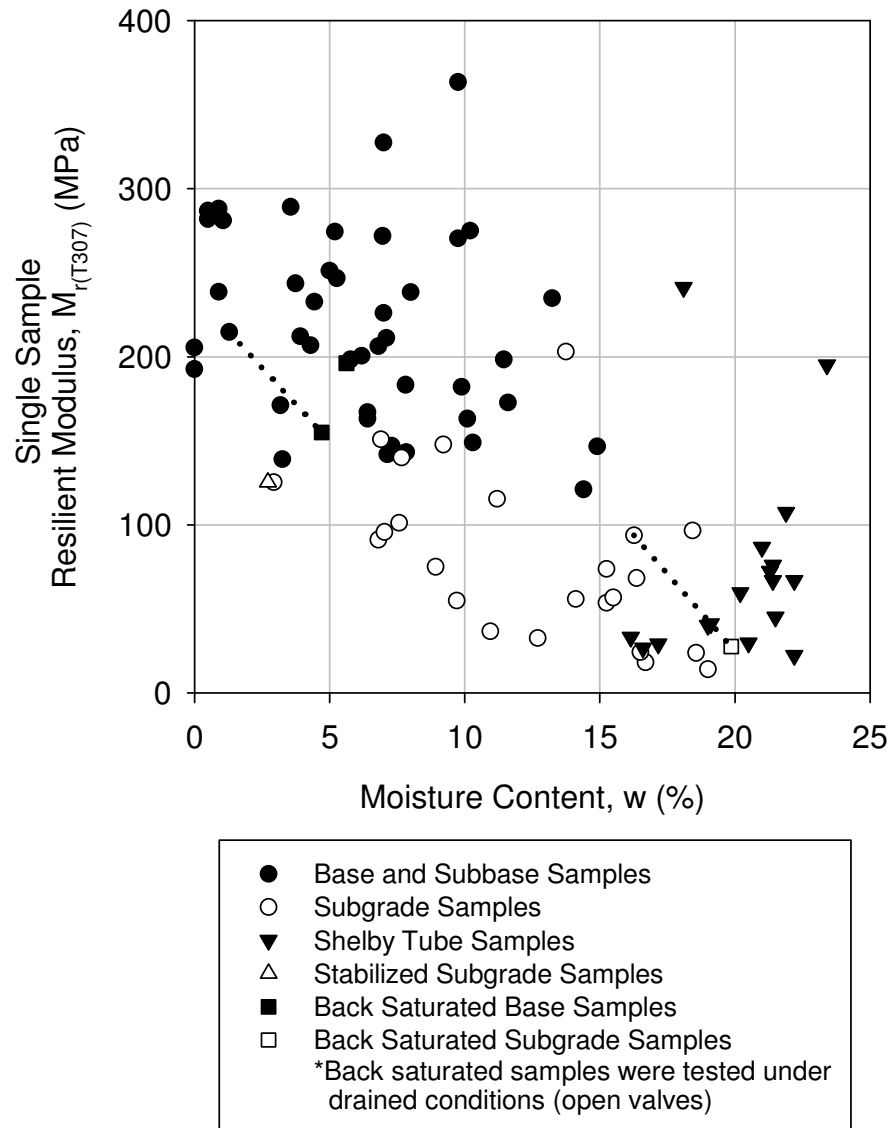
Figure 65. Summary of moisture content (w) during testing as a function of

average $M_{r(T307)}$ for single material samples

Degree of saturation

The degree of saturation (S) influences the resilient modulus and is calculated from three parameters, dry unit weight, moisture content, and specific gravity. An increase in S indicates a combination of lower densities and higher moisture contents. Drumm et al. (1997) noted that increasing either moisture content or degree of saturation decreases the resilient modulus.

Further, S influences soil suction, which could account for some of the differences in $M_{r(T307)}$ seen in this study. Soil suction consists of two parts—osmotic suction and matric suction. Osmotic suction develops from the attraction of water due to dissolved salts in the pore fluid. However, osmotic suction has negligible effects, especially on coarse to fine grained soils; therefore, matric suction is the major factor of total suction (Liang et al. 2008, Terzaghi et al. 1996). Matric suction develops from the attraction of capillary and surface adsorptive forces (Liang et al. 2008).

In this study, as the degree of saturation transitioned from about 40% to 60%, $M_{r(T307)}$ values for all materials decreased markedly. Base material $M_{r(T307)}$ and S values between 40%–80% had stronger inverse relationships than at lower degrees of saturation. Additionally, base material $M_{r(T307)}$ values were more constant at degrees of saturation less than 40%. The inverse relationship between degree of saturation and $M_{r(T307)}$ values is very clear for a majority of subgrade samples. Lower degrees of saturation correlate to increased matric suction between soil particles, pulling them tightly together and making the soil structure stiffer. Yang et al. (2008) found that increases in matric suction reduced the resilient strain, which indicated that high matric suction increased the effective stress and decreased deformation. At higher degrees of saturation, matric suction and effective stresses decrease, reducing the $M_{r(T307)}$ values.

Dotted lines link back saturated samples to corresponding partially saturated samples. The back saturated samples were untrimmed base from Michigan I-94, class 2A subbase from Pennsylvania US-22, and subgrade from Pennsylvania US-22. Resilient modulus tests were performed with the drainage valves open—that is a drained test. One resilient modulus test on class 2A subbase was performed with closed drainage valves to simulate a worst-case, ponded foundation system. Overall, increased saturation lead to 25–70% decrease in single material $M_{r(T307)}$ values. However, the class 2A subbase indicated a slight improvement with saturation. The closed valve test had a lower $M_{r(T307)}$ value than the open valve test on the class 2A subbase. Figure 66 summarizes the relationship between the degree of saturation during testing and the resilient moduli for single material samples.
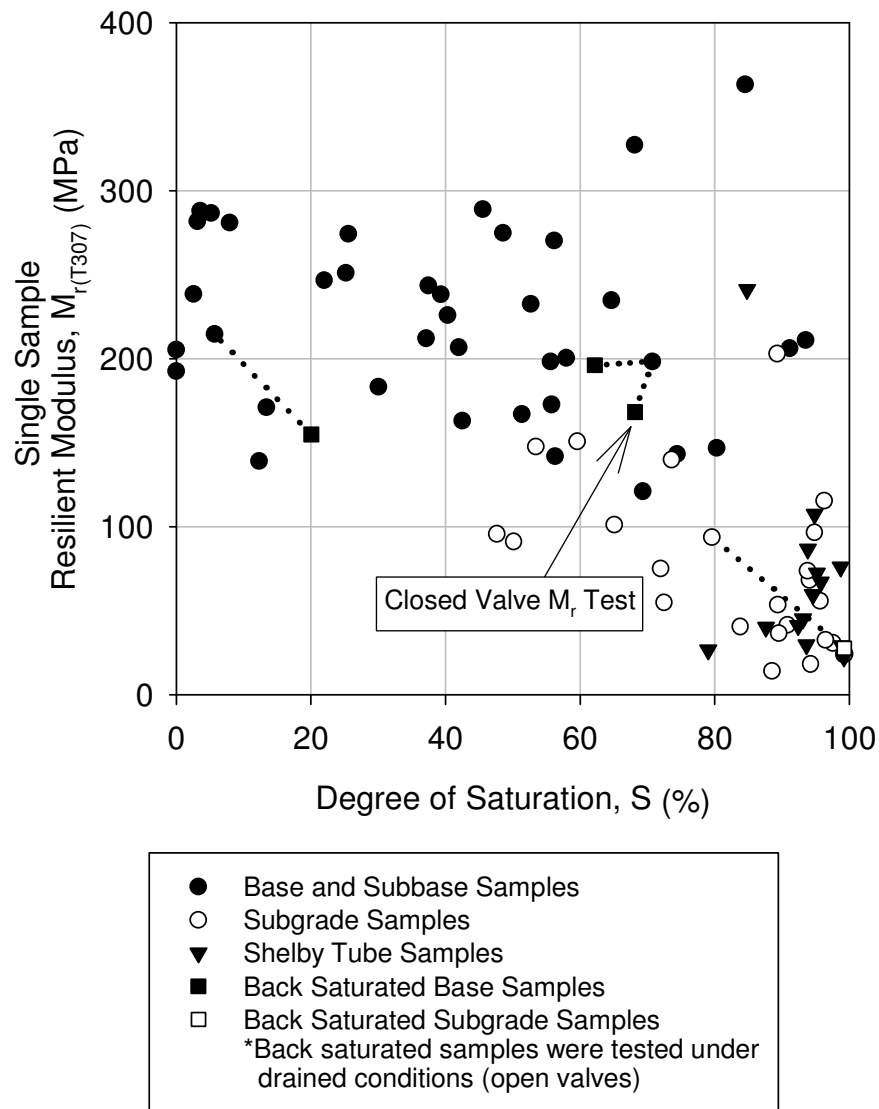
Figure 66. Summary of degree of saturation (S) during testing as a function of average

$\mathbf{M_{r(T307)}}$ **for single material samples**

Composite material sample resilient moduli

Single material samples were compared to composite material samples fabricated with layers made from materials found in the single material samples. Composite samples should provide the closest relationship between laboratory and in situ data. Dry unit weights and moisture content values were selected from in situ conditions. Composite material samples were prepared in two ways: 1) single material samples corresponded to composite material sample layers with dry unit weights within ±1.0 kN/m³ and moisture contents within ±3%

and 2) dry unit weights and moisture content values were intentionally varied beyond the selected range to investigate effects on resilient moduli (Figure 67). The variation of dry density and moisture content between single and composite material samples is shown in Figure 68.

Single Material Samples   Composite Material Samples   Single Material Samples

$\gamma_d \pm 1.0$ kN/m^3
w% ± 3%

$\gamma_d \pm >1.0$ kN/m^3
w% ± > 3%
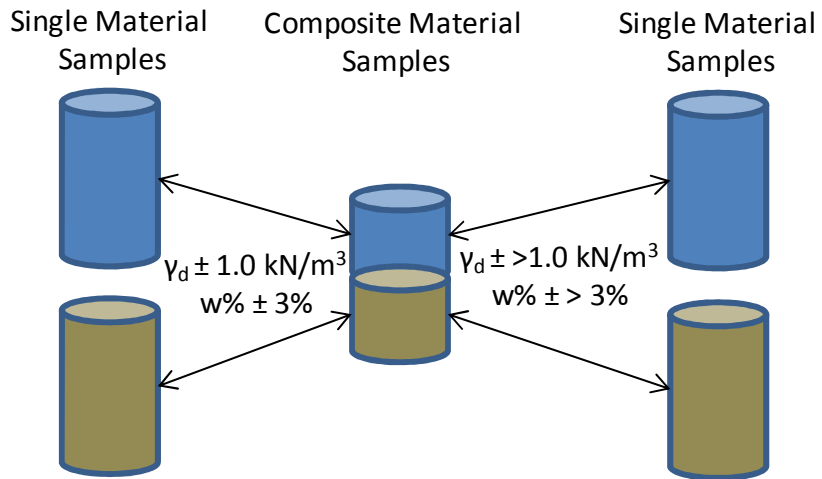
Figure 67. Comparison of single and composite material samples
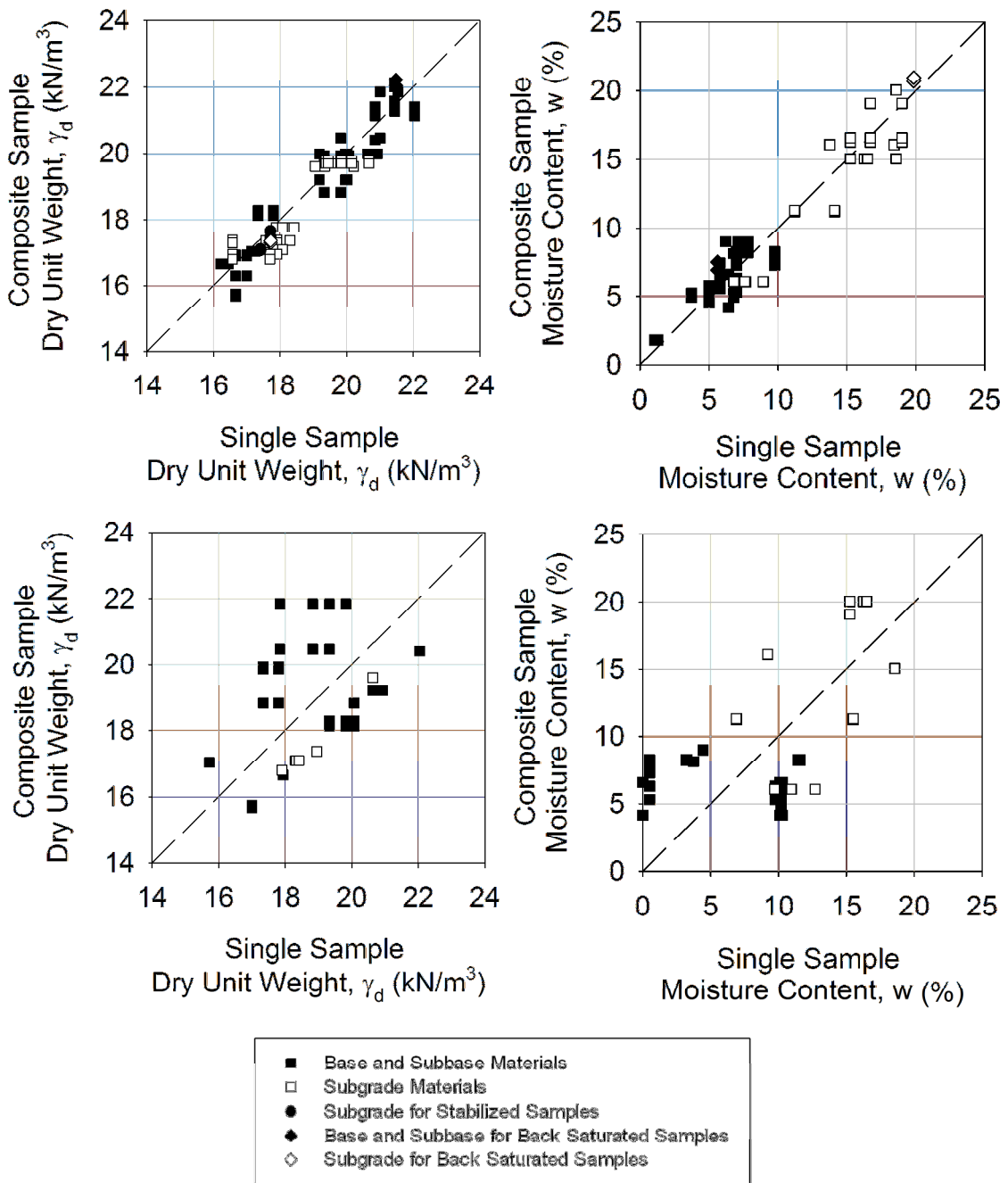
Figure 68. Composite and single material sample dry unit weight and moisture content variations meeting dry unit weight and moisture content criteria range (top) and varied beyond criteria range (bottom)

For most tests, composite material sample $M_{r(T307)}$ and permanent strain (ε_p) values were between the stiffer and weaker single material sample values. All single material back saturated samples had larger ε_p at the end of testing than non-back saturated samples. Only one composite material back saturated sample had a smaller ε_p at the end of testing than the corresponding non-back saturated sample.

Deviations from the expected outcomes are attributed to variations in the soil unit weight and moisture values. Large differences between single material and composite material $M_{r(T307)}$ values were from samples that had a large differences in unit weight and moisture contents.

Several samples were also used to investigate the differences in $M_{r(T307)}$ and ε_p values with and without a geosynthetic layer. The geosynthetic layer was a woven geofabric material from CSI Geoturf (Model W270), seen in Figure 69. Laboratory samples from Michigan I-96, Pennsylvania US-22, and Wisconsin US-10 were tested with the geofabric layer at the interface between the subbase and subgrade layers. Differences were seen in the $M_{r(T307)}$ values for the samples with and without the geofabric material, but these results were minor and could be caused by unit weight and moisture variations. Increases in stiffness from geosynthetic layers (typically geogrids but woven geofabrics can be applicable) are often obtained by laterally restraining the base or subbase (i.e., decreasing the shear stresses on the subgrade) (Christopher et al. 2006). In the small diameter samples used in this study, the geofabric layers did not experience high lateral stresses and were not restrained laterally. Nazzal et al. (2007) reported that, at a 95% confidence level, geogrid type and arrangement did not significantly improve the resilient modulus of a crushed limestone base material. Typically, geofabric layers are used as a separation layer to prevent aggregate-subgrade mixing and therefore loss of base or subbase thickness (Christopher et al. 2006). The results from this study further reinforce the idea that geofabric layers may not provide high resilient moduli increases for laboratory samples. Higher number of test cycles (e.g., 100,000 or greater) may be needed to fully evaluate the effects of geofabric on composite samples.
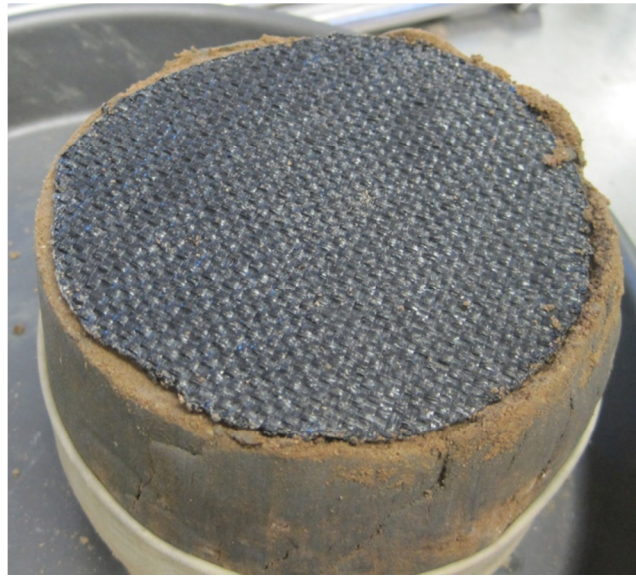
Figure 69. Woven geofabric on top of Michigan I-96 subgrade after completion

of composite material M_r test

Pennsylvania US-22, Pennsylvania US-422, and Iowa I-29 had samples that were stabilized with the addition of cement, high-density polyurethane foam, and fly ash, respectively. The sample results for these materials are discussed in further detail under the Stabilization Techniques section in this chapter but are included in this section for comparison to the other samples.

Some of the Pennsylvania US-22 composite material samples were made with a layer of cement treated base (CTB) over the class 2A subbase. The CTB is a porous material made from a large diameter, uniformly graded crushed limestone. Portland cement bonds the particles together into a stiff but pervious matrix. The CTB used in this study was made in the laboratory using a large box and coring a cylinder to a 101.6 mm (4.0 in.) diameter. The ends were trimmed flat so the sample was 101.6 mm (4.0 in.) tall. The resulting CTB over class 2A sample is shown in Figure 70.

Figure 70. Pennsylvania US-22 composite material sample of CTB over class

2A subbase after M$_r$ testing

Single and composite materials from Michigan I-94 are compared in Figure 71 and Table 29; Michigan I-96 are compared in Figure 72 and Table 30; Pennsylvania US-22 are compared in Figure 73 and Table 31; Pennsylvania US-422 are compared in Figure 74 and Table 32; Iowa I-29 are compared in Figure 75, Figure 76, Table 33, and Table 34; and Wisconsin US-10 are compared in Figure 77 and Table 35.
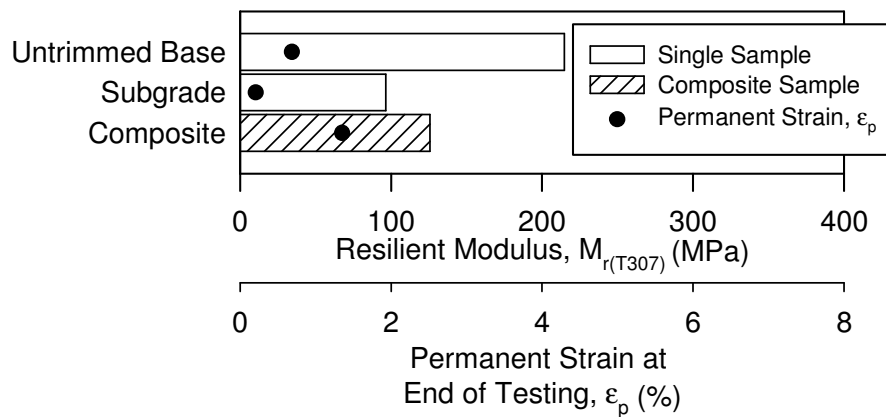
Figure 71. Comparison of single and composite samples of base and subgrade

M$_{r(T307)}$ values from Michigan I-94

Table 29. Michigan I-94 single and composite sample comparisons

Sample Description	Upper Layer Material		Lower Layer Material		$M_{r(T307)}$ (MPa)	ε_p (%)[§]
	γ_d (kN/m³)	w (%)	γ_d (kN/m³)	w (%)		
Untrimmed Base	16.45	1.3	—	—	214.7	0.69
Subgrade	—	—	17.58	18.4	96.6	0.21
Composite	16.65	1.6	17.37	15.6	125.8	1.35

[§] = at end of test per AASHTO T307 criteria
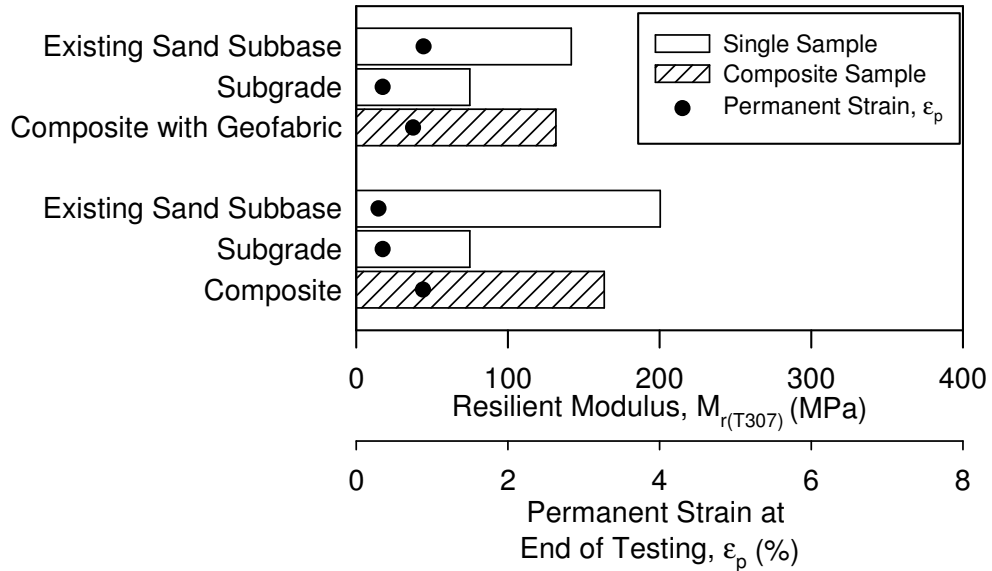
Figure 72. Comparison of single and composite samples of subbase and

subgrade $M_{r(T307)}$ values from Michigan I-96

Table 30. Michigan I-96 single and composite sample comparisons

Sample Description	Upper Layer Material		Lower Layer Material		$M_{r(T307)}$ (MPa)	ε_p (%)[§]
	γ_d (kN/m³)	w (%)	γ_d (kN/m³)	w (%)		
Existing Subbase Sand	19.18	7.1	—	—	141.9	0.89
Subgrade	—	—	19.84	8.9	75.0	0.35
Composite with Geofabric	19.19	6.1	19.69	9.0	131.7	0.75
Existing Subbase Sand	19.96	6.2	—	—	200.5	0.29
Subgrade	—	—	19.84	8.9	75.0	0.35
Composite with Geofabric	19.98	6.1	19.78	9.0	163.5	0.88

[§] = at end of test per AASHTO T307 criteria
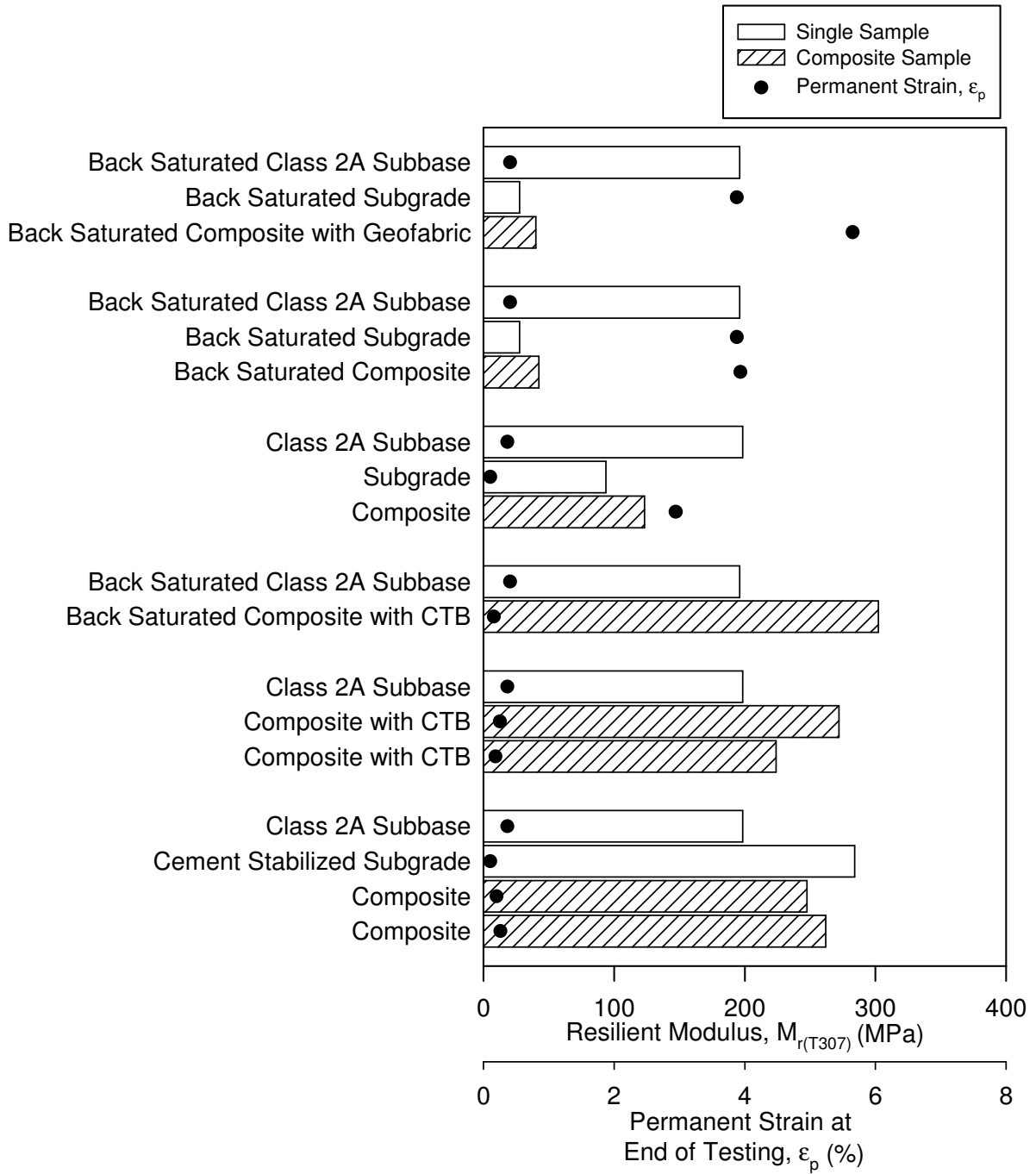
Figure 73. Comparison of single and composite samples of subbase and subgrade

$M_{r(T307)}$ **values from Pennsylvania US-22**

Table 31. Pennsylvania US-22 single and composite sample comparisons

Sample Description	Upper Layer Material		Lower Layer Material		$M_{r(T307)}$ (MPa)	ε_p (%)[§]
	γ_d (kN/m^3)	w (%)	γ_d (kN/m^3)	w (%)		
Back Saturated Class 2A Subbase	21.48	6.4	—	—	196.2	0.41
Back Saturated Subgrade	—	—	17.72	19.2	27.6	3.88
Back Saturated Composite with Geofabric	22.22	6.9	17.36	20.1	40.2	5.65
Back Saturated Class 2A Subbase	21.48	6.4	—	—	196.2	0.41
Back Saturated Subgrade	—	—	17.72	19.2	27.6	3.88
Back Saturated Composite	22.03	7.5	17.30	20.7	42.5	3.94
Class 2A Subbase	21.44	7.3	—	—	198.4	0.37
Subgrade			17.88	16.3	93.8	0.11
Composite	22.14	5.9	17.77	15.1	123.4	2.94
Back Saturated Class 2A Subbase	—	—	21.48	6.4	196.2	0.41
Back Saturated Composite with CTB	CTB	CTB	21.55	6.2	302.2	0.16
Class 2A Subbase	—	—	21.44	7.3	198.4	0.37
Composite with CTB	CTB	CTB	21.58	5.7	272.0	0.25
Composite with CTB	CTB	CTB	21.58	6.1	224.0	0.18
Class 2A Subbase	21.44	7.3	—	—	198.4	0.37
Cement Stabilized Subgrade	—	—	17.71	—	284.2	0.11
Composite	21.43	5.4	17.46	—	247.6	0.20
Composite	21.27	5.4	17.66	—	262.0	0.26

[§] = at end of test per AASHTO T307 criteria
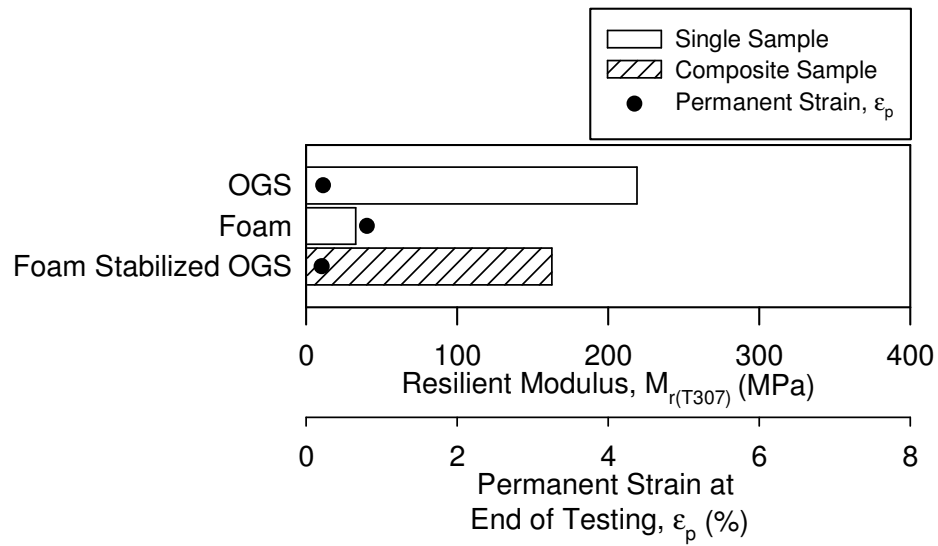
Figure 74. Comparison of single and composite samples of base and foam

$M_{r(T307)}$ values from Pennsylvania US-422

Table 32. Pennsylvania US-422 single and composite sample comparisons

Sample Description	Upper Layer Material		Lower Layer Material		$M_{r(T307)}$ (MPa)	ε_p (%)[§]
	γ_d (kN/m³)	w (%)	γ_d (kN/m³)	w (%)		
OGS	1.44	—	—	—	32.8	0.81
Foam	18.54	0.2	—	—	219.1	0.23
Foam and OGS	14.92	—	—	—	162.8	0.21

[§] = at end of test per AASHTO T307 criteria
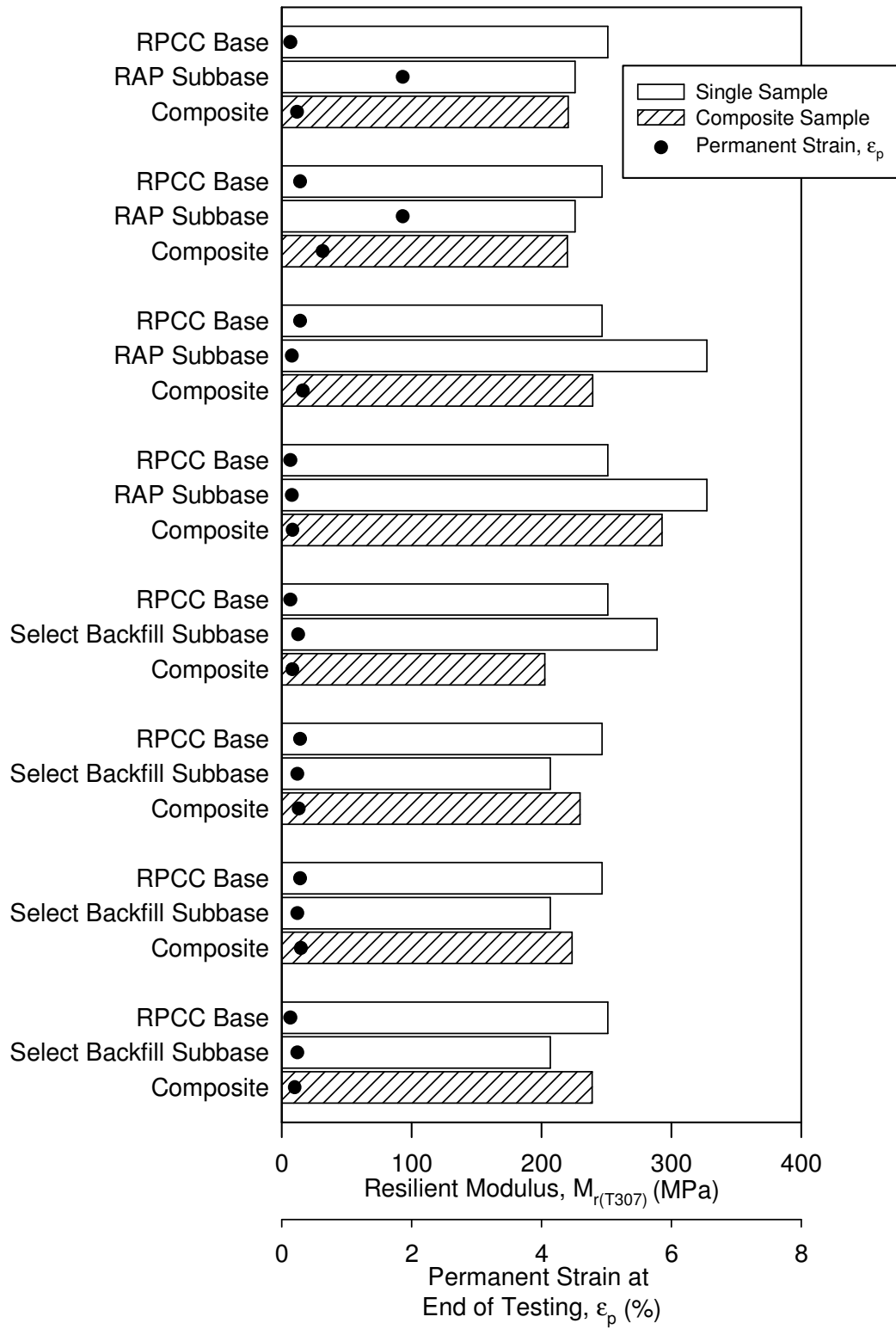
Figure 75. Comparison of single and composite samples of base and

subbase $M_{r(T307)}$ values from Iowa I-29

Table 33. Iowa I-29 single and composite sample comparisons

Sample Description	Upper Layer Material		Lower Layer Material		$M_{r(T307)}$ (MPa)	ε_p (%)[§]
	γ_d (kN/m³)	w (%)	γ_d (kN/m³)	w (%)		
RPCC Base	17.00	5.0	—	—	251.1	0.13
RAP Subbase	—	—	17.34	7.0	226.0	1.86
Composite	16.93	4.9	18.29	5.3	220.6	0.23
RPCC Base	15.86	5.3	—	—	246.7	0.29
RAP Subbase	—	—	17.34	7.0	226.0	1.86
Composite	15.67	5.0	18.12	6.3	219.9	0.63
RPCC Base	15.86	5.3	—	—	246.7	0.29
RAP Subbase	—	—	19.82	7.0	327.4	0.16
Composite	15.75	4.5	19.86	7.7	239.5	0.33
RPCC Base	17.00	5.0	—	—	251.1	0.13
RAP Subbase	—	—	19.82	7.0	327.4	0.16
Composite	16.93	4.9	19.94	7.3	292.9	0.17
RPCC Base	17.00	5.0	—	—	251.1	0.13
Select Backfill Subbase	—	—	21.87	3.6	289.1	0.25
Composite	16.92	5.7	21.41	4.9	202.7	0.16
RPCC Base	15.86	5.3	—	—	246.7	0.29
Select Backfill Subbase	—	—	20.75	4.3	206.8	0.24
Composite	15.73	5.3	20.41	5.0	229.6	0.26
RPCC Base	15.86	5.3	—	—	246.7	0.29
Select Backfill Subbase	—	—	20.75	4.3	206.8	0.24
Composite	15.67	5.7	21.35	5.2	223.6	0.29
RPCC Base	17.00	5.0	—	—	251.1	0.13
Select Backfill Subbase	—	—	20.75	4.3	206.8	0.24
Composite	16.90	5.8	20.41	4.9	239.0	0.20

[§] = at end of test per AASHTO T307 criteria
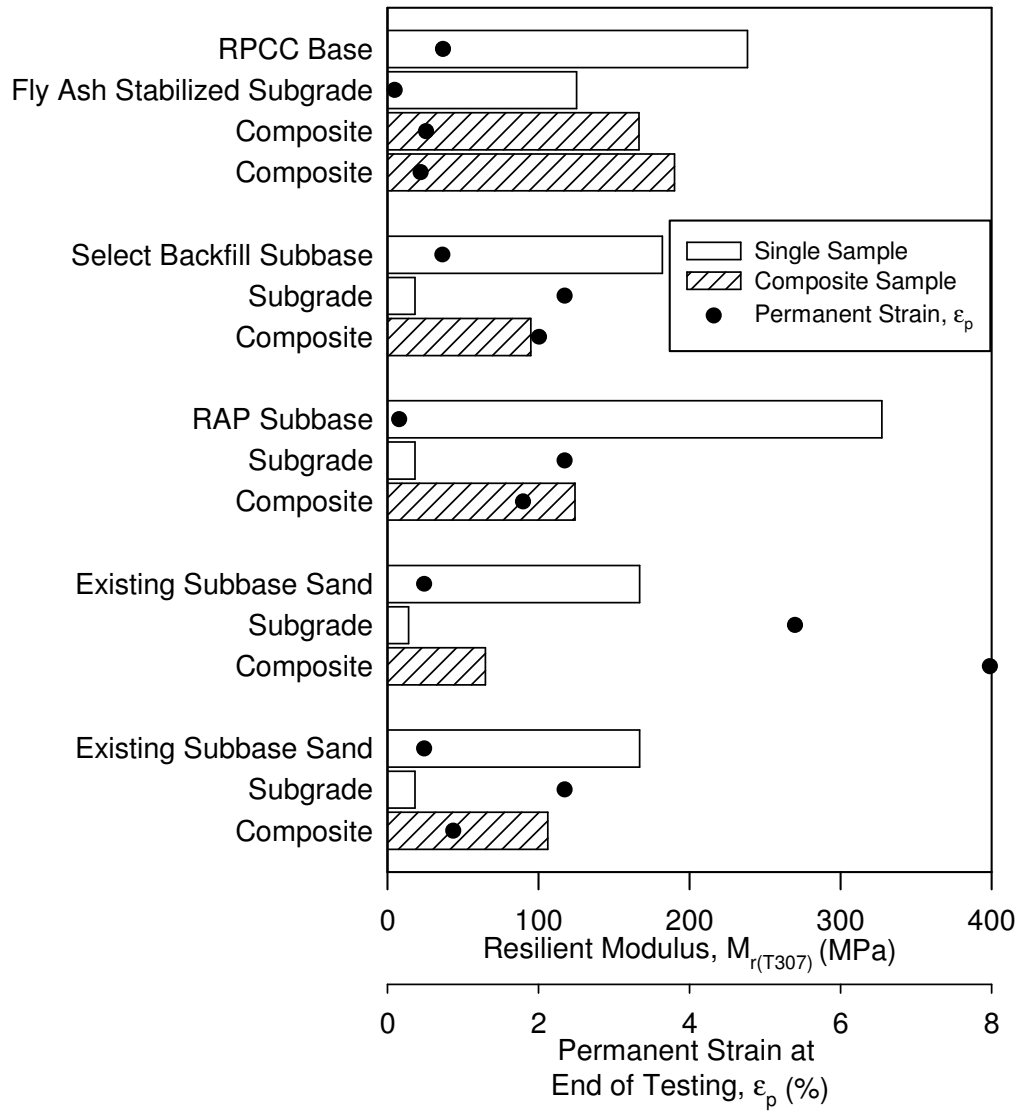
Figure 76. Comparison of single and composite samples of subbase and

subgrade $M_{r(T307)}$ values from Iowa I-29

Table 34. Iowa I-29 single and composite sample comparisons (con't)

Sample Description	Upper Layer Material		Lower Layer Material		$M_{r(T307)}$ (MPa)	ε_p (%)[§]
	γ_d (kN/m³)	w (%)	γ_d (kN/m³)	w (%)		
RPCC	16.85	8.0	—	—	238.4	0.74
Fly Ash Stabilized Subgrade	—	—	17.41	—	125.3	0.10
Composite	16.29	8.2	17.10	—	166.7	0.51
Composite	16.29	8.2	17.07	—	190.1	0.44
Select Backfill Subbase	21.89	9.9	—	—	182.0	0.73
Subgrade	—	—	17.69	16.7	18.2	2.35
Composite	21.13	8.1	17.39	16.3	95.0	2.01
RAP Subbase	19.82	7.0	—	—	327.4	0.16
Subgrade	—	—	17.69	16.7	18.2	2.35
Composite	18.82	8.3	17.29	16.6	124.2	1.80
Existing Sand Subbase	19.82	6.4	—	—	167.0	0.49
Subgrade	—	—	16.57	19.0	14.1	5.40
Composite	21.85	5.7	16.80	19.1	64.8	7.98
Existing Sand Subbase	19.82	6.4	—	—	167.0	0.49
Subgrade	—	—	17.69	16.7	18.2	2.35
Composite	20.46	6.6	16.95	16.5	106.2	0.87

[§] = at end of test per AASHTO T307 criteria
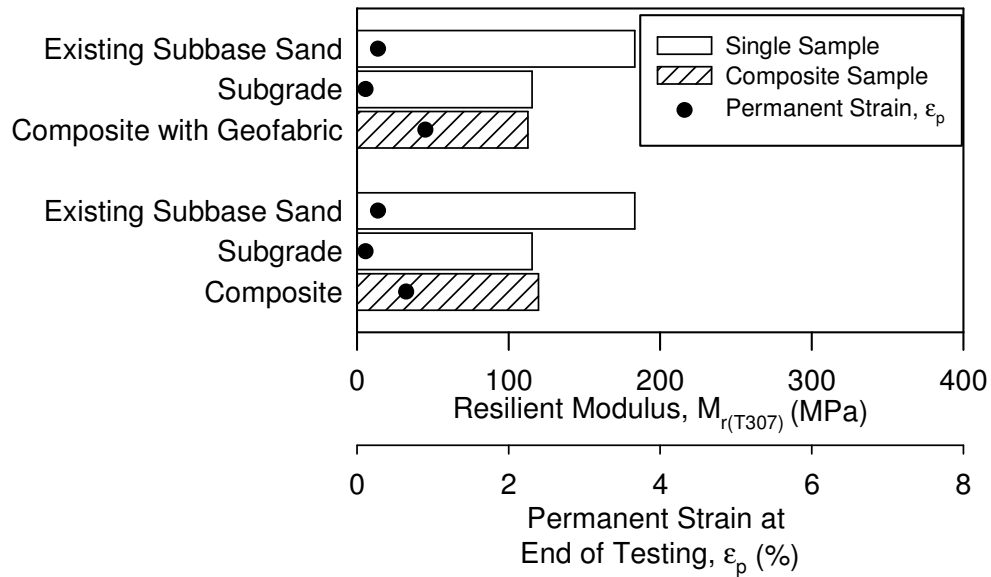
Figure 77. Comparison of single and composite samples of subbase and

subgrade $M_{r(T307)}$ values from Wisconsin US-10

Table 35. Wisconsin US-10 single and composite sample comparisons

Sample Description	Upper Layer Material		Lower Layer Material		$M_{r(T307)}$ (MPa)	ε_p (%)[§]
	γ_d (kN/m^3)	w (%)	γ_d (kN/m^3)	w (%)		
Existing Subbase Sand	17.25	7.8	—	—	183.3	0.28
Subgrade	—	—	20.21	12.1	115.5	0.12
Composite with Geofabric	17.04	8.2	19.60	11.3	119.8	0.65
Existing Subbase Sand	17.25	7.8	—	—	183.3	0.28
Subgrade	—	—	20.21	12.1	115.5	0.12
Composite with Geofabric	17.04	8.3	19.60	11.2	112.9	0.90

[§] = at end of test per AASHTO T307 criteria

Base and subbase materials tended to have lower composite sample $M_{r(T307)}$ values and higher single sample $M_{r(T307)}$ values. Subgrade materials tended to be have higher composite sample $M_{r(T307)}$ values and lower single sample $M_{r(T307)}$ values. These trends indicate that layering of materials affects composite $M_{r(T307)}$ values. Layering materials increases composite characteristics of weak soil layers. Stiff materials in upper layers increase the

moduli of weak material in lower layers. The resilient moduli of single materials would need to be corrected to account for the composite behavior. The MEPDG (NCHRP 2004b) recognized the layering effect as a consideration for structural design of pavement layers and stated that composite behavior is commonly somewhere between the two extremes of stiff granular behavior and soft subgrade behavior.

The composite reaction depends on the relative moduli differences between the soil layers and thickness of the granular layer. Christopher et al. (2006) suggested that weak lower natural soil layers could be improved with the use of granular upper layers (e.g., increase the support capacity, provide uniform support over highly variable soil conditions, etc.). Additionally, Christopher et al. (2006) stated that granular base contribution to the overall structural capacity could be as high as 50% for low subgrade CBR values or nearly zero for high subgrade CBR values.

Changes in resilient moduli for stabilized and back saturated samples were marked by dotted lines. Some Iowa I-29 and Pennsylvania US-22 subgrade samples were stabilized with Class C fly ash and portland cement, respectively. However, Iowa I-29 fly ash-stabilized composite samples did not correspond to any unstabilized samples. Dotted lines link stabilized Pennsylvania samples to corresponding unstabilized samples. Composite fly ash stabilized samples experienced a 100–112% increase in $M_{r(T307)}$ values compared to unstabilized composite samples, after a seven day oven cure. Subgrade samples stabilized with 10% cement by dry unit weight experienced a 203% increase in $M_{r(T307)}$ values compared to unstabilized subgrade samples. Subgrades samples stabilized with 15% fly ash by dry unit weight experienced a 588% increase in $M_{r(T307)}$ values compared to unstabilized subgrade samples.

Another dotted line links a back saturated Pennsylvania subgrade sample to a corresponding partially saturated sample. The partially saturated single material sample had an increase in resilient modulus by nearly four times. The partially saturated composite material $M_{r(T307)}$ value increased by approximately 5% over the back saturated sample.

Overall, stabilized and back saturated samples indicate that composite material $M_{r(T307)}$ values are influenced by weak subgrades. Increasing the M_r values of subgrades increases the M_r values of composite samples. Statistical analyses to quantify the significance of weak

lower layer materials are discussed below. Single and composite $M_{r(T307)}$ values were compared in Figure 78.
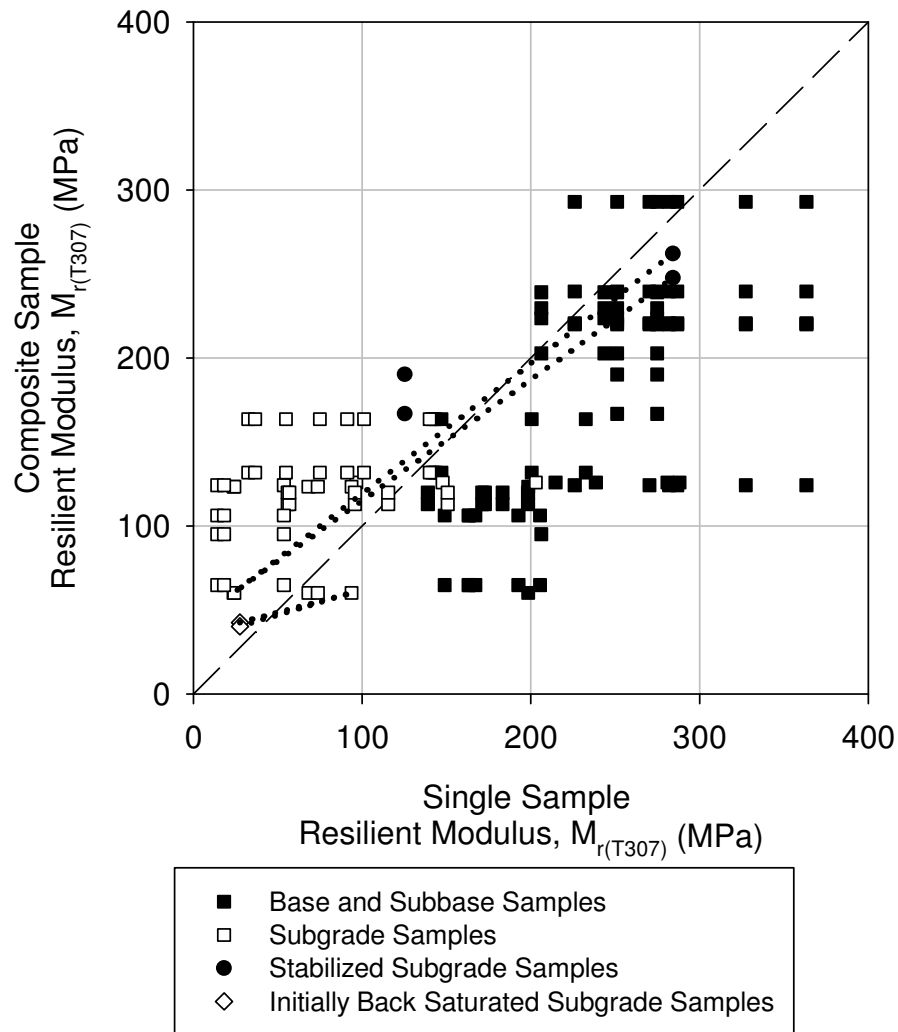
Figure 78. Comparison of average composite $M_{r(T307)}$ and corresponding single base, subbase, and subgrade average $M_{r(T307)}$ values

Statistical analyses

Statistical analysis software was used to investigate the effects of 1) the resilient moduli of each layer in composite material samples, and 2) moisture content, dry unit weight, and layering on composite material resilient moduli values. Single material samples were compared to composite material samples to determine if the different variables had a significant effect on the resilient moduli. Additionally, corrections for moisture content

differences were performed on single material $M_{r(T307)}$ values and compared to composite material $M_{r(T307)}$ values.

When performing statistical analyses, considerations must be made if a variable did not vary quantitatively (i.e., the tested dry unit weight or moisture content ranges were very small). A limitation of this study was that few experiments were set up to investigate the effects of variables over a broad range of values. Additionally, the low number of specimens with corresponding materials made comparisons between the specimens difficult to broadly interpret.

The t ratio indicates relative significance, and the p-value indicates the global significance of a parameter. When t ratios had absolute values greater than two, they were considered relatively significant. Between variables in the same dataset, larger absolute values indicate higher relative significance. Variables were considered significant in explaining the variation in resilient moduli if the p-value (prob>|t|) was less than 0.05. If the p-value was between 0.05 and 0.10, the variable was considered possibly significant. All other p-values were considered not significant.

Depending on the number of tested samples, some analyses investigated many of the variables together, while other analyses (with fewer samples and therefore fewer degrees of freedom) were only able to investigate a few variables together.

If a variable had very low p-values or t ratios, that variable was considered insignificant. By being an insignificant variable, the value might have masked the significance of the other variables. The variable was removed from the analysis and another analysis was performed on the remaining variables.

Resilient moduli of layers

Statistical analyses were performed on composite samples (i.e., base over subgrade, base over subbase, and subbase over subgrade) to determine if a layer was significant in explaining the variation in composite $M_{r(T307)}$ values.

Single material $M_{r(T307)}$ values corresponded to composite material sample layers when dry unit weights were within ±1.0 kN/m^3 and moisture contents were within $\pm3\%$. Chemically stabilized materials (i.e., fly ash-treated or cement-treated subgrades) were not included. The analyzed materials are provided in Table 29 through Table 35. Most composite

material samples were fabricated as a stiff layer over a soft layer. Only three composite material samples were fabricated as a soft layer over a stiff layer.

Overall, lower layers were significant in explaining the variation in $M_{r(T307)}$ values, but upper layers were not significant. In this study, lower layers were most often weaker layers. Therefore, characterizing weak lower layers is critical to determining the composite behavior of pavement foundations. The results of the statistical analyses for composite material resilient moduli layers are summarized in Table 36.

Table 36. Statistical analysis results for composite material resilient moduli layers

Layer Location	Parameter Estimate	Standard Error	t ratio	Prob>|t|	Significant?
Intercept	18.777	37.058	0.51	0.6189	No
Upper Layer	0.2844	0.1865	1.52	0.1457	No
Lower Layer	0.5552	0.0755	7.35	<0.0001	Yes

Moisture content, unit weight, layering

It is well documented that resilient moduli are influenced by moisture content, dry unit weight, and back saturation conditions (Alam et al. 2010; Drumm et al. 1997; Seed et al. 1962; Southgate and Mahboub 1994), but layering and sample disturbance also affect the resilient moduli. Layering refers to whether the sample was fabricated from two materials or a single material. Disturbance refers to subgrade samples and whether the material was undisturbed (i.e., Shelby tube sample) or remolded in the laboratory. Frost et al. (2004) found that remolding soil had increased resilient moduli possibly from the collapse of fissures found in natural soils or from the effects of compaction and shearing the overconsolidated material.

Overall, large variances in moisture and unit weight values between specimens tended to cause the variables to be significant in explaining the variation in resilient moduli. As expected, layering was a significant variable in many analyses for both granular and cohesive materials. Many times, variables had smaller p-values when combined with other variables. This indicated that combinations of variables are important factors when judging significance and therefore other multiple variables affected the resilient moduli values. Statistical analyses for each of the sites are summarized in Table 37 through Table 43.

Table 37. Summary of statistical analysis for Michigan I-94 materials

Site	Specimen #1	Specimen #2	Variable	t Ratio	Prob>|t|	Significant Y/N	Notes
MI I-94	Untrimmed Base	Untrimmed Base/ Subgrade	w%	0.14	0.9113	N	n_1= 4, n_2 = 1 $w\%_1$ = 0.9–1.4 $w\%_2$ = 1.6 γ_{d1} = 13.63–17.93 γ_{d2} = 16.65
			γ_d	0.01	0.9454	N	
			Layering	1.09	0.4727	N	
	Untrimmed Base	Untrimmed Base/ Subgrade	Layering	3.32	0.045	Y	
	Subgrade	Untrimmed Base/ Subgrade	w%	0.56	0.6756	N	n_1= 3, n_2 = 1 $w\%_1$ = 9.2–18.4 $w\%_2$ = 15.0 γ_{d1} = 17.58–18.85 γ_{d2} = 17.37
	Subgrade	Untrimmed Base/ Subgrade	Layering	0.17	0.8937	N	
	Subgrade	Untrimmed Base/ Subgrade	γ_d	19.11	0.0333	Y	
	Subgrade	Untrimmed Base/ Subgrade	Layering	-8.04	0.0787	Possibly	
	Subgrade	Untrimmed Base/ Subgrade	Layering	0.38	0.741	N	

w% = moisture content (%);
γ_d = dry unit weight (kN/m^3);
n_1 = number of tests on specimen #1; and
n_2 = number of tests on specimen #2.

Table 38. Summary of statistical analysis for Michigan I-96 materials

Site	Specimen #1	Specimen #2	Variable	t Ratio	Prob>|t|	Significant Y/N	Notes
MI I-96	Sand	Sand/ Subgrade	w%	-3.56	0.0378	Y	$n_1 = 5$, $n_2 = 2$ $w\%_1 = 4.4–7.8$ $w\%_2 = 9.0$ $\gamma_{d1} = 19.18–20.92$ $\gamma_{d2} = 19.23–19.98$
			γ_d	0.81	0.4748	N	
			Layering	-2.11	0.125	Y	
	Sand	Sand/ Subgrade	w%	-4.76	0.0089	Y	
			Layering	-2.27	0.0862	Possibly	
	Sand	Sand/ Subgrade	w%	-3.38	0.0197	Y	
	Sand	Sand/ Subgrade	Layering	0.79	0.4635	N	
	Sand	Sand/Geo/ Subgrade	Layering	0.21	0.8435	N	$n_1 = 5$, $n_2 = 1$ $w\%_1 = 4.4–7.8$ $w\%_2 = 9.0$ $\gamma_{d1} = 19.18–20.92$ $\gamma_{d2} = 19.23–19.98$
	Subgrade	Sand/ Subgrade	w%	-4.18	0.0139	Y	$n_1 = 6$, $n_2 = 2$ $w\%_1 = 6.8–12.1$ $w\%_2 = 6.1–8.7$ $\gamma_{d1} = 19.38–20.66$ $\gamma_{d2} = 19.68–19.78$
			γ_d	0.87	0.4316	N	
			Layering	-2.73	0.0527	Y	
	Subgrade	Sand/ Subgrade	w%	-4.40	0.0070	Y	
			Layering	-2.76	0.0397	Y	
	Subgrade	Sand/ Subgrade	w%	-5.60	0.0014	Y	
	Subgrade	Sand/ Subgrade	Layering	-3.66	0.0106	Y	
	Subgrade	Sand/Geo/ Subgrade	Layering	-3.19	0.0242	Y	$n_1 = 6$, $n_2 = 1$ $w\%_1 = 6.8–12.1$ $w\%_2 = 6.1–8.7$ $\gamma_{d1} = 19.38–20.66$ $\gamma_{d2} = 19.68–19.78$
	Subgrade	Shelby Tube	w%	-5.64	0.0049	Y	$n_1 = 6$, $n_2 = 2$ $w\%_1 = 6.8–12.1$ $w\%_2 = 16.2–17.2$ $\gamma_{d1} = 19.23–19.98$ $\gamma_{d2} = 18.03–18.52$
			γ_d	0.62	0.5664	N	
			Dist	-2.64	0.0576	Possibly	
	Subgrade	Shelby Tube	w%	-6.21	0.0016	Y	
			Dist	-3.32	0.021	Y	
	Subgrade	Shelby Tube	Dist	1.61	0.1591	N	

w% = moisture content (%);
γ_d = dry unit weight (kN/m^3);
n_1 = number of tests on specimen #1;
n_2 = number of tests on specimen #2; and
Dist = disturbance (i.e., undisturbed versus remolded).

Table 39. Summary of statistical analysis for Pennsylvania US-22 materials

Site	Specimen #1	Specimen #2	Variable	t Ratio	Prob>|t|	Significant Y/N	Notes
PA US-22	Class 2A Subbase	2A Subbase/ Subgrade	Layering	1.95	0.3023	N	$n_1= 1$, $n_2 = 2$ $w\%_1 = 7.3$ $w\%_2 = 5.9$–7.4 $\gamma_{d1} = 21.44$ $\gamma_{d2} = 22.00$–22.14
	Subgrade	2A Subbase/ Subgrade	w%	-5.31	0.013	Y	$n_1= 5$, $n_2 = 2$ $w\%_1 = 15.3$–18.6 $w\%_2 = 15.6$–20.1 $\gamma_{d1} = 17.88$–18.41 $\gamma_{d2} = 17.09$–17.77
			γ_d	0.58	0.6038	N	
			Layering	2.25	0.1104	N	
	Subgrade	2A Subbase/ Subgrade	Layering	-1.21	0.2796	N	
	Subgrade	2A Subbase/ Geo/ Subgrade	Layering	-1.94	0.1246	N	$n_1= 5$, $n_2 = 1$ $w\%_1 = 15.3$–18.6 $w\%_2 = 15.6$–20.1 $\gamma_{d1} = 17.88$–18.41 $\gamma_{d2} = 17.09$–17.77
	2A Subbase/ Subgrade - Back Saturated	2A Subbase/ Subgrade	Saturation	-1.59	0.2525	N	$n_1= 2$, $n_2 = 2$
	Subgrade	Subgrade - Back Saturated	Saturation	0.85	0.4433	N	$n_1= 5$, $n_2 = 1$ $w\%_1 = 15.3$–18.6 $w\%_2 = 19.2$ $\gamma_{d1} = 17.88$–18.41 $\gamma_{d2} =17.72$

w% = moisture content (%);
γ_d = dry unit weight (kN/m^3);
n_1 = number of tests on specimen #1; and
n_2 = number of tests on specimen #2.

Table 40. Summary of statistical analysis for Iowa I-29 materials

Site	Specimen #1	Specimen #2	Variable	t Ratio	Prob>|t|	Significant Y/N	Notes
IA I-29	RPCC Base	RPCC Base/ Select Backfill Subbase	w%	0.42	0.6901	N	n_1= 5, n_2 = 4 $w\%_1$ = 5.0–10.2 $w\%_2$ = 5.3–5.8 γ_{d1} = 15.86–17.03 γ_{d2} = 15.67–16.92
			γ_d	-0.09	0.9339	N	
			Layering	2.30	0.0701	Possibly	
	RPCC Base	RPCC Base/ Select Backfill Subbase	w%	0.45	0.6652	N	
			Layering	2.58	0.0416	Y	
	Select Backfill Subbase	RPCC Base/ Select Backfill Subbase	w%	-2.61	0.0309	Y	n_1= 8, n_2 = 4 $w\%_1$ = 3.6–9.9 $w\%_2$ = 4.9–5.2 γ_{d1} = 20.61–22.49 γ_{d2} = 20.41–21.41
			γ_d	1.9	0.09	Possibly	
			Layering	-0.24	0.8188	N	
	Select Backfill Subbase	RPCC Base/ Select Backfill Subbase	w%	-1.6	0.1412	N	
	Select Backfill Subbase	RPCC Base/ Select Backfill Subbase	Layering	0.21	0.837	N	
	RPCC Base	RPCC Base/ RAP Subbase	w%	0.19	0.8533	N	n_1= 5, n_2 = 4 $w\%_1$ = 5.0–10.2 $w\%_2$ = 4.5–5.0 γ_{d1} = 15.86–17.03 γ_{d2} = 15.67–16.93
			γ_d	0.91	0.4065	N	
			Layering	0.27	0.7952	N	
	RPCC Base	RPCC Base/ RAP Subbase	Layering	0.8	0.4485	N	
	RAP Subbase	RPCC Base/ RAP Subbase	w%	1.28	0.2466	N	n_1= 6, n_2 = 4 $w\%_1$ = 0.5–9.8 $w\%_2$ = 5.3–7.7 γ_{d1} = 17.34–20.07 γ_{d2} = 18.12–19.94
			γ_d	2.91	0.027	Y	
			Layering	3.15	0.0197	Y	
	RAP Subbase	RPCC Base/ RAP Subbase	γ_d	2.68	0.0314	Y	
			Layering	2.86	0.0244	Y	
	RAP Subbase	RPCC Base/ RAP Subbase	Layering	1.78	0.1135	N	

w% = moisture content (%);
γ_d = dry unit weight (kN/m^3);
n_1 = number of tests on specimen #1; and
n_2 = number of tests on specimen #2.

Table 41. Summary of statistical analysis for Iowa I-29 materials (con't)

Site	Specimen #1	Specimen #2	Variable	t Ratio	Prob>|t|	Significant Y/N	Notes
IA I-29	Select Backfill Subbase	Select Backfill Subbase/ Subgrade	w%	-4.57	0.006	Y	
			γ_d	4.00	0.0103	Y	
			Layering	2.85	0.0359	Y	
	Select Backfill Subbase	Select Backfill Subbase/ Subgrade	w%	-1.40	0.2124	N	$n_1 = 8, n_2 = 1$ $w\%_1 = 3.6$–9.9 $w\%_2 = 8.1$ $\gamma_{d1} = 20.61$–22.49 $\gamma_{d2} = 21.13$
			Layering	2.92	0.0265	Y	
	Select Backfill Subbase	Select Backfill Subbase/ Subgrade	γ_d	0.67	0.5279	Y	
			Layering	3.05	0.0224	Y	
	Select Backfill Subbase	Select Backfill Subbase/ Subgrade	Layering	3.41	0.0114	Y	

w% = moisture content (%);
γ_d = dry unit weight (kN/m^3);
n_1 = number of tests on specimen #1; and
n_2 = number of tests on specimen #2.

142

Table 42. Summary of statistical analysis for Iowa I-29 materials (con't)

Site	Specimen #1	Specimen #2	Variable	t Ratio	Prob>|t|	Significant Y/N	Notes
IA I-29	Subgrade	Select Backfill Subbase/ Subgrade	w%	-1.6	0.356	N	
			Layering	0.35	0.7866	N	
	Subgrade	Select Backfill Subbase/ Subgrade	γ_d	0.96	0.5127	N	$n_1= 3$, $n_2 = 1$ $w\%_1 = 15.3–19.0$ $w\%_2 = 16.3$ $\gamma_{d1} = 16.57–17.91$ $\gamma_{d2} = 17.39$
			Layering	0.14	0.9086	N	
	Subgrade	Select Backfill Subbase/ Subgrade	Layering	-2.65	0.118	N	
	Sand Subbase	Sand Subbase/ Subgrade	w%	-1.47	0.2145	N	$n_1= 6$, $n_2 = 2$ $w\%_1 = 0.0–9.4$ $w\%_2 = 6.6–7.2$ $\gamma_{d1} = 19.84–21.53$ $\gamma_{d2} = 20.64–21.85$
			γ_d	-0.46	0.6707	N	
			Layering	4.82	0.0085	Y	
	Sand Subbase	Sand Subbase/ Subgrade	Layering	4.74	0.0032	Y	
	Subgrade	Sand Subbase/ Subgrade	w%	-9.27	0.0684	Possibly	
			γ_d	-8.37	0.0757	Possibly	
			Layering	3.17	0.1948	N	$n_1= 3$, $n_2 = 2$ $w\%_1 = 15.3–19.0$ $w\%_2 = 16.5–19.1$ $\gamma_{d1} = 16.57–17.91$ $\gamma_{d2} = 16.80–16.95$
	Subgrade	Sand Subbase/ Subgrade	w%	-0.70	0.5587	N	
			Layering	0.16	0.89	N	
	Subgrade	Sand Subbase/ Subgrade	γ_d	-0.17	0.8788	N	
			Layering	-0.84	0.4895	N	
	Subgrade	Sand Subbase/ Subgrade	Layering	-2.54	0.0845	Possibly	

w% = moisture content (%);
γ_d = dry unit weight (kN/m^3);
n_1 = number of tests on specimen #1; and
n_2 = number of tests on specimen #2.

Table 43. Summary of statistical analysis for Wisconsin US-10 materials

Site	Specimen #1	Specimen #2	Variable	t Ratio	Prob>|t|	Significant Y/N	Notes
WI US-10	Sand Subbase	Sand Subbase/ Subgrade	w%	0.51	0.6469	N	$n_1 = 5$, $n_2 = 2$ $w\%_1 = 2.8–11.6$ $w\%_2 = 8.2–8.3$ $\gamma_{d1} = 15.72–17.81$ $\gamma_{d2} = 17.04$
			γ_d	5.08	0.0147	Y	
			Layering	10.12	0.0021	Y	
	Sand Subbase	Sand Subbase/ Subgrade	γ_d	7.14	0.002	Y	
			Layering	11.42	0.0003	Y	
	Subgrade	Sand Subbase/ Subgrade	w%	-3.01	0.057	Possibly	$n_1 = 5$, $n_2 = 2$ $w\%_1 = 6.9–15.5$ $w\%_2 = 11.2–11.3$ $\gamma_{d1} = 19.06–20.63$ $\gamma_{d2} = 19.6$
			γ_d	5.65	0.011	Y	
			Layering	-3.64	0.0359	Y	
	Subgrade	Sand Subbase/ Subgrade	w%	-2.46	0.0694	Possibly	
			Layering	-1.00	0.3727	N	
	Subgrade	Sand Subbase/ Subgrade	γ_d	5.01	0.0074	Y	
			Layering	-2.21	0.0913	Possibly	
	Subgrade	Sand Subbase/ Subgrade	Layering	-0.71	0.5109	N	

w% = moisture content (%);
γ_d = dry unit weight (kN/m^3);
n_1 = number of tests on specimen #1; and
n_2 = number of tests on specimen #2.

Moisture correction

Moisture is known to influence the resilient modulus values, especially for cohesive materials (Seed et al. 1962). Linear regression analyses were performed on granular and cohesive samples to obtain a constant multiplier for moisture content as a function of resilient modulus. Single sample resilient moduli were then altered by Equation 21.

$$\text{Corrected } M_{r(Single)} = M_{r(Single)} + \Gamma\left(w_{Composite} - w_{Single}\right) \tag{21}$$

where: Corrected $M_{r(Single)}$ = single sample resilient modulus corrected to composite sample moisture content;

$M_{r(Single)}$ = single sample resilient modulus;

Γ = linear regression constant multiplier (See Table 44);

$w_{Comosite}$ = composite sample moisture content; and

w_{Single} = single sample moisture content.

Table 44. Moisture content linear regression results to obtain Γ

Material Type	Parameter Estimate, Γ value (%)	Standard Error	t ratio	Prob>|t|	Significant?
Cohesive	-5.674	1.932	-2.94	0.0076	Yes
Granular	-4.385	2.122	-2.07	0.0452	Yes

Corrected M_r values only apply to the base, subbase, and subgrade samples. There was a slight change in the corrected single sample $M_{r(T307)}$ values for cohesive materials. The minimal change makes sense because most single material samples had moisture contents that were close to the composite material samples. A larger shift in $M_{r(T307)}$ values occurred with the granular samples. There was less scatter at higher $M_{r(T307)}$ values after correcting for moisture content. The overall trend for both types of materials, however, stayed the same—granular materials had higher single material $M_{r(T307)}$ values than composite values and cohesive materials had lower single material $M_{r(T307)}$ values than composite values. Comparisons between composite sample $M_{r(T307)}$ values and single sample $M_{r(T307)}$ values corrected for the composite sample moisture contents are seen in Figure 79.
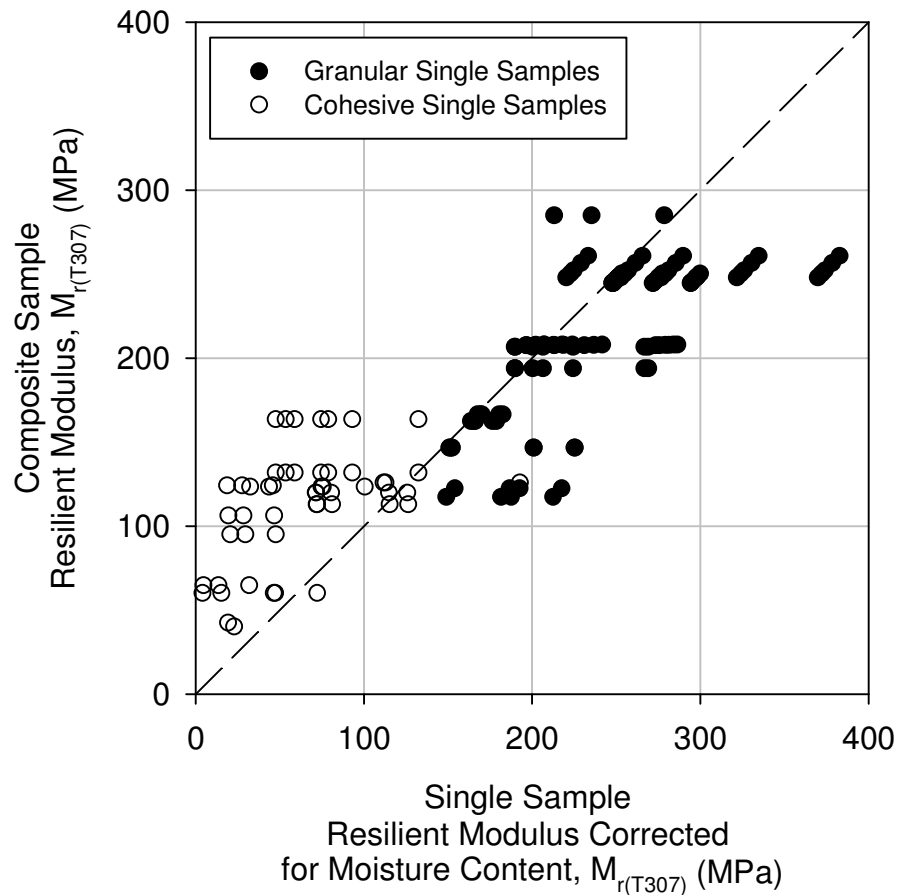
Figure 79. Comparison of average composite $M_{r(T307)}$ and corresponding single

granular and cohesive average $M_{r(T307)}$ values corrected for moisture content

Material index property correlations

The compared index properties included gradation, Atterberg limits, undrained shear strength, dry unit weight-moisture content ratio, and degree of saturation. These index properties were chosen because they are widely used and easily determined. The comparisons between these index properties and resilient moduli are only valid over the range of materials tested.

A general trend is seen for the percent passing No. 200 sieve and percent passing No. 4 sieve. As expected, higher fines content tends to reduce the resilient moduli. Hicks (1971) also determined that lower fines content tends to increase resilient moduli. Fines content is related to cohesive material, and an increase in cohesive material reduces the resilient

moduli. There was no distinct trend between coefficient of uniformity (c_u) and coefficient of curvature (c_c) values compared with resilient moduli.

There was also no clear link between the Atterberg limits and resilient moduli. Atterberg limits are used to classify soils using ranges of moisture content. Nazzal and Mohammad (2010) found that the liquid limit (LL) and plasticity index (PI) of clay soils were influential variables in the regression coefficient models when combined with other factors including percent passing the No. 200 sieve, maximum dry unit weight, and a moisture content variable. Although the data in this study did not have a trend for PI and LL individually, the inclusion of other variables may help describe the resilient behavior.

The strongest relationships involve several index properties that directly influence the resilient moduli, such as the undrained shear strength and dry unit weight-moisture content ratio. The undrained shear strength (s_u) was graphed according to 1) the ultimate s_u or s_u at 5% vertical strain (ε_v)—whichever occurred first—and 2) s_u at 1% ε_a ($s_{u1\%}$). The s_u value was determined from quick shear test data after the end of the resilient modulus procedure, according to AASHTO T307. Lee et al. (1997) observed that M_r and $s_{u1\%}$ were correlated to moisture content. A nonlinear curve between M_r and $s_{u1\%}$ data showed a strong coefficient of determination for three soils used in the study (Lee et al. 1997). Thompson and Robnett (1979) also found strong positive correlations between M_r and static stress-strain data— through unconfined compressive strength and static modulus, for fine-grained soils. In this study, granular materials had more scatter than the cohesive materials. The scatter was most likely a result of confining stress dependency for the granular materials. The cohesive materials are more dependant on deviator stress than confining stress. Additionally, for most of the tests performed, the granular materials had higher $M_{r(T307)}$ and s_u values than the cohesive materials.

A comparison that was described in the literature (Mohammad et al. 2008) was M_r versus dry unit weight-moisture content ratio. Four points with high dry unit weight-moisture content ratio values were untrimmed base from Michigan I-94 that had very low moisture contents (about 1%). The low moisture contents contributed to the higher dry unit weight-moisture content ratio values. Cohesive materials had less scatter than granular materials for the dry unit weight-moisture content ratio and $M_{r(T307)}$ relationships. In situ cohesive soils are

rarely dry, so it is expected for the dry unit weight-moisture content ratio to be lower than granular materials. In situ granular materials can have moisture contents that range from very dry to almost saturated. The positive relationship between dry unit weight-moisture content ratio and single sample $M_{r(T307)}$ is expected because as dry unit weight increases and moisture content decreases, samples tend to become stiffer. The ratio is a possible way to view the relationships between cohesive and granular samples together. Degree of saturation is another way to view this relationship. An increase in the degree of saturation relates to decreasing unit weight and increasing moisture. Therefore, an increase in the degree of saturation corresponds to decreasing $M_{r(T307)}$ values.

These methods provide general relationships to quickly assess resilient moduli from common laboratory tests. Better relationships might be developed by investigating the individual materials more closely. The benefit to plotting the results from several types of materials from across the country is the ability to see widespread trends that provide a basic idea of how the materials will behave under different conditions. Figure 80 and Figure 81 summarize the relationships between several soil gradation properties and index properties, respectively, as functions of $M_{r(T307)}$ values for single material samples.
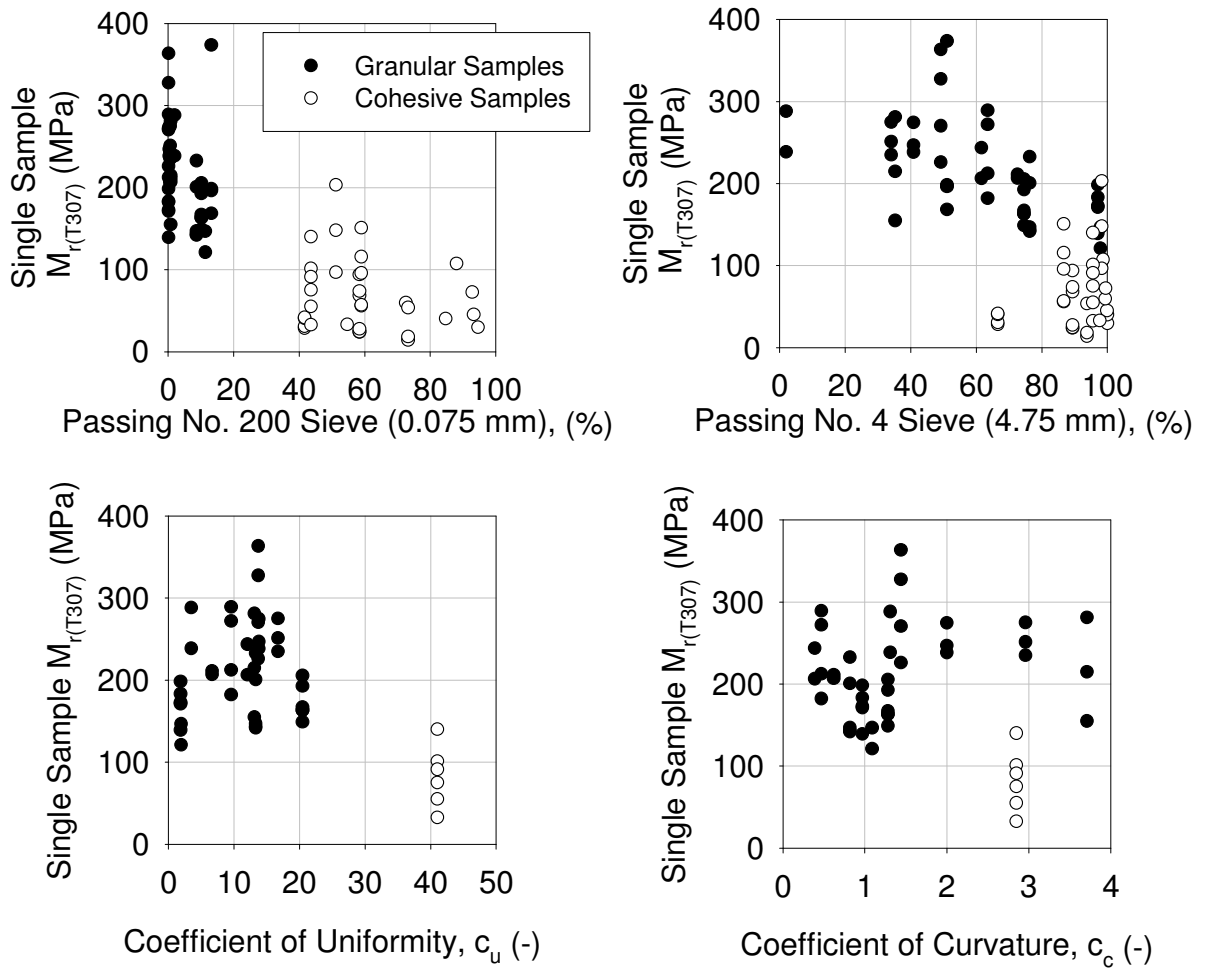
Figure 80. Summary of gradation properties as functions of average resilient moduli for single material samples
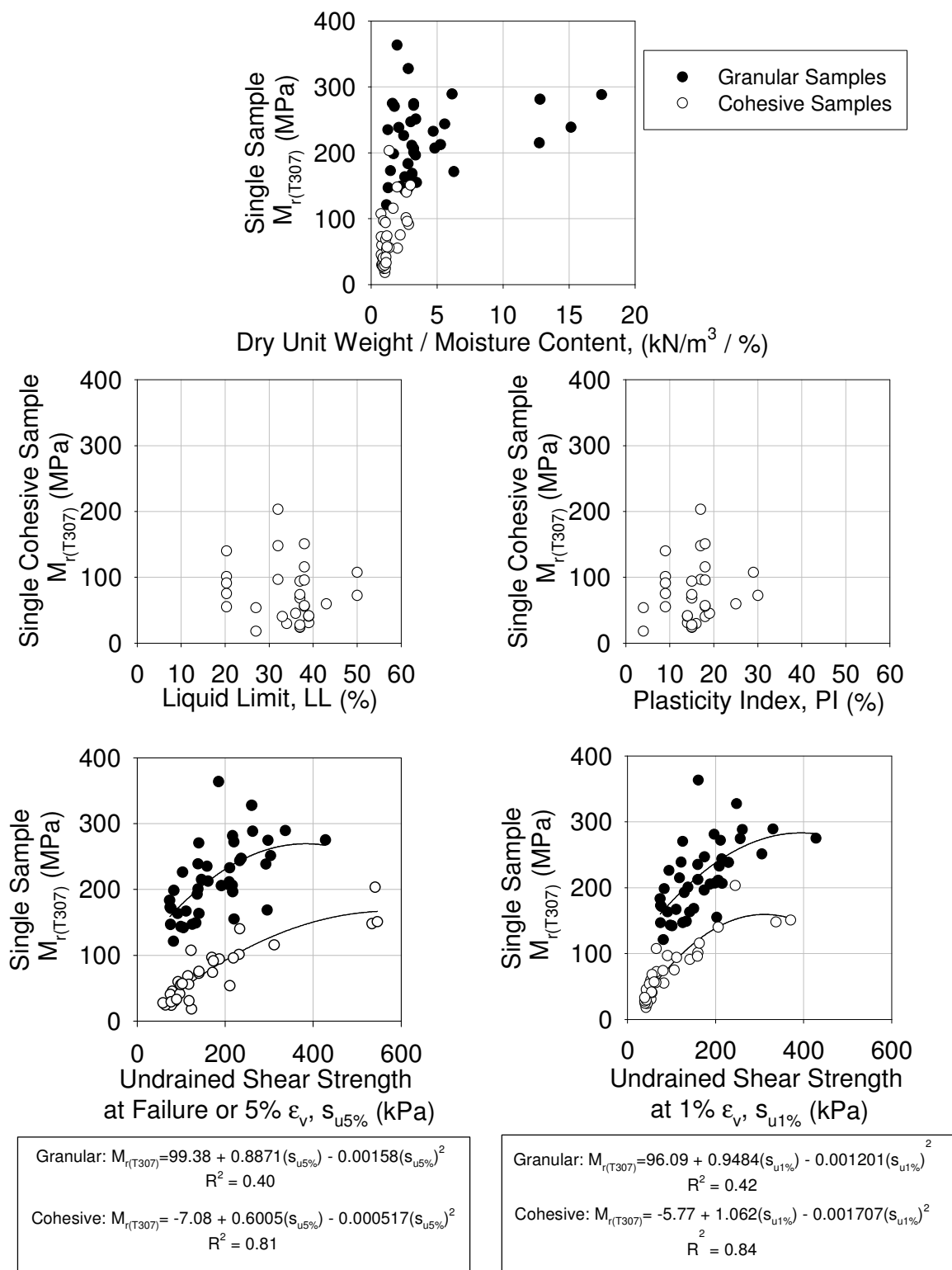
Figure 81. Summary of index properties as functions of average resilient moduli

for single material samples

Statistical analyses were performed with each index property for granular and cohesive materials. The properties that were significant in explaining the variation in $M_{r(T307)}$ values were then ranked according to t ratio. For both granular and cohesive materials, the undrained shear strength properties ($s_{u5\%}$ and $s_{u1\%}$) were among the most significant values in explaining variations in $M_{r(T307)}$ values. These findings verify what the data illustrates in Figure 81. Additionally, the percent passing No. 200 and No. 4 sieves were significant for granular materials. Statistical analysis results for granular and cohesive materials are summarized in Table 45 and Table 46.

Table 45. Statistical analysis results for granular material index properties

Property	Parameter Estimate	Standard Error	t ratio	Prob>|t|	Significant?	Rank
Passing No. 200 Sieve	-4.6783	1.6224	-2.88	0.0060	Yes	4
Passing No. 4 Sieve	-1.4825	0.3059	-4.85	<0.0001	Yes	1
LL	No Data					
PI	No Data					
c_u	1.3445	1.4821	0.91	0.3696	No	—
c_c	13.7076	9.5997	1.43	0.1609	No	—
$s_{u5\%}$ or failure	0.4001	0.0853	4.69	<0.0001	Yes	2
$s_{u1\%}$	0.4302	0.0922	4.66	<0.0001	Yes	3
$\gamma_d/w\%$	2.3894	1.1131	2.15	0.0375	Yes	5

Table 46. Statistical analysis results for cohesive material index properties

Property	Parameter Estimate	Standard Error	t ratio	Prob>|t|	Significant?	Rank
Passing No. 200 Sieve	-0.4094	0.4698	-0.87	0.3898	No	—
Passing No. 4 Sieve	1.1751	0.7626	1.54	0.1332	No	—
LL	-0.3012	0.9778	-0.31	0.7595	No	—
PI	1.7935	1.2826	1.40	0.1719	No	—
c_u	No Variation					
c_c	No Variation					
$s_{u5\%}$ or failure	0.2897	0.0292	9.91	<0.0001	Yes	1
$s_{u1\%}$	0.4497	0.0483	9.31	<0.0001	Yes	2
$\gamma_d/w\%$	36.8082	9.3786	3.92	0.0004	Yes	3

Secant moduli

This investigation focused on developing laboratory conditions similar to in situ conditions (i.e., repeated pulse loading, small cyclic strains, and accumulation of permanent

strains) to identify significant correlations between laboratory and in situ elastic moduli investigations.

Secant modulus, a type of elastic modulus, is determined from the slope of the line connecting the origin to a selected point on the stress-strain curve of a material. Two variations of secant moduli were determined from laboratory data—cyclic secant moduli and dynamic secant moduli. The difference between secant moduli and resilient moduli is the use of permanent strain instead of resilient strain for the determination of the moduli. A simplified comparison for resilient, cyclic secant, and dynamic secant moduli is shown in Figure 82. The two stress levels represent the AASHTO T307 changes in applied stresses (Table 27 and Table 28).
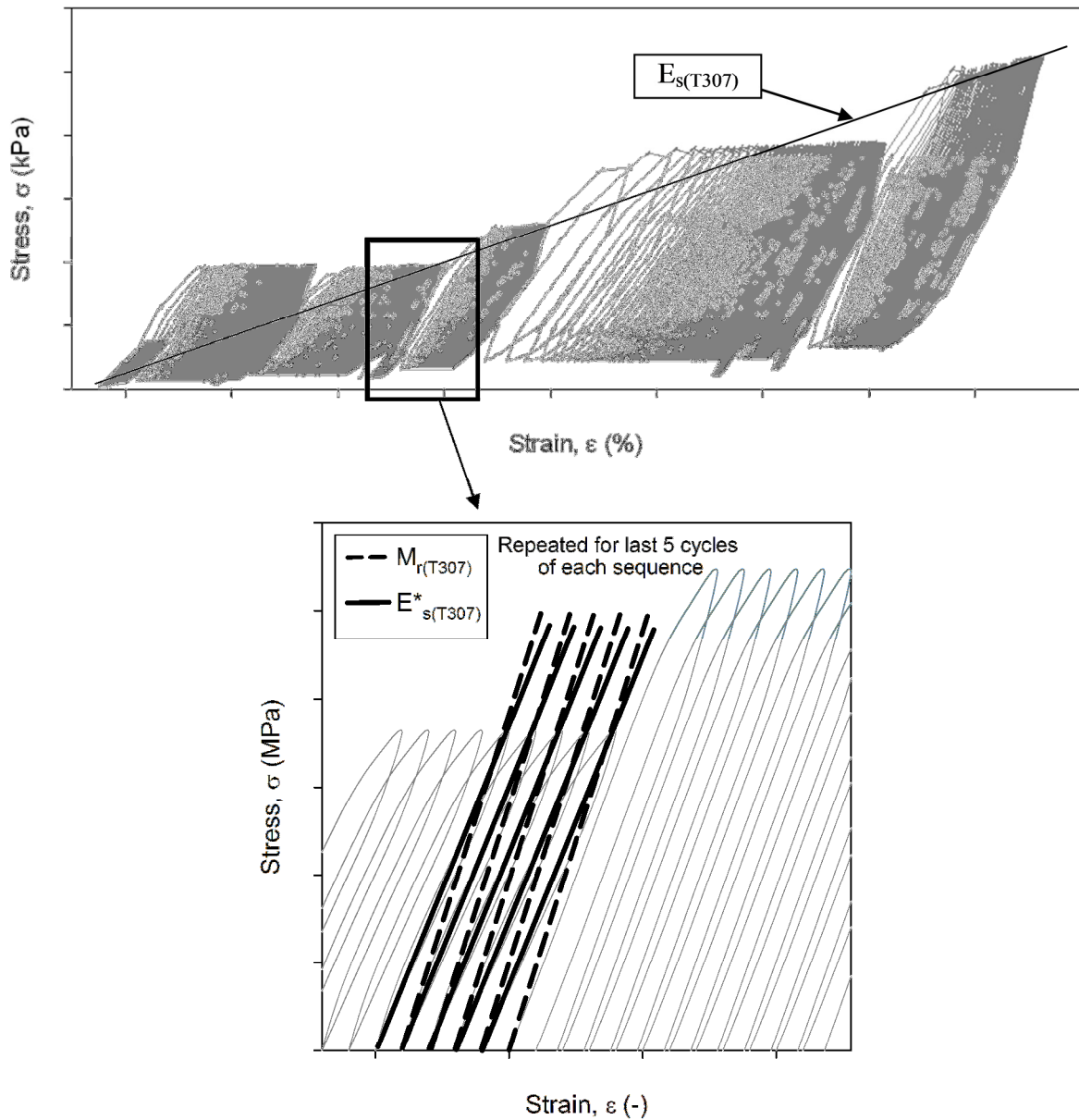
Figure 82. Comparison of resilient ($M_{r(T307)}$), cyclic secant ($E^*_{s(T307)}$), and

dynamic secant ($E_{s(T307)}$) modulus values

Cyclic secant moduli

The cyclic secant modulus ($E^*_{s(T307)}$) was determined using same five cycles from each test sequence as resilient modulus but using the sum of permanent and resilient strain (i.e., strain at beginning of cycle to strain at peak stress) to calculate the modulus. The process was repeated for all 15 load sequences. $E^*_{s(T307)}$ values are the average values for all load

sequences for each sample. Sample calculations for cyclic secant modulus were performed in Equation 22.

$$E^*_{s(T307)} = \frac{\sigma_d}{\Delta\varepsilon_{pi} + \varepsilon_{ri}} = \frac{0.011499\text{MPa}}{(0.013542 - 0.013558) + 0.000869} = 13.72\text{MPa} \tag{22}$$

where: σ_d = deviator stress (MPa);

ε_{ri} = resilient strain for the ith cycle (-); and

$\Delta\varepsilon_{pi}$ = additional permanent strain between the i-1 and i^{th} cycle (-).

A near one to one relationship (i.e., $E^*_{s(T307)} = M_{r(T307)}$) was determined between the calculated $E^*_{s(T307)}$ and $M_{r(T307)}$ values. This very close relationship is due to the extremely small permanent strain values that accumulate during each resilient modulus cycle. Overall, the permanent strains could be large, but on a cycle by cycle basis, the resilient and cyclic secant moduli are nearly identical. These findings indicate that the calculated $E^*_{s(T307)}$ values are very closely related to the M_r values for the range of materials and conditions tested. Figure 83 summarizes the relationship between $E^*_{s(T307)}$ and $M_{r(T307)}$ values.
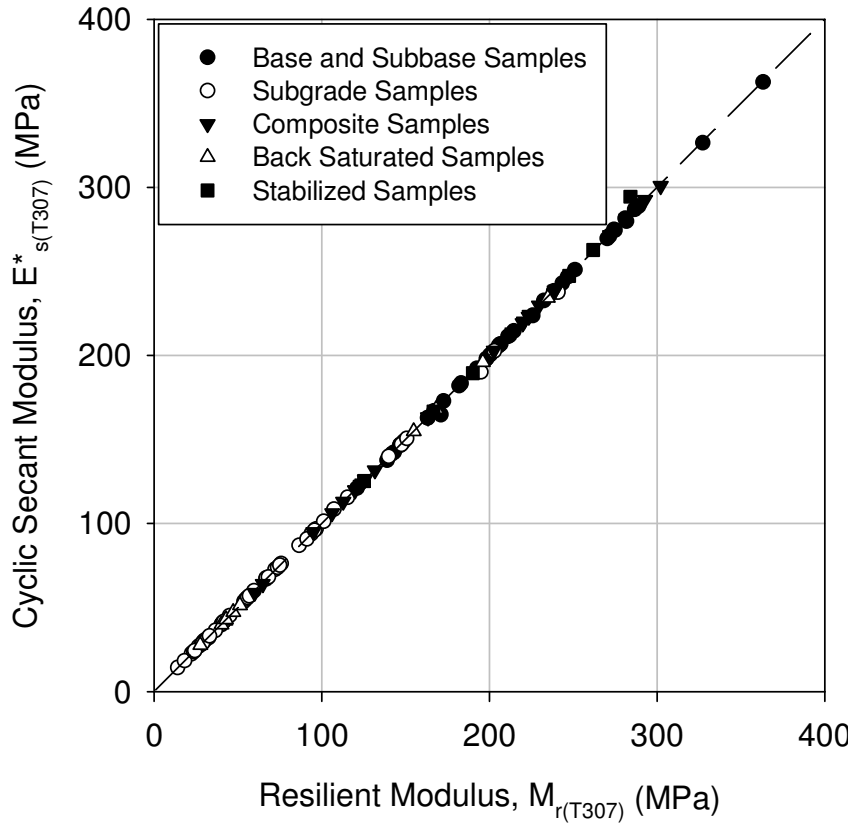
Figure 83. Summary of the relationships between cyclic secant moduli ($E^*_{s(T307)}$) and

$M_{r(T307)}$ values for all samples

Dynamic secant moduli

The dynamic secant modulus ($E_{s(T307)}$) was determined by dividing the change in applied stresses (determined from the first and last cycles) by the change in permanent strains from the first to last cycles. $E_{s(T307)}$ was calculated using Equation 23. Sample calculations of $E_{s(T307)}$ can be found below in Equation 24, and Table 47.

$$E_{s(T307)} = \frac{(\sigma_1)_{15} - (\sigma_1)_1}{(\varepsilon_p)_{15} - (\varepsilon_p)_1} \tag{23}$$

where: $(\sigma_1)_1$ = maximum applied vertical stress during the 1st sequence,

$(\sigma_1)_{15}$ = maximum applied vertical stress during the 15th sequence,

$(\varepsilon_p)_1$ = permanent strain at the end of the 1st sequence, and

$(\varepsilon_p)_{15}$ = permanent strain at the end of the 15th sequence.

Table 47. Example of stress and strain values for $E_{s(T307)}$ calculation

Sequence No.	Confining Stress, σ_3 (kPa)	Max. Deviator Stress, σ_d (kPa)	Max. Vertical Stress, $\sigma_1{}^*$ (kPa)	Permanent Strain, ε_p (%)	Resilient Modulus, M_r (MPa)
0	41.4	27.6	68.9	—	—
1	41.0	12.7	53.7	0.78	26.2
2	40.9	26.1	66.9	0.82	18.0
3	40.7	38.5	79.2	1.39	16.6
4	41.1	50.9	91.9	2.46	18.6
5	40.7	65.7	106.4	3.65	22.3
6	26.8	12.6	39.4	3.46	59.1
7	27.1	25.6	52.7	3.47	20.8
8	27.2	39.1	66.3	3.54	17.7
9	27.4	51.8	79.3	3.71	19.3
10	26.9	65.2	92.2	4.22	22.3
11	13.1	12.9	25.9	4.01	45.6
12	13.7	25.9	39.6	4.02	21.2
13	13.1	39.4	52.5	4.08	17.0
14	13.0	53.2	66.2	4.23	18.8
15	13.2	66.7	79.9	4.63	20.6

* $\sigma_1 = \sigma_d + \sigma_c$

$$E_{s(T307)} = \frac{(\sigma_1)_{15} - (\sigma_1)_1}{(\varepsilon_p)_{15} - (\varepsilon_p)_1} = \frac{(79.9\text{kPa}) - (53.7\text{kPa})}{0.0463 - 0.0078} = 680.5\text{kPa} = 0.68\text{MPa}$$

(24)

Most of the $E_{s(T307)}$ values were less than the $M_{r(T307)}$ values. The regression of the data indicated a relatively weak R^2 value and a slope that was less than a 1:1 relationship (i.e., $E_{s(T307)} = M_{r(T307)}$) when analyzing all of the data points. Seen from Equation 23, the $E_{s(T307)}$ data characterizes the permanent strain from all of the load sequences. High permanent strains (seen in soft samples such as subgrades) led to lower $E_{s(T307)}$ values. When the permanent strains are low, higher $E_{s(T307)}$ values are seen (e.g., dense base or subbase samples). The one subgrade outlier was from Wisconsin US-10 had a much larger $E_{s(T307)}$ value than $M_{r(T307)}$ value. The sample experienced very small permanent strains because it was batched at a low moisture content (7.0%) and a high unit weight (20.63 kN/m^3), relative

to the optimum values of the material (standard Proctor: $w_{opt} = 12.4\%$ and

$\gamma_{dmax} = 18.70$ kN/m^3). As expected, these findings indicate that $E_{s(T307)}$ values are related to

$M_{r(T307)}$ values but tend to be lower because the permanent strain is greater than the resilient

strain. Additionally, by comparing the same type of moduli (i.e., elastic moduli), better

correlations between laboratory and in situ data can be developed. The 95% confidence

interval provides the range of values that define the region containing the true mean

relationship between $M_{r(T307)}$ and $E_{s(T307)}$ values. Figure 84 summarizes the relationships

between $E_{s(T307)}$ and $M_{r(T307)}$. The *Mechanistic-Empirical Pavement Design Guide: A Manual

of Practice* (AASHTO 2008) recommends using a correction value to convert in situ

calculated layer moduli (e.g., E_{FWD}, etc) to equivalent laboratory resilient moduli. The

correction values for several layer types and locations are summarized in Table 5.
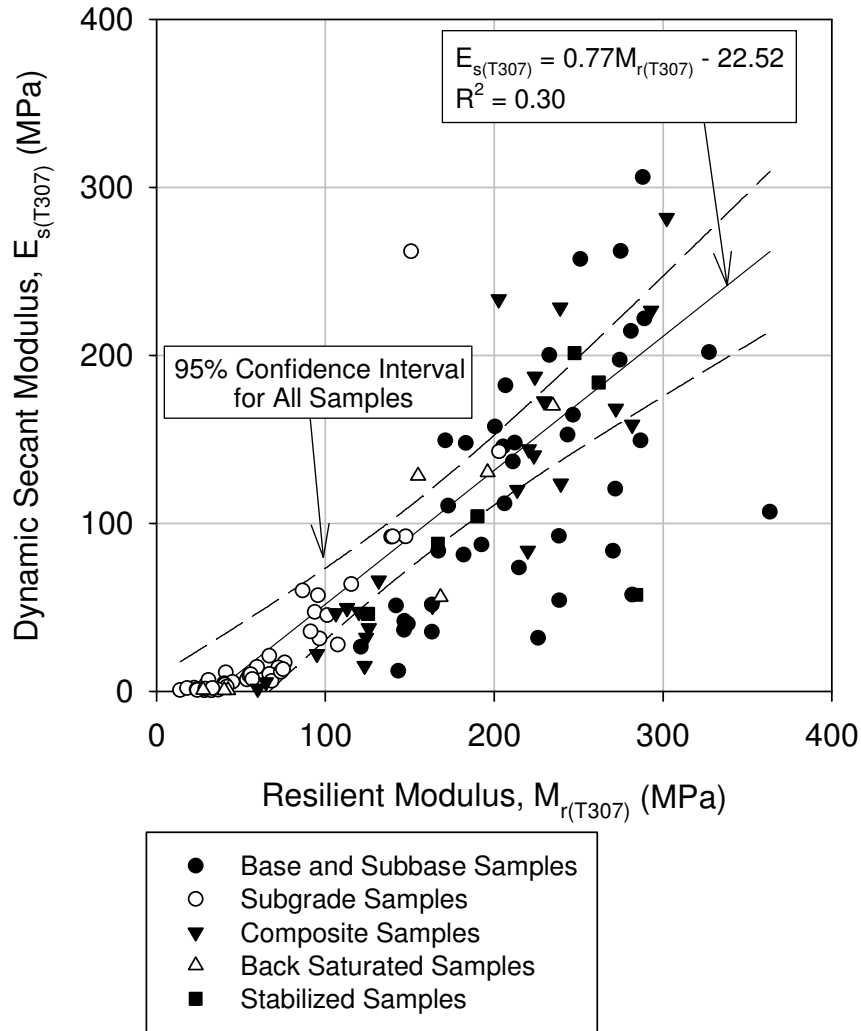
Figure 84. Summary of the relationship between average $E_{s(T307)}$ and average $M_{r(T307)}$

Table 48. Summary of average values to convert in situ calculated layer moduli

to equivalent laboratory resilient moduli (AASHTO 2008)

Layer Type	Location	C-Value (M_r/E_{FWD} Ratio)
Aggregate Base/Subbase	Between stabilized and HMA layer	1.43
	Below PCC layer	1.32
	Below HMA layer	0.62
Subgrade-Embankment	Below stabilized subgrade/embankment	0.75
	Below HMA or PCC layer	0.52
	Below unbound aggregate base	0.35
This study	$M_{r(T307)}/E_{s(T307)}$ for $E_{s(T307)} > 22.5$ MPa	1.30

IN SITU STUDIES

In situ studies included tests that directly measured elastic moduli of in situ materials as well as tests that were correlated to resilient moduli.

Elastic moduli measured from plate load tests (E_{PLT}), falling weight deflectometer tests (E_{FWD}), and light weight deflectometer tests (E_{LWD}) were compared to single and composite material resilient moduli with similar dry unit weights and moisture contents.

Dynamic cone penetrometer indices (DCPI) and E_{LWD} values were correlated to resilient moduli through empirical correlations. Gradation and plasticity values were also used to determine resilient moduli through correlations with CBR. Additionally, single material sample resilient moduli were converted to equivalent composite sample resilient moduli ($M_{r(Equiv\ Composite)}$) through an equation from Von Quintus and Killingsworth (1997). Calculated $M_{r(Equiv\ Composite)}$ values were then compared to composite $M_{r(T307)}$ values.

In situ moduli

Several points from each test site were chosen to compare in situ and laboratory moduli. Plate load tests (PLT), falling weight deflectometer (FWD) tests, and light weight deflectometer (LWD) tests were performed on base, subbase, and subgrade layers at each site to measure elastic moduli in situ. Additionally, at each test point, a nuclear moisture-density gauge (NG) was used to determine in situ dry unit weights and moisture contents. PLT, FWD, and LWD data points were compared to laboratory resilient modulus tests when the in situ and laboratory materials met the following criteria: dry unit weights = ±1.0 kN/m^3 and moisture contents = $\pm2\%$. For some tests, comparisons of data points were limited because materials did not meet the dry unit weight and moisture content criteria. Additionally, it was not expected for the in situ and laboratory moduli to be perfectly correlated. George (2003) discusses residual stress and stress-dependant nonlinearity of soils that affect the results of in situ and laboratory tests.

Plate load test

PLTs were conducted in general accordance with ASTM D1196 directly on base, subbase, and subgrade layers. A static load was applied to a 300 mm diameter bearing plate. The bearing plate was placed directly pavement foundation layers. Bearing plate deflection was measured using three linear voltage displacement transducers (LVDTs). The average

deflection values from the three LVDTs were used in calculations. A data logger continuously recorded the load and deflection readings during the test. An initial stress was applied to the material (0.2 MPa for subgrades and 0.4 MPa for base and subbases) and released. The material was then reloaded to the same stress and released.

Initial (E_{v1}) and reload (E_{v2}) elastic moduli readings were determined by Equation 25 (Vennapusa and White 2009). Load and deformation readings were taken from stress ranges of 0.2 to 0.4 MPa (29 to 58 psi) for granular materials and 0.1 to 0.2 MPa (14.5 to 29 psi) for non-granular subgrade soils (White et al. 2009). Appendix A provides PLT sample calculations.

Laboratory and in situ materials met the dry unit weight and moisture content criteria at the Michigan I-94, Michigan I-96, and Wisconsin US-10 sites.

$$E = \frac{(1-v^2)\sigma_0 a}{d_0} f \tag{25}$$

where: E = elastic modulus (MPa);

d_0 = measured deflection (mm);

v = Poisson's ratio;

σ_0 = applied stress (MPa);

a = radius of the loading plate (mm); and

f = shape factor depending on stress distribution (for the segmented plate FWD: f = 2; for PLT or LWD on clay: f = π/2; for PLT or LWD on sand: f = 8/3 (Vennapusa and White 2009)).

E_{v1} and E_{v2} values were lower than $M_{r(T307)}$ and $E_{s(T307)}$ values. The E_{v1} and E_{v2} values also had litter variation when compared to $M_{r(T307)}$ and $E_{s(T307)}$ values. One possible reason for the differences between in situ and laboratory moduli is that the PLT is a static load test and therefore does not model the cyclic response of pavement foundations. Additionally, PLTs measure maximum deflections. Maximum deflections are related to total strains (the sum of permanent and resilient strains). M_r tests use the resilient strain to determine $M_{r(T307)}$ values. The number of cycles may also affect the determined moduli; PLTs had two cycles, while M_r tests had 1500 cycles. E_{v1} and E_{v2} values are compared to $M_{r(T307)}$ and $E_{s(T307)}$ values in Figure 85.
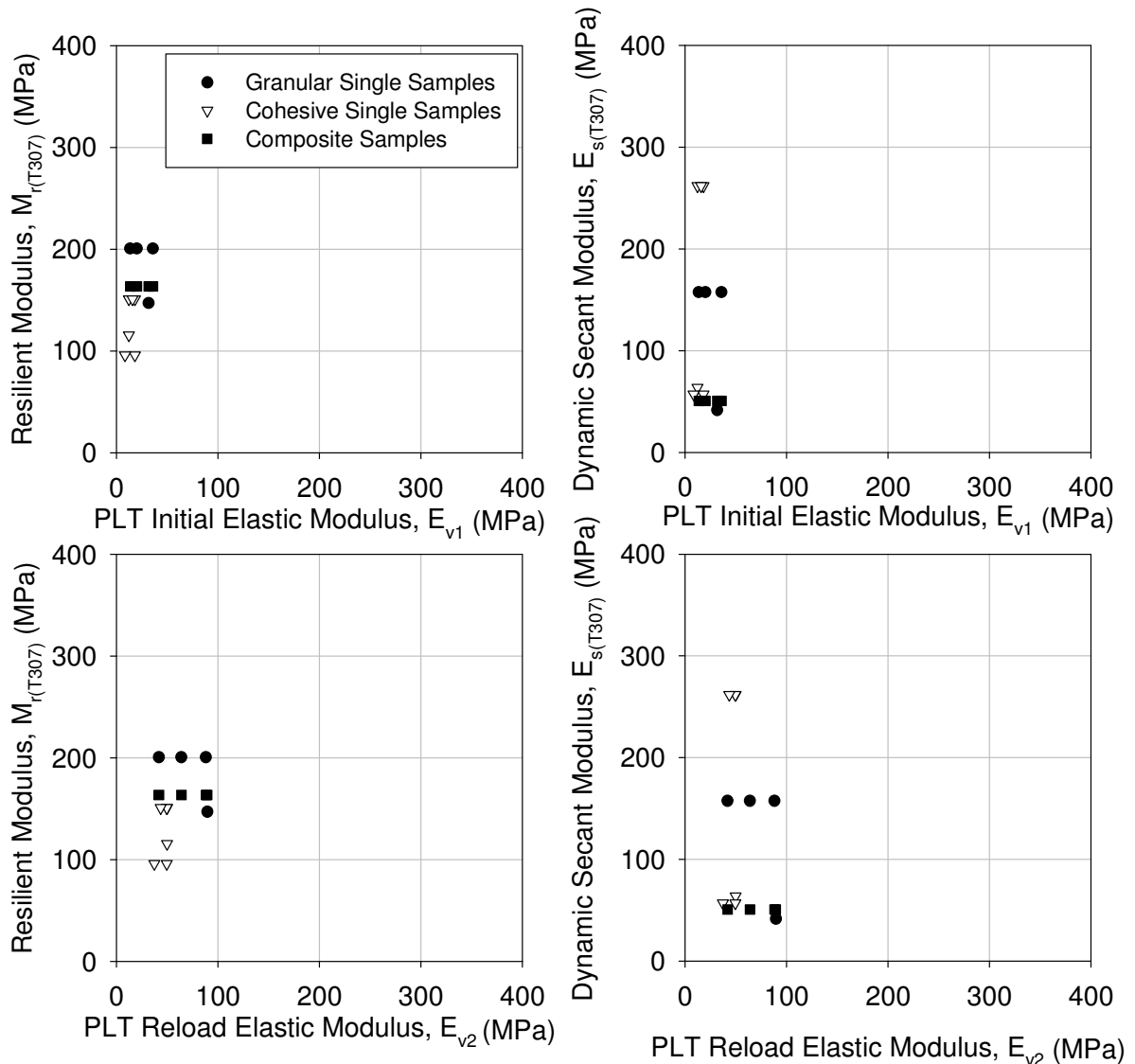
Figure 85. Comparison of M$_{r(T307)}$ and E$_{s(T307)}$ versus E$_{v1}$ and E$_{v2}$

Falling weight deflectometer

A KUAB 2m-FWD 150 was used to perform FWD tests directly on pavement foundation layers. Only FWD data from Michigan I-94 had materials that met the dry unit weight and moisture content criteria that correlated to laboratory tested materials. The FWD tests from Michigan I-94 were performed on the base layer of the reconstructed pavement foundation.

The load sequence involved one seating impact and three recorded impacts with nominal applied loads of 21.40 kN (4811 lbf), 32.50 kN (7306 lbf), and 32.69 kN (7349 lbf) for the three recorded impacts. Deflections were measured by sensors placed at the center of the

plate, and at 0.2 m, 0.3 m, 0.5 m, 0.6 m, 0.8 m, 0.9 m, 1.2 m, 1.52 m, and 1.8 m offsets from the center of the plate.

Elastic moduli were calculated from FWD data (E_{FWD}) using Equation 25 and the deflection reading at the center of the load plate. This method determined composite elastic moduli of pavement layers directly under the FWD plate, which should relate to laboratory resilient and dynamic moduli from composite material samples.

E_{FWD} values were lower than $M_{r(T307)}$ and $E_{s(T307)}$ values. The poor correlation between in situ and laboratory moduli is illustrated through low variation of E_{FWD} values. One of the possible reasons for the differences between E_{FWD} and $M_{r(T307)}$ values is that the FWD measures maximum deflection (i.e., total strain), and M_r tests measure resilient strain (i.e., a portion of total strain). For cyclic loading, total strain is simplified as the sum of permanent strain and resilient strain. Moduli are calculated by dividing applied stresses by strain values. Therefore, small resilient strains would lead to larger $M_{r(T307)}$ values, compared to E_{FWD} values. Additionally, the FWD is a dynamic test that only applies a small number of impacts to test points. M_r tests, on the other hand, apply 1500 impacts to soil samples over a range of stress conditions. E_{FWD} values are compared to $M_{r(T307)}$ and $E_{s(T307)}$ values in Figure 86.
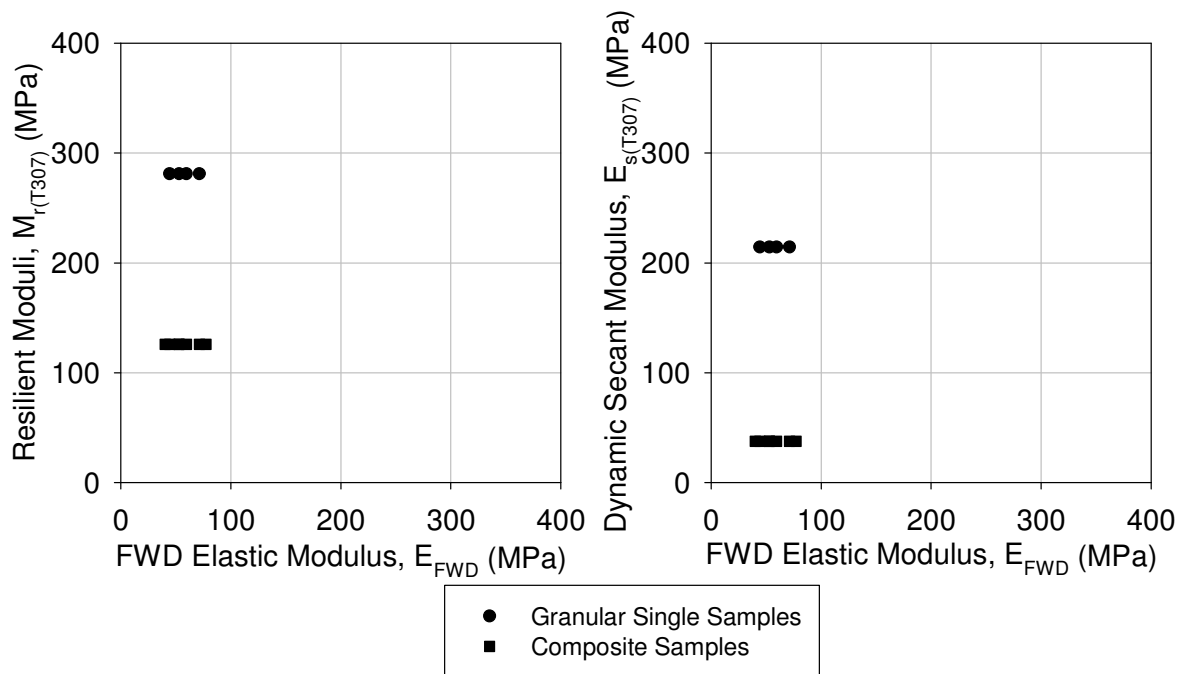

Figure 86. Comparison of $M_{r(T307)}$ and $E_{s(T307)}$ versus E_{FWD}

Light weight deflectometer

Zorn ZFG 2000 was used to perform the LWD tests directly on base, subbase, and subgrade layers. The drop height was 720 mm, and the plate diameter was 300 mm. Prior to performing the LWD test, a flat area on the material surface was prepared. Three seating drops were performed, and three test drops were recorded. Deflections for each test drop were recorded and averaged at each point. The applied stress was assumed constant for the known plate diameter, drop weight, drop height, and spring constant.

Elastic moduli were calculated from LWD data ($E_{LWD-Z3(72)}$) using the average deflection reading and Equation 25. This method determined composite elastic moduli of pavement layers directly under the LWD plate, which should relate to laboratory resilient and dynamic secant moduli values from composite material samples.

Like E_{FWD} values, $E_{LWD-Z3(72)}$ values were low compared to $M_{r(T307)}$ and $E_{s(T307)}$ values. Although, many more data points were tested, the resulting low variance in $E_{LWD-Z3(72)}$ values illustrates a poor correlation between in situ and laboratory moduli. Differences between $E_{LWD-Z3(72)}$ and $M_{r(T307)}$ and $E_{s(T307)}$ values were most likely due to the measured strains. LWD tests measured maximum deflection (i.e., total strain) and M_r tests measured resilient strain. Because E_s values were calculated from M_r values, the strains were still very small and may not have matched the in situ conditions. Total strain is much greater than resilient strain, which would then lead to smaller $E_{LWD-Z3(72)}$ values compared to $M_{r(T307)}$ values. $E_{LWD-Z3(72)}$ values are compared to $M_{r(T307)}$ and $E_{s(T307)}$ values in Figure 87.
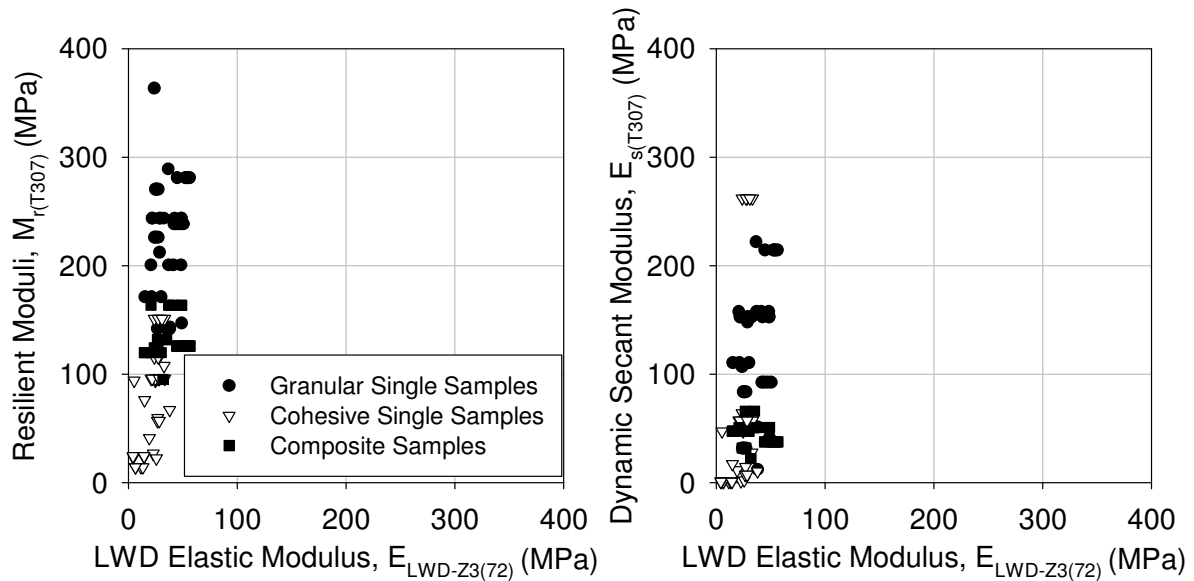
Figure 87. Comparison of $M_{r(T307)}$ and $E_{s(T307)}$ versus $E_{LWD-Z3(72)}$

Empirical correlations

DCP and LWD test points were compared to laboratory resilient modulus tests when materials matched the following criteria: dry unit weights = ±1.0 kN/m^3 and moisture contents = ±2%. The DCPI values and E_{LWD} values were converted to $M_{r(DCPI)}$ and $M_{r(LWD)}$ values through equations provided by the MEPDG (NCHRP 2004b) and Mohammaed et al. (2008).

Gradation and plasticity values were also correlated to resilient moduli of single material samples using equations provided in the MEPDG (NCHRP 2004b). Additionally, Von Quintus and Killingsworth (1997) reported an equation to calculate composite resilient moduli ($M_{r(Equiv\ Composite)}$) from in situ determined single layer resilient moduli. In this study, the equation was used with single material $M_{r(T307)}$ values to calculate composite material $M_{r(Equiv\ Composite)}$ values. $M_{r(Equiv\ Composite)}$ values were then compared to measured $M_{r(T307)}$ values.

Dynamic cone penetrometer

DCP tests were performed in accordance with ASTM D6951-03. The DCP works by dropping an 8 kg (17.6 lb) hammer onto a rod with a cone tip from a height of 575 mm (22.6 in.) and measuring the penetration distance for a given number of blows. Tests were performed to a depth of 1 m with the typical DCP apparatus and extended to 2 m using

extension rods. Dynamic cone penetration index (DCPI) was calculated for each test. Weighted average DCPIs were calculated for each foundation layer using Equation 26 (White et al. 2009).

$$DCPI_z = \frac{DCPI_i \cdot z_i + DCPI_{i+1} \cdot z_{i+1} + ... + DCPI_n \cdot z_n}{\sum z_n} \tag{26}$$

where: $DCPI_z$ = DCPI for the foundation layer of thickness z (mm/blow) and $DCPI_{i,i+1,...n}$ = DCPI of blows i to n (mm/blow).

In order to determine the average dynamic cone penetrometer index ($DCPI_{Ave}$) for each pavement layer, DCPI values were first converted to CBR values according to Equations 27, 28, and 29 (ASTM D6951). Weighted CBR values were determined for each recorded DCP blow using Equation 26 but substituting CBR values for the DCPI values. Pavement foundation layers were chosen by observing where a clear change in slope occurred on depth versus weighted CBR graphs (Figure 88). Some test points did not have a clear change in slope, and engineering judgment was applied using graphs of depth versus DCPI values to determine the layer boundaries.

Strength and stiffness values of granular materials are highly dependant on confining stresses. Near the surface (the first one to three blows or approximately the first 150 mm (Siekmeier et al. 2009)), very little confining stress is present, and the strength and stiffness values were low. The portion of the layer with very low confining stresses was considered unconfined and was not used to determine $DCPI_{Ave}$ values for the rest of the layer. On graphs of DCP data in Appendix E, the unconfined portions of granular layers are clearly indicated, as illustrated in Figure 88.
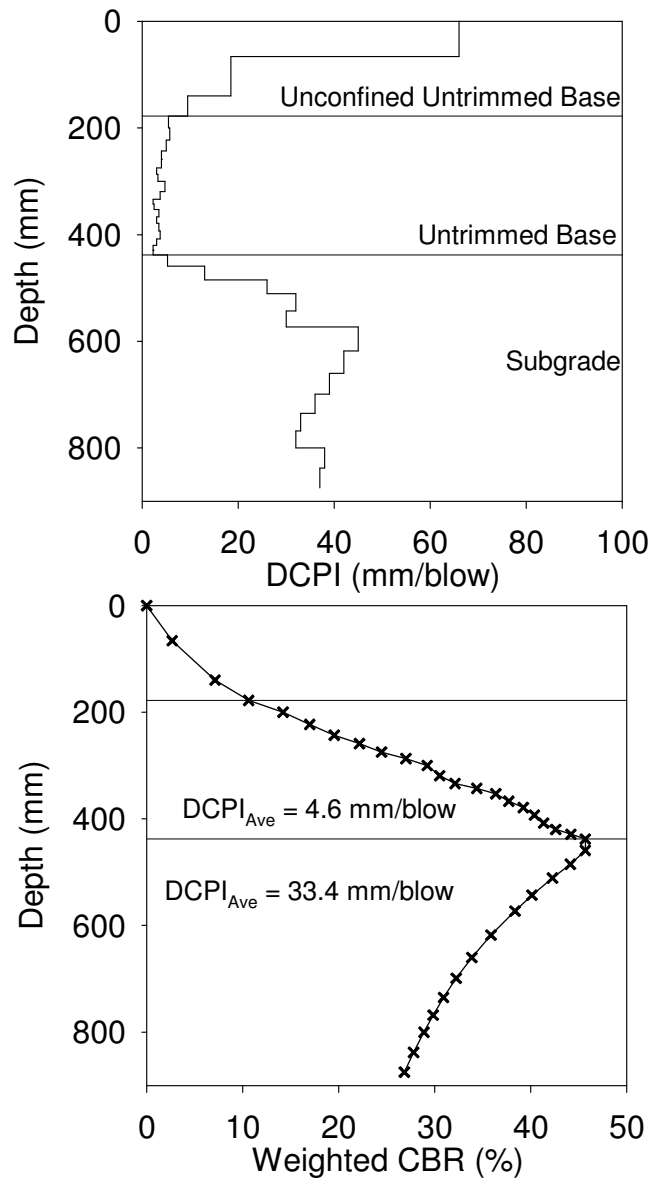
Figure 88. Determination of DCPI$_{Ave}$ and pavement foundation layers

To compare in situ and laboratory moduli, DCPI$_{Ave}$ values for each layer were used to determine M$_{r(DCPI)}$. Resilient moduli were calculated from the DCPI$_{Ave}$ for each layer using Equations 27, 28, 29, and 30 (ASTM D6951) and Equations 31 and 32 from Mohammad et al. (2008). Equations 31 and 32 are specific to cohesive and granular materials, respectively, whereas Equation 30 is used for all soil types.

The MEPDG only lists Equations 27 and 30 to correlate DCPI to CBR to M$_r$ values. However, the MEPDG also references ASTM D6951 which recommends using Equations

27, 28, and 29 to determine DCPI values. DCPI correlated values are considered level 2 design inputs in the MEPDG, which indicates the values are not as rigorous as level 1 inputs, but require more investigation than level 3 inputs. Appendix A provides sample calculations for the $M_{r(DCPI)}$.

$$CBR = \frac{292}{DCPI^{1.12}} \text{ ; for all soils except for CH and CL soils with CBR} < 10 \qquad (27)$$

$$CBR = \frac{1}{(0.017019 \cdot DCPI)^2} \text{ ; for CL soils with CBR} < 10 \qquad (28)$$

$$CBR = \frac{1}{(0.002871 \cdot DCPI)} \text{ ; for CH soils} \qquad (29)$$

$$M_{r(DCPI)} = 17.6(CBR)^{0.64} \text{ ; for all materials} \qquad (30)$$

$$M_{r(DCPI))} = \frac{1046.6}{DCPI^{1.096}} \text{ ; for cohesive materials} \qquad (31)$$

$$M_{r(DCPI)} = \frac{391.1}{DCPI^{0.23}} \text{ ; for granular materials} \qquad (32)$$

where: DCPI = dynamic cone penetrometer index (mm/blow);

CBR = California bearing ratio (%); and

M_r = resilient modulus (MPa).

Overall, the use of $DCPI_{Ave}$ values from each layer resulted in $M_{r(DCPI)}$ values being lower than $M_{r(T307)}$ values which means that in situ DCPI values may provide more conservative values than laboratory tests. Granular and cohesive material $M_{r(DCPI)}$ values using Equations 27 and 30 are less than $M_{r(T307)}$ values in all but four instances. Lower values may provide a built in factor of safety when using DCPI-M_r correlations. Equation 31 tends to also underestimate the $M_{r(T307)-12}$ values for cohesive materials by an average of 34%, while Equation 32 tends to overestimate the $M_{r(T307)-5}$ values for granular materials by 71%. George and Uddin (2000) noted that relatively poor correlations were developed between DCPI and M_r directly, but the correlations were improved when the equations incorporated dry unit weight, moisture content, liquid limit, and plasticity index for cohesive materials and dry unit

weight, moisture content, log of the coefficient of uniformity, and percent passing No. 200 sieve for granular materials. Mohammad et al. (2009) also determined that incorporating additional soil parameters (e.g., moisture content) increased the coefficient of determination (R^2) value. Mohammad et al. 2009 reported that DCPI and resilient moduli results were influenced by moisture content. Both George and Uddin (2000) and Mohammad et al. (2009) determined laboratory M_r values at $\sigma_d = 37$ kPa (5.4 psi) and $\sigma_3 = 14$ kPa (2.0 psi), whereas the results from this study averaged the M_r values from all 15 sequences ($M_{r(T307)}$) for each sample.

DCP tests measure a very small portion of the soil, and soil on a given site can be highly non-homogeneous. Therefore, a single DCP test may not describe the subsurface soil conditions for an entire site; additional test points are needed.

Overall, strain may be one possible reason for the discrepancies between $M_{r(DCPI)}$ and $M_{r(T307)}$ values. DCP tests provide a measure of the shear strength of the soil. High localized strain develops around the cone tip as the DCP apparatus penetrates into the soil, whereas small strains are experienced by laboratory M_r samples.

Resilient moduli of granular materials are also highly dependant on confining stresses. Higher confining stresses increase the resilient moduli. If laboratory procedures involve less confining stress than in situ conditions, the in situ granular soils will be stiffer. Cohesive materials are much more sensitive to differences in moisture, unit weight, and deviator stresses. Therefore, if laboratory conditions are different than in situ conditions, the laboratory resilient moduli could be different. The relationships between $M_{r(DCPI)}$ and $M_{r(T307)-5/12}$ for remolded and Shelby tube samples are summarized in Figure 89 and Figure 90, respectively.
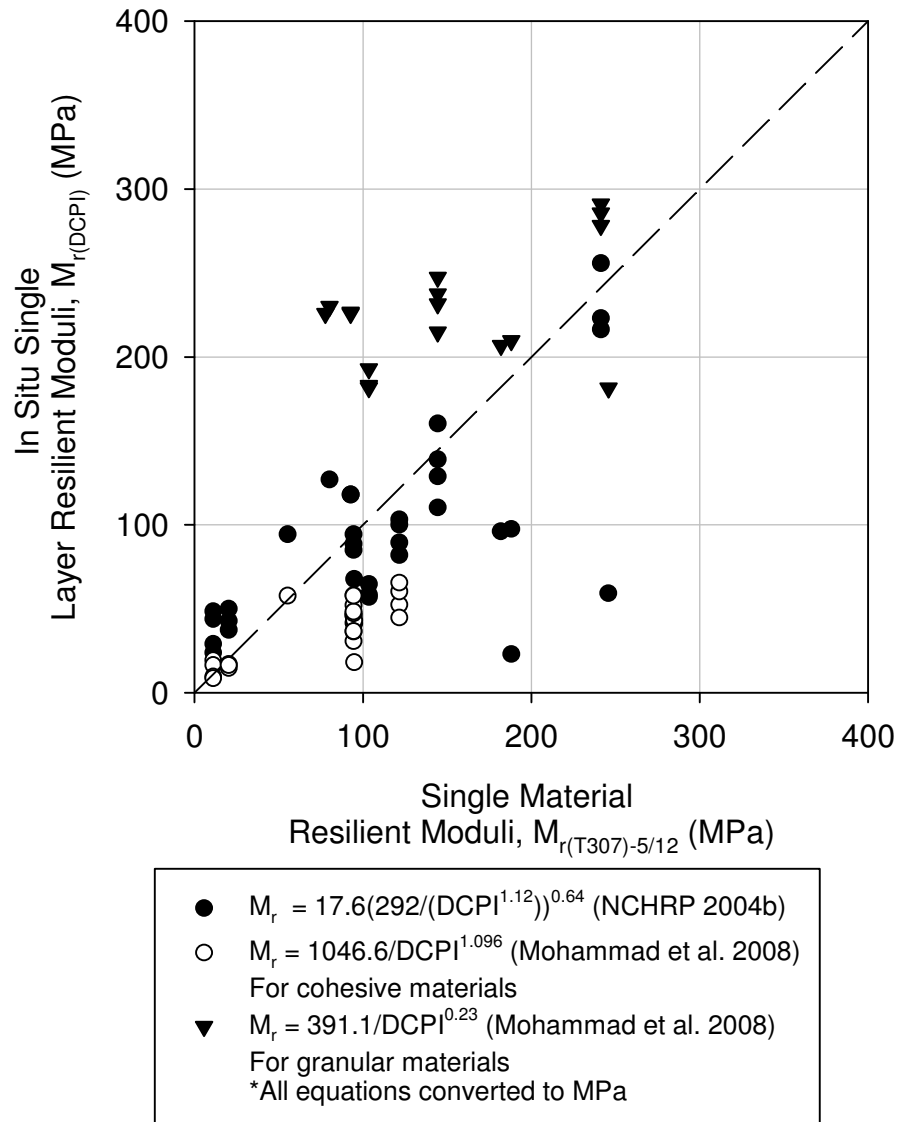
Figure 89. Single layer $M_{r(DCPI)}$ determined using three equations versus single material

$M_{r(T307)-5/12}$
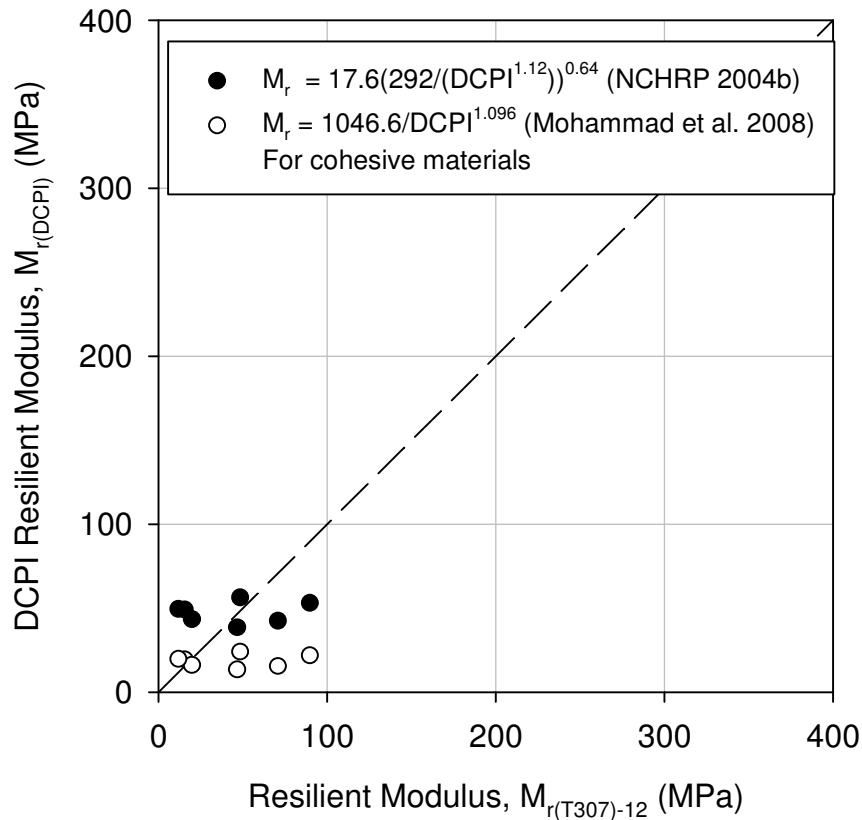
Figure 90. $M_{r(DCPI)}$ (NCHRP 2004b) of corresponding in situ points versus $M_{r(T307)}$

for Shelby tube samples from Michigan I-94

Light weight deflectometer

LWD tests were performed directly on base, subbase, and subgrade layers. Methods and calculations were the same as described above under the In Situ Moduli section. Data from LWD devices used in this study and studies by White et al. (2007) and Mohammad et al. (2008) were used to compare correlations between $M_{r(LWD)}$ and laboratory M_r values.

In situ tests from this study used a Zorn LWD device with a 720 mm drop height and a 300 mm plate diameter. $M_{r(T307)}$ values from Sequence 5 ($M_{r(T307)-5}$), Sequence 12 ($M_{r(T307)-12}$), and $M_{r(T307)}$ values were compared to $E_{LWD-Z3(72)}$ values.

White et al. (2007) used a Zorn LWD device with a 630 mm drop height and a 200 mm plate diameter. Only cohesive materials were investigated. $M_{r(T307)}$ values were determined from single material samples.

Mohammad et al. (2008) used a Prima LWD device with an 850 mm drop height and a 200 mm plate diameter. Granular and cohesive materials were investigated, and two equations for each material were developed to relate $E_{LWD-P2(85)}$ to $M_{r(T294)}$ at specific stress states. Granular material $M_{r(T294)}$ values were determined from a stress state of $\sigma_{cyclic} = 103.4$ kPa (15.0 psi) and $\sigma_3 = 34.5$ kPa (5.0 psi). Cohesive material $M_{r(T294)}$ values were determined from a stress state of $\sigma_{cyclic} = 41.3$ kPa (6.0 psi) and $\sigma_3 = 14.0$ kPa (2.0 psi).

Equation 33 was used for granular materials to calculate M_r values directly from E_{LWD-P} values. Equation 34 was used for granular materials to calculate M_r values using E_{LWD-P} and percent passing the No. 4 sieve (P_4). Equation 35 was used for cohesive materials to calculate M_r values directly from E_{LWD-P} values. Equation 36 was used for cohesive materials to calculate M_r values using E_{LWD-P} and the soil moisture content. Two boxes outline the calculated M_r values for the range of moisture contents, P_4, and E_{LWD-P} values used in the study by Mohammad et al. (2008) in Figure 91.

$$M_{r(LWD)} = 18.69 E_{LWD-P2(85)}^{0.21} \tag{33}$$

$$M_{r(LWD)} = 27.48 E_{LWD-P2(85)}^{0.11} - 0.08 P_4 \tag{34}$$

$$M_{r(LWD)} = 5.70 E_{LWD-P2(85)}^{0.18} \tag{35}$$

$$M_{r(LWD)} = 1.63 + 2.7 E_{LWD-P2(85)}^{0.2} + 35.17 \frac{1}{w} \tag{36}$$

where: $E_{LWD-P(85)}$ = elastic moduli determined by Prima LWD with 850 mm drop height;

P_4 = percent passing No. 4 sieve; and

w = moisture content.

The Prima LWD had a much larger range of E_{LWD} values than the Zorn LWD. Prima LWD measured deflections of the ground with a geophone, while Zorn LWD measured deflections of the plate with accelerometers (Vennapusa and White 2009). The differences in deflection measurements may affect the range of E_{LWD} values.

The different LWD devices had different plate diameters and drop heights. Increased drop heights or decreased plate diameters lead to increases in applied stresses to the material. Vennapusa and White (2009) reported increasing Zorn E_{LWD} values for increasing applied

stresses but an inverse trend (with less variation at applied stresses greater than 0.1 MPa) between applied stress and Keros and Dynatest E_{LWD} values.

With the exception of the data from Mohammad et al. (2008), all of the laboratory M_r values were larger than the in situ E_{LWD} values. M_r tests measure resilient strains, while E_{LWD} is based on the maximum strain. Differences in moduli can be attributed to different strains used in calculations and different applied stresses. The relationships between $M_{r(T307)}$ and $E_{LWD-Z2(63)}$, $E_{LWD-Z3(72)}$, $E_{LWD-P2(85)}$, values are shown in Figure 91.
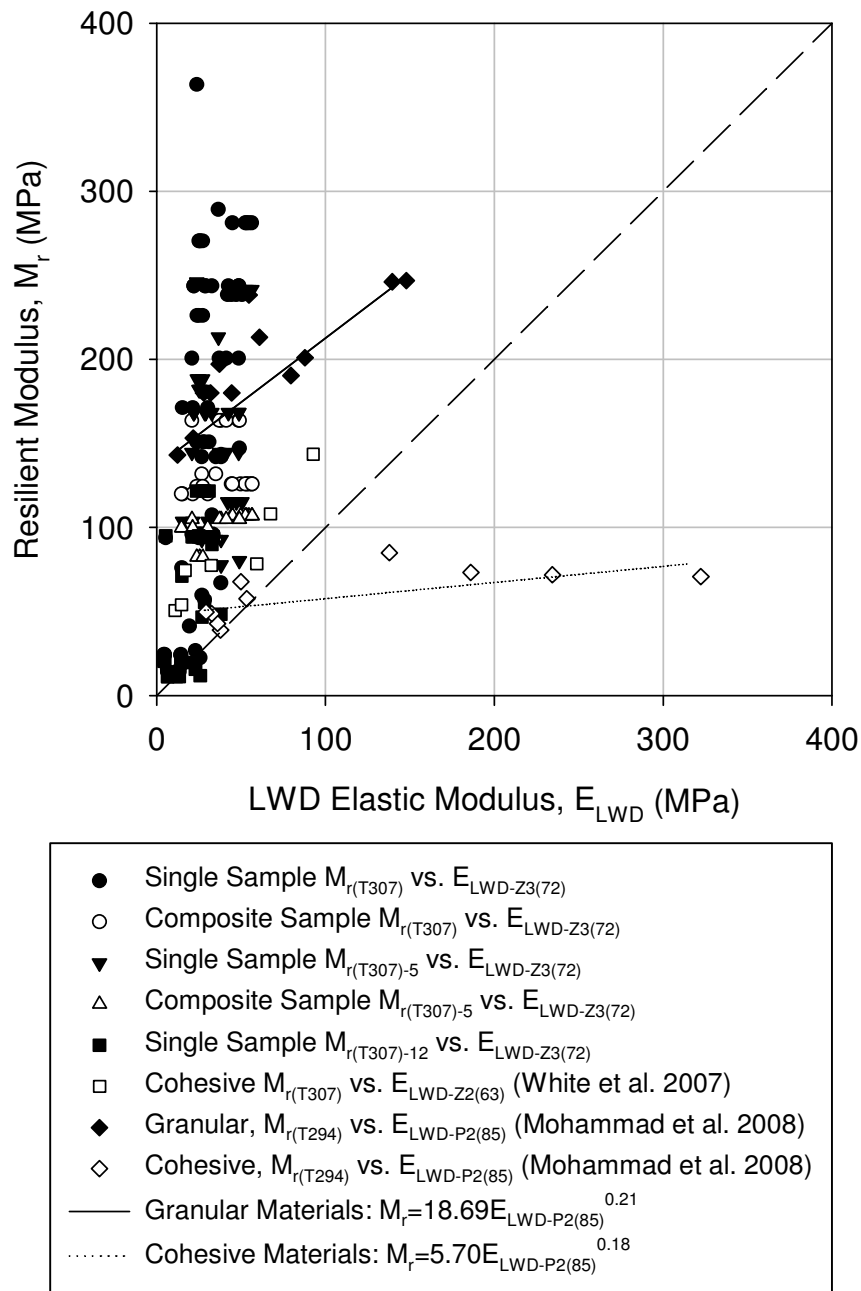
Figure 91. Comparison of laboratory M_r values and in situ E_{LWD} values using three LWD devices

$M_{r(T307)}$ values from Sequence 5 for granular and composite samples and Sequence 12 for cohesive samples were compared to $M_{r(LWD)-P}$ values using the equations from Mohammad et al. (2008) and data from White et al. (2007) and this study. Most granular materials had

higher $M_{r(LWD)-P}$ values than $M_{r(T307)-5}$ values. However, cohesive materials were evenly scattered around both sides of the equality line at low $M_{r(LWD)-P}$ and $M_{r(T307)-12}$ values.

Differences between $M_{r(LWD)-P}$ and $M_{r(T307)}$ values are most likely the result of Equations 33 to 36 not being developed from the Zorn LWD devices. Additionally, different applied stresses from LWD devices would also contribute to the $M_{r(LWD)-P}$ variances. The Prima LWD devices applied greater stresses to the soil surface because of larger the drop height and smaller plate diameter compared to the Zorn LWD devices. When using empirical equations, it is important to select equations that were developed using similar equipment and applied stresses. The relationships between $M_{r(T307)-5/12}$ and $M_{r(LWD)-P}$ values are shown in Figure 92.
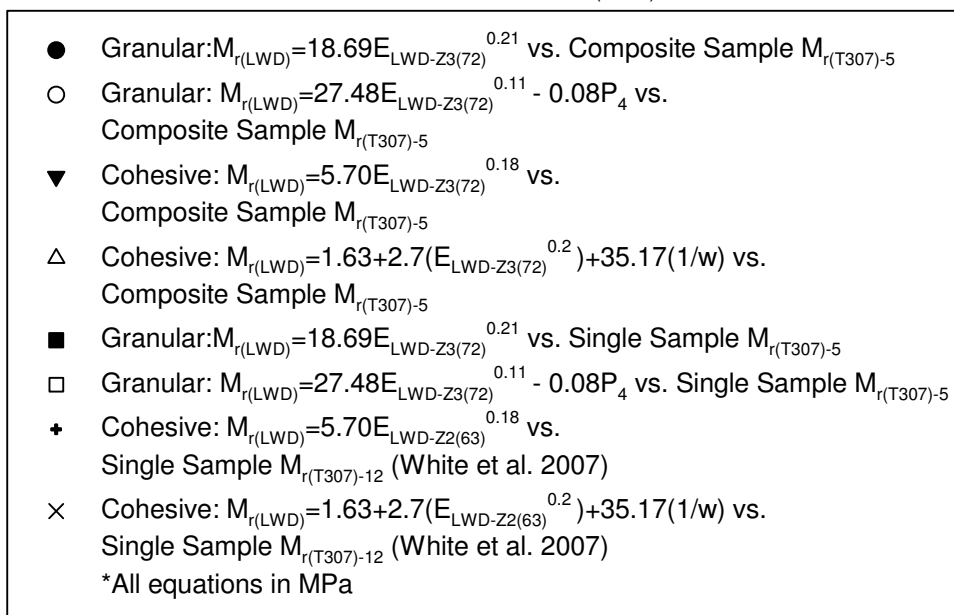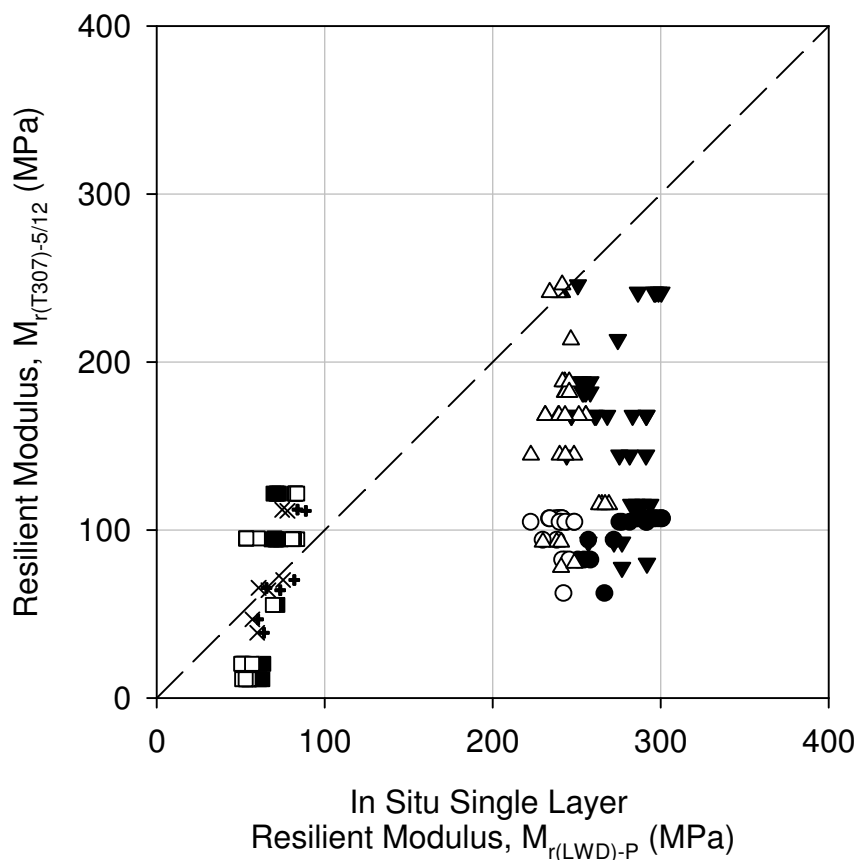
Figure 92. Comparison of $M_{r(LWD)-P}$ values and $M_{r(T307)}$ values from Sequences 5 and 12

for composite and single material samples

Gradation and plasticity index

The MEPDG included equations to predict resilient moduli from gradation and plasticity index values. As with the DCPI correlations, Equations 37 and 38 are level 2 design inputs. Level 2 inputs provide intermediate accuracy and are derived from limited tests or through correlations with other determined properties.

Equations 37 and 38 (NCHRP 2004b) are related empirically to resilient moduli through Equation 30. Both equations produced relatively accurate correlations to single material sample $M_{r(T307)}$ values. However, the use of these equations should be cautioned. The MEPDG appendix was the only place where the applicable ranges of values for the equations were described. Originally, the equations were used to obtain an estimate of resilient moduli for frozen materials (NCHRP 2004b). The equations can provide an estimate of resilient modulus based on the material properties of the soils, indicated in Figure 93.

$$CBR = 28.09 (D_{60})^{0.358} \tag{37}$$

$$CBR = \frac{75}{1 + 0.728 (P_{200} \times PI)} \tag{38}$$

where: D_{60} = diameter at 60% passing from the grain size distribution (mm);

P_{200} = percent passing the No. 200 sieve (decimal); and

PI = plasticity index (%).

Some of the discrepancies between empirical $M_{r(CBR)}$ values and laboratory $M_{r(T307)}$ values can be attributed to the parameters that influence resilient moduli (e.g., unit weight, moisture content, stress conditions, material type, etc.). Gradations can affect the unit weight (and therefore the resilient moduli) depending on the range of particle sizes to fill voids in the soil matrix. Plasticity index describes the range of moisture contents where the soil remains plastic. The M_r values of granular materials are known to be sensitive to unit weight and confining stresses (Alam et al. 2010; Seed et al. 1962; Southgate and Mahboub 1994), whereas the M_r values of cohesive materials are known to be sensitive to the deviator stress, unit weight, and moisture content (Seed et al. 1962 and Drumm et al. 1997).

Equations 37 and 38 include terms that account for gradation and moisture parameters, but stress parameters are neglected. Leaving out parameters that define the specific soil

condition introduces scatter in the resilient moduli relationships. The increased scatter of cohesive materials when compared to granular materials may indicate that cohesive materials were more sensitive to parameters not included in the equations, rather than P_{200} and PI values. These gradation and plasticity index equations are compared to $M_{r(T307)}$ values in Figure 93.
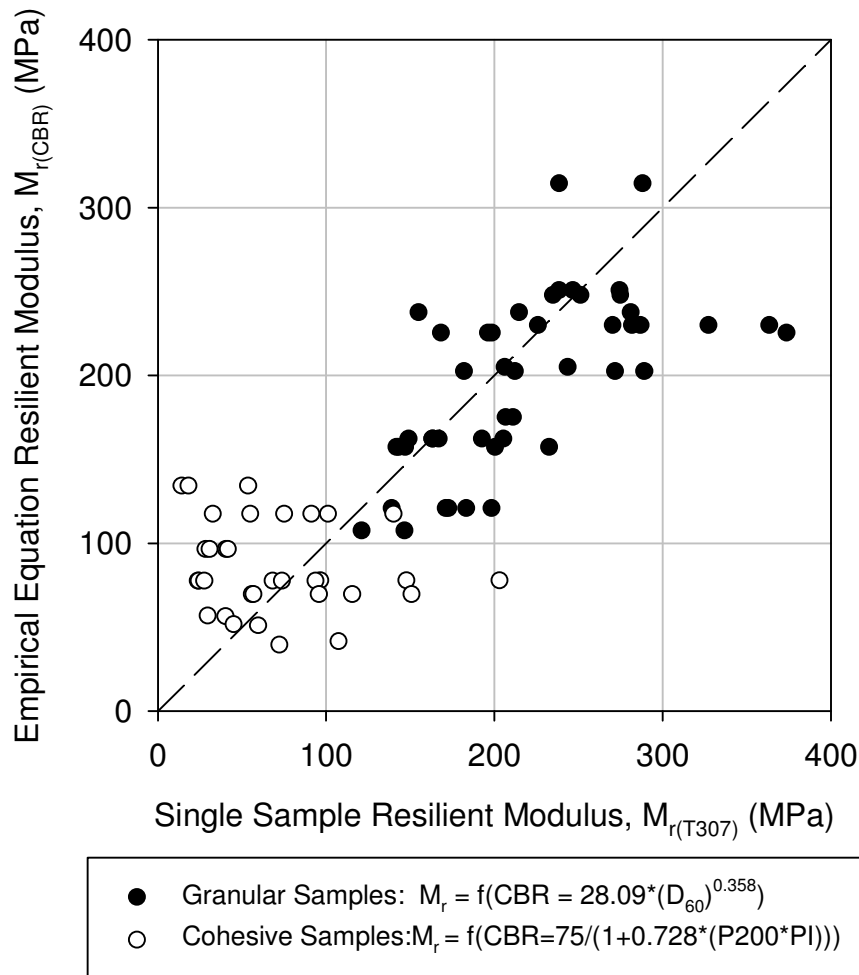

Figure 93. M_r values derived from equations provided in the MEPDG (NCHRP 2004b) compared to the single sample average $M_{r(T307)}$ values

Layered equivalent resilient moduli

Layered equivalent composite resilient moduli ($M_{r(Equiv\ Composite)}$) were determined from $M_{r(T307)}$ values of single material samples and combined in Equation 39 (Von Quintus and Killingsworth 1997). Equation 39 was developed to be used with resilient moduli determined

from in situ tests. To match the laboratory conditions, thicknesses of 10.2 cm (4 in.) were used for each layer to calculate $M_{r(Equiv\ Composite)}$.

$$M_{r(EquivComposite)} = \frac{D_{s1}^3 M_{r1} + D_{s2}^3 M_{r2}}{\left(D_{S1}\right)^3 + \left(D_{S2}\right)^3} \tag{39}$$

where: M_{r1} = resilient modulus of the upper layer;

M_{r2} = resilient modulus of the lower layer;

D_{S1} = thickness of the upper layer; and

D_{S2} = thickness of the lower layer.

$M_{r(T307)}$ and $M_{r(Equiv\ Composite)}$ values were strongly related and close to the equality line (i.e. $M_{r(Equiv\ Composite)} = M_{r(T307)}$). When calculating $M_{r(Equiv\ Composite)}$, care was taken to compare single material samples that had unit weight and moisture contents within ± 1.0 kN/m^3 and $\pm 3\%$, respectively, to the corresponding layers in composite samples.

Although Equation 39 was developed for in situ data, it provides a good relationship to determine composite M_r values from laboratory data. However, care should be exercised when comparing the laboratory determined M_r values with in situ M_r values because of the boundary effects. Comparisons of $M_{r(T307)}$ and $M_{r(Equiv\ Composite)}$ are summarized in Figure 94.
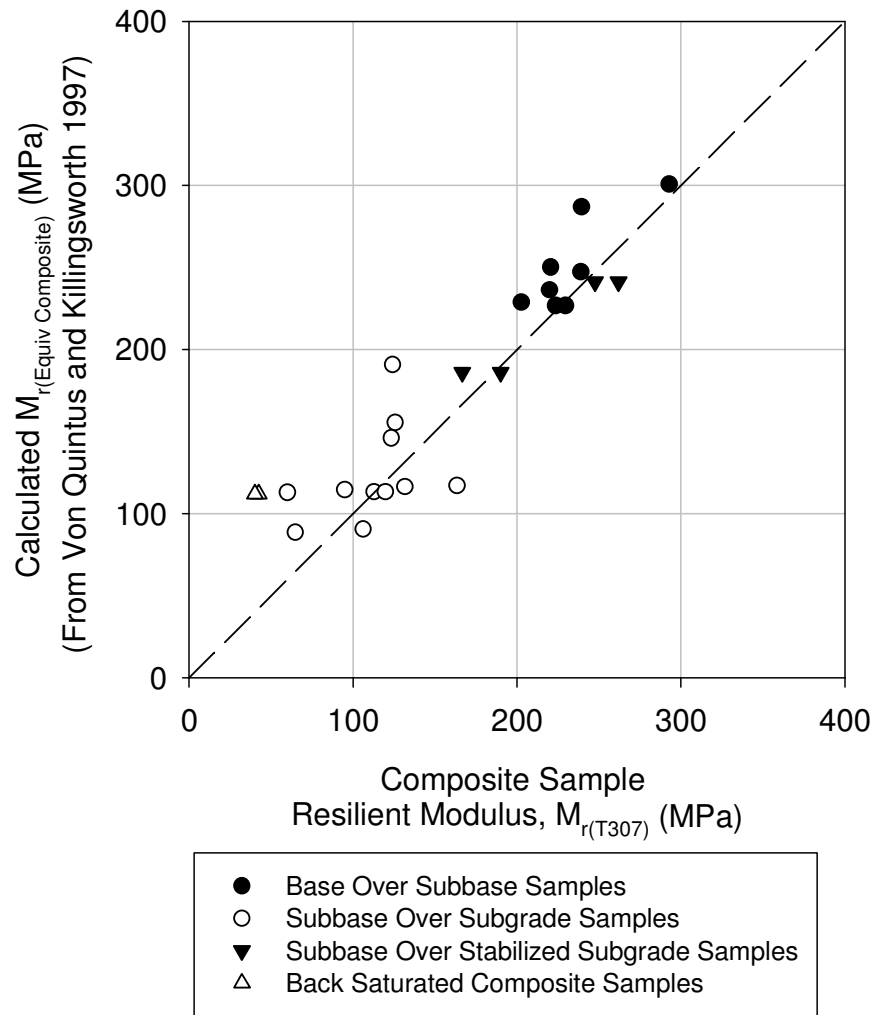
Figure 94. Layered equivalent M_r derived from Von Quintus and Killingsworth (1997) equation compared to the $M_{r(T307)}$ for composite samples

$M_{r(Equiv\ Composite)}$ values might differ from $M_{r(T307)}$ values because the boundary conditions and edge effects from in situ data were not present in the laboratory data. The ends of laboratory specimens were in contact with steel platens. This condition was analogous to having an infinitely stiff layer right below the in situ subgrade. In situ layers also had stress bulbs and shear stresses that develop, illustrated in Figure 95. These effects will alter the M_r values used to calculate $M_{r(Equiv\ Composite)}$ values. Additionally, if the differences in unit weight and moisture content between single material samples and composite sample layers were too

large, the resilient moduli would be affected and lead to errors in determining the $M_{r(Equiv\ Composite)}$ values.
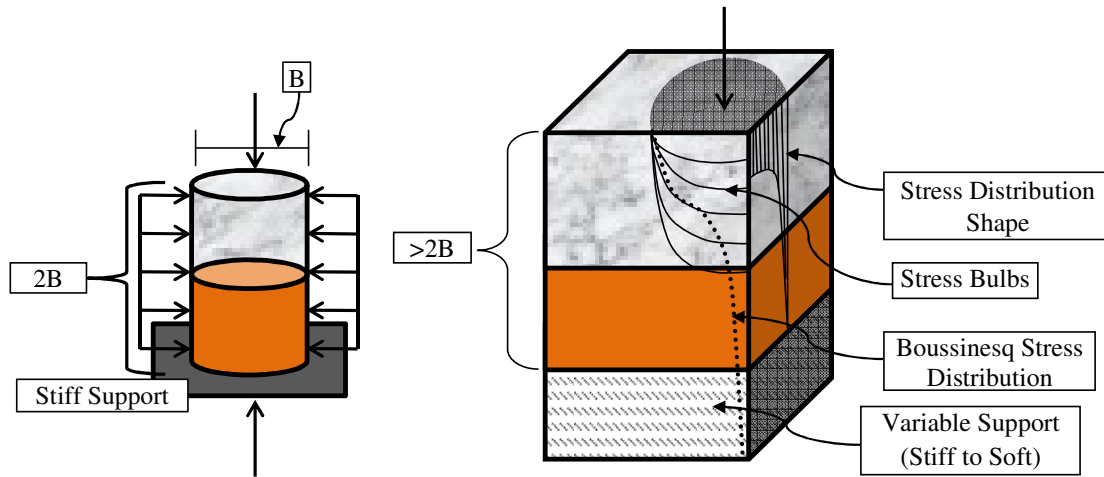

Figure 95. Idealized comparison between laboratory (left) and in situ (right) boundary conditions

DESIGN VALUES

This section discusses the parameters and values that are used in pavement design. Common parameters include resilient modulus, regression coefficients, and modulus of subgrade reaction. This section focuses on parameters determined from laboratory data— resilient moduli and regression coefficients. The section concludes with an example of the differences between design assumptions and measured moduli from the Michigan I-94 site.

Resilient modulus

When resilient modulus tests are not performed, values based on regional experience or material type can be assumed. These assumed values are considered level 3 inputs by the MEPDG (NCHRP 2004b). Level 3 inputs are the least accurate and are the default values based on regional experience. Level 3 inputs should be used when the consequences for early failure are minimal (e.g., low volume roads). For comparison, $M_{r(T307)}$ values were compared to the M_r value ranges provided in the MEPDG. As expected, the general trend was for the resilient moduli to decrease for the cohesive and fine grained soils and increase for the granular soils. $M_{r(T307)}$ values do not always precisely match up to the ranges provided by the MEPDG. The MEPDG M_r value ranges often tended to overestimate the resilient moduli,

when compared to the laboratory specimens. The $M_{r(T307)}$ values are compared to MEPDG M_r value ranges by AASHTO and USCS soil type in Figure 96.
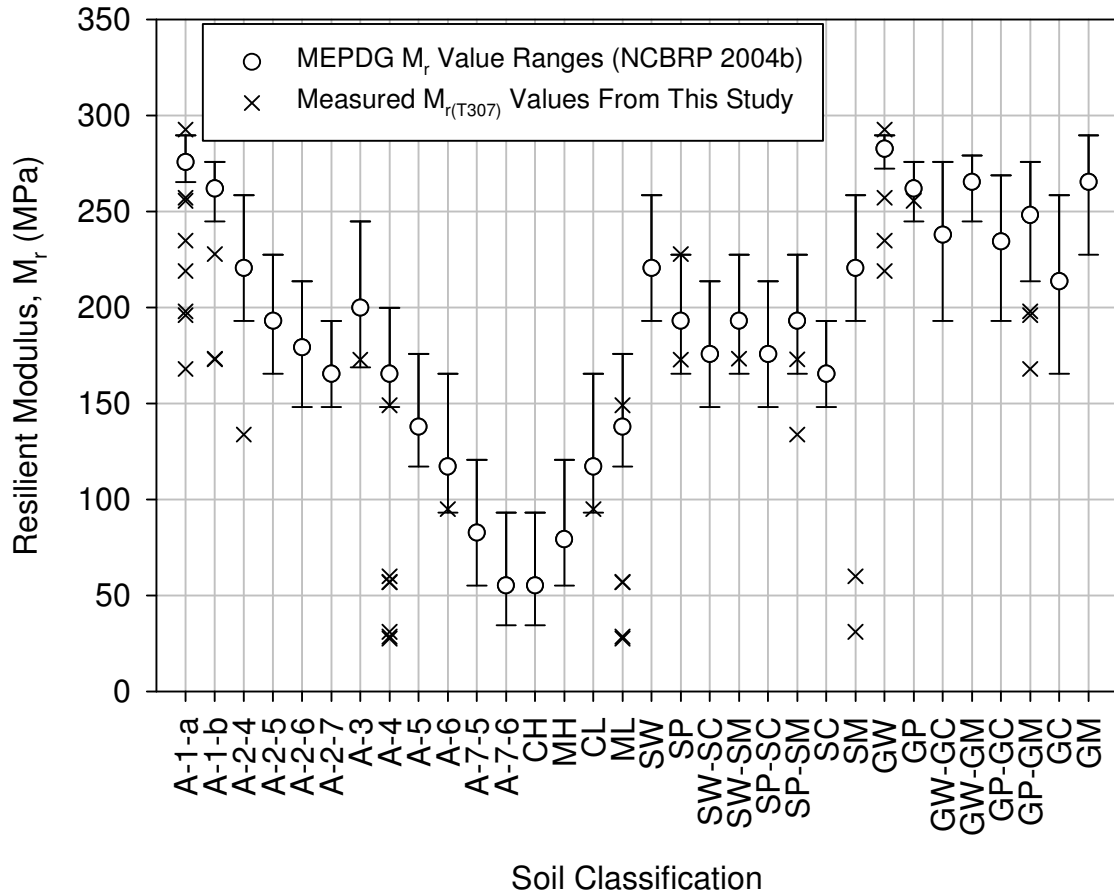

Figure 96. $M_{r(T307)}$ values and MEPDG M_r value ranges compared according to soil classification

Regression coefficients

Many models have been developed to account for nonlinear soil behavior. This study focused on the MEPDG recommended "universal model" (Witczak and Uzan 1988). The MEPDG uses the regression coefficients (k_1, k_2, k_3) as level 1 design inputs for flexible pavements. The coefficients model the relationship between resilient modulus and confining and deviator stresses, which are incorporated into the "universal model" (Equation 40) by the octahedral and bulk stress parameters.

$$M_r = k_1 P_a \left(\frac{\sigma_B}{P_a} \right)^{k_2} \left(\frac{\tau_{oct}}{P_a} + 1 \right)^{k_3} \tag{40}$$

where: P_a = atmospheric pressure (MPa);

σ_B = bulk stress (MPa) = $\sigma_1 + \sigma_2 + \sigma_3$;

τ_{oct} = octahedral shear stress (MPa) $= \dfrac{\sqrt{(\sigma_1 - \sigma_2)^2 + (\sigma_2 - \sigma_3)^2 + (\sigma_3 - \sigma_1)^2}}{3}$;

σ_1, σ_2, σ_3 = principal stresses; and

k_1, k_2, k_3 = regression coefficients.

Resilient modulus is fairly proportional with k_1. As resilient modulus increased, the k_1 value also increased fairly linearly. The outlier is a very stiff cement stabilized subgrade sample from Pennsylvania US-22 which had a 1406 kPa applied stress at 1% axial strain. Overall, subgrade materials tended to have higher k_1 values than base or subbase materials. Resilient modulus tests on subgrade materials used lower stress states than base or subbase materials (as seen in Table 27 and Table 28). Generally, lower stress states would result in σ_B and τ_{oct} being fairly small, leading the k_2 and k_3 values to be smaller, as well. Therefore, the k_1 value would become a larger constituent of the M_r relationship in Equation 40.

The k_2 regression coefficient is related to the behavior of the material due to changes in volumetric (e.g., bulk) stress. Bulk stress is made up of the three orthogonal stresses, as described in Equation 40. For triaxial specimens the intermediate and confining stresses are assumed to be equal ($\sigma_2 = \sigma_3$), so bulk stress is more an indicator of the confining stress applied to the sample than the deviator stress. The granular materials tended to have higher k_2 values than the cohesive materials. The cohesive materials had k_2 values that ranged from -0.56 to 0.71. Most of the lower k_2 values can are found at low M_r values, for cohesive materials. The Michigan I-96 samples tended to have a more linear $M_{r(T307)}$-σ_B relationship. For negative k_2 values, the cohesive samples tended to show decreasing M_r values with increasing bulk stress. The trends for the cohesive materials $M_{r(T307)}$-σ_B relationships are not as clear as granular samples. This indicates that granular materials are more dependant on the bulk (and therefore confining) stresses than the cohesive materials. $M_{r(T307)}$-σ_B relationships

for select samples are compared in Figure 98. Additional examples are provided in Appendix G.

Granular materials tend to have k_3 values near zero, while samples with cohesive materials (single and composite material specimens) tend to have larger negative k_3 values and smaller average resilient modulus values. The octahedral stress is made up of primarily the deviator stress. It is well documented (Seed et al. 1962; Huang 1993; Lee et al. 1997; Andrei et al. 2004) that the deviator stress is an important factor in resilient moduli determination for cohesive materials and less so for granular materials. The stiffness of granular materials is more dependant on confinement stress, thus the bulk stress parameter is more closely related to the behavior of granular materials. The k_3 value illustrates the effect of shear softening of cohesive samples. Shear softening was less apparent over the range of tested densities and moisture contents for the granular samples, as indicated by k_3 being approximately equal to zero. Figure 97 is a summary of the regression coefficients (k_1, k_2, and k_3) versus the laboratory average resilient modulus values.
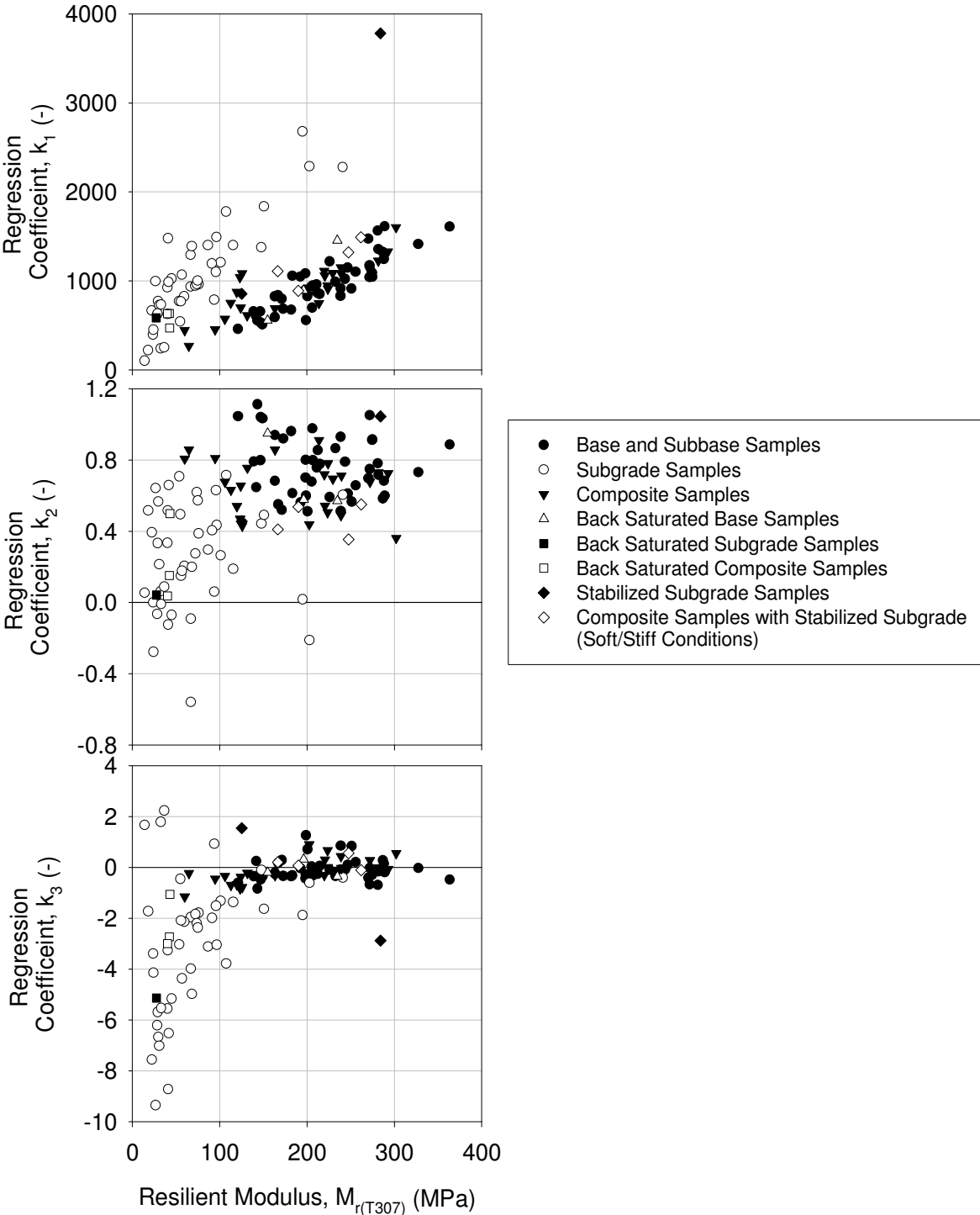
Figure 97. Summary of regression coefficients (k₁, k₂, and k₃) versus the

**laboratory average resilient modulus**
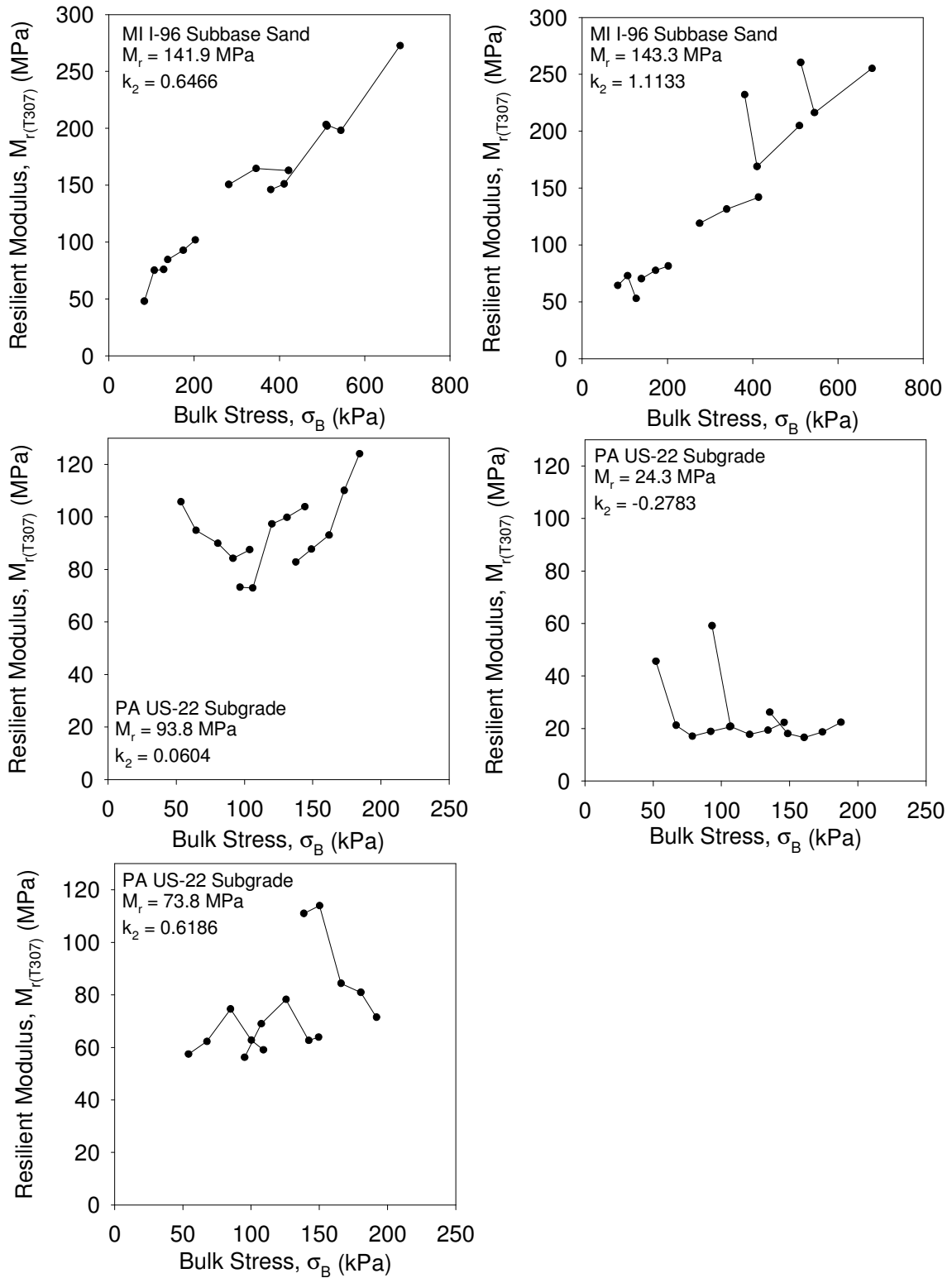
Figure 98. $M_{r(T307)}$-σ_B relationships for samples with various k_2 values

Base samples tended to have a lower than unity regression coefficient relationships (i.e., the composite sample value was less than the single sample value), and subgrade samples tend to have a higher than unity relationship. This trend is also seen in composite versus single material resilient modulus graph in Figure 78. The reason for this trend is that layering of materials of different moduli affects the overall modulus. For most tests in this study, composite samples had a stiffer upper layer (base material) and a softer lower layer (subgrade material). Layering causes the composite sample M_r values to be between the extremes of the stiffer and softer layers.

Base and subbase single material samples had larger M_r and k values than the corresponding base and subbase layers in composite samples. Also, subgrade single material samples had smaller M_r and k values than corresponding subgrade layers in composite samples. These trends were true for k_1, k_2, and k_3 values. Being able to determine the modulus of a layered system, rather than just the individual materials, would lead to less uncertainty in design and more economical construction practices. Figure 99 summarizes the regression coefficients (k_1, k_2, and k_3) for composite samples versus single samples.
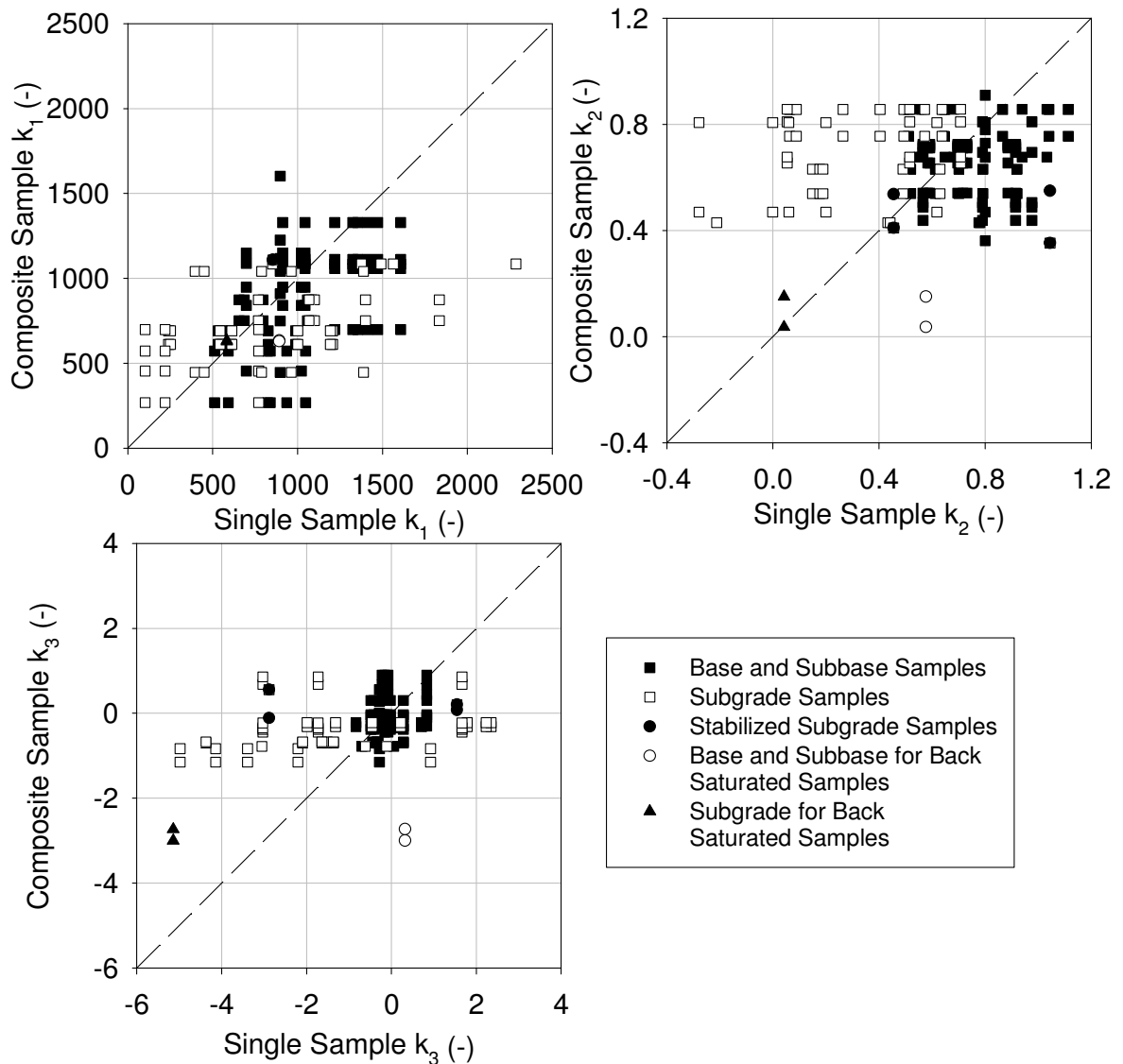
Figure 99. Summary of regression coefficients (k_1, k_2, and k_3) for composite samples

and single samples

Site example

Michigan I-94

Information was obtained from the Michigan Department of Transportation (MDOT) about the design process for the I-94 test location. The following is a comparison between the design assumptions and measured laboratory and in situ values.

The *AASHTO Guide for Design of Pavement Structures* (1993) was used to determine the design values for the Michigan I-94 test location. The design was for jointed plain concrete pavement.

Laboratory and in situ moduli were determined as described above and in the Methods chapter. The in situ composite modulus of subgrade reaction (k_{comp}) was determined by the PLT. The in situ k_{comp} values had to be corrected from a 300 mm (12 in.) plate diameter to a 762 mm (30 in.) plate diameter used in determining the design value. Equations 41 and 42 (Terzaghi 1955) were used to correct the plate size.

$$k_s = k_1 \left[\frac{B + B_1}{2B} \right]^2 \text{; footings on sand} \tag{41}$$

$$k_s = k_1 \left[\frac{B_1}{B} \right] \text{; footings on clay} \tag{42}$$

where: B_1 = side dimension of a square plate used in the load test;

B = width of footing;

k_s = modulus of subgrade reaction; and

k_1 = stiffness estimated from a static plate load test.

The laboratory modulus values were tested under a range of moisture and unit weight values to simulate in situ conditions. For the unit weight and moisture contents tested, the laboratory Shelby tube M_r values were slightly larger than the design values. The elastic modulus of the subbase (E_{SB}) design value matched up very well the laboratory values, but the measured PLT (E_{v1}), LWD ($E_{LWD-Z3(72)}$), and FWD (E_{FWD}) values were much lower. Additionally, k_{comp} design values were determined by MDOT through charts and correlations with the pavement thickness, subgrade M_r value, E_{SB}, and the loss of support (LS) value. The in situ k value was determined from the plate load test as described earlier in the In Situ Studies section. Again, the measured E_{SB} and k_{comp} values were much lower than the design values.

For the tested moistures and densities, the laboratory M_r value indicates that the design value might be slightly conservative. A possible reason for the discrepancy between the values is that the provided design values correspond to the average over the year, while the

tested values correspond to a specific season. Different moduli are used during different seasons to account for changes due to spring thaw or midwinter freezing. If the moduli actually indicated that the foundation is not stiff enough, pavement deterioration could be accelerated from the increased slab movement (due to decreased stiffness). The predicted long term performance of the pavement structure could be affected. Increased in situ moduli could also develop over time due to thixotropy and further compaction from equipment during construction before traffic is allowed to use the roadway.

These findings demonstrate the inconsistencies between the assumed values used in design and what is actually measured in the laboratory and in situ. If more accurate values are input into the design process, more accurate results can be predicted about the performance of the pavement. The cost differences for increased testing, long term performance, maintenance, and replacement need to be quantified. The values used in the design process for Michigan I-94 are summarized and compared to in situ and laboratory measured values in Table 49.

Table 49. Summary of design, in situ, and laboratory values from Michigan I-94

Design Parameter	Design Value	In Situ Value	Laboratory Value
Subgrade M_r	20.7 MPa (3.0 ksi)	34.1–47.6 MPa (4.9–6.9 ksi)[a]	29.7–86.6 MPa[b] (4.3–12.6 ksi)
Slag base elastic modulus (E_{SB})	165.5 MPa (24.0 ksi)	$E_{v1} =$ 11.1–32.9 MPa (1.61–4.47 ksi) $E_{LWD\text{-}Z3(72)} =$ 22.7–105.2 MPa (3.29–15.3 ksi) $E_{FWD} =$ 19.5–83.7 MPa[c] (2.83–12.1 ksi)	$E_s =$ 73.6–214.4 MPa (10.7–31.1 ksi)
Composite modulus of subgrade reaction (k_{comp})	0.084 MPa/mm (310 pci)[d]	0.016–0.048 MPa/mm[d] (58.9–176.8 pci)	—[e]

[a] = values determined from DCPI values of the subgrade converted to M_r as a function of CBR according to Equations 27 and 30 at the same locations as the Shelby tube samples
[b] = determined from six Shelby tube samples obtained from 1.0–1.7 m (1.5–5.5 ft) below the ground surface;
[c] = E_{FWD} determined from the average of three drops (applied stresses range 0.28–0.45 MPa) with deflections measured directly under the loading plate;
[d] = design value determined using a 762 mm (30 in.) plate, in situ PLT values converted from 300 mm (12 in.) plate to 762 mm plate using Equation 41 (Terzaghi 1955); and
[e] = cannot be determined from measured values.

Michigan I-96

Information was obtained from the Michigan Department of Transportation (MDOT) about the design process for the I-96 test location. The following is a comparison between the design assumptions and measured laboratory and in situ values.

The *AASHTO Guide for Design of Pavement Structures* (1993) was used to determine the design values for the Michigan I-96 test location. The design was for jointed plain concrete pavement.

In situ and laboratory M_r values were larger than the design value. The design value was based on classifying the subgrade soil as a frost susceptible poorly drained loam, with MDOT borings indicating primarily sandy silty clay and no water table. Because only one value was selected, it is likely that the modulus is conservative and may represent the worst case conditions (i.e., spring thaw).

A possible reason for the discrepancy between the measured and design values is that the provided design values correspond to the average over the year. Different moduli are used during different seasons to account for changes due to spring thaw or midwinter freezing. If the moduli actually indicated that the foundation is not stiff enough, pavement deterioration could be accelerated from the increased slab movement (due to decreased stiffness). The predicted long term performance of the pavement structure could be affected. Increased in situ moduli could also develop over time due to thixotropy and further compaction from equipment during construction before traffic is allowed to use the roadway.

According to MDOT, E_{SB} value is a weighted average of the base and subbase values. The I-96 site used an open-graded cement treated base and sand subbase. FWD testing was performed directly on the cement treated base layer overlying the sand subbase and subgrade layers. In situ E_{FWD} values ranged from well below to slightly above the design value, with an average of 214.5 MPa (31.1 ksi).

The laboratory E_s value was based on only the sand subbase material and had a maximum value less than half of the design value. The $E_{LWD-Z3(72)}$ value was also performed on the sand subbase layer but was much less than the E_s value. Because neither of these values incorporates the cement treated base, they cannot be reliably compared to the design E_{SB} value.

The range of in situ k_{comp} values were less than the design value. The PLT was used to determine k_{comp}, and the test was performed on the sand subbase layer.

The values used in the design process for Michigan I-94 are summarized and compared to in situ and laboratory measured values in Table 50.

Table 50. Summary of design, in situ, and laboratory values from Michigan I-96

Design Parameter	Design Value	In Situ Value	Laboratory Value
Subgrade M_r	20.7 MPa (3.0 ksi)	116.5–290.3 MPa[a] (16.9–42.1 ksi)	29.1–33.1 MPa[b] (4.22–4.80 ksi)
Subbase elastic modulus (E_{SB})	E_{SB}: 413.7 MPa[c] (60 ksi)	$E_{LWD-Z3(72)} =$ 9.9–52.3 MPa[d] (1.44–7.59 ksi) $E_{FWD} =$ 46.2–496.8 MPa[e] (6.7–72.1 ksi)	$E_s =$ 12.1–200.1 MPa[f] (17.5–29.0 ksi)
Composite modulus of subgrade reaction (k_{comp})	0.136 MPa/mm (500 pci)	0.014–0.053 MPa/mm[g] (51.9–193.9 pci)	—[h]

[a] = values determined from DCPI values of the subgrade converted to M_r as a function of CBR according to Equations 27 and 30 at the same locations as the Shelby tube samples
[b] = determined from two Shelby tube samples obtained from 0.0762-0.308 m (0.25-1 ft) below the ground surface;
[c] = weighted average of cement treated base and sand subbase (per MDOT correspondence);
[d] = measured from $E_{LWD-Z3(72)}$ performed directly on sand subbase;
[e] = E_{FWD} determined from a single drop on CTB over sand subbase with an applied stresses range of 0.32–0.39 MPa with deflections measured directly under the loading plate;
[f] = single material sample of subbase sand;
[g] = design value determined using a 762 mm (30 in.) plate, in situ PLT values converted from 300 mm (12 in.) plate to 762 mm plate using Equation 41 (Terzaghi 1955); and
[h] = cannot be determined from measured values.

Pennsylvania US-22

Information was obtained from the Pennsylvania Department of Transportation (PennDOT) about the design process for the US-22 test location. The following is a comparison between the design assumptions and measured laboratory and in situ values.

The *AASHTO Guide for Design of Pavement Structures* (1993) was used to determine the design values for the Pennsylvania US-22 test location. The design method was for jointed plain concrete pavement. Foundation layer design parameters (i.e., E_{SB}, subgrade M_r) were selected using CBR relationships and the PennDOT Pub 242 Pavement Policy manual. The AASHTO 1993 Design Guide did not include methods to account for structural effects from the CTB.

A possible reason for the discrepancy between the values is that the provided design values correspond to the average over the year. Different moduli are used during different seasons to account for changes due to spring thaw or midwinter freezing. If the moduli

actually indicated that the foundation is not stiff enough, pavement deterioration could be accelerated from the increased slab movement (due to decreased stiffness). The predicted long term performance of the pavement structure could be affected. Increased in situ moduli could also develop over time due to thixotropy and further compaction from equipment during construction before traffic is allowed to use the roadway.

Laboratory modulus values were tested under a range of moisture and unit weight values to simulate in situ conditions. For the unit weight and moisture contents tested, the laboratory M_r values indicate that the design value was not being attained. The lower laboratory M_r values could increase the required pavement thickness. Increased quantities of pavement materials would lead to increased project costs. However, in situ correlations between DCPI and M_r values indicate that some areas may be reaching the design values but other areas are well below specifications.

Both the in situ ($E_{LWD-Z3(72)}$) and laboratory (E_s) elastic moduli were lower than the design E_{SB} value for the summer test period. These low values would lead to increases in the pavement thickness. Additionally, the predicted long term performance of the pavement structure could be affected. If the foundation is not stiff enough, the deterioration could be accelerated from the increased slab movement (due to decreased stiffness). In situ and laboratory k_{comp} values were not determined at this site and, therefore, could not be compared to the design value.

Overall, there appears to be inconsistencies between the design and measured values. The modulus values used in the design process for Pennsylvania US-22 are summarized and compared to in situ and laboratory modulus values in Table 51.

Table 51. Summary of design, in situ, and laboratory values from Pennsylvania US-22

Design Parameter	Design Value	In Situ Value	Laboratory Value
Subgrade M_r	206.8 MPa (30 ksi)	40.4–277.8 MPa[a] (5.86–40.3 ksi)	23.8–93.8 MPa (3.45–13.6 ksi)
Class 2A subbase elastic modulus (E_{SB})	*Summer/fall:* 206.8 MPa (30 ksi) *Winter:* 344.7 MPa (50 ksi) *Spring:* 103.4 MPa (15 ksi)	*Summer:* 7.23–95.4 MPa[b] (1.05–13.8 ksi)	$E_s =$ 111.8 MPa (16.2 ksi)
Composite modulus of subgrade reaction (k_{comp})	0.143 MPa/mm (526 pci)	—[c]	—[d]

[a] = values determined from DCPI values of the subgrade converted to M_r as a function of CBR according to Equations 27 and 30 from approximately the top 300 mm of subgrade;
[b] = measured from $E_{LWD-Z3(72)}$ performed directly on class 2A subbase during the summer of 2009;
[c] = not measured; and
[d] = cannot be determined from measured values.

STABILIZATION TECHNIQUES

Three materials were stabilized using different chemical techniques. Fly ash was mixed into Iowa I-29 subgrade, cement was mixed into Pennsylvania US-22 subgrade, and a high-density polyurethane (HDP) foam was injected into Pennsylvania US-422 open graded stone (OGS) subbase. Fly ash was added to the Iowa subgrade at 15% by dry unit weight, and cement was added to the Pennsylvania subgrade at 10% by dry unit weight. The Pennsylvania US-22 specimen could be classified as a soft over stiff layered condition.

The Iowa fly ash-stabilized subgrade specimen experienced a 40% increase in $M_{r(T307)}$ values when layered with the RPCC base. The Pennsylvania cement-stabilized subgrade experienced a 10% decrease in $M_{r(T307)}$ values when layered with the Class 2A subbase. The Pennsylvania OGS experienced a 25% decrease in M_r when injected with the foam. However, it should be noted that the dry unit weight of the OGS sample ($\gamma_d = 18.54$ kN/m^3) was considerably higher than the foam and OGS sample ($\gamma_d = 14.92$ kN/m^3), and the difference in densities could have caused the difference in M_r values. Because the fly ash-

and cement-treated subgrades were kept at constant densities for the single and composite material samples, the changes in M_r are more likely due to the properties of the upper layers (i.e., RPCC base and Class 2A subbase).

Solanki et al. (2010) demonstrated that lime, class C fly ash and cement kiln dust increase the design resilient moduli of subgrade clay soils. At low application rates (3–6%), lime treatment increased M_r values by 140–810%, depending on soil type. Greater applications of lime decreased the strength values of the soil. High application rates (10–15%) of class C fly ash and cement kiln dust also increased M_r values by 130–1100% and 400–2000%, respectively, depending on soil type.

Overall, the resilient moduli are dependant on the composite stiffness of the layered system. Increasing the stiffness of the weakest layer will increase the stiffness of the composite system. Using the weakest layer as the design value is too conservative and does not represent the increased stiffness from other layers. The results for the stabilized materials are summarized in Figure 100.
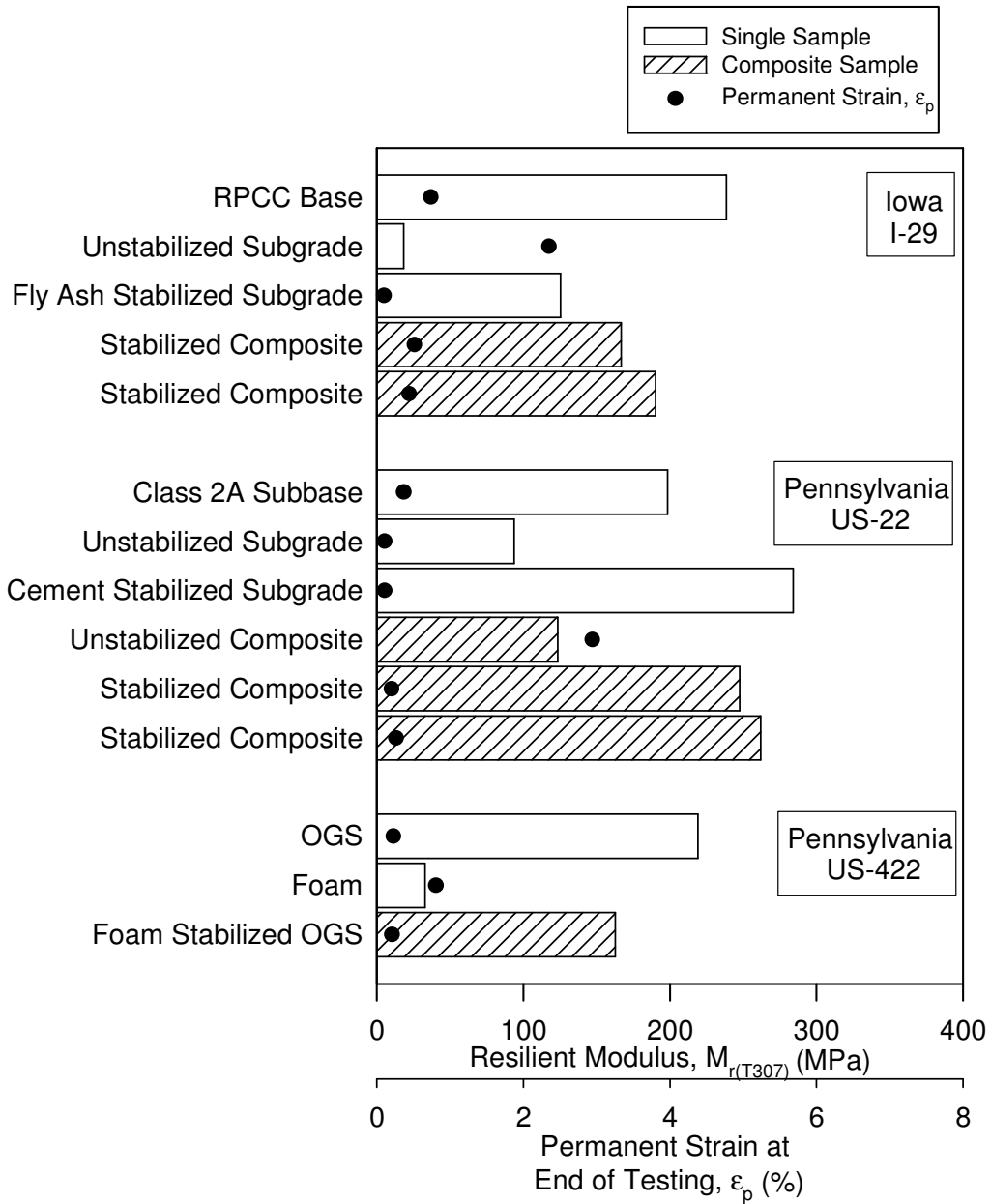
Figure 100. Summary of resilient moduli for stabilized materials

FINE MATERIAL MIGRATION

The migration of fine particles (silt and clay size) is thought to affect the pavement foundation performance. Over the life of pavement structures, fine particles from lower layers tend to infiltrate into upper layers with larger void ratios. The fine particle

contamination of the upper layers affects the permeability and may also affect the overall stiffness of the foundation.

Resilient modulus tests were performed according to AASHTO T307-99 on materials from several states as summarized in Table 52. Sample back saturation was performed according to the method described in Chapter 3. Two methods for the 10,000 cycle M_r test were used and are described in Appendix C. The first method was performed on the Pennsylvania US-22 Class 2A subbase specimen; the second was performed on the Iowa composite RPCC-loess specimen.

Table 52. Summary of tests to analyze migration of fine particles

Material Origin	Materials Tested	Type of Test
Michigan I-94	Slag Base	M_r
Michigan I-96	Sand subbase	M_r
Pennsylvania US-22	Class 2A subbase	10,000 cycle M_r
Iowa	Composite RPCC/loess	M_r, back saturated M_r, 10,000 cycle back saturated M_r
	Special backfill subbase	M_r
	RPCC	M_r

After the completion of the M_r test sequences, the materials from Michigan I-94, Michigan I-96, and Pennsylvania US-22 were analyzed by dividing each specimen into three equal portion (i.e., top, middle, and bottom) and performing particle distribution tests on each portion.

The Michigan I-94 particle distribution shows a slight decrease in sand content in the top portion, but the change in fine particle content is negligible for each of the three portions. The Michigan I-96 particle distribution shows almost no change in fine particle content throughout the entire specimen. The particle distributions for Michigan I-94 and I-96 are plotted in Figure 101 and Figure 102, respectively.
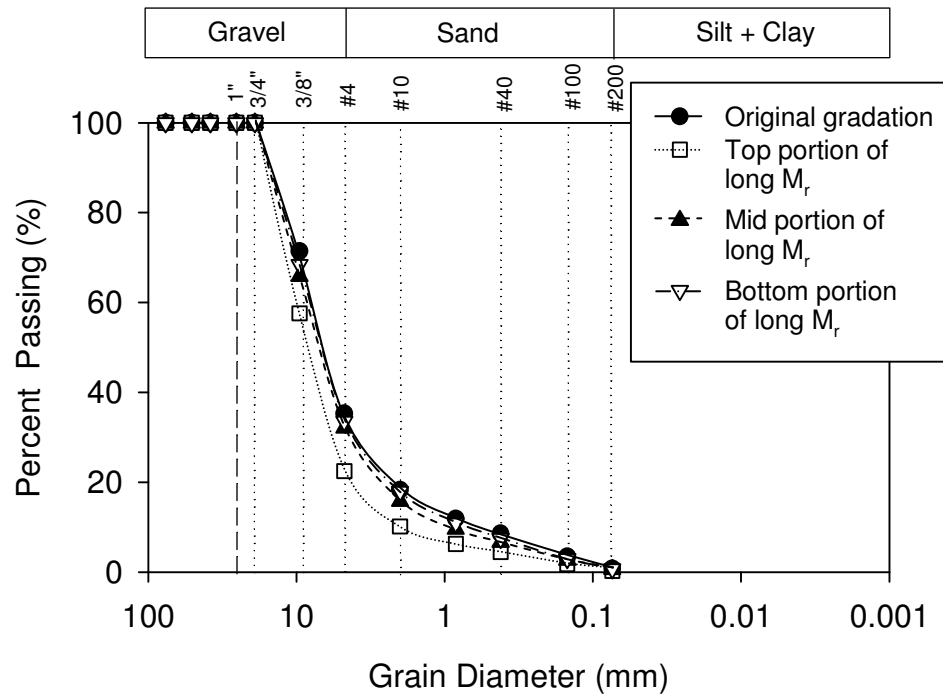
Figure 101. Particle distribution of Michigan I-94 slag base after M$_r$ test
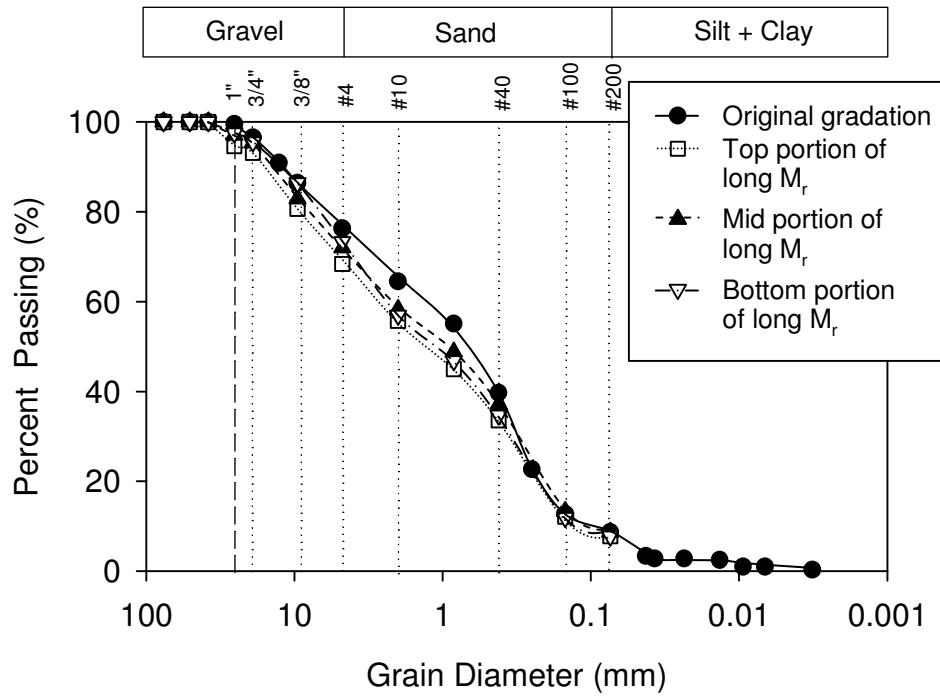


Figure 102. Particle distribution of Michigan I-96 sand subbase after M$_r$ test

The original particle distribution of the Pennsylvania US-22 specimen is approximately equal to the mid portion gradation. Both the top and bottom portions had increases in fine particles. Because of the high axial stresses applied during the 10,000 cycle resilient modulus test and the fact that the percent of fine particles did not increase in the middle portion, particle breakage near the end surfaces was probably the cause of the increase in fine particles. The top and bottom portions most likely absorbed more of the applied stresses, and therefore, the mid portion did not incur much particle breakage. The results show that there was almost no determinable movement of fine particles after the 10,000 cycle M_r test. The particle distributions of the Pennsylvania US-22 specimen are plotted in Figure 103.

Figure 103. Particle distribution of Pennsylvania US-22 Class 2A subbase

after 10,000 cycle M_r test

The tests on the Iowa composite specimen of RPCC over loess were not analyzed by particle distributions. Instead a visual check was used to determine whether any of the loess particles infiltrated the porous RPCC void structure. The M_r, back saturated M_r, and 10,000 cycle back saturated M_r tests showed no movement of fine particles. The loess seen around the RPCC particles at the interface of the back saturated M_r test specimen was due to

the compaction of the RPCC into the loess. No loess is seen above the level where the RPCC penetrated into top of the loess (Figure 104). In both of the back saturated specimens, as the membrane was cut, water poured out of the RPCC at the RPCC-loess interface. The water was clear as seen in Figure 105, indicating no loess in suspension.

**Figure 104. Interface of Iowa RPCC-Loess specimen after back saturated M_r testing**
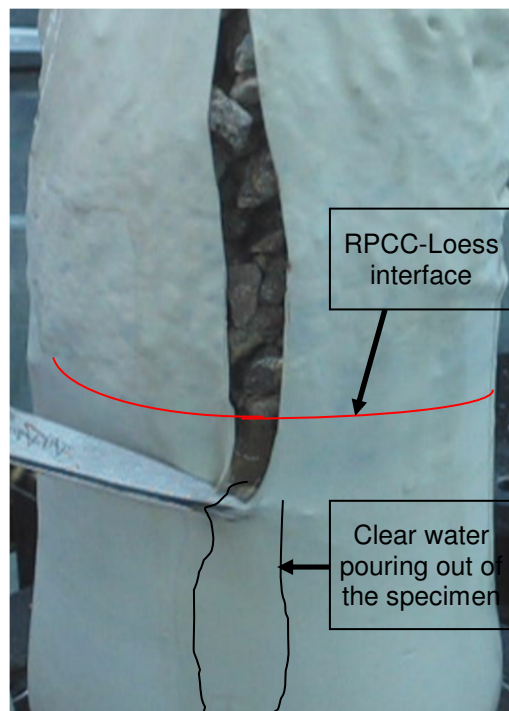
Figure 105. Clear water pouring out of the Iowa RPCC-loess back saturated

10,000 cycle M_r specimen

Through the several resilient modulus tests and observations, it became apparent that either 10,000 cycles are not enough, the applied stresses do not adequately correlate to vehicle movements, a wider range of densities needs to be tested, or there is another condition which has not been accounted for (e.g., loss of support creating slab movement, etc.) to induce significant fine particle movement in this material.

CHAPTER 6. CONCLUSIONS AND RECOMMENDATIONS

This chapter presents three categories of conclusions—laboratory moduli, in situ moduli, and design values—as well as recommendations for immediate impact, long-term impact, and future research.

The three conclusion categories summarize the major ideas derived from the data. The three recommendation categories discuss short- and long-term ideas that could impact pavement foundation design and construction practices and also provide several ideas to further advance the knowledge gained from this study.

LABORATORY MODULI CONCLUSIONS

Single material sample resilient moduli

The AASHTO T307 standard uses single material samples tested over a range of confining and deviator stress conditions to quantify resilient moduli model parameter values. This study expanded the variables of the standard test to include factors including moisture and density variation and two layer composite samples. Test results showed that increased moisture contents and degree of saturation resulted in decreased $M_{r(T307)}$ values. Incrementally increasing the degree of saturation by approximately 15% resulted in a 28% decrease in $M_{r(T307)}$ value for a granular sample. Incrementally increasing the degree of saturation by approximately 30% resulted in a 70% decrease in $M_{r(T307)}$ value for a cohesive sample. The inverse relationship between matric suction and degree of saturation may explain the decreases in resilient moduli with increasing saturation. Additionally, all single material back saturated samples had larger permanent strain, ε_p, at the end of testing than non-back saturated samples. Yang et al. (2008) found that increases in matric suction reduced the resilient strain, which indicated that high matric suction increased the effective stress and decreased deformation. At higher degrees of saturation, matric suction and effective stresses decrease, reducing the $M_{r(T307)}$ values and increasing the ε_p experienced by the sample.

Resilient moduli are dependent on the stress condition (i.e., confining and deviator stresses). The National Highway Cooperative Research Program (NCPRP) Project 1-28A (2004a) suggested that a resilient modulus value be determined by interpolating the resilient moduli values using $\sigma_{cyclic} = 103$ kPa (15 psi) and $\sigma_3 = 35$ kPa (5 psi) for granular materials and $\sigma_{cyclic} = 41$ kPa (6 psi) and $\sigma_3 = 14$ kPa (2 psi) for cohesive materials, where σ_{cyclic} is

defined as $\sigma_{maximum}$ minus $\sigma_{contact}$. The specific stress states described by NCHRP lie within the range of applied stresses according to the AASHTO T307 standard. In this study, the Zorn LWD applied approximately 100 kPa to the material surface and the FWD applied a range of stresses (from 300 kPa to over 500 kPa). These stresses align with the NCHRP stresses for base materials but are large for tests on subgrade materials. To accurately model responses of pavement foundation layers, analyzed stress states must match the stress states experienced in situ (i.e., higher stresses for base and subbase layers than for subgrade layers). Discrepancies may occur between laboratory and in situ values because of differences in boundary conditions and applied stresses during QC/QA testing.

Composite material sample resilient moduli

Laboratory testing on composite samples creates an opportunity to evaluate the layered nature of pavement foundation conditions and directly factors interface effects and composite behavior into the measurements. Design methods often use composite moduli to characterize several layers of the pavement foundation layers into thickness design calculations, but the methods do this based on single layer measurements and theoretical relationships instead of laboratory composite test samples. Laboratory test results in this study showed statistically that the laboratory $M_{r(T307)}$ values are affected by individual layer modulus values. Using a statistical criteria approach, lower layers that were weaker than upper layers were significant (p-values<0.05) in determining $M_{r(T307)}$ values. Typically, pavement foundation layers are comprised on a stiff layer over a weak layer. Additionally, increasing $M_{r(T307)}$ values of lower layers significantly increased composite sample $M_{r(T307)}$ values. This would be analogous to stabilizing a weak subgrade layer underlying an aggregate base layer. For most samples, $M_{r(T307)}$ and ε_p values for composite materials fell between $M_{r(T307)}$ and ε_p values of the stiffer and softer layers.

The addition of geofabric at the interface between soil layers did not significantly increase $M_{r(T307)}$ values because of the small restraining stresses. Geofabrics are more commonly used as separation layers rather than reinforcement layers. The larger aperture size of geogrids (more commonly used for reinforcement) did not allow for testing with the 101.6 mm (4 in.) diameter samples used in this study.

Only one composite back saturated sample had a smaller ε_p at the end of testing than the corresponding composite non-back saturated sample. This data illustrates the inverse relationship between moisture content and resilient modulus.

Stabilization techniques

Soil stabilization is an important practice in pavement foundation construction. This study investigated a limited set of stabilization techniques. Subgrade samples stabilized with 10% cement by dry unit weight experienced a 203% increase in $M_{r(T307)}$ values compared to unstabilized subgrade samples. Subgrades samples stabilized with 15% fly ash by dry unit weight experienced a 588% increase in $M_{r(T307)}$ values compared to unstabilized subgrade samples. Composite fly ash stabilized samples experienced a 100–112% increase in $M_{r(T307)}$ values compared to unstabilized composite samples. The soil characteristics, amount of stabilizer, and type of stabilizer will affect the level of change in resilient moduli (Solanki et al. 2010). This topic should continue to be analyzed and refined in future studies.

Material index property correlations

Resilient modulus tests are expensive, time consuming, and require special training to measure quality data. To obtain enough information to accurately characterize foundation layers over an entire project site, other cost effective and less time consuming tests have been correlated to resilient modulus values (Thompson and Robnett 1979; George 2004; Roy 2007; Puppula 2008) Based on statistical criteria, this study found percent passing No. 200 sieve (0.075 mm) and percent passing No. 4 sieve (4.75 mm) were significant in determining resilient moduli for granular materials. Undrained shear strength results were found to be significant (p-values < 0.0001) in determining resilient moduli for both granular and cohesive materials. However, coefficient of uniformity, coefficient of curvature, Atterberg limits, and ratio of dry unit weight-moisture content to not be significant in determining resilient moduli for any material type.

Secant moduli

Secant moduli were calculated to investigate direct comparisons between laboratory and in situ moduli. Comparing the same type of moduli (i.e., laboratory composite elastic moduli compared to in situ elastic moduli), limits the discrepancies between the values.

Cyclic secant moduli ($E*_{s(T307)}$) were closely related to $M_{r(T307)}$ values for all materials. The cycle by cycle increase in permanent strain was very small which caused the $E*_{s(T307)}$ and $M_{r(T307)}$ values to be nearly equal.

For dynamic secant moduli ($E_{s(T307)}$) greater than 22.5 MPa, the $M_{r(T307)}$-Es(T307) ratio for all materials equaled 1.30. This value corresponds to the M_r-E_{FWD} ratio in the Mechanistic-Empirical Pavement Design Guide: A Manual of Practice: Interim Edition (AASHTO 2008) for aggregate base or subbase below a PCC layer.

IN SITU MODULI CONCLUSIONS

In situ moduli

In situ tests provide a means for QC/QA of the pavement foundation materials. However, in situ and laboratory determined moduli are weakly linked. Plate load test elastic moduli (E_{v1} and E_{v2}), falling weight deflectometer elastic moduli (E_{FWD}), and light weight deflectometer elastic moduli ($E_{LWD-Z3(72)}$) were all less than $M_{r(T307)}$ values. There was little variation in the range of in situ elastic modulus values compared to the range of $M_{r(T307)}$ values. The discrepancies between in situ and laboratory data may be due to the differences in boundary conditions (George 2003).

Empirical correlations

Typical pavement design methods accept the use of empirical correlations to obtain moduli values. Future research should focus on evaluating the statistical significance of the differences between calculated values and measured values to quantify the level of uncertainty when determining design or QC/QA values.

Correlations using equations from MEPDG (NCHRP 200b) underestimated $M_{r(DCPI)}$ values in relation to $M_{r(T307)}$ values for most materials. Additional correlations using equations from Mohammad et al. (2008) underestimated $M_{r(DCPI)}$ values for cohesive materials by an average of 34% and overestimated $M_{r(DCPI)}$ values for granular materials by an average of 71% in relation to $M_{r(T307)-5/12}$ values. The discrepancies between $M_{r(DCPI)}$ and $M_{r(T307)}$ values may be due to strain differences. DCP tests provide a measure of the shear strength of the soil. High localized strain develops around the cone tip as the DCP apparatus penetrates into the soil, whereas small strains are experienced by laboratory Mr samples.

Most granular materials had higher $M_{r(LWD)-P}$ values than $M_{r(T307)-5}$ values, while $M_{r(LWD)-P}$ values for cohesive materials were evenly scattered around $M_{r(T307)-12}$ values. Measured LWD moduli were determined using a Zorn LWD device, while $M_{r(LWD)-P}$ was derived using a Prima LWD device. The different LWD devices had different plate diameters and drop heights. Increased drop heights or decreased plate diameters lead to increases in applied stresses to the material, which have been shown to affect the measured moduli (Vennapusa and White 2009).

$M_{r(CBR)}$ values (determined from D_{60} values for granular materials and P_{200} and PI values for cohesive materials) were correlated to $M_{r(T307)}$ values. The limited number of parameters incorporated in $M_{r(CBR)}$ correlations may introduce scatter to the relationship because the parameters that define the specific soil condition (e.g., unit weight, moisture content, soil classification, etc.) are neglected.

The equation by Von Quintus and Killingsworth (1997) provided agreement between composite $M_{r(T307)}$ values and $M_{r(Equiv\ Composite)}$ values, if dry unit weight and moisture contents were within ±1.0 kN/m3 and ±3%, respectively. The equation $M_{r(Equiv\ Composite)}$ was developed to analyze in situ layer moduli. $M_{r(T307)}$ values might differ from $M_{r(Equiv\ Composite)}$ values because the boundary conditions and edge effects from in situ data were not present in the laboratory data.

CONCLUSIONS FROM DESIGN VALUES

Regression coefficients

Regression coefficients (k_1, k_2, and k_3) account for nonlinear soil behavior. Each coefficient is related to specific stress parameters. Bulk stress dependence for granular materials was illustrated by positive k_2 values. Granular materials had k_3 values near zero, while cohesive materials had negative k_3 values. This illustrated shear softening of cohesive materials. As expected, just as for the $M_{r(T307)}$ values, layering influenced the composite sample k_1, k_2, and k_3 values.

Site examples

Design parameter values collected from state departments of transportation were compared to measured moduli. Many of the provided moduli values appear to be based on regional experience rather than detailed in situ investigations.

Both laboratory and in situ moduli were compared to design moduli. In general, laboratory resilient moduli were greater than the design values, and laboratory elastic moduli (E_s) were less than the design values. Boundary conditions and edge effects may have been a key factor in the differences between laboratory and design moduli. In situ moduli were scattered both greater and less than the design moduli, which indicated non-uniform pavement foundation conditions along the test site.

IMMEDIATE IMPACT

Laboratory and in situ test methods currently measure two different soil parameters—resilient moduli and elastic moduli. Both are used to characterize pavement foundations, but resilient moduli are more closely linked to pavement performance than elastic moduli. This study has shown that care needs to be taken when using resilient moduli values correlated from in situ elastic measurements, as they may not be directly related.

Additionally, pavement foundation layers have a significant effect on composite stiffness characteristics. Weak subgrades decrease composite moduli of foundation systems. Identifying weak areas at a site and using methods to increase the moduli of weak layers will have a significant impact on composite moduli.

LONG-TERM IMPACT

The industry problem discussed in the introduction chapter involved the need to properly evaluate the as-constructed values in relation to the design moduli. Improved test methods and correlations between in situ and laboratory tests can assist in analyzing foundation behaviors over a range of conditions (e.g., varying unit weights, moistures, etc.) experienced during the life of pavement structures. Better measurements over larger ranges of variables could also reduce the need for conservative assumptions during the design process, thus developing a more economical and better performing pavement system.

FUTURE RESEARCH RECOMMENDATIONS

The research presented in previous chapters investigated a limited number of variables and samples. To advance pavement foundation design and construction, additional in-depth investigations need to occur.

The lifetime load cycles experienced by pavement systems are poorly modeled by the current AASHTO resilient modulus standard. Additional sequences of cyclic loads could be used to investigate degradation of materials and movements of fine particles between foundation layers. Over time, foundation materials tend to degrade under cyclic loads. Permanent strains, changes in stiffness, and changes in particle gradation could be investigated at high number of cycles (e.g., 100,000 cycles) to better simulate in situ pavement conditions. Movements of fine particles between foundation layers are a known issue for long term pavement performance. Future research should include deeper investigations to study how the number of cycles, different materials, different boundary conditions (e.g., to simulate slab pumping, loss of slab support, etc.), and different densities could affect fine particle movements within pavement foundations.

Composite material samples were prepared using equal layer thicknesses and only studied permanent strains of the whole sample. Future research could investigate the effects of different thicknesses of layers on the composite moduli. Additionally, research should evaluate the permanent and resilient strains of individual layers in composite samples. Advanced measurement and analysis techniques may need to be used to account for vertical and horizontal strains that develop with cyclic loading (e.g., photo measurement software). Permanent strain of weak foundation layers could be related to permanent strain of the entire sample.

Many mechanistic and empirical design methods include the assumption that pavement foundation systems consist of stiff over soft layers. As seen from Pennsylvania cement stabilized subgrade and some base over subbase composite samples, certain situations can create a soft over stiff layer foundation systems. Future research should investigate how design assumptions change for these situations.

To build better performing pavement structures, new methods need to be developed to measure construction quality. Both in situ and laboratory measurements should be included to link design assumptions and actual measurements of materials. For example, to improve relationships between E_{LWD} and $M_{r(LWD)}$, correlations must be developed using the same equipment and applied stresses (e.g., only use equations developed for the Prima LWD on

data from the Prima LWD, do not use equations developed for Zorn applied stress of 0.1 MPa for Zorn applied stress of 0.5 MPa, etc.).

WORKS CITED

AASHTO. (2008). *Mechanistic-Empirical Pavement Design Guide: A Manual of Practice*, Interim Edition. American Association of State Highway and Transportation Officials, Washington, D.C.

AASHTO. (1993). *AASHTO Guide for Design of Pavement Structures*. American Association of State Highway and Transportation Officials, Washington, D.C.

AASHTO T307-99. "Standard method of test for determining the resilient modulus of soils and aggregate materials" American Association of State Highway and Transportation Officials (AASHTO), Washington, D.C.

American Coal Ash Association (ACAA) (2008), *Soil Stabilization and Pavement Recycling with Self-Cementing Coal Fly Ash*, Revised Ed., Aurora, CO

ASTM C127-07. "Standard Test Method for Density, Relative Density (Specific Gravity), and Absorption of Coarse Aggregate." American Standards for Testing Methods (ASTM), West Conshohocken, PA.

ASTM D422-63. "Standard Test Method for Particle-Size Analysis of Soils." American Standards for Testing Methods (ASTM), West Conshohocken, PA.

ASTM D698-07e1. "Standard Test Method for Laboratory Compaction Characteristics of Soil Using Standard Effort (12,400 ft-lbf/ft^3 (600 kN-m/m^3))." American Standards for Testing Methods (ASTM), West Conshohocken, PA.

ASTM D854-10. "Standard Test Method for Specific Gravity of Soil Solids by Water Pycnometer." American Standards for Testing Methods (ASTM), West Conshohocken, PA.

ASTM D1196-93. "Standard Test Method for Nonrepetitive Static Plate Load Tests of Soils and Flexible Pavement Components, for Use in Evaluation and Design of Airport and Highway Pavements." American Standards for Testing Methods (ASTM), West Conshohocken, PA.

ASTM D1557-09. "Standard Test Method for Laboratory Compaction Characteristics of Soil Using Modified Effort (56,000 ft-lbf/ft^3 (2,700 kN-m/m^3))." American Standards for Testing Methods (ASTM), West Conshohocken, PA.

ASTM D1587-08. "Standard Practice for Thin-Walled Tube Sampling of Soils for Geotechnical Purposes." American Standards for Testing Methods (ASTM), West Conshohocken, PA.

ASTM D4253-00. "Standard Test Methods for Maximum Index Density and Unit Weight of Soils Using a Vibratory Table." American Standards for Testing Methods (ASTM), West Conshohocken, PA.

ASTM D4254-00. "Standard Test Methods for Minimum Index Density and Unit Weight of Soils and Calculation of Relative Density." American Standards for Testing Methods (ASTM), West Conshohocken, PA.

ASTM D4318-10. "Standard Test Methods for Liquid Limit, Plastic Limit, and Plasticity Index of Soils." American Standards for Testing Methods (ASTM), West Conshohocken, PA.

ASTM D4718-87. "Standard Practice for Correction of Unit Weight and Water Content for Soils Containing Oversize Particles." American Standards for Testing Methods (ASTM), West Conshohocken, PA.

ASTM D4767-04. "Standard Test Method for Consolidated Undrained Triaxial Compression Test for Cohesive Soils." American Standards for Testing Methods (ASTM), West Conshohocken, PA.

ASTM D6938-10. "Standard Test Method for In-Place Density and Water Content of Soil and Soil-Aggregate by Nuclear Methods (Shallow depth)." American Standards for Testing Methods (ASTM), West Conshohocken, PA.

ASTM D6951-03. "Standard Test Method for Use of the Dynamic Cone Penetrometer in Shallow Pavement Applications." American Standards for Testing Methods (ASTM), West Conshohocken, PA.

Alam, T.B., Abdelrahman, M., Schram, S.A. (2010). "Laboratory Characterization of Recycled Asphalt Pavement as a Base Layer." *International Journal of Pavement Engineering*, Taylor & Francis, 11(2), 123–131.

Andrei, D., Witczak, M. W., Schwartz, C. W., Uzan, J. (2004). "Harmonized Resilient Modulus Test Method for Unbound Pavement Materials." *Transportation Research Record No. 1874*, Transportation Research Board, Washington, D. C., 29–37.

Bhatti, M.A., Barlow, J.A., Stoner, J.W. (1996). "Modeling Damage to Rigid Pavements Caused by Subgrade Pumping." *Journal of Transportation Engineering*, American Society of Civil Engineers, 122(1), 12–21.

Briaud, J.-L. (2001). "Introduction to Soil Moduli." Geotechnical News, BiTech Publishers Ltd, Richmond, B.C., Canada.

Brown, S.F. (1974). "Repeated Load Testing of a Granular Material." *Journal of the Geotechnical Engineering Division*, American Society of Civil Engineers, 100(GT7), 825–841.

Christopher, B.R., Schwartz, C., Boudreau, R. (2006). Geotechnical Aspects of Pavements, Reference Manual/Participant Workbook for NHI Course No. 132040, Federal Highway Administration, U.S. Department of Transportation, Washington, D.C., FHWA NHI-05-037, 888p.

Crisman, B. and Facchin, G. (2009). "Multilayer elastic theory applied to stress-dependant materials for pavement response," *Proceedings, International Conference on Maintenance and Rehabilitation of Pavements and Technological Control Sixth Proceedings*, International Society for Maintenance and Rehabilitation of Transportation Infrastructure and Transportation Research Board, Turin, Italy.

Drumm, E.C., Boateng-Poku, Y., Pierce, T.J. (1990). "Estimation of Subgrade Resilient Modulus from Standard Tests." *Journal of Geotechnical Engineering*, American Society of Civil Engineers, 116(5), 774–789.

Drumm, E.C., Reeves, J.S., Madgett, M.R., Torlinger, W.D. (1997). "Subgrade Resilient Modulus Correction for Saturation Effects." *Journal of Geotechnical and Geoenvironmental Engineering*, American Society of Civil Engineers, 123(7), 663–670.

Federal Highway Administration (FHWA). (1996). "Protocol 46: Resilient Modulus of Unbound Granular Base/Subbase Materials and Subgrade Soils." Long Term Pavement Performance Program, Pavement Performance Division, U.S. Department of Transportation. McLean, VA.

FHWA. (2000). "LTPP Manual for Falling Weight Deflectometer Measurements Operational Field Guidelines: Version 3.1." Long Term Pavement Performance Program, Pavement Performance Division, U.S. Department of Transportation. McLean, VA.

Fleming, P.R., Frost, M.W., Rogers, C.D.F. (2000). "A Comparison of Devices for Measuring Stiffness In-Situ." *Proceedings of the Fifth International Conference on Unbound Aggregate In Roads*, Nottingham, United Kingdom.

Frost, M.W., Fleming, P.R., Rogers, D.F. (2004). "Cyclic Triaxial Tests on Clay Subgrades for Analytical Pavement Design." Journal of Transportation Engineering, American Society of Civil Engineers, 130(3), 378–386.

George, K.P. (2003). "Falling Weight Deflectometer for Estimating Subgrade Resilient Moduli." *Report No. FHWA/MS-DOT-RD-03-153*, Federal Highway Administration (FHWA), U.S. Department of Transportation, Washington, D.C.

George, K.P. (2004). "Prediction of Resilient Modulus from Soil Index Properties." *Report No. FHWA/MS-DOT-RD-04-172*, Federal Highway Administration, U.S. Department of Transportation, Washington, D.C.

George, K.P. and Uddin, W. (2000). "Subgrade Characterization for Highway Pavement Design." Department of Civil Engineering, University of Mississippi, University, MS.

Groeger, J.L., Rada, G.R., Lopez, A. (2003). "AASHTO T307 – Background and Discussion," *Resilient Modulus Testing for Pavement Components*, *ASTM STP 1437*. West Conshohocken, PA: ASTM International. 16–29.

Hicks, R.G. and Monismith, C.L. (1971). "Factors Influencing the Resilient Response of Granular Materials." *Highway Research Record No. 345*. Highway Research Board, Washington, D.C., 15–31.

Hilf, J.W. (1991). "Compacted Fill," in *Foundation Engineering Handbook*, 2nd Edition. Ed. F. Hsai-Yang. Van Nostrand Reinhold, New York, NY. 249–316.

Huang, Y.H. (1993). *Pavement Analysis and Design*, 1st Ed., Prentice Hall, Inc., Englewood Cliffs, New Jersey.

Hveem, F.N. (1955). "Pavement Deflections and Fatigue Failures." Bulletin No. 114, Highway Research Board, Washington, D.C., 43–87.

Khoury, N.N. and Zaman, M.M. (2004). "Correlation Between Resilient Modulus, Moisture Variation, and Soil Suction for Subgrade Soils." *Journal of the Transportation Research Board, No. 1874*, Transportation Research Board, Washington, D.C., 99–107.

Kiekmeir, J., Pinta, C., Merth, S., Jensen, J., Davich, P., Camargo, F., Beyer, M. (2009). *Using the Dynamic Cone Penetrometer and Light Weight Deflectometer for Construction Quality Assurance.* Final Report submitted to Minnesota Department of Transportation, Office of Materials and Road Research, MNDOT, Maplewood, MN.

Koerner, R.M. (1991). "Geosynthetics in Geotechnical Engineering," in *Foundation Engineering Handbook*, 2nd Edition. Ed. F. Hsai-Yang. Van Nostrand Reinhold, New York, NY. 796–813.

Koerner, R.M. and Soong, T.-Y. (1995). "Use of Geosynthetics in Infrastructure Remediation." *Journal of Infrastructure Systems*, American Society of Civil Engineers, 1(1), 66–75.

Kouassi, P., Breysse, D., Girard, H., Poulain, D. (2000). "A New Technique of Kneading Compaction in the Laboratory." *Geotechnical Testing Journal*, ASTM International, 23(1), 72-82.

Lee, W., Bohra, N.C., Altschaeffl, A.G., and White, T.D. (1997). "Resilient Modulus of Cohesive Soils." *Journal of Geotechnical and Geoenvironmental Engineering*, American Society of Civil Engineers, 123(2), 131–136.

Liang, R.Y., Rabab'ah, S., Khasawneh, M. (2008). "Predicting Moisture-Dependant Resilient Modulus of Cohesive Soils Using Soil Suction Concept." *Journal of Transportation Engineering*, American Society of Civil Engineers, 134(1), 34–40.

Loulizi, A., Al-Qadi, I.L., Bhutta, S.A., Flintsch, G.W. (1999). "Evaluation of Geosynthetics Used as Separators." *Journal of the Transportation Research Record No 1687*. Transportation Research Board, Washington, D.C., 104–111.

Maheshwari, P. (2011). "Foundation-Soil Interaction" in *Geotechnical Engineering Handbook*. Ed. B.M. Das. J. Ross Publishing, Inc., Fort Lauderdale, FL. 4-22–4-25.

Mayrberger, T. and Hodek, R. J. (2007). *Resilient Modulus at the Limits of Gradation and Varying Degrees of Saturation*, Research Report RC-1497, Michigan Technological University, Houghton, MI.

Mohammad, L.N., Gaspard, K., Herath, A., Nazzal, M. (2007). Comparative Evaluation of Subgrade Resilient Modulus from Non-destructive, In-situ, and Laboratory Methods. Final report submitted to Louisiana Department of Transportation and Development, Louisiana Transportation Research Center, Baton Rouge, LA.

Mohammad, L.N., Herath, A., Gudishala, R., Abu-Farsakh, M.Y., Alshibli, K. (2008). Development of Models to Estimate the Subgrade and Subbase Layers' Resilient Modulus from In Situ Devices Test Results for Construction Control. Final report submitted to Louisiana Department of Transportation and Development, Louisiana Transportation Research Center, Baton Rouge, LA.

Mohammad, L.N., Nazzal, D.M., Abu-Farsakh, M.Y., Alshibli, K. (2009). "Estimation of Subgrade Soils Resilient Modulus from In-situ Devices Test Results." Journal of Testing and Evaluation, ASTM International, 37(3), DOI: 10.1520/JTE101993.

Nataatmadja, A. and Tan, Y.L. (2001). "Resilient Response of Recycled Concrete Road Aggregates." *Journal of Transportation Engineering*, American Society of Civil Engineers, 127(5), 450–453.

National Cooperative Highway Research Program (NCHRP). (2004a). "Laboratory Determination of Resilient Modulus for Flexible Pavement Design." *NCHRP Research Results Digest for NCRHP 1-28A Project*, Washington, D.C.

National Cooperative Highway Research Program (NCHRP). (2004b). "Guide for Mechanistic-Empirical Design of New and Rehabilitated Pavement Structures." *NCHRP Final Report for NCHRP 1-37A Project*, Washington, D.C. http://onlinepubs.trb.org /onlinepubs/archive/mepdg/guide.htm (accessed March 1, 2010).

Nazzal, M., Abu-Farsakh, M., Mohammad, L. (2007). "Laboratory Characterization of Reinforced Crushed Limestone under Monotonic and Cyclic Loading." *Journal of Materials in Civil Engineering*, American Society of Civil Engineers, 19(9), 772–783.

Packard, R.G. (1973). "Design of Concrete Airport Pavement." Engineering Bulletin, Portland Cement Association, Skokie, IL.

Papagiannakis, A.T. and Masad, E.A. (2008). Pavement Design and Materials. John Wiley and Sons, Inc., New Jersey.

Puppala, A.J. (2008). "Estimating Stiffness of Subgrade and Unbound Materials for Pavement Design: A Synthesis of Highway Practice." *NCHRP Synthesis 382*, Transportation Research Board, Washington, D.C.

Robnett, Q.L. and Thompson, M.R. (1973), *Interim Report: Resilient Properties of Subgrade Soils, Phase I, Development of Testing Procedure*, Transportation Research Laboratory, Department of Civil Engineering, University of Illinois, Champaign, IL.

Saeed, A. (2008). "Performance-Related Tests of Recycled Aggregates for Use in Unbound Pavement Layers." *NCHRP Report 598*, Transportation Research Board, Washington, D.C.

Seed, H.B., Chan, C.K., Lee, C.E. (1962). "Resilience Characteristics of Subgrade Soils and Their Relation to Fatigue failures in Asphalt Pavements." *Proceedings, International Conference on the Structural Design of Asphalt Pavements*. University of Michigan, Ann Arbor, MI, 611–636.

Seed, H.B., Chan, C.K., Monismith, C.L. (1955). "Effects of Repeated Loading on the Strength and Deformation of Compacted Clay." *Proceedings, Thirty Fourth Annual Meeting of the Highway Research Board*. Washington, D. C., 541–558.

Shukla, S.K. and Sivakugan, N. (2011). "Foundation-Soil Interaction" in *Geotechnical Engineering Handbook*. Ed. B.M. Das. J. Ross Publishing, Inc., Fort Lauderdale, FL. 10-60–10-63.

Siekmeier, J.A., Young, D., Breberg, D. (1999). "Comparison of the Dynamic Cone Penetrometer with Other Tests During Subgrade and Granular base Characterization in Minnesota," *Nondestructive Testing of Pavements and Backcalculation of moduli: Third Volume, ASTM STP 1375*, S.D. Tayabji and E.O. Lukanen, Eds., American Society for Testing and Materials, West Conshohocken, PA.

Solanki, P. Zaman, M.M., Dean, J. (2010). "Resilient Modulus of Clay Subgrades Stabilized with Lime, Class C Fly Ash, and Cement Kiln Dust for Pavement Design." Transportation Research Board 2010 Annual Meeting (CD-ROM), January 10–14, 2010, Washington, D.C.

Southgate, H.F. and Mahboub, K.C. (1994). "Proposed Uniform Scale for Stiffness of Unbound Pavement Materials for Pavement Design." *Journal of Transportation Engineering*, American Society of Civil Engineers, 120(4), 940–952.

Stubstad, R.N., Jiang, Y.J., Clevenson, M.L., Lukanen, E.O. (2006). "Review of the Long-Term Pavement Performance Backcaluculation Results–Final Report." *Report No. FHWA-HRT-05-150*, Federal Highway Administration, U.S. Department of Transportation, Washington, D.C.

Terzaghi, K. (1955). "Evaluation of Coefficient of Subgrade Reaction," *Geotechnique*, 5(4), 297–326.

Terzaghi, K., Peck, R.B., Mesri, G. (1996). Soil Mechanics in Engineering Practice, 3rd Edition. John Wiley and Sons, Inc., New York, NY.

Texas Department of Transportation (TxDOT). (2004). "Test Procedure for Determining Flakiness Index." Construction Division, Texas Department of Transportation, Austin, TX.

Thompson, M.R. and Robnett, Q.L. (1979). "Resilient Properties of Subgrade Soils." *Transportation Engineering Journal*, American Society of Civil Engineers, 105(TE1), 71–89.

Tingle, J.S. and Jersey, S.R. (2005). "Cyclic Plate Load Testing of Geosynthetic-Reinforced Unbound Aggregate Roads." *Journal of the Transportation Research Board No. 1936,* Transportation Research Board, Washington D.C., 60–69.

Ullidtz, P. (1987). Pavement Analysis: Developments in Civil Engineering, Vol. 19, Elsevier Science Publishers, New York.

Vennapusa, P.K.R. and White, D.J. (2009). "Comparison of Light Weight Deflectometer Measurements for Pavement Foundation Materials." *Geotechnical Testing Journal*, ASTM International, 32(3).

Vinson, T.S. (1989). "Fundamentals of Resilient Modulus Testing." Presented at Workshop on Resilient Modulus Testing, Oregon State University, Corvallis, OR, March 28–30.

Von Quintus, H. and Killingsworth, B. (1997). "Design Pamphlet for the Determination of Design Subgrade in Support of the 1993 AASHTO Guide for the Design of Pavement Structures." *Report No. FHWA-RD-97-083,* Federal Highway Administration, U.S. Department of Transportation, Washington, D.C.

Werkmeister, S., Dawson, A.R., Wellner, F. (2004). "Pavement Design Model for Unbound Granular Materials." *Journal of Transportation Engineering*, American Society of Civil Engineers, 130(5), 665–674.

White, D., Thompson, M., Vennapusa, P. (2007). *Field Validation of Intelligent Compaction Monitoring Technology for Unbound Materials*. Final report submitted to Minnesota Department of Transportation, Center for Transportation Research and Education, Iowa State University, Ames, IA.

White, D.J. and Gieselman, H. (2009). "Plate Load Test Device." Tech Brief, Earthworks Engineering Research Center, Iowa State University, Ames, IA.

White, D.J., Bergeson, K.L., Jahren, C.T. (2002). *Embankment Quality: Phase III*, Center for Transportation Research and Education, Iowa State University, Ames, IA.

White, D.J., Steffes, R., Gieselman, H., Zimmerman, B. (2008). "Hydraulic Tube Sampling Attachment for Geotechnical Mobile Lab Truck," Tech Brief, Earthworks Engineering Research Center, Iowa State University, Ames, IA.

White, D.J., Vennapusa, P., Zhang, J., Gieselman, H., Morris, M. (2009). *Implementation of Intelligent Compaction Performance Based Specifications in Minnesota*. Final report submitted to Minnesota Department of Transportation, Earthworks Engineering Research Center, Department of Civil, Construction, and Environmental Engineering, Iowa State University, Ames, IA

Winterkorn, H.F. (1991). "Soil Stabilization and Grouting" in *Foundation Engineering Handbook*, 2nd Edition. Ed. F. Hsai-Yang. Van Nostrand Reinhold, New York, NY. 317–378.

Witczak, M., and Uzan, J. (1988). "The Universal Airport Design System, Report I of IV. Granular Material Characterization." Department of Civil Engineering, University of Maryland, College Park, MD.

Yang, S., Lin, H, Kung, J.H.S., Huang, W. (2008). "Suction-Controlled Laboratory Test on Resilient Modulus of Unsaturated Compacted Subgrade Soils." *Journal of Transportation Engineering*, American Society of Civil Engineers, 134(9), 1375–1384.

Zaman, M., Chen, D., Laguros, J. (1994). "Resilient Moduli of Granular Materials." *Journal of Geotechnical and Geoenvironmental Engineering*, American Society of Civil Engineers, 120(4), 940–952.

Zehgal, M. (2004). "Discrete-Element Method Investigation of the Resilient Behavior of Granular Materials." *Journal of Transportation Engineering*, American Society of Civil Engineers, 130(6), 503–509.

APPENDIX A. SAMPLE CALCULATIONS

The resilient and cyclic secant moduli will use data from Table 1 for sample calculations. The static secant moduli will use data from Table 2.

Table 1. Last five cycles of resilient modulus load sequence 1 for a subgrade sample

Cycle #	Applied Max Dev Stress, σ_d (kPa)	Applied Cyclic Dev Stress, σ_{cyclic} (kPa)	Applied Contact Dev Stress, σ_c (kPa)	Deflection LVDT (mm)	Resilient Strain, ε_r (%)	Resilient Modulus, M_r (MPa)	Permanent Strain, ε_p (%)	Cyclic Secant Modulus, E^*_S (MPa)
96	12.917	11.499	1.418	0.177	0.0869	13.2	1.3558	—
97	13.279	11.922	1.356	0.180	0.0885	13.5	1.3542	13.72
98	12.696	11.414	1.282	0.162	0.0796	14.3	1.3558	14.05
99	12.802	11.500	1.302	0.178	0.0877	13.1	1.3554	13.18
100	12.833	11.496	1.337	0.168	0.0825	13.9	1.3534	14.29
Ave.	12.906	11.567	1.339	0.173	0.0850	13.6	1.355	13.81

Table 2. All load sequences for a subgrade sample

Sequence No.	Confining Pressure, σ_c (kPa)	Max Deviator Stress, σ_d (kPa)	Mean Bulk Stress, σ_B (kPa)	Average M_r (MPa)	Permanent Strain, ε_p (%)	Avg E_s^* (MPa)
—	41.4	27.6	151.7	12.8	1.4	—
1	41.6	12.9	137.7	13.6	1.4	13.8
2	41.8	26.4	151.6	12.3	1.4	12.1
3	41.6	40.2	165.2	12.1	2.4	12.0
4	41.8	54.7	180.0	14.9	3.6	14.8
5	41.6	68.2	193.1	18.0	4.7	17.8
6	27.6	13.0	95.9	13.5	4.5	13.5
7	27.6	26.2	109.1	11.9	4.5	11.9
8	28.1	41.1	125.5	13.1	4.6	13.1
9	27.8	56.7	140.2	15.4	4.8	15.4
10	28.3	69.8	154.7	18.1	5.1	18.1
11	14.1	13.2	55.4	12.3	4.8	12.2
12	13.7	27.0	68.2	11.2	4.9	11.2
13	13.9	41.2	82.8	12.3	5.0	12.3
14	13.9	56.8	98.5	15.1	5.1	15.1
15	13.9	70.9	112.6	18.1	5.4	18.0
Ave.	—	—	—	14.1	—	14.1

RESILIENT MODULI

Using the data in Table 1, the resilient modulus for Sequence No. 1was calculated using Equation 1.

$$M_r = \frac{\sigma_{cyclic}}{\varepsilon_r} = \frac{0.011567 \text{MPa}}{0.000850} = 13.61 \text{MPa} \tag{1}$$

The process was repeated for all 15 load sequences (Table 2). The values reported are the average value ($M_{r(T307)}$) of all load sequences for each test specimen.

LABORATORY EQUATIONS

PI-Gradation

The M-E PDG (NCHRP 2004b) describes several equations to determine M_r values without performing M_r tests. Equations 2 and 3 incorporate gradation and Atterberg limit parameters to determine M_r. This equation is typically applicable to cohesive materials. The parameters are converted to a CBR value then using Equation 3, the CBR value is converted to M_r values, as seen below.

$$CBR = \frac{75}{1 + 0.728(P_{200} \times PI)} = \frac{75}{1 + 0.728(0.15 \times 20\%)} = 23.6\% \tag{2}$$

$$M_{r(PI-P200)} = 17.6(CBR)^{0.64} = 17.6(23.6\%)^{0.64} = 132.9 \text{MPa} \tag{3}$$

where: P_{200} = percent passing the No. 200 sieve (decimal);

PI = plasticity index (%);

M_r = resilient modulus (MPa).

Gradation

The M-E PDG (NCHRP 2004b) describes several equations to determine M_r values without performing M_r tests. Equations 4 and 5 incorporate a gradation parameter to determine M_r. This equation is typically applicable to granular materials. The parameters are converted to a CBR value then using Equation 5, the CBR value is converted to M_r values, as seen in the following:

$$CBR = 28.09(D_{60})^{0.358} = 28.09(2.5 \text{mm})^{0.358} = 39.0\% \tag{4}$$

$$M_{r(D60)} = 17.6(CBR)^{0.64} = 17.6(39.0\%)^{0.64} = 183.6 \text{MPa} \tag{5}$$

where: D_{60} = diameter at 60% passing from the grain size distribution (mm) and

M_r = resilient modulus (MPa).

Von Quintus and Killingsworth Equivalent Layered Composite Moduli

Equation was obtained form Von Quintus and Killingsworth (1997). It was used to compare single material samples to the composite samples. Equation 6 illustrates the sample calculation.

$$M_{r(EquivComposite)} = \frac{D_{s1}^3 M_{r1} + D_{s2}^3 M_{r2}}{(D_{S1})^3 + (D_{S2})^3} = \frac{(10.2\text{cm})^3 * 150\text{MPa} + (10.2\text{cm})^3 * 40\text{MPa}}{(10.2\text{cm})^3 + (10.2\text{cm})^3} = 95.0 \text{MPa} \tag{6}$$

where: M_{r1} = resilient modulus of the upper layer;

M_{r2} = resilient modulus of the lower layer;

D_{S1} = thickness of the upper layer; and

D_{S2} = thickness of the lower layer.

IN SITU EQUATIONS

DCPI

DCP tests were performed in accordance with ASTM D6951-03. The DCP works by dropping an 8 kg (17.6 lb) hammer onto a rod with a cone tip from a height of 575 mm (22.6 in.) and measuring the penetration distance for a given number of blows. Tests were performed to a depth of 1 m with the typical DCP apparatus and extended to 2 m using extension rods. Dynamic cone penetration index (DCPI) was calculated for each test. Weighted average DCPIs were calculated for each foundation layer using Equation 7 (White et al. 2009).

Weighted CBR values were determined for each recorded DCP blow using Equation 7 but substituting CBR values for the DCPI values. Pavement foundation layers were chosen by observing where a clear change in slope occurred on depth versus weighted CBR graphs (Figure 1 and Table 3). Some test points did not have a clear change in slope, and engineering judgment was applied using graphs of depth versus DCPI values to determine the layer boundaries.

$$DCPI_z = \frac{DCPI_i \cdot z_i + DCPI_{i+1} \cdot z_{i+1} + ... + DCPI_n \cdot z_n}{\sum z_n}$$
(7)

$$DCPI_z = \frac{9.5 \cdot (178 - 140mm) + 5.5 \cdot (200 - 178mm) + ... + 2.3 \cdot (438 - 429mm)}{438 - 178mm} = 4.6 blow/mm$$

where: $DCPI_z$ = DCPI for the foundation layer of thickness z (mm/blow) and

$DCPI_{i,i+1,...n}$ = DCPI of blows i to n (mm/blow).

Table 3. Table of values for determination of DCPI$_{Ave}$ example

Number of Blows	Depth (mm)	Corrected Depth (mm)	DCPI (mm/blow)	CBR (%)	Weighted CBR (%)
0	45	0	66.0	2.7	0.0
1	111	66	66.0	2.7	2.7
4	185	140	18.5	11.1	7.1
4	223	178	9.5	23.5	10.6
4	245	200	5.5	43.3	14.2
4	268	223	5.8	41.2	17.0
4	288	243	5.0	48.1	19.6
4	304	259	4.0	61.8	22.2
4	320	275	4.0	61.8	24.5
4	332	287	3.0	85.3	27.0
4	345	300	3.3	78.0	29.2
4	364	319	4.8	51.0	30.5
4	379	334	3.8	66.4	32.1
4	388	343	2.3	117.7	34.4
4	398	353	2.5	104.6	36.4
4	412	367	3.5	71.8	37.7
4	424	379	3.0	85.3	39.2
4	438	393	3.5	71.8	40.4
4	453	408	3.8	66.4	41.3
4	465	420	3.0	85.3	42.6
4	474	429	2.3	117.7	44.2
4	483	438	2.3	117.7	45.7
4	504	459	5.3	45.6	45.7
2	530	485	13.0	16.5	44.1
1	556	511	26.0	7.6	42.3
1	588	543	32.0	6.0	40.1
1	618	573	30.0	6.5	38.4
1	663	618	45.0	4.1	35.9
1	705	660	42.0	4.4	33.9
1	744	699	39.0	4.8	32.3
1	780	735	36.0	5.3	30.9
1	813	768	33.0	5.8	29.9
1	845	800	32.0	6.0	28.9
1	883	838	38.0	5.0	27.8
1	920	875	37.0	5.1	26.9
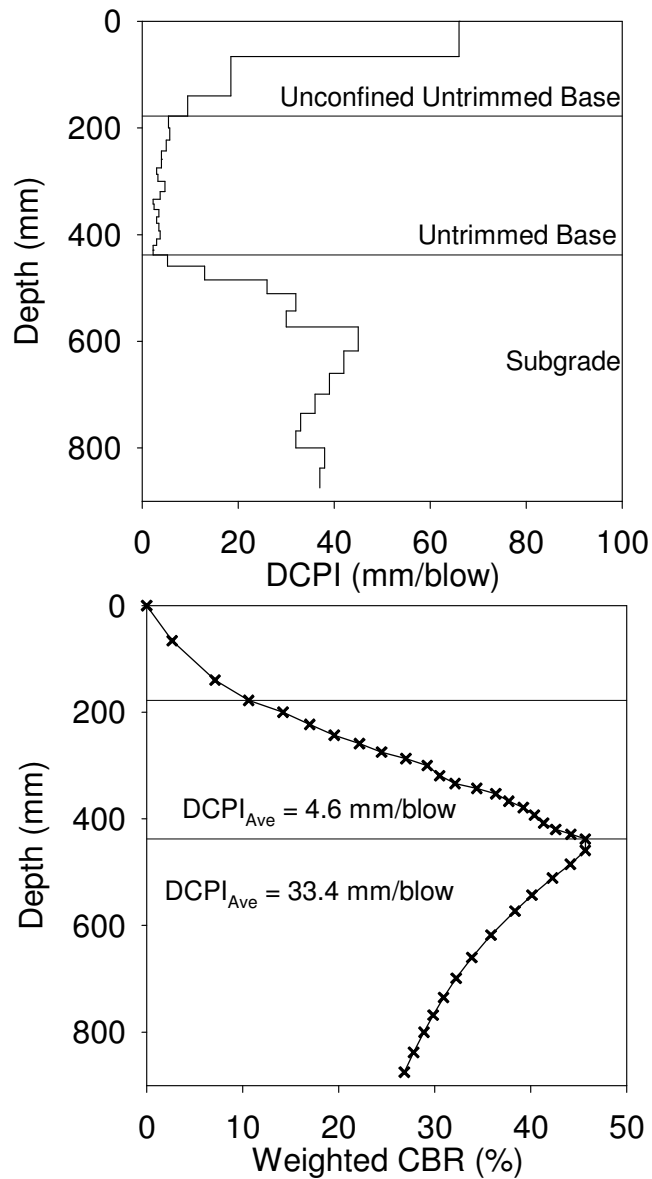
Figure 1. Determination of DCPI$_{Ave}$ example

Four equations were used to relate DCPI to M_r. Equation 8 from the MEPDG (NCHRP 2004b) converts DCPI into a CBR value, and Equation 9 converts the CBR value into M_r. Mohammad et al. (2008) developed two equations—one for cohesive materials (Equation 10), one for granular materials (Equation 11)—to related DCPI to M_r. The following illustrates sample calculations for each equation.

$$\text{CBR} = \frac{292}{\text{DCPI}^{1.12}} = \frac{292}{15^{1.12}} = 14.07\% \tag{8}$$

$$M_{r(DCPI)} = 17.6(CBR)^{0.64} = 17.6(14.07\%)^{0.64} = 95.6 \text{MPa} \tag{9}$$

$$M_{r(DCPI))} = \frac{1046.6}{DCPI^{1.096}} = \frac{1046.6}{15^{1.096}} = 53.8 \text{MPa} \tag{10}$$

$$M_{r(DCPI)} = \frac{391.1}{DCPI^{0.23}} = \frac{391.1}{15^{0.23}} = 209.8 \text{MPa} \tag{11}$$

where: DCPI = dynamic cone penetrometer index (mm/blow);

CBR = California bearing ratio (%); and

M_r = resilient modulus (MPa).

FWD

The composite E_{FWD} value was determined using the deflection measured directly under the FWD plate. Because the FWD used a segmented plate, the shape factor was assumed to be f=2. The assumed Poisson's ratio was $\upsilon = 0.4$.

$$E_{FWD} = \frac{(1-v^2)\sigma_0 a}{d_0} f = \frac{(1-0.4^2)0.2\text{MPa}*150.1\text{mm}}{2.12\text{mm}}(2) = 23.8 \text{MPa} \tag{12}$$

where: E = elastic modulus (MPa);

d_0 = measured displacement (mm);

υ = Poisson's ratio;

σ_0 = applied stress (MPa);

a = radius of the loading plate (mm); and

f = shape factor depending on stress distribution (for the segmented plate FWD: f = 2).

PLT

The PLT used a rigid plate to determine the load and reload elastic moduli (E_{v1} and E_{v2}) and modulus of subgrade reaction (k_s) as discussed in Chapter 3. Different shape factors needed to be used to determine the E_{v1} and E_{v2} values. When the PLT was performed directly on clay materials, $f = \pi/2$, and when the PLT was performed on sandy material $f = 8/3$. The assumed Poisson's ratio was $\upsilon = 0.4$. Equation 13 illustrates the calculation for E_{v1}.

$$E_{v1} = \frac{(1-v^2)\sigma_0 a}{d_0} f = \frac{(1-0.4^2)0.2\text{MPa}*150.1\text{mm}}{2.12\text{mm}}\left(\frac{8}{3}\right) = 31.7 \text{MPa} \tag{13}$$

where: E = elastic modulus (MPa);

d_0 = measured displacement (mm);

υ = Poisson's ratio;

σ_0 = applied stress (MPa);

a = radius of the loading plate (mm); and

f = shape factor depending on stress distribution (for PLT on clay: f = π/2; for PLT on sand: f = 8/3).

The modulus of subgrade reaction (k_s) was determined using the "load" data from the PLT. The stress used was 0.2 MPa (measured from the initial applied stress of 0.2 MPa to 0.4 MPa) and divided by the measured deflection over that stress range. The plate had a 150 mm (6 in.) radius. Equation 14 illustrates the calculation of k_s.

$$k_s = \frac{\sigma_v}{\delta} = \frac{0.2\text{MPa}}{2.12\text{mm}} = 0.093\text{MPa/mm} = 342\text{pci} \tag{14}$$

When comparing the k_s values using different sized PLTs, a correction to the calculated value needs to be applied. For footings on sand and clay, Vennapusa and White (2009) recommend Equations 15 and 16, respectively.

$$k_s = k_1 \left[\frac{B + B_1}{2B} \right]^2 = 300\text{pci} \left[\frac{30\text{in.} + 12\text{in.}}{2 * 30\text{in.}} \right]^2 = 147\text{pci} \tag{15}$$

$$k_s = k_1 \left[\frac{B_1}{B} \right] = 300\text{pci} \left[\frac{12\text{in.}}{30\text{in.}} \right] = 120\text{pci} \tag{16}$$

LWD

When the LWD was performed directly on clay materials, f = π/2, and when the LWD was performed on sandy material f = 8/3. The assumed Poisson's ratio was υ = 0.4. The calculation for E_{LWD} is identical to Equation 12.

APPENDIX B. STATISTICAL ANALYSIS

UPPER AND LOWER LAYER ANALYSIS
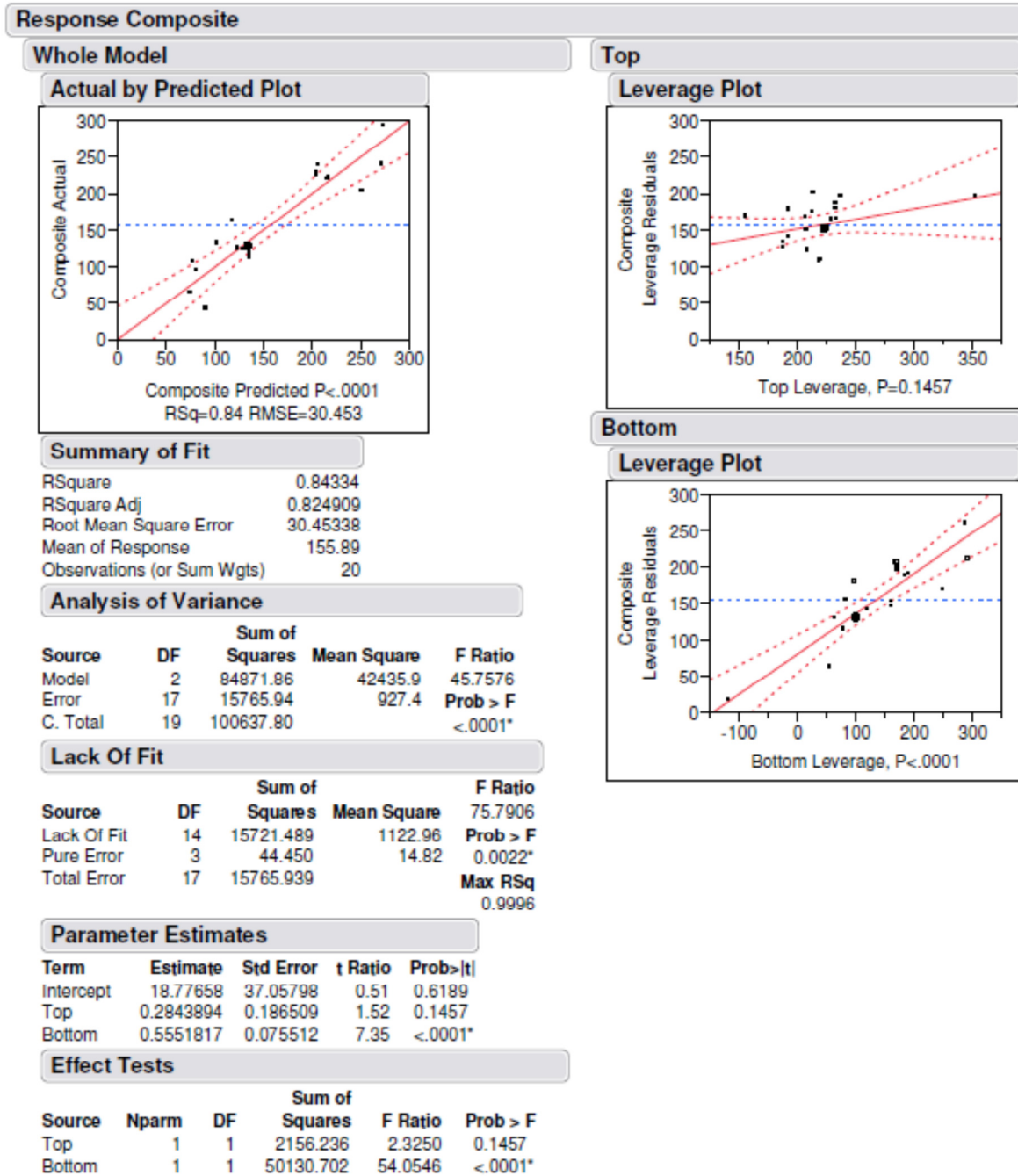
Figure 2. JMP results of M_r significance for upper and lower layers

MOISTURE CORRECTION
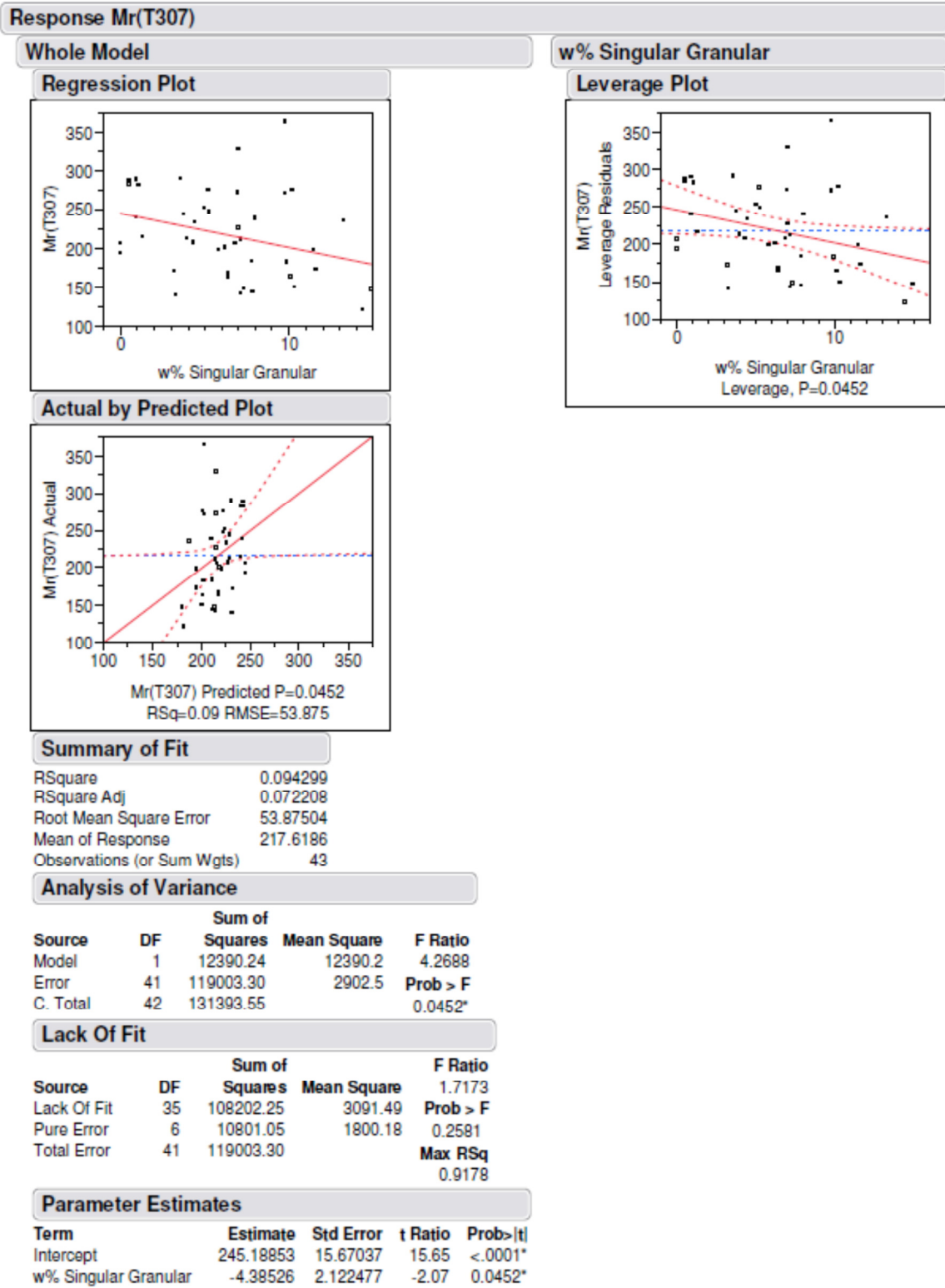
Figure 3. JMP results of least fit squares analysis for granular samples
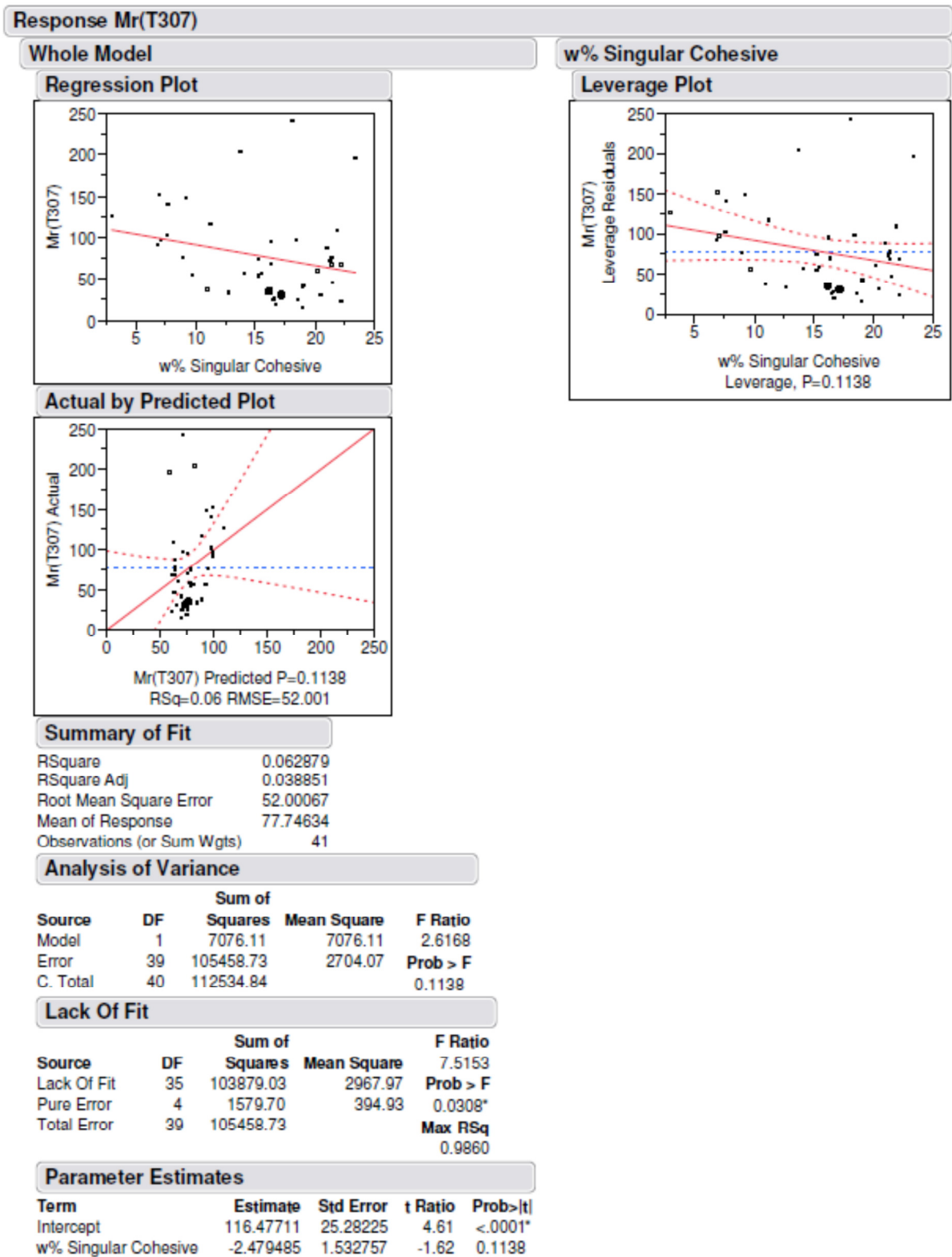
Figure 4. JMP results of least fit squares analysis for cohesive and Shelby tube samples

Response Mr(T307)

Whole Model

Regression Plot

Actual by Predicted Plot

P=0.0076 RSq=0.28 RMSE=42.03

w% Singular Cohesive

Leverage Plot

w% Singular Cohesive
Leverage, P=0.0076

Summary of Fit

RSquare	0.281565
RSquare Adj	0.248909
Root Mean Square Error	42.03016
Mean of Response	81.19167
Observations (or Sum Wgts)	24

Analysis of Variance

Source	DF	Sum of Squares	Mean Square	F Ratio
Model	1	15231.290	15231.3	8.6221
Error	22	38863.748	1766.5	Prob > F
C. Total	23	54095.038		0.0076*

Lack Of Fit

Source	DF	Sum of Squares	Mean Square	F Ratio
Lack Of Fit	21	38659.728	1840.94	9.0233
Pure Error	1	204.020	204.02	Prob > F
Total Error	22	38863.748		0.2575
				Max RSq
				0.9962

Parameter Estimates

Term	Estimate	Std Error	t Ratio	Prob>|t|
Intercept	151.48615	25.43034	5.96	<.0001*
w% Singular Cohesive	-5.674248	1.932418	-2.94	0.0076*

Figure 5. JMP results of least fit squares analysis for cohesive samples

APPENDIX C. 10,000 CYCLE RESILIENT MODULUS TESTS

METHOD #1

This method was performed on the Pennsylvania US-22 Class 2A subbase specimen to investigate the migration of fine particles. The sample was prepared according to the "Granular Materials" section of the methods chapter. The sample was then subjected to the load cycles and sequences summarized in Table 4.

Table 4. Resilient modulus test sequences and stress values for 10,000 cycle test on Pennsylvania US-22 specimen (adapted from Saeed 2008)

Sequence No.	Confining stress		Max. axial stress		No. of cycles
	kPa	psi	kPa	psi	
1	103.4	15	68.9	10	1000
2	103.4	15	137.9	20	1000
3	103.4	15	275.8	40	1000
4	103.4	15	413.7	60	1000
5	103.4	15	551.6	80	1000
6	103.4	15	689.5	100	1000
7	103.4	15	827.4	120	1000
8	103.4	15	965.3	140	1000
9	103.4	15	1103.2	160	1000
10	103.4	15	1241.1	180	1000

METHOD #2

This method was performed on the Iowa composite RPCC-loess specimen to investigate the migration of fine particles. The sample was prepared according to the "Composite Samples" section of the methods chapter. The sample was then subjected to the load cycles and sequences summarized in Table 5.

Table 5. Resilient modulus test sequences and stress values for 10,000 cycle test on Iowa

RPCC-loess specimen

Sequence No.	Confining stress		Max. axial stress		No. of cycles
	kPa	psi	kPa	psi	
0	41.4	6	27.6	4	500
1	27.6	4	41.4	6	1000
2	27.6	4	41.4	6	1000
3	27.6	4	41.4	6	1000
4	27.6	4	41.4	6	1000
5	27.6	4	41.4	6	1000
6	27.6	4	41.4	6	1000
7	27.6	4	41.4	6	1000
8	27.6	4	41.4	6	1000
9	27.6	4	41.4	6	1000
10	27.6	4	41.4	6	1000

APPENDIX D. FWD LOAD SEQUENCES

Different FWD load sequences were performed at different site due to differences in surface materials. Table 6 summarizes the FWD load sequences.

Table 6. FWD load sequences for three sites

Site	Test Bed	Drop #	Average Applied Stress (MPa)
MI I-94	3 (Untrimmed Base)	1	Seating
		2	0.302
		3	0.459
		4	0.462
MI I-96	2 (CTB)	1	Seating
		2	0.371
		3	0.564
PA US-22	4 (CTB)	1	Seating
		2	0.361
		3	0.546
		4	0.733

APPENDIX E. DETERMINATION OF DCPI VALUES AND SOIL LAYERS
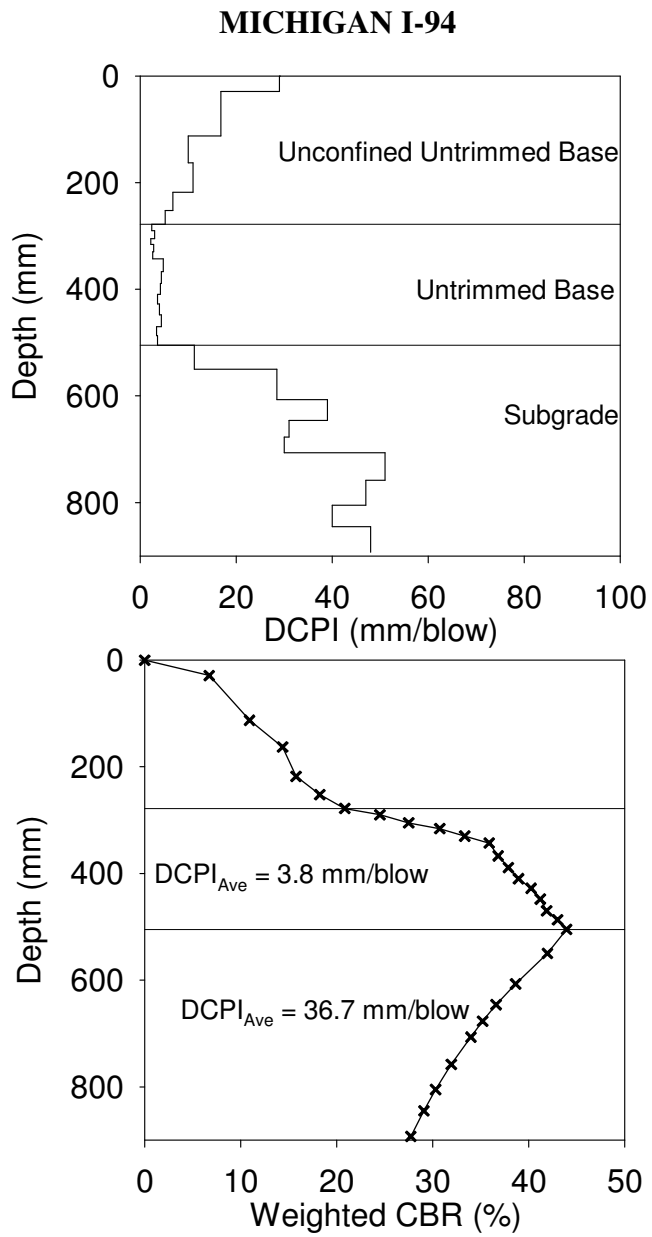
MICHIGAN I-94

Figure 6. Michigan I-94 Test Bed 3 Point 839+50-O DCPI determination for each layer
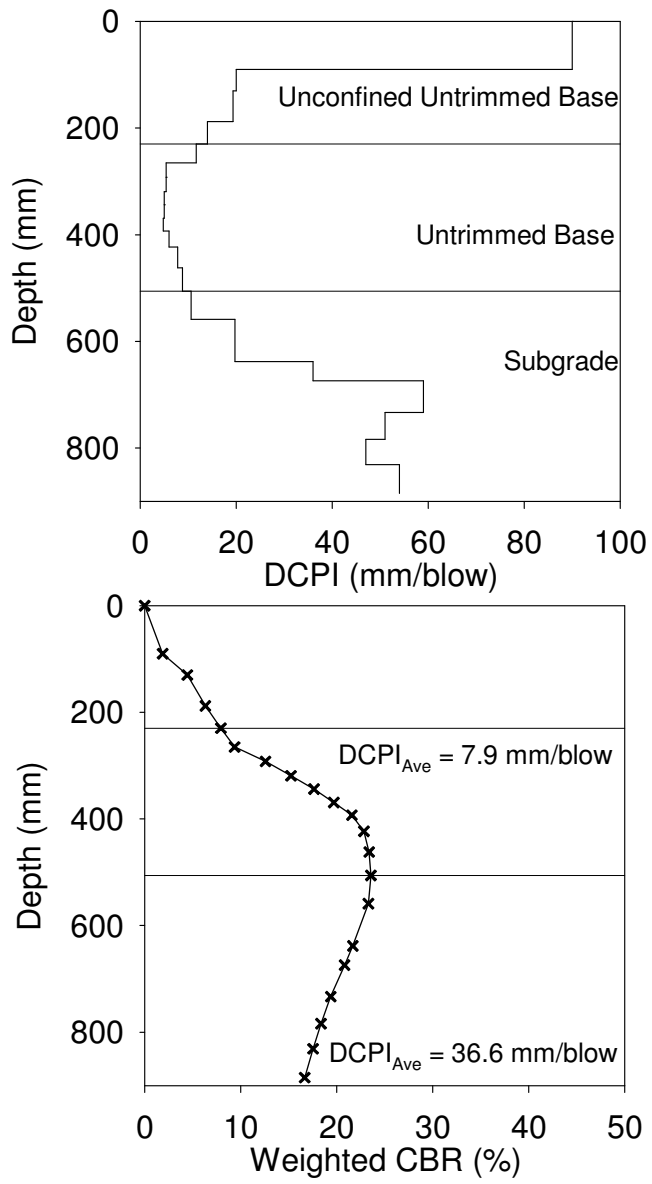
Figure 7. Michigan I-94 Test Bed 3 Point 846+00-I DCPI determination for each layer
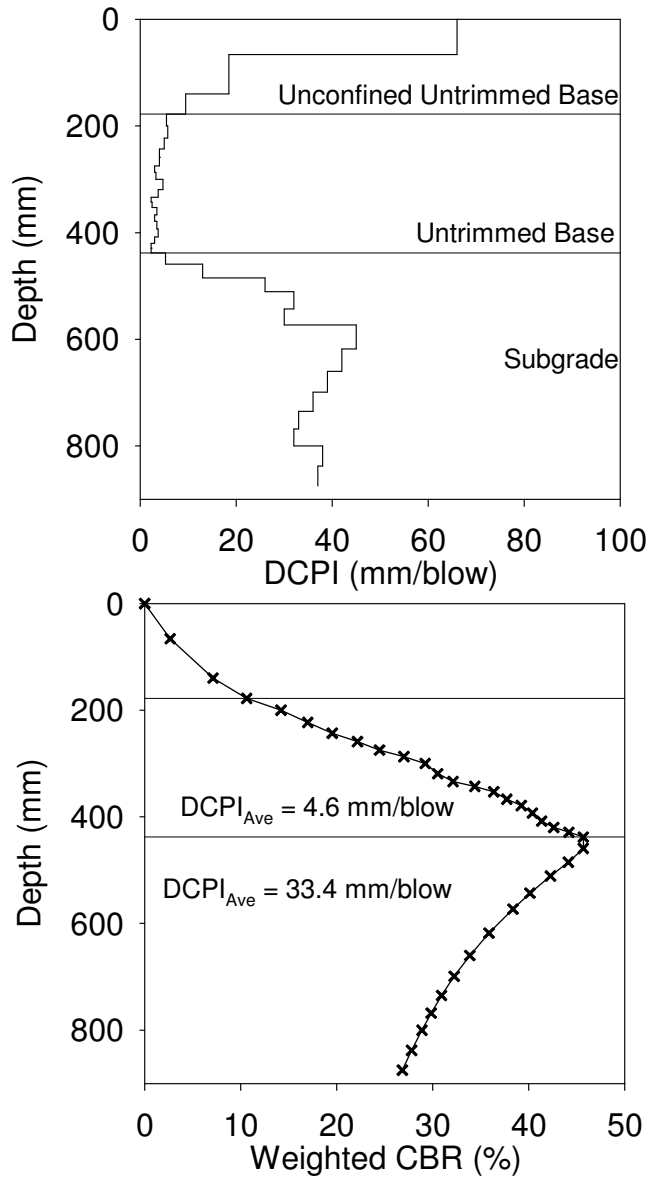
Figure 8. Michigan I-94 Test Bed 3 Point 847+00-O DCPI determination for each layer
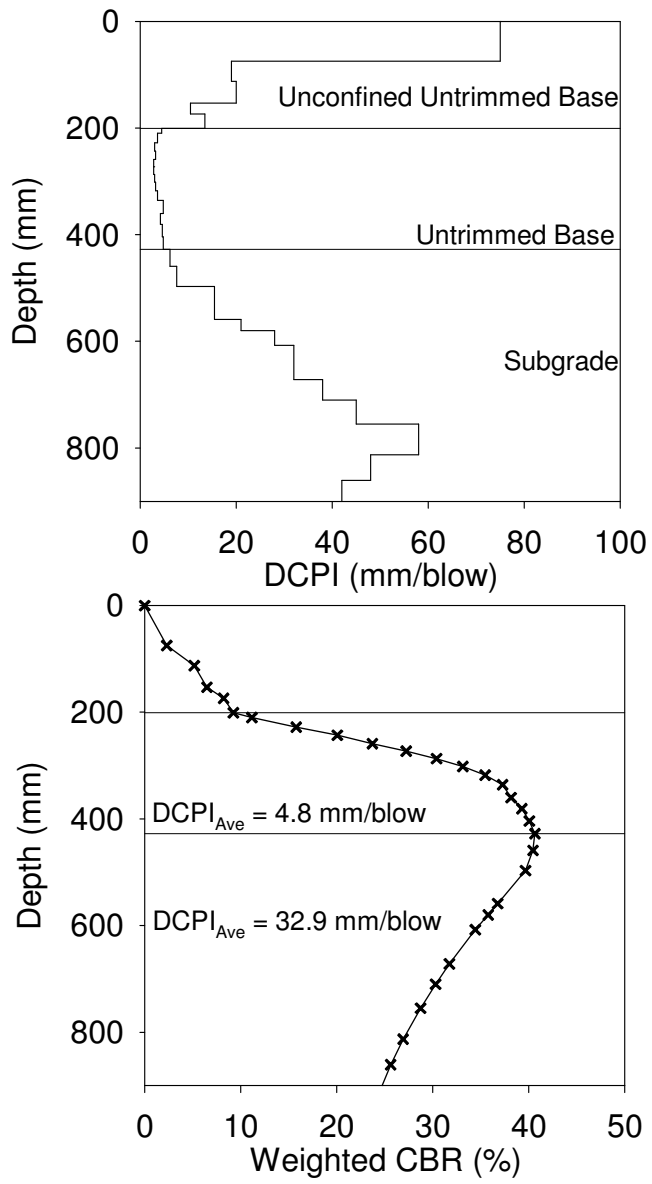
Figure 9. Michigan I-94 Test Bed 3 Point 848+00-I DCPI determination for each layer
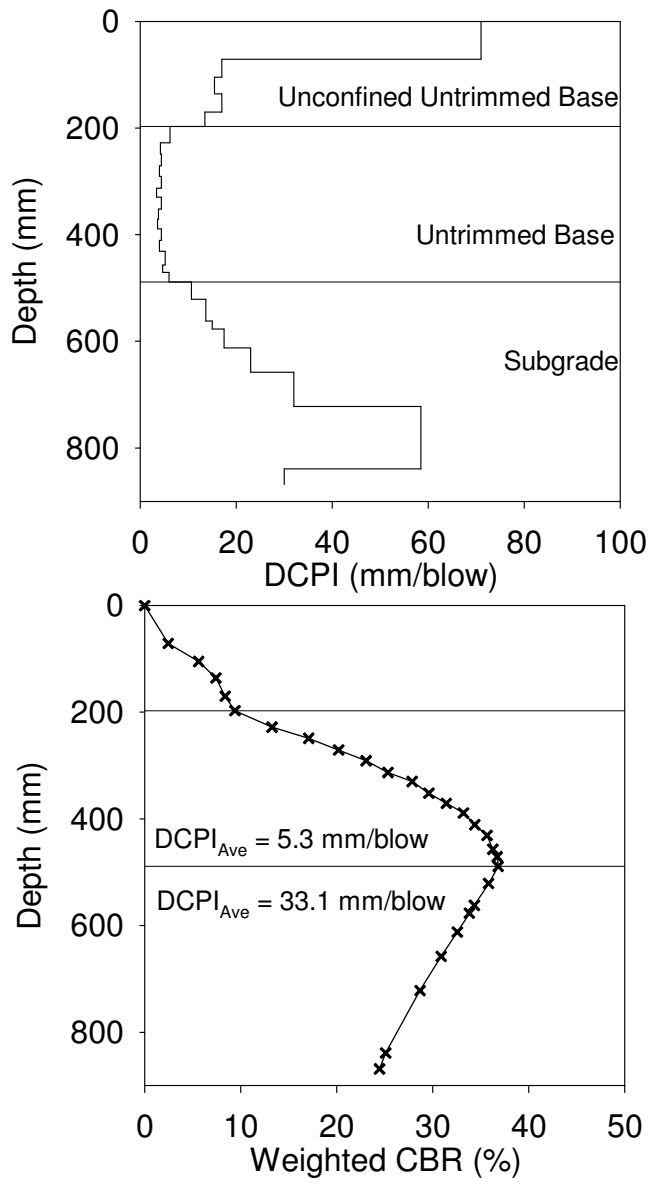
Figure 10. Michigan I-94 Test Bed 3 Point 848+00-O DCPI determination for each layer
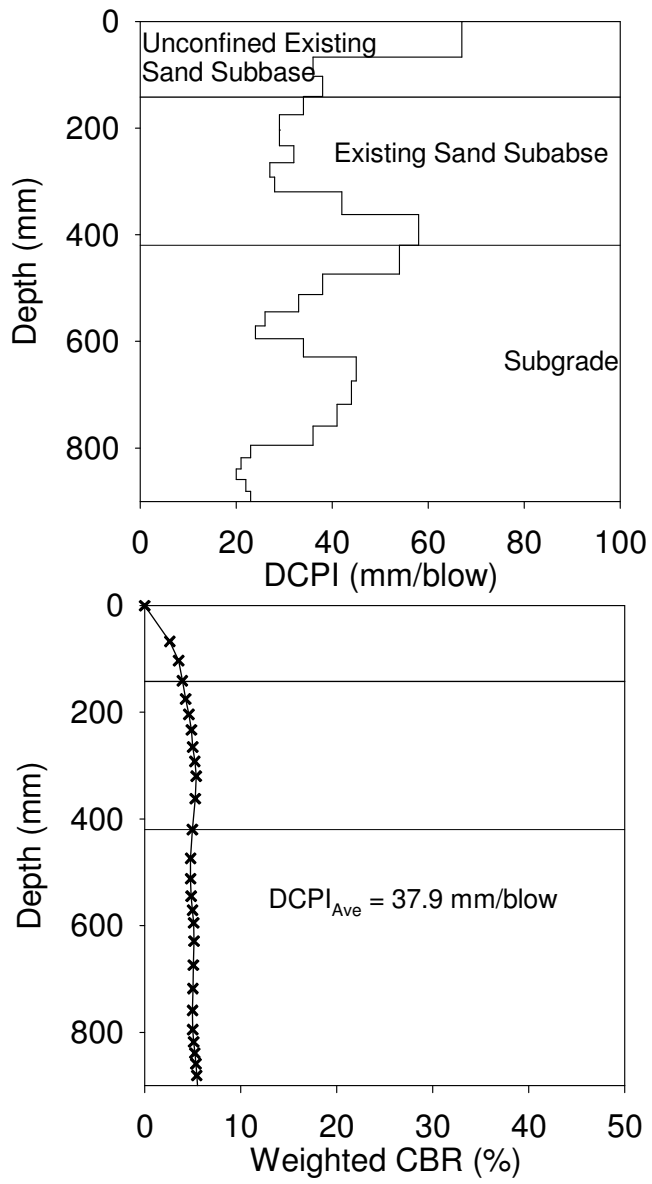
Figure 11. Michigan I-94 Test Bed 2 Point A4 DCPI determination for each layer
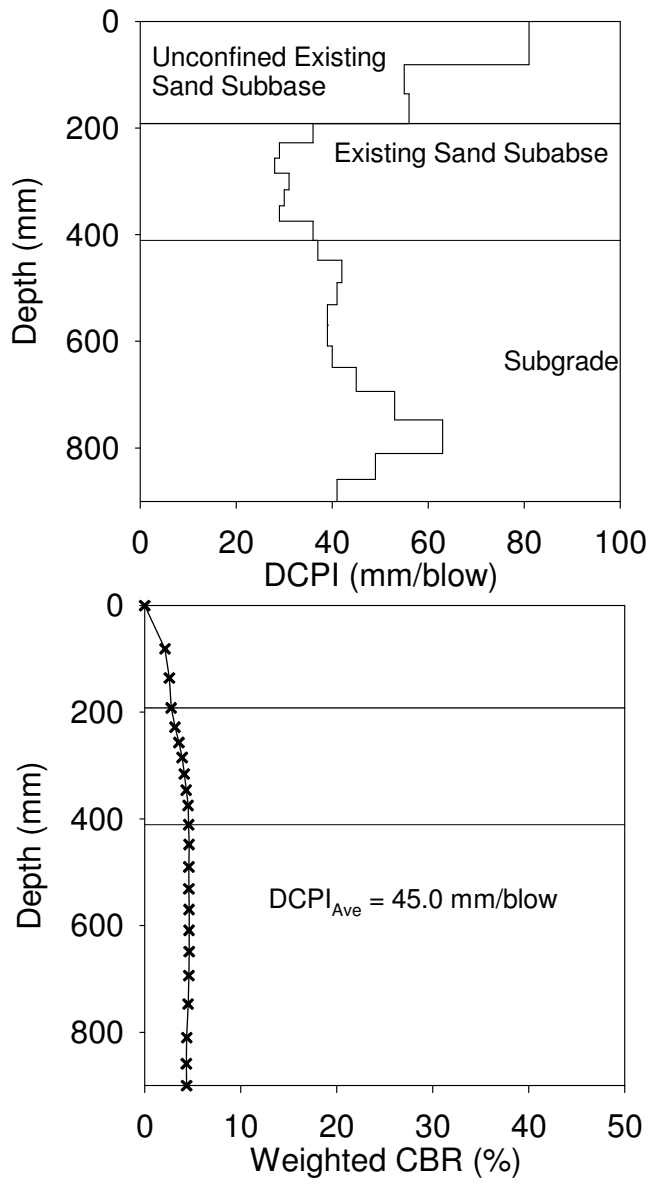
Figure 12. Michigan I-94 Test Bed 2 Point C2 DCPI determination for each layer
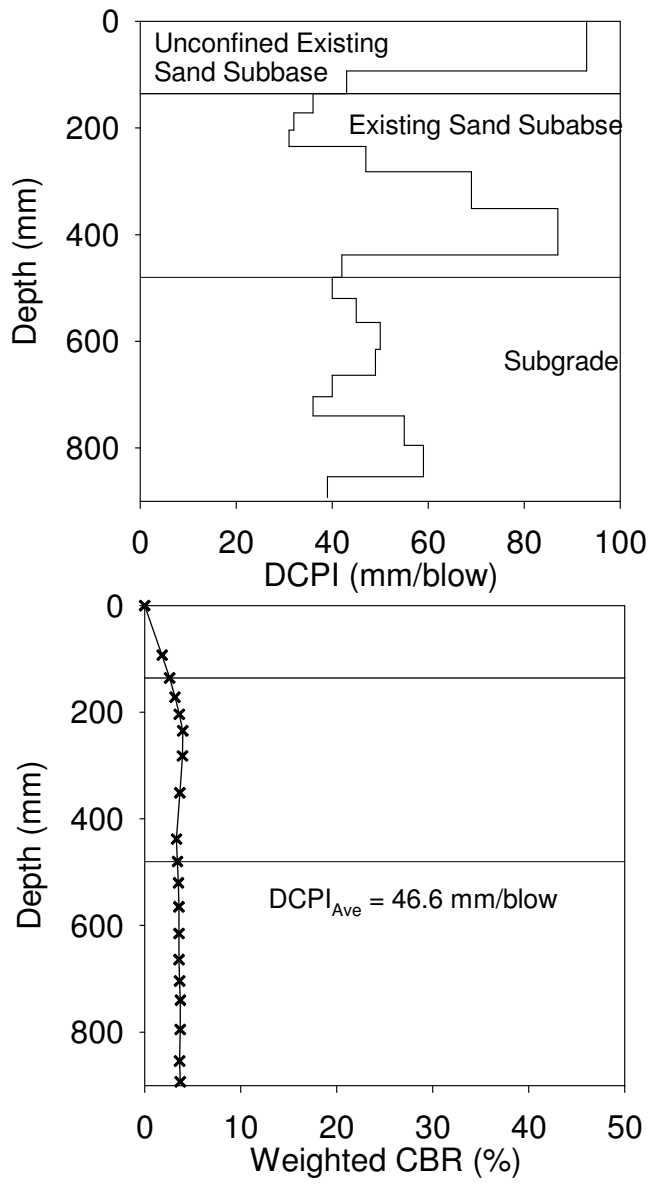
Figure 13. Michigan I-94 Test Bed 2 Point C4 DCPI determination for each layer
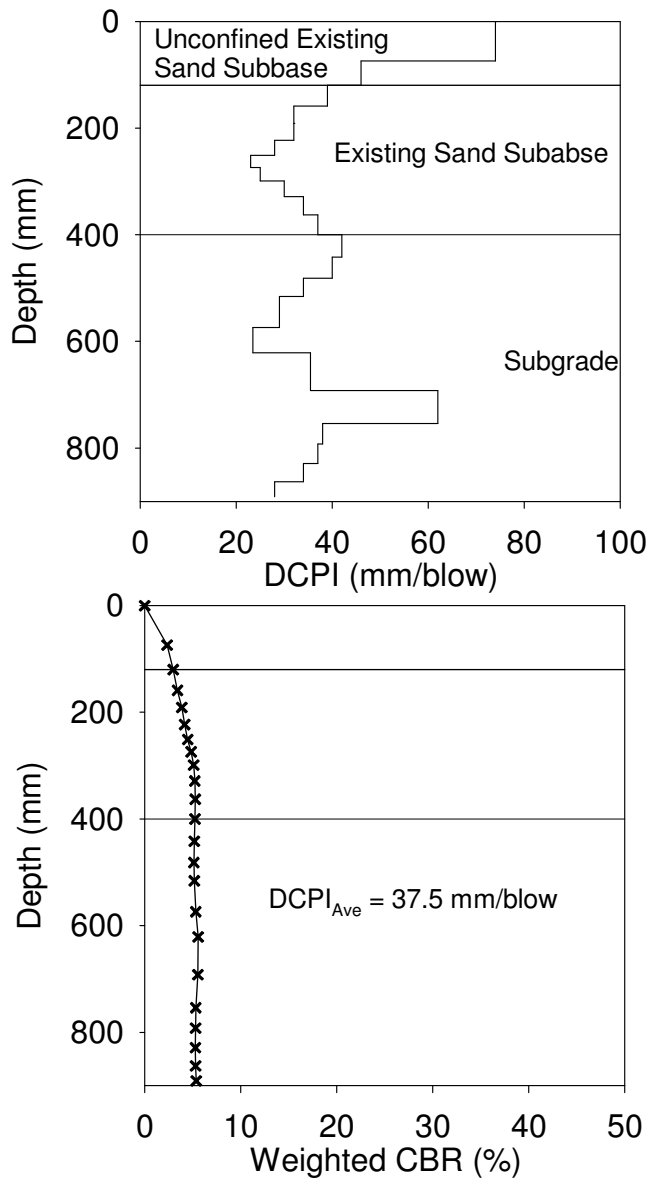
Figure 14. Michigan I-94 Test Bed 2 Point E2 DCPI determination for each layer
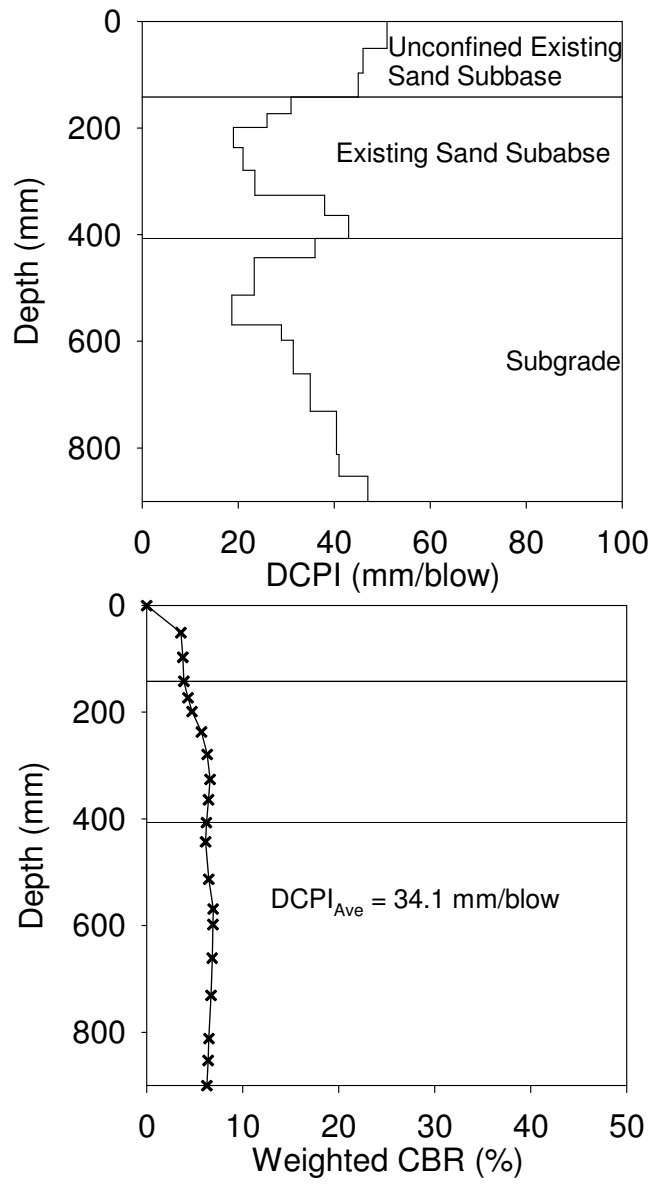
Figure 15. Michigan I-94 Test Bed 2 Point E4 DCPI determination for each layer
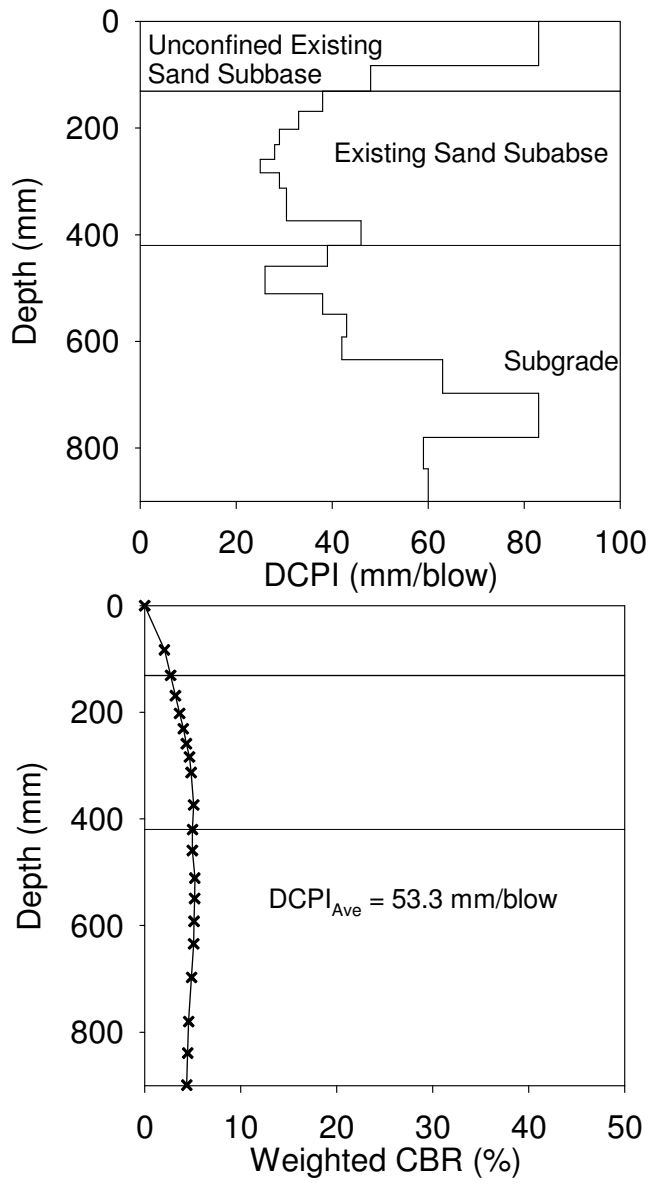
Figure 16. Michigan I-94 Test Bed 2 Point G1 DCPI determination for each layer
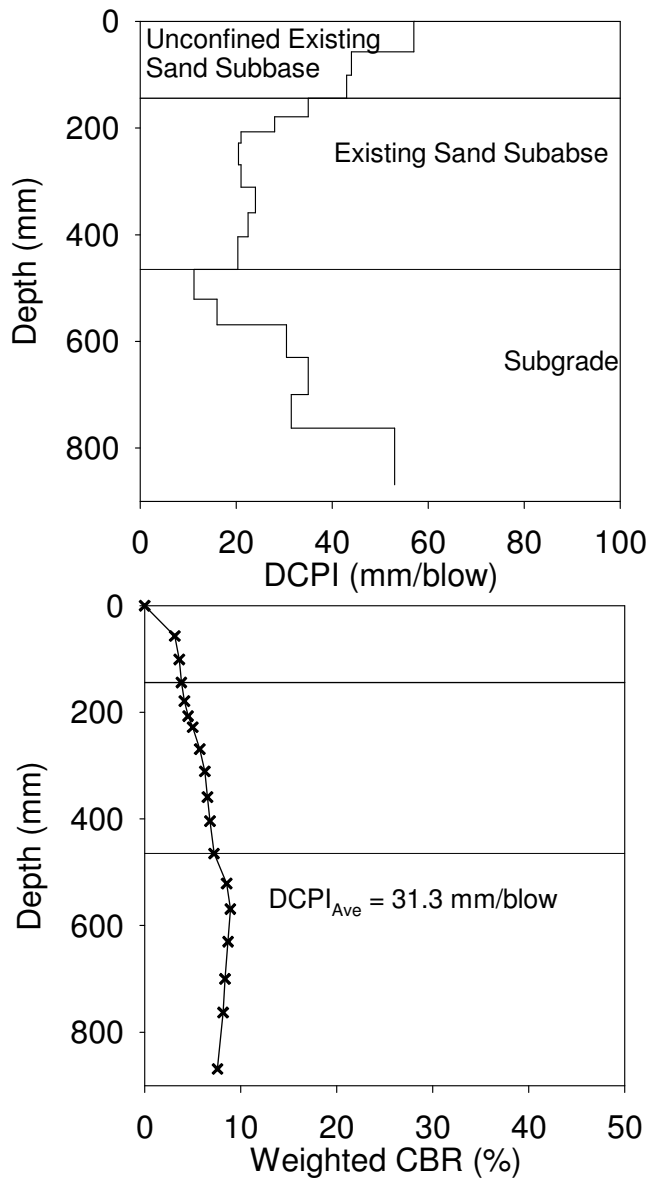
Figure 17. Michigan I-94 Test Bed 2 Point G3 DCPI determination for each layer

MICHIGAN I-96
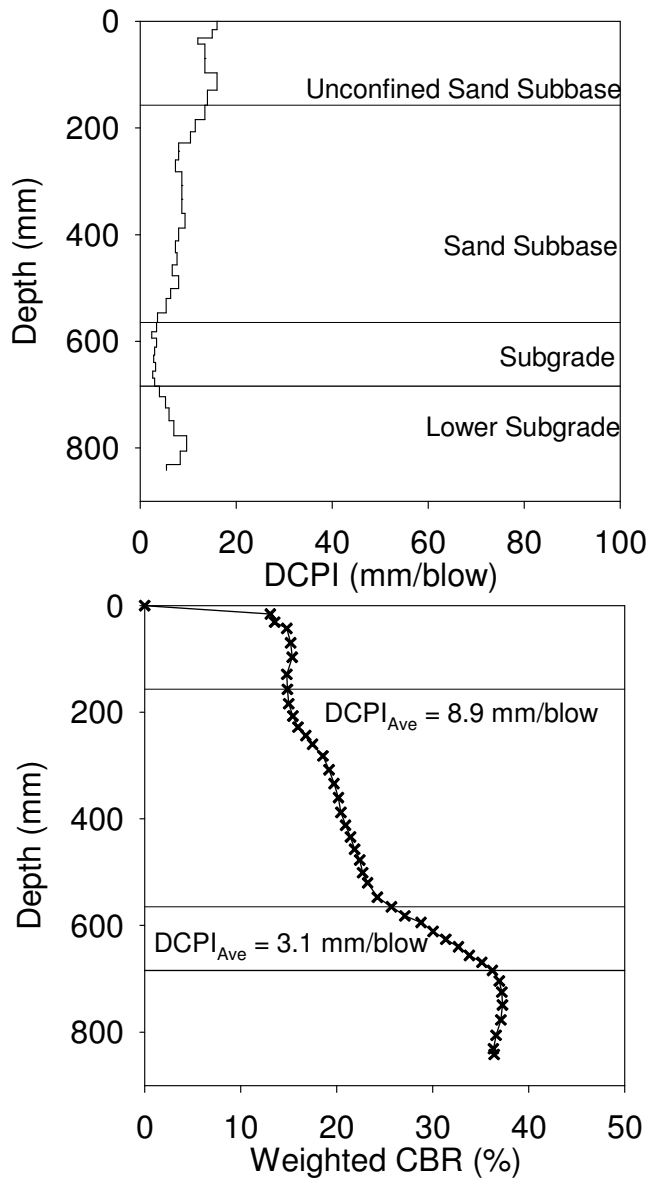
Figure 18. Michigan I-96 Test Bed 1 Point E8 DCPI determination for each layer
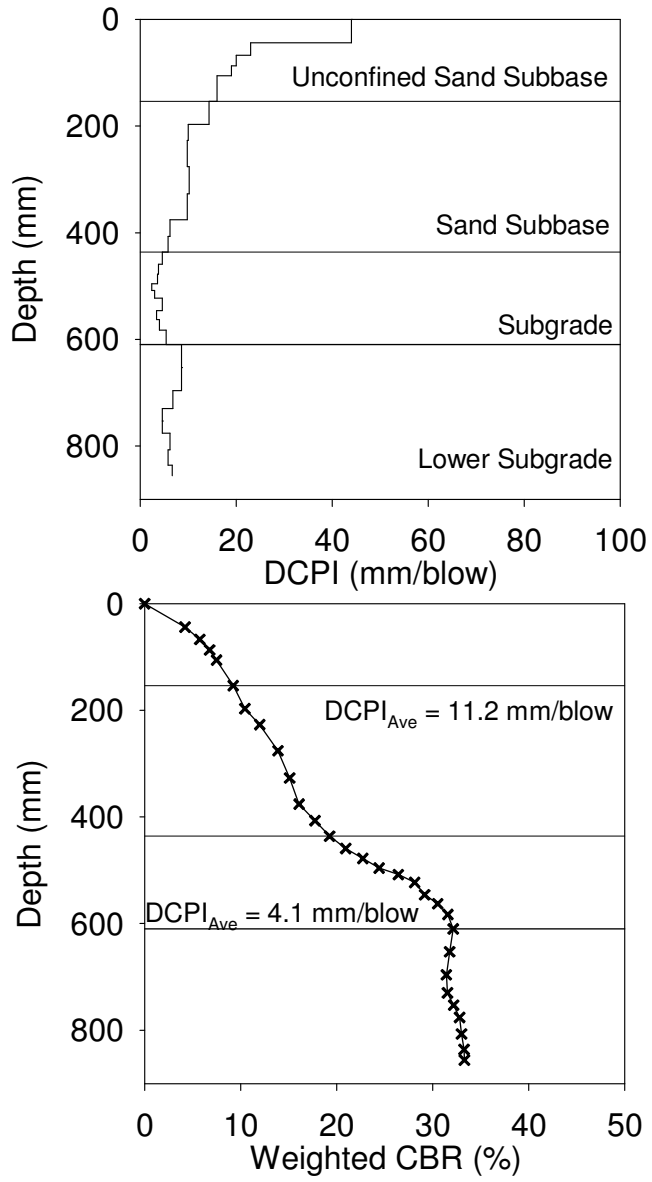
Figure 19. Michigan I-96 Test Bed 1 Point G6 DCPI determination for each layer
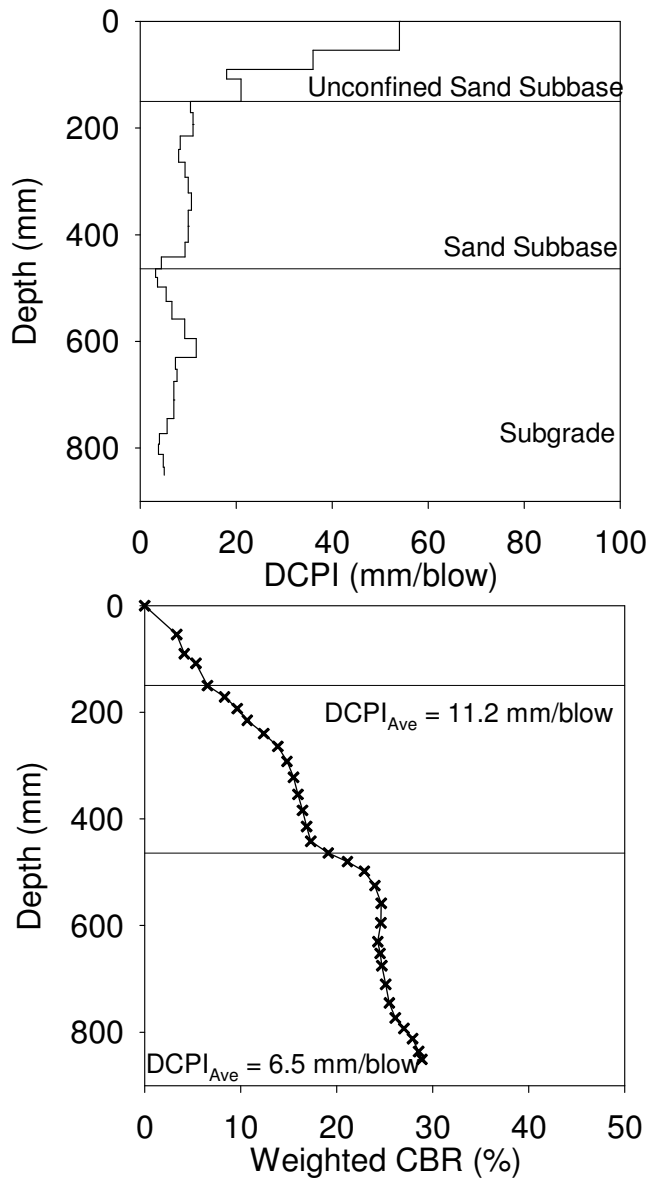
Figure 20. Michigan I-96 Test Bed 1 Point I8 DCPI determination for each layer
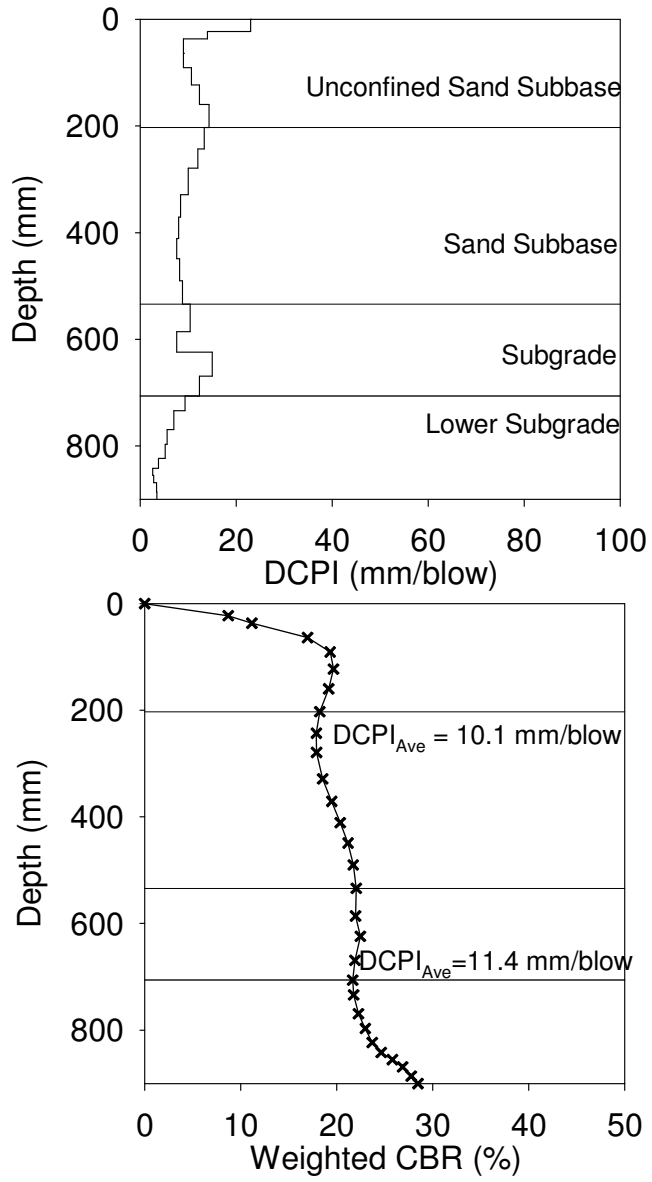
Figure 21. Michigan I-96 Test Bed 3 Point 459+50 DCPI determination for each layer
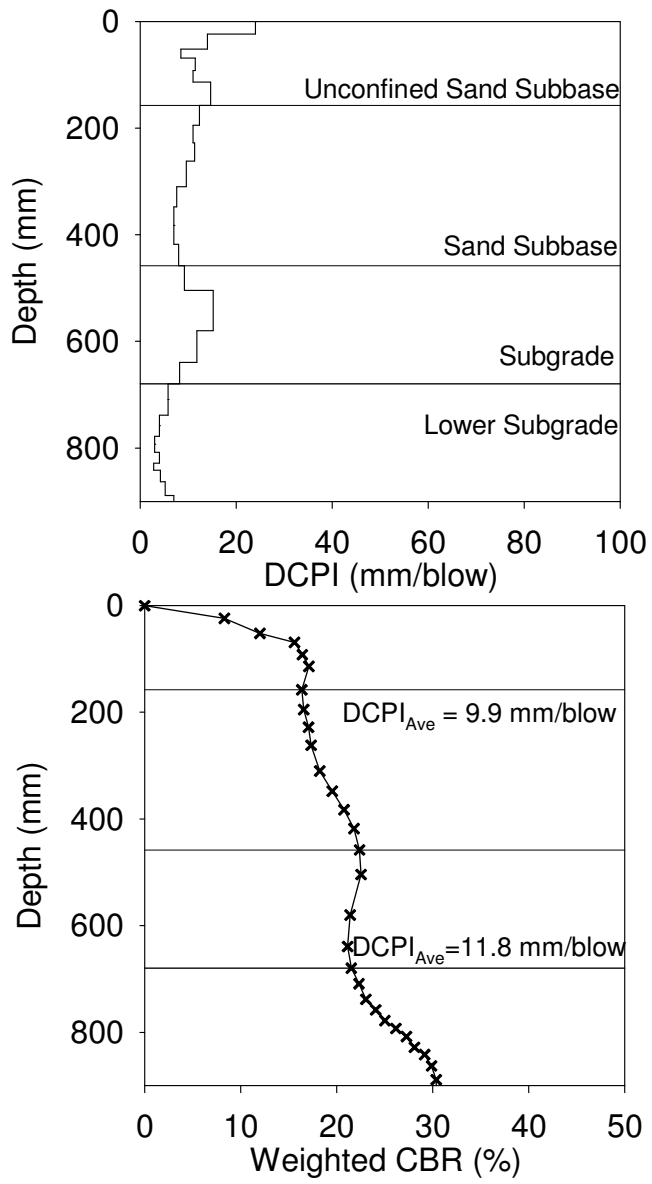
Figure 22. Michigan I-96 Test Bed 3 Point 460+50 DCPI determination for each layer
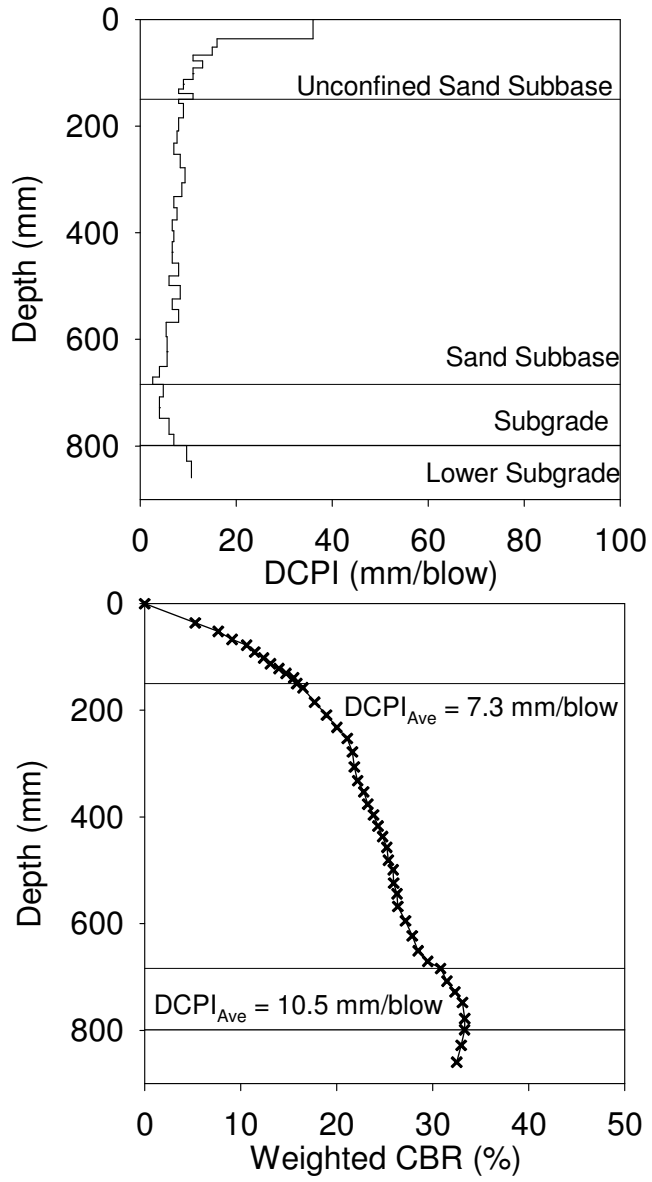
Figure 23. Michigan I-96 Test Bed 3 Point 467+50 DCPI determination for each layer
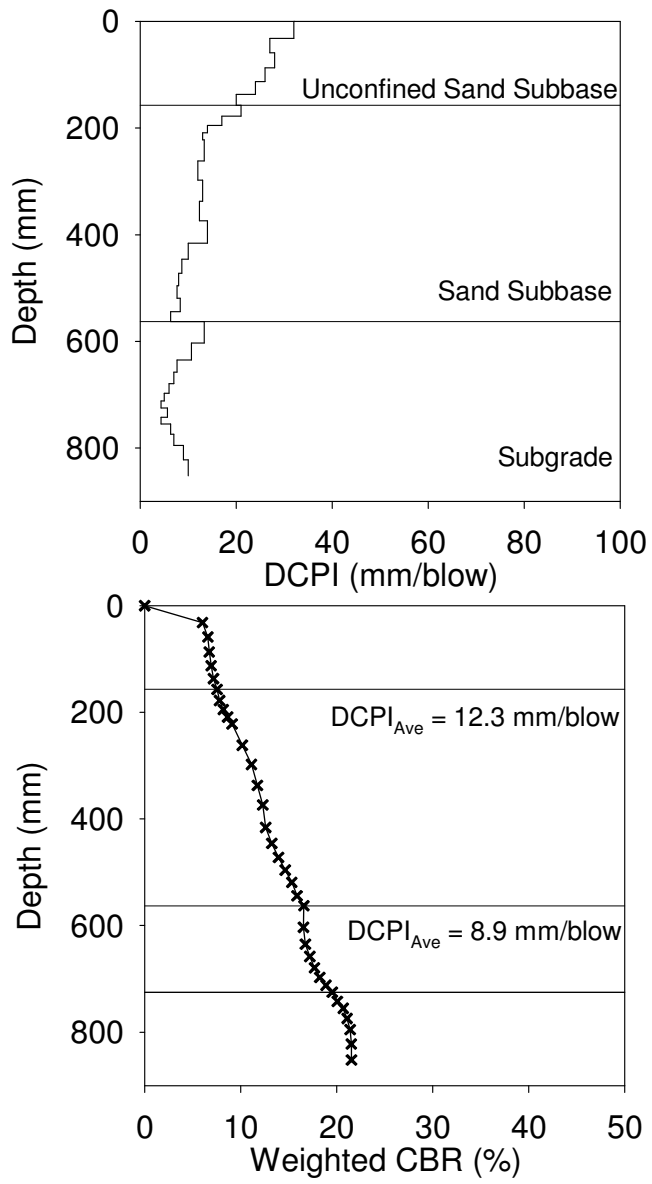
Figure 24. Michigan I-96 Test Bed 3 Point 468+50 DCPI determination for each layer
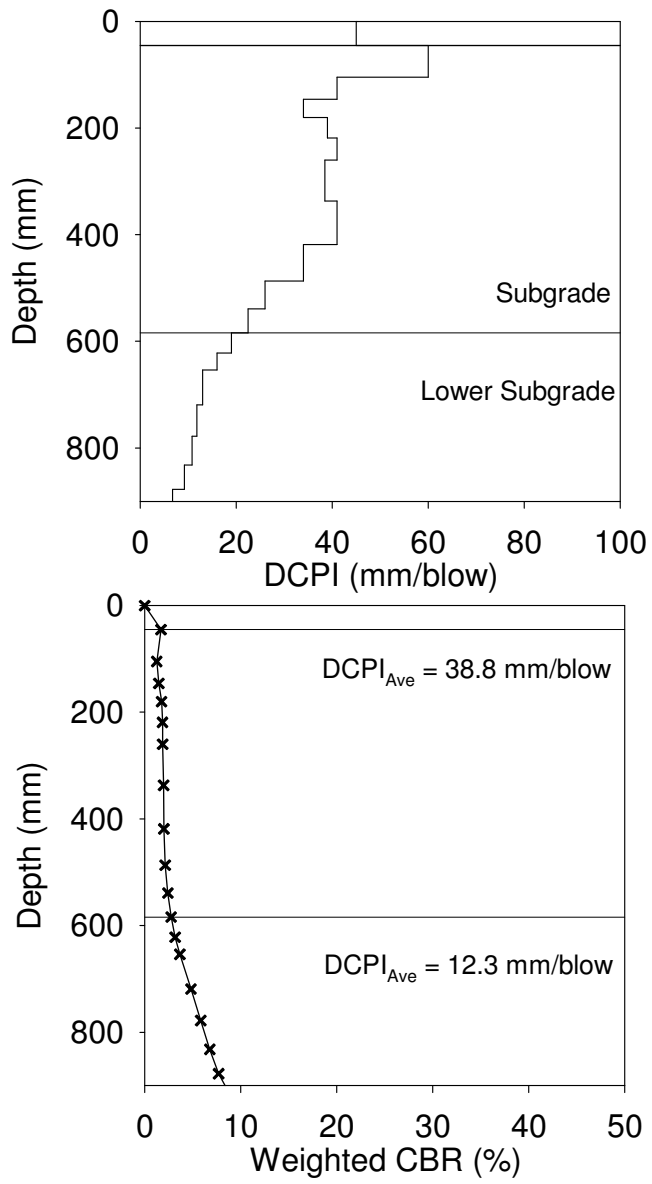
IOWA I-29

Figure 25. Iowa I-29 Test Bed 1 Point 3 DCPI determination for each layer
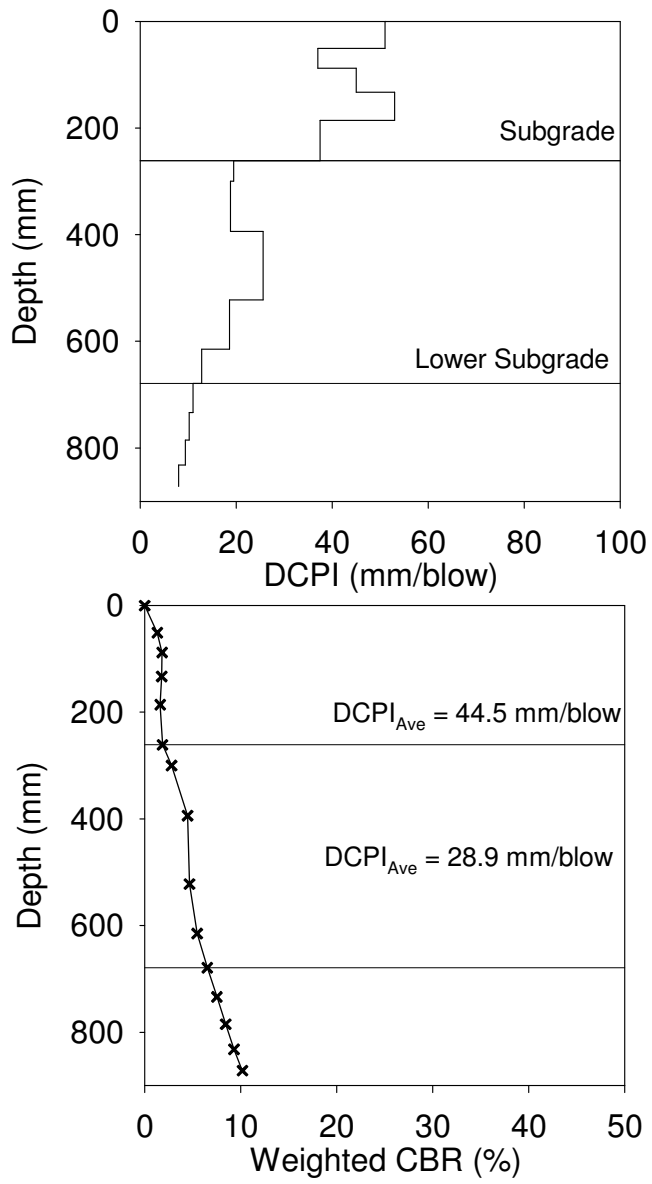
Figure 26. Iowa I-29 Test Bed 1 Point 4 DCPI determination for each layer
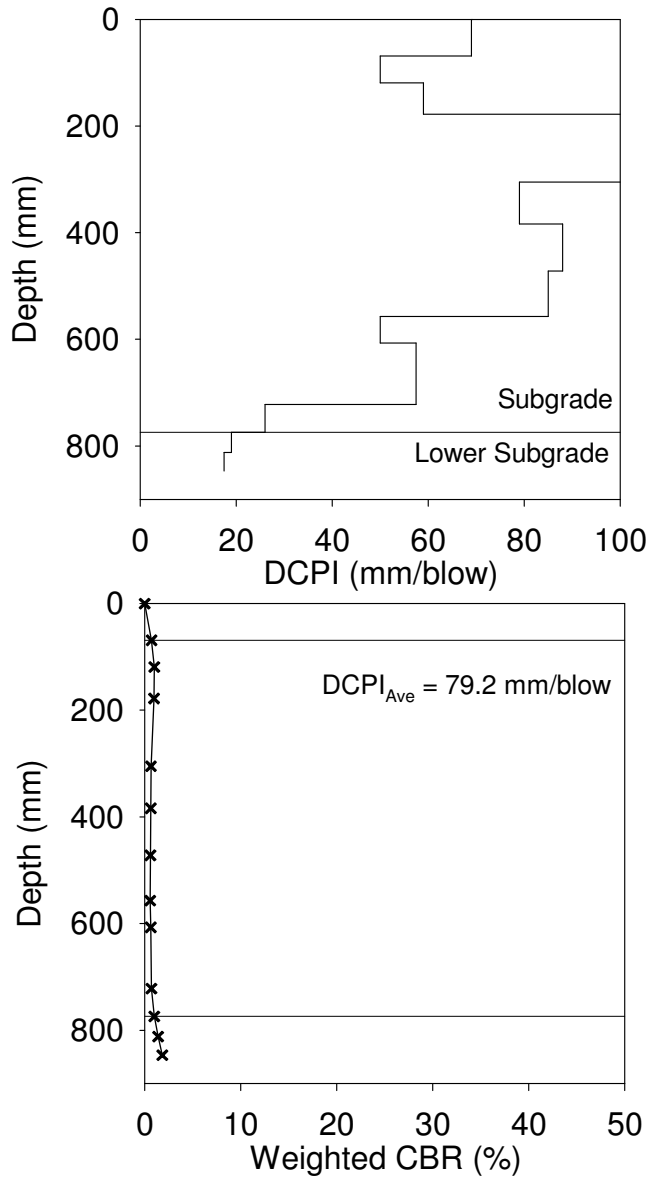
Figure 27. Iowa I-29 Test Bed 2 Pass 1-Point 1 DCPI determination for each layer
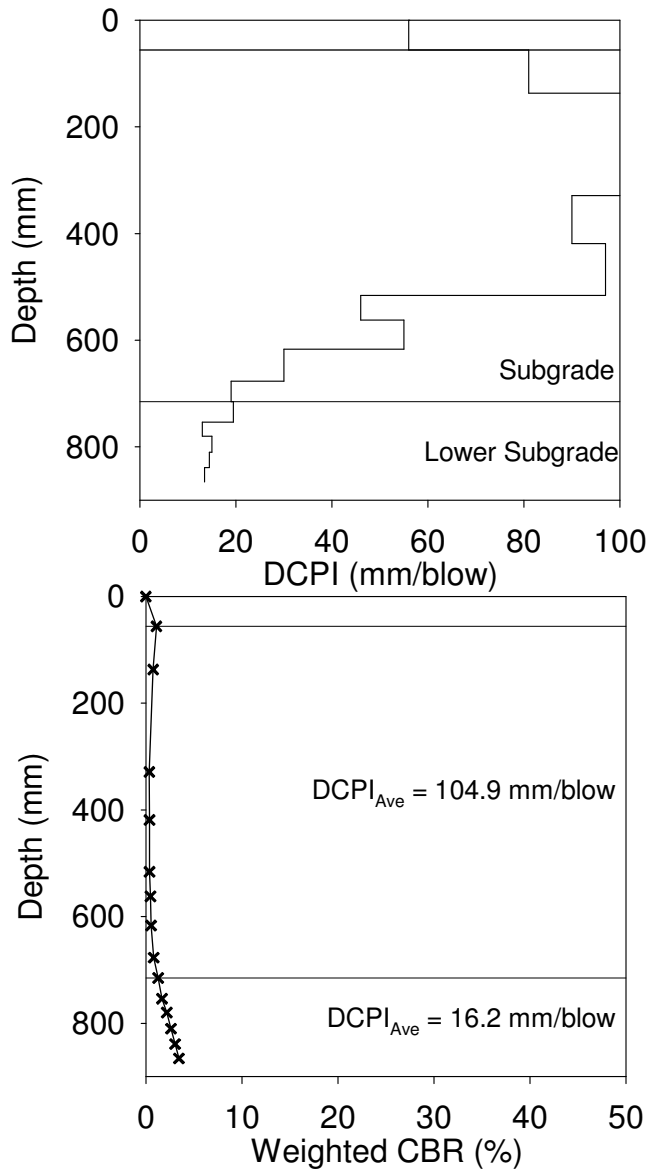
Figure 28. Iowa I-29 Test Bed 2 Pass 2-Point 1 DCPI determination for each layer
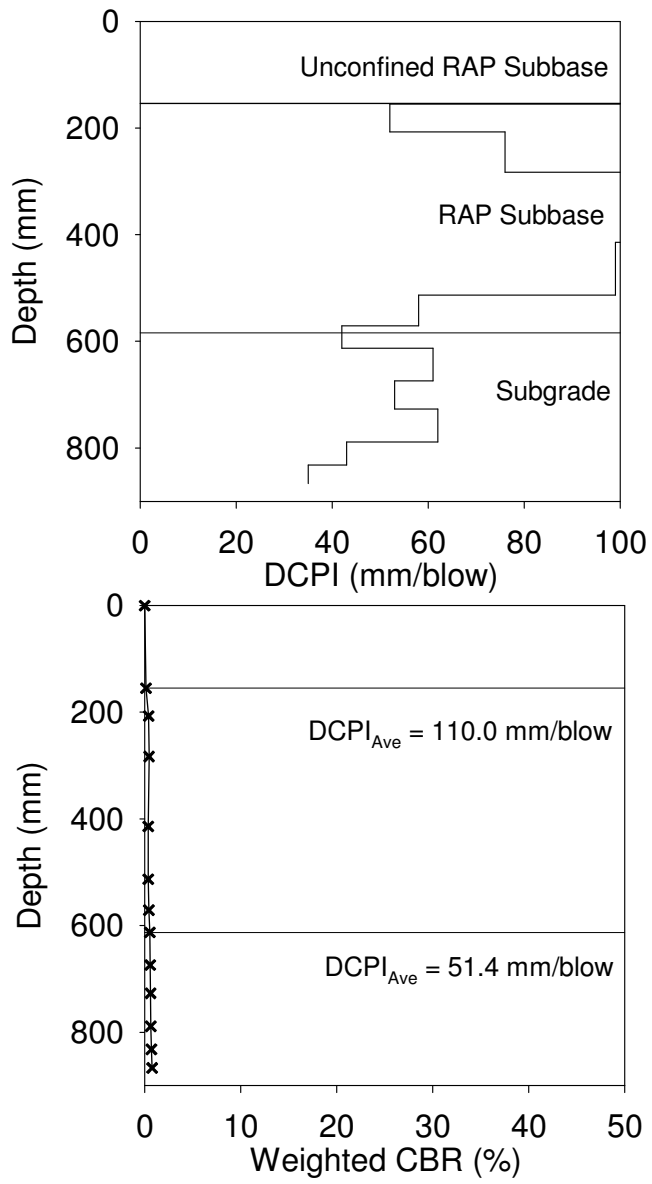
Figure 29. Iowa I-29 Test Bed 4 Pass 1-Point 1 DCPI determination for each layer
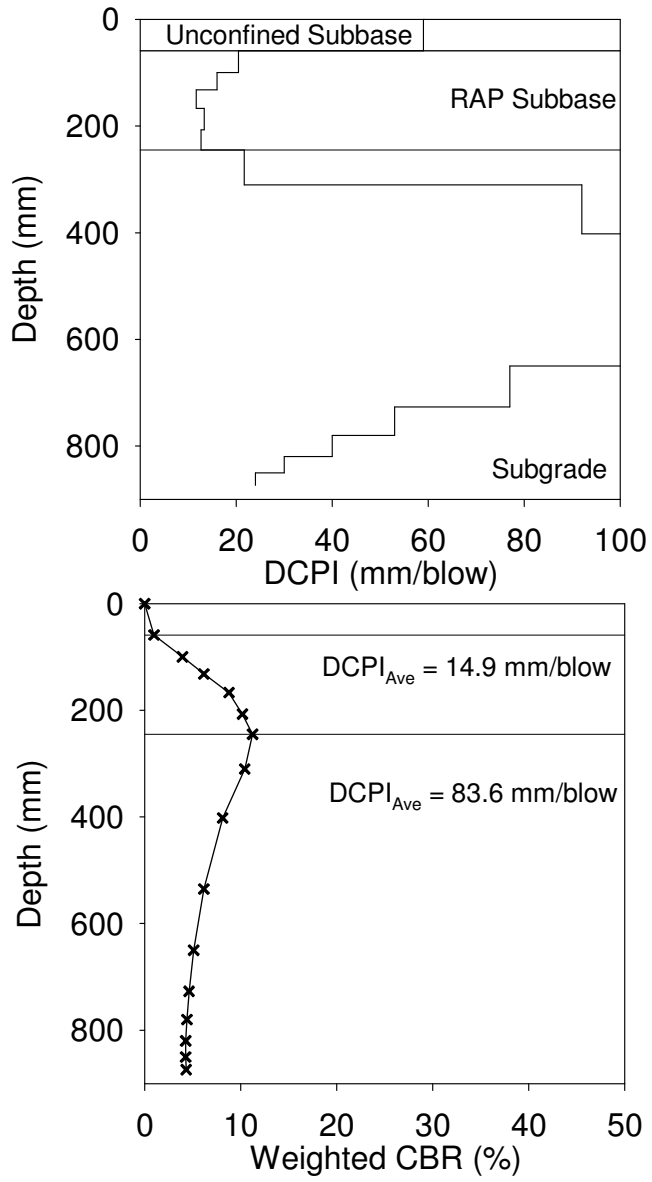
Figure 30. Iowa I-29 Test Bed 4 Pass 4-Point 2 DCPI determination for each layer
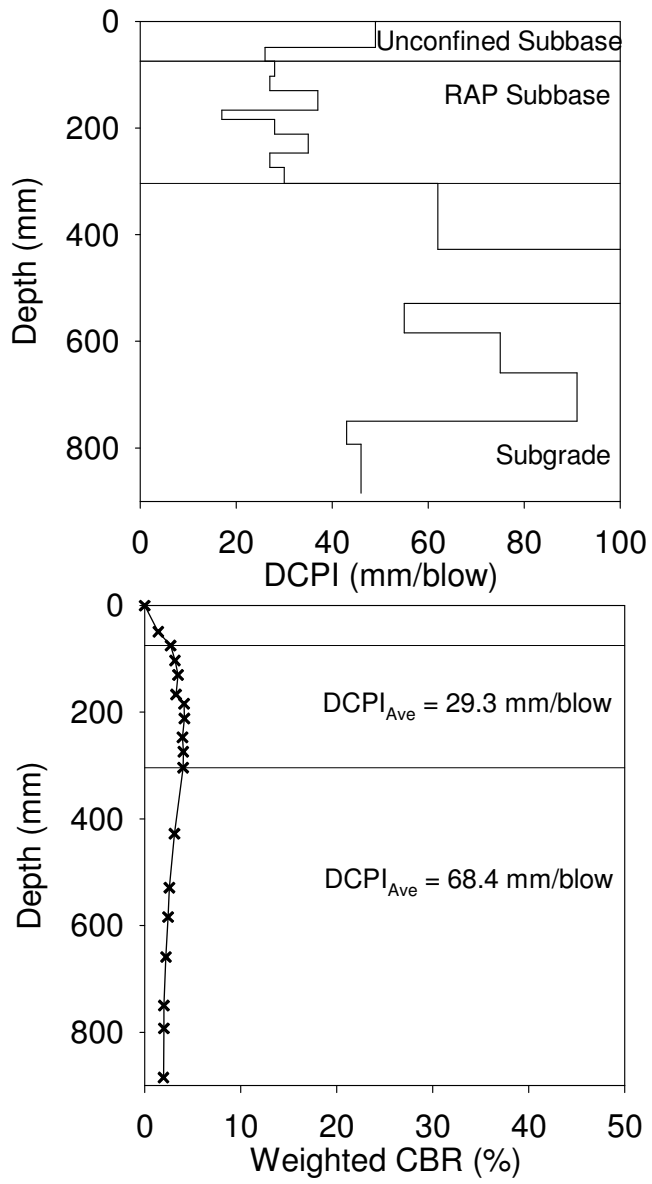
Figure 31. Iowa I-29 Test Bed 4 Pass 4-Point 4 DCPI determination for each layer
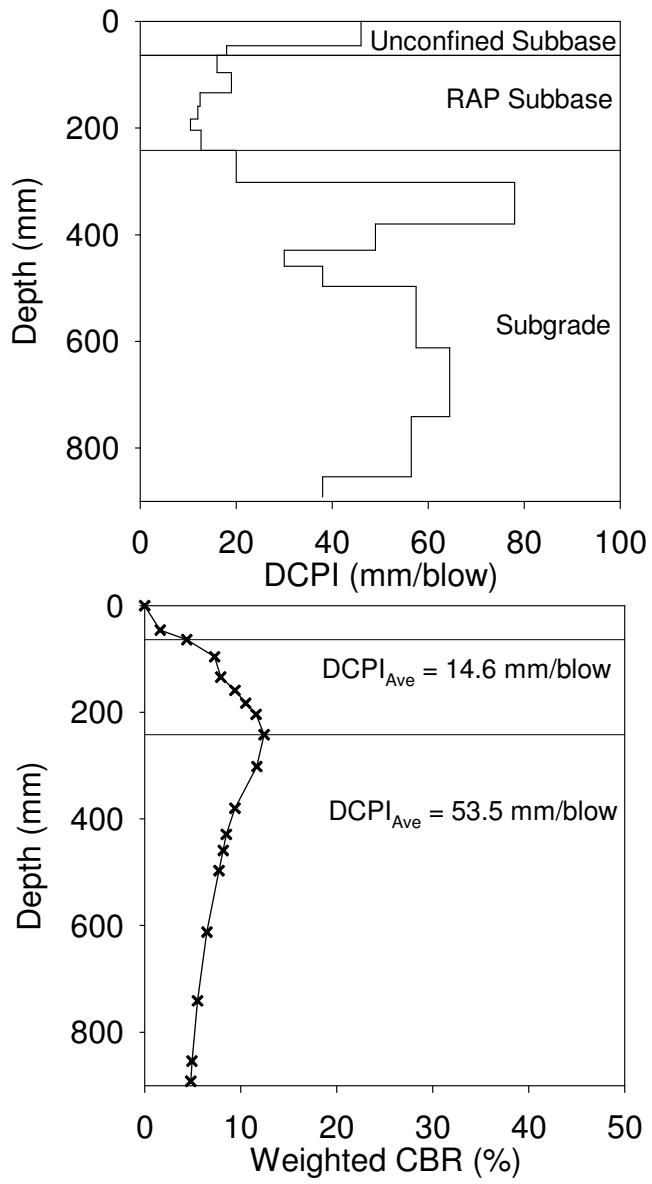
Figure 32. Iowa I-29 Test Bed 4 Pass 8-Point 2 DCPI determination for each layer

PENNSYLVANIA US-22
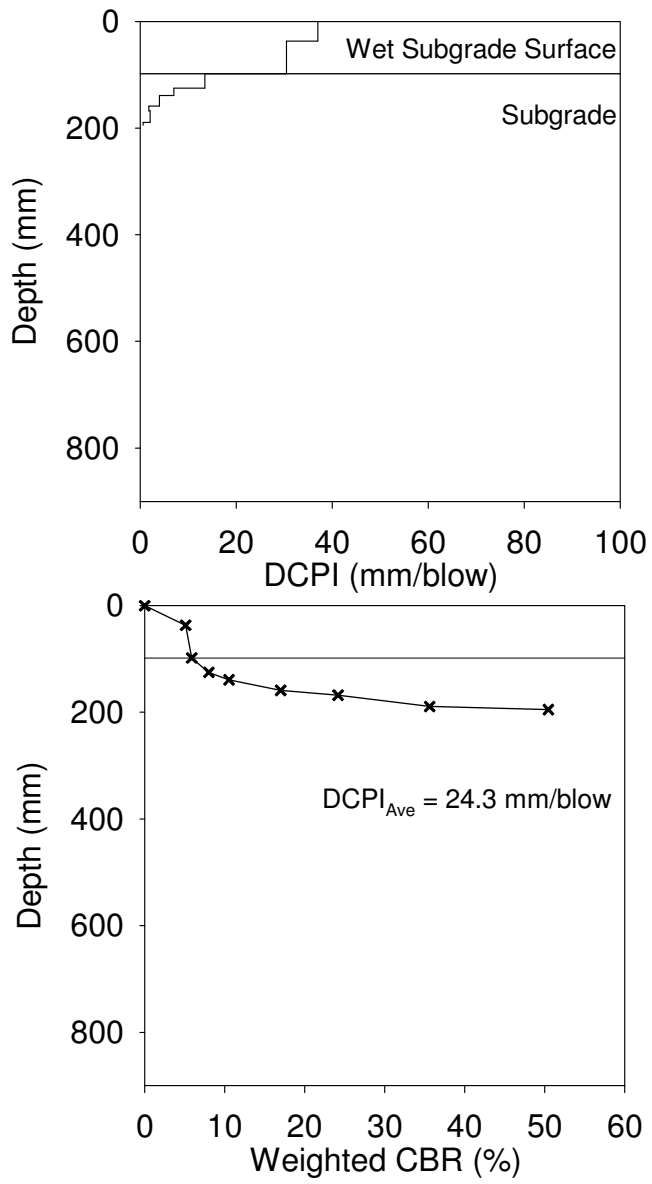
Figure 33. Pennsylvania US-22 Test Bed 6 Point P9 DCPI determination for each layer
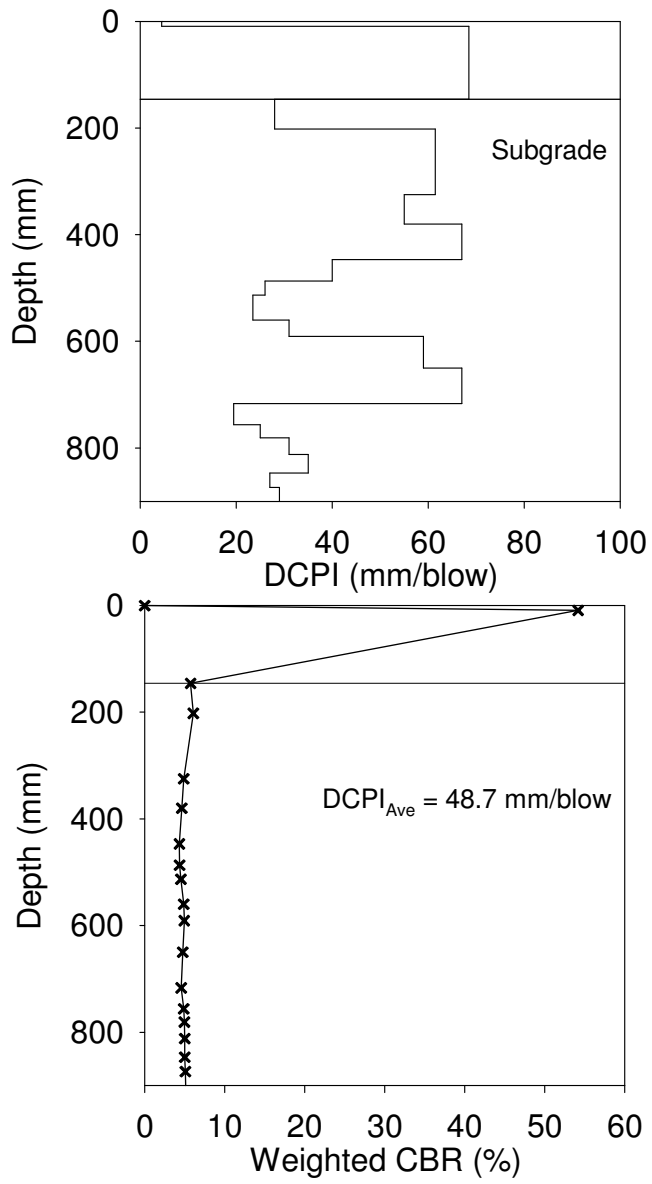
Figure 34. Pennsylvania US-22 Test Bed 6 Point P14 DCPI determination for each layer
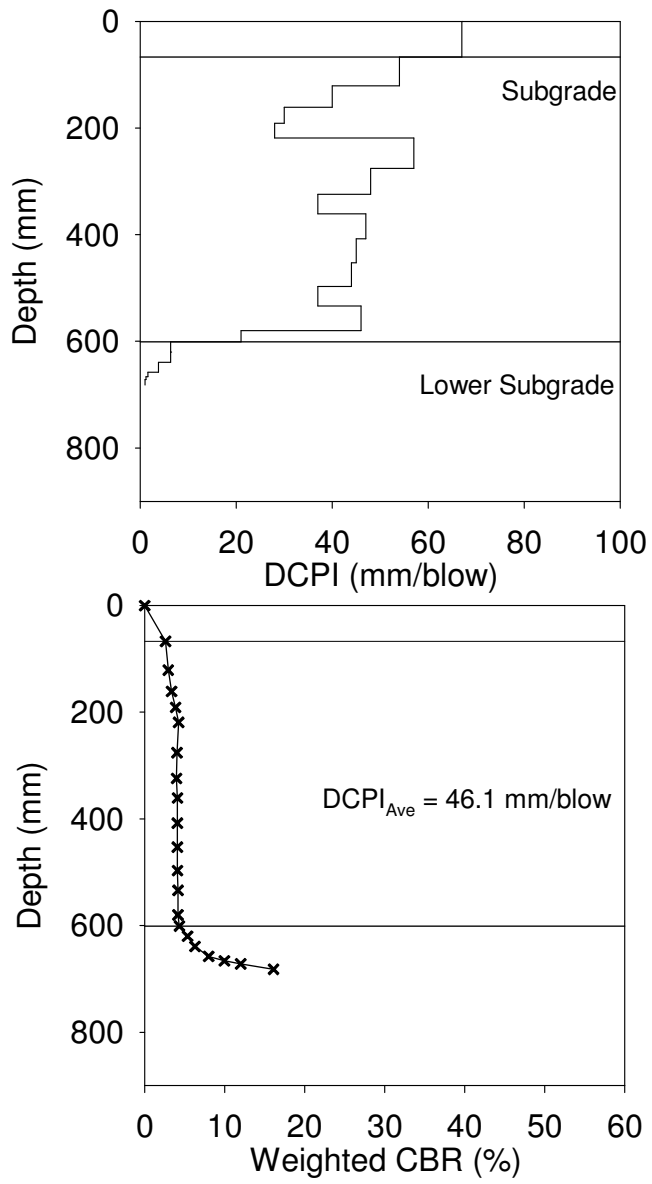
Figure 35. Pennsylvania US-22 Test Bed 6 Point P15 DCPI determination for each layer
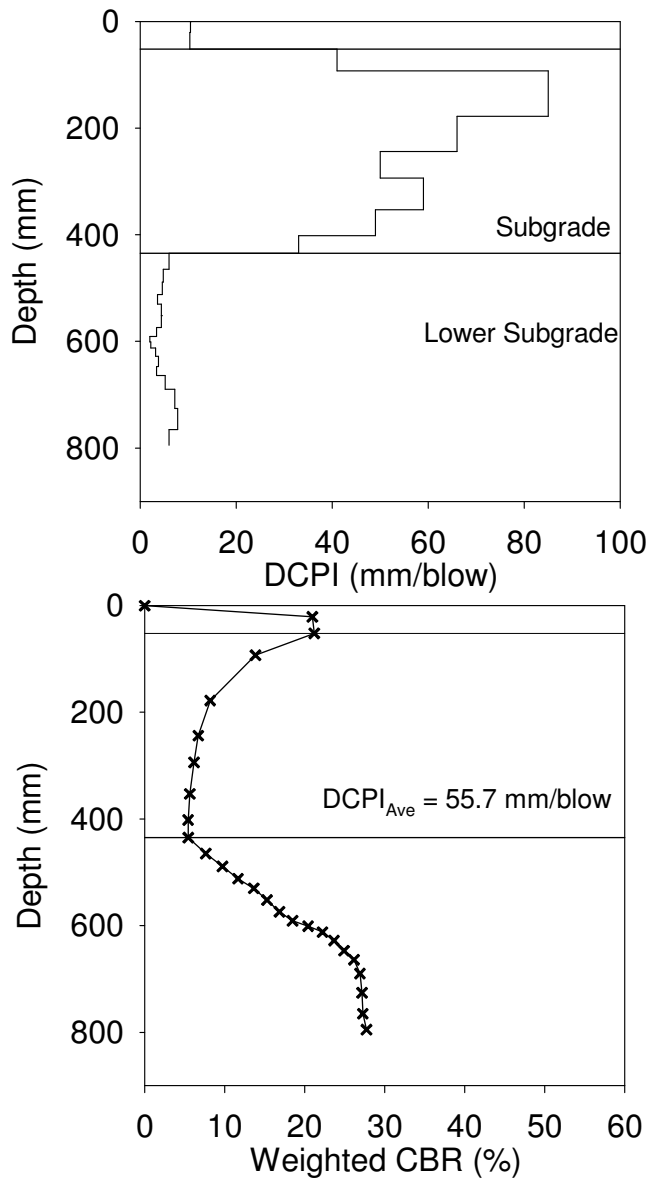
Figure 36. Pennsylvania US-22 Test Bed 6 Point P18 DCPI determination for each layer
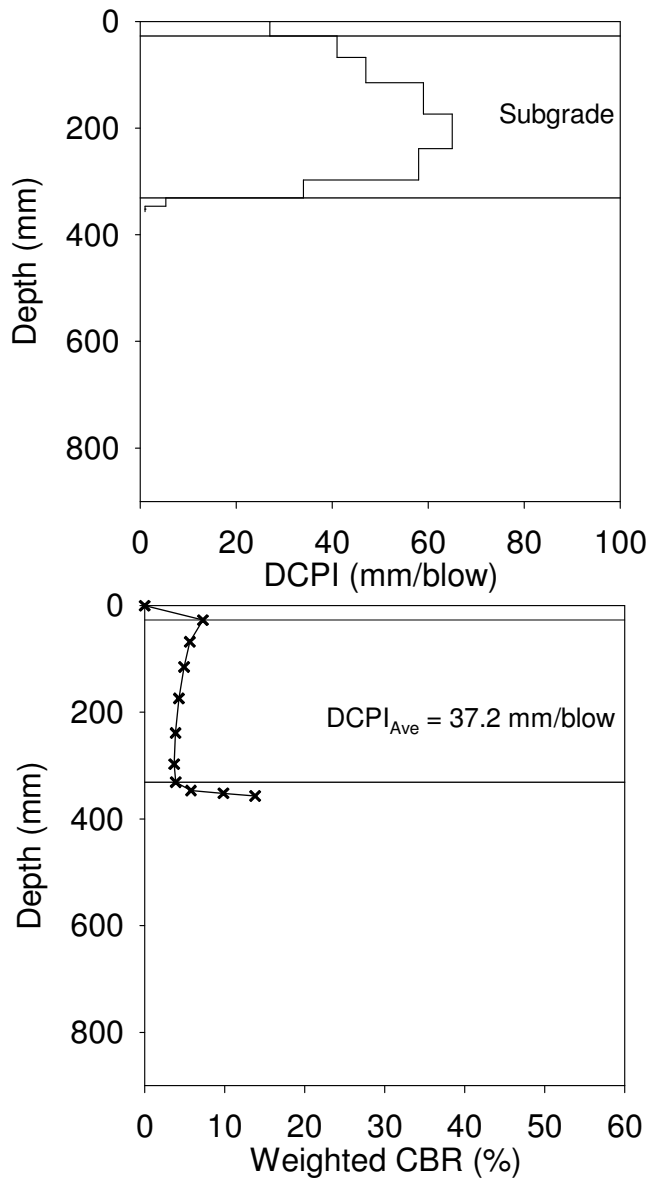
Figure 37. Pennsylvania US-22 Test Bed 6 Point P21 DCPI determination for each layer

WISCONSIN US-10
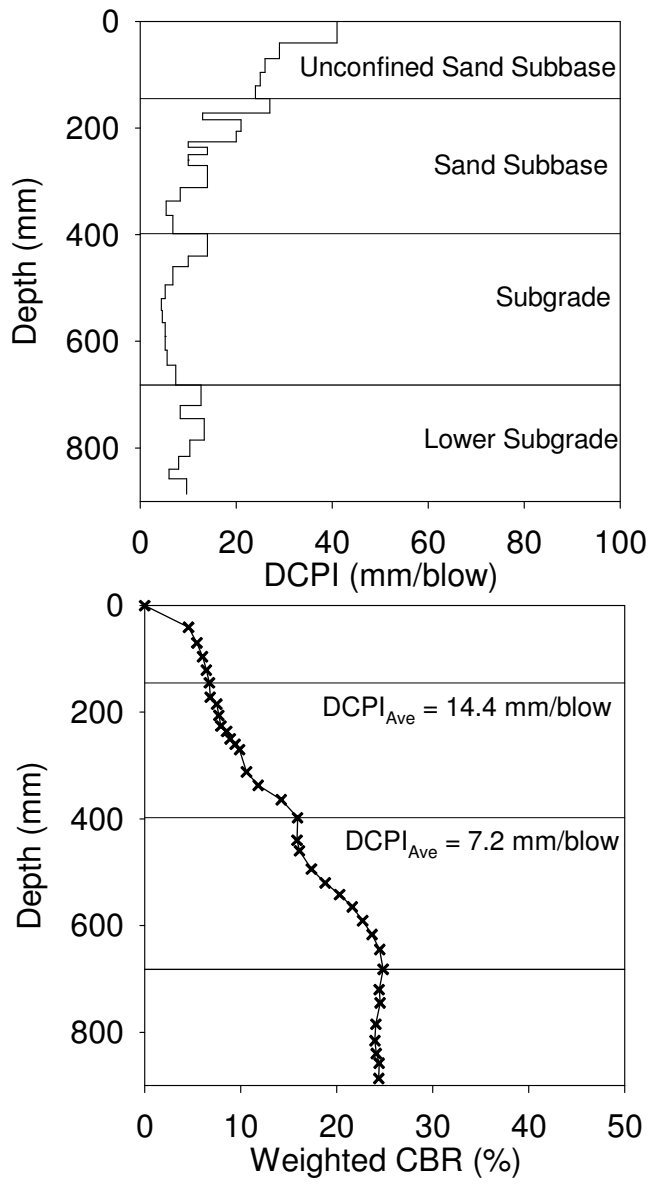
Figure 38. Wisconsin US-10 Test Bed 1 Point A2 DCPI determination for each layer
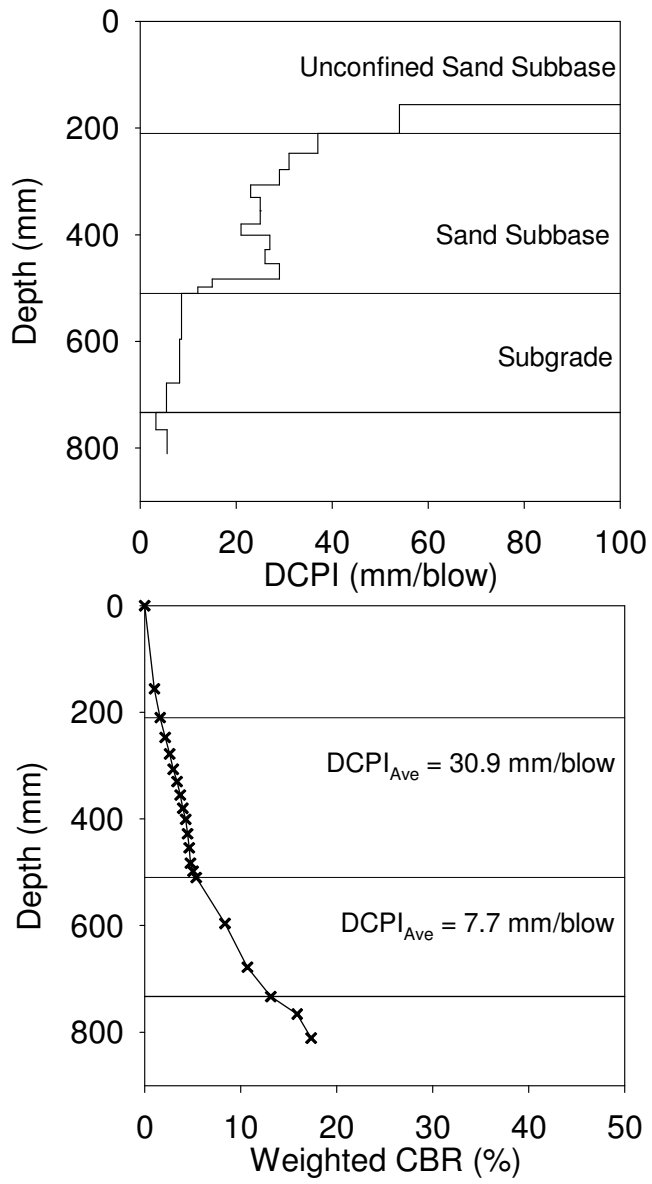
**Figure 39. Wisconsin US-10 Test Bed 1 Point D3 DCPI determination for each layer**
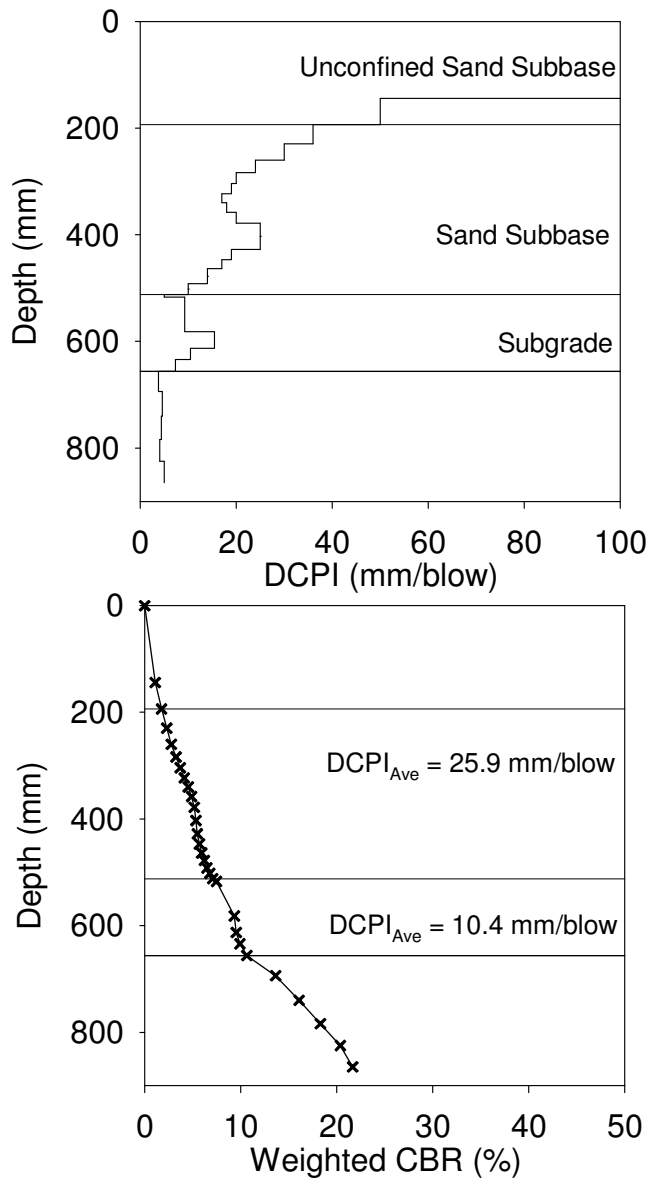
**Figure 40. Wisconsin US-10 Test Bed 1 Point D5 DCPI determination for each layer**
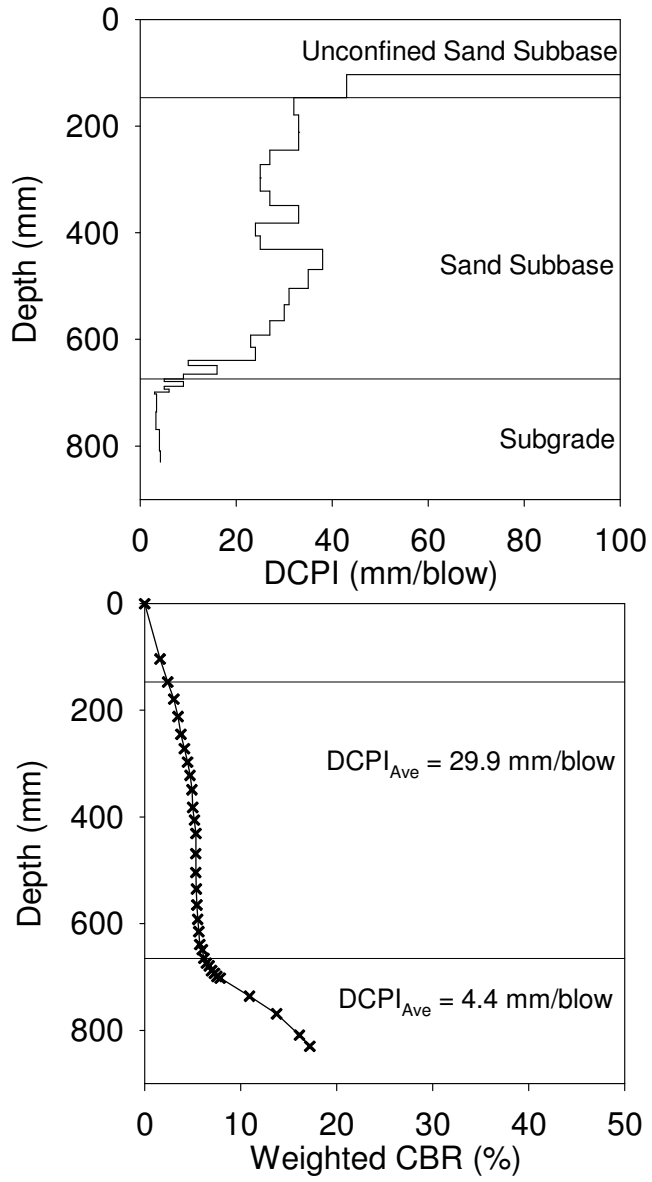
Figure 41. Wisconsin US-10 Test Bed 1 Point D10 DCPI determination for each layer
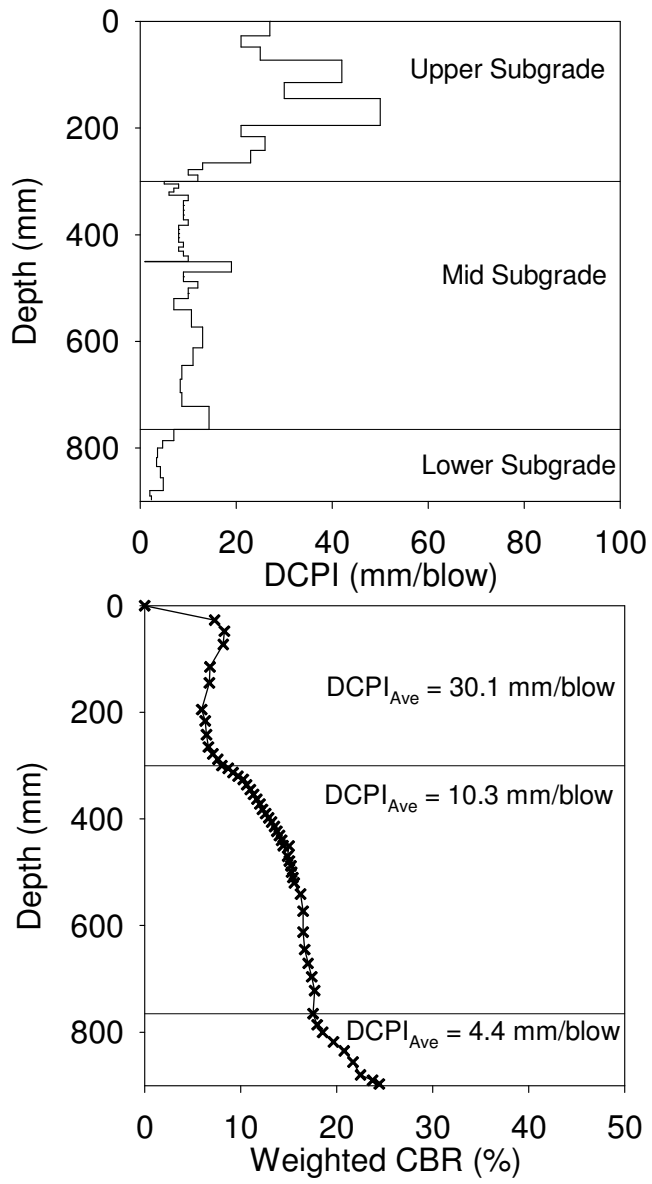
Figure 42. Wisconsin US-10 Test Bed 2 Point A1 DCPI determination for each layer
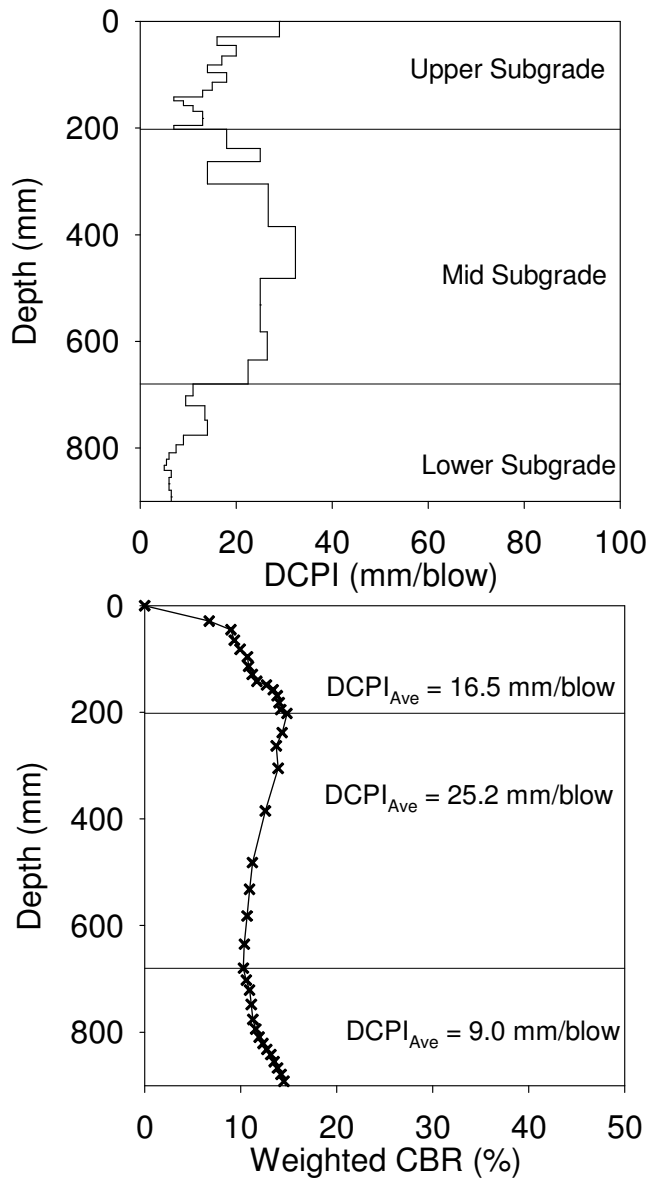
Figure 43. Wisconsin US-10 Test Bed 2 Point A8 DCPI determination for each layer
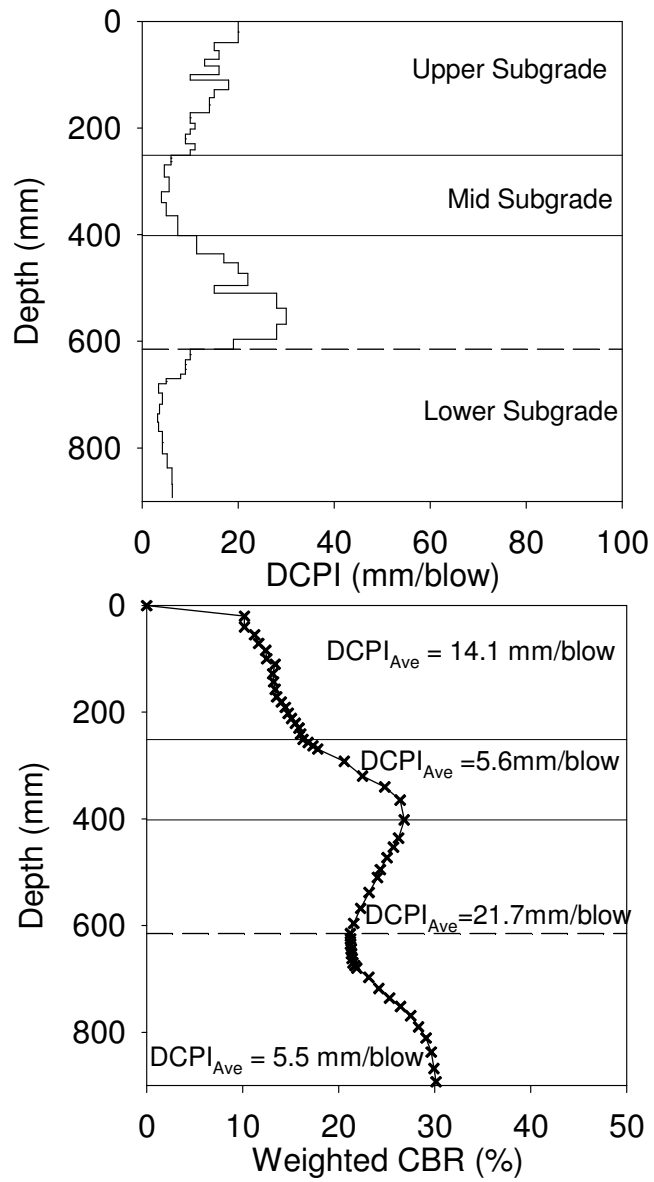
Figure 44. Wisconsin US-10 Test Bed 2 Point B5 DCPI determination for each layer
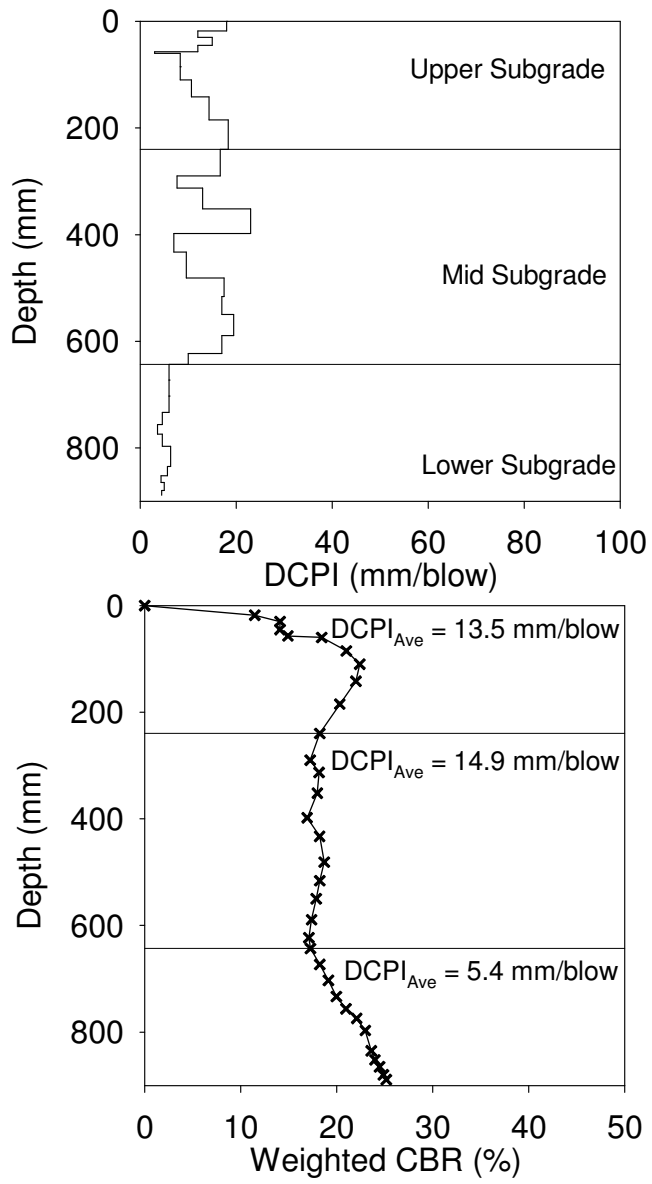
**Figure 45. Wisconsin US-10 Test Bed 2 Point C7 DCPI determination for each layer**
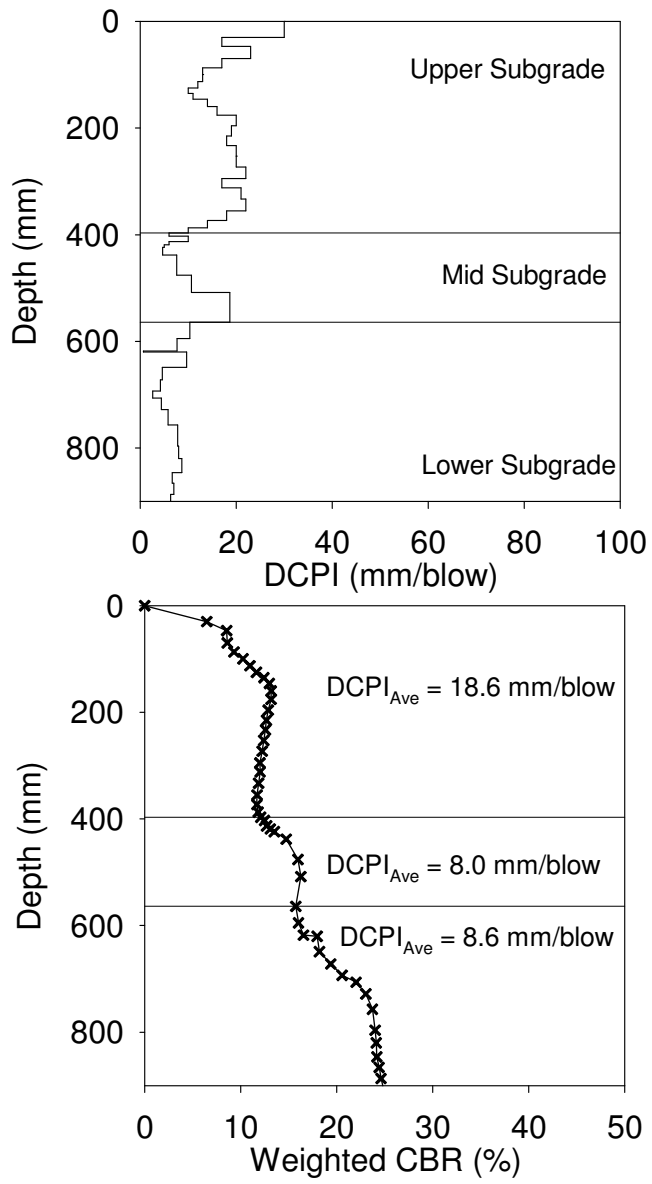
Figure 46. Wisconsin US-10 Test Bed 2 Point D8 DCPI determination for each layer
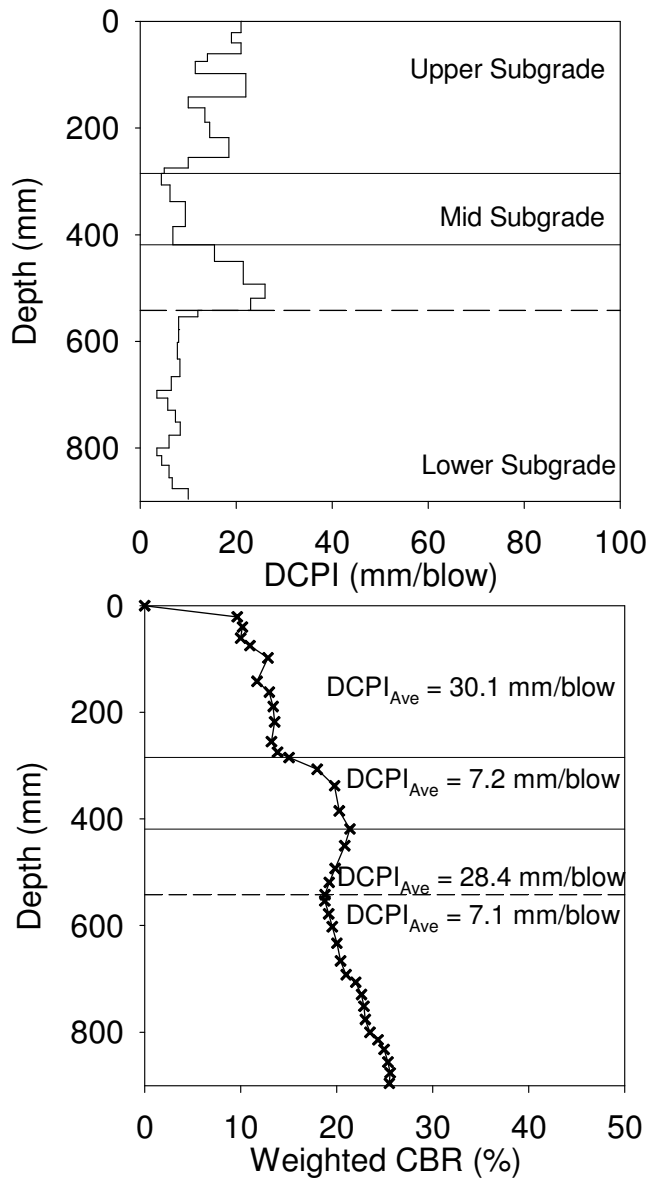
Figure 47. Wisconsin US-10 Test Bed 2 Point D9 DCPI determination for each layer
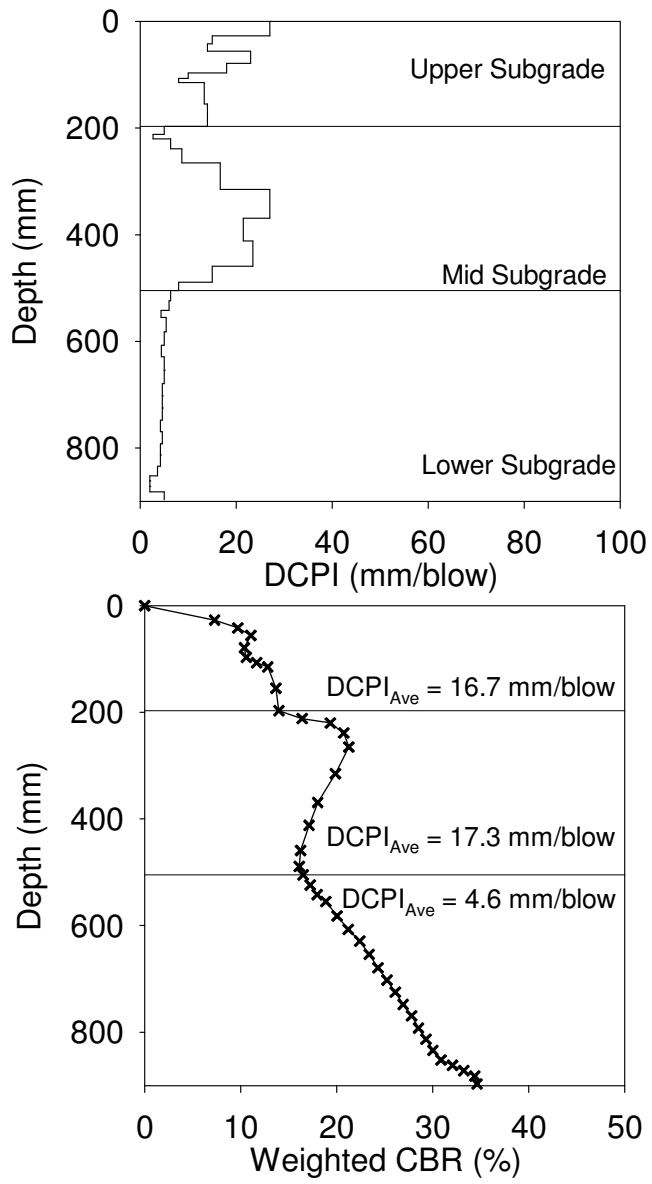
Figure 48. Wisconsin US-10 Test Bed 2 Point D12 DCPI determination for each layer
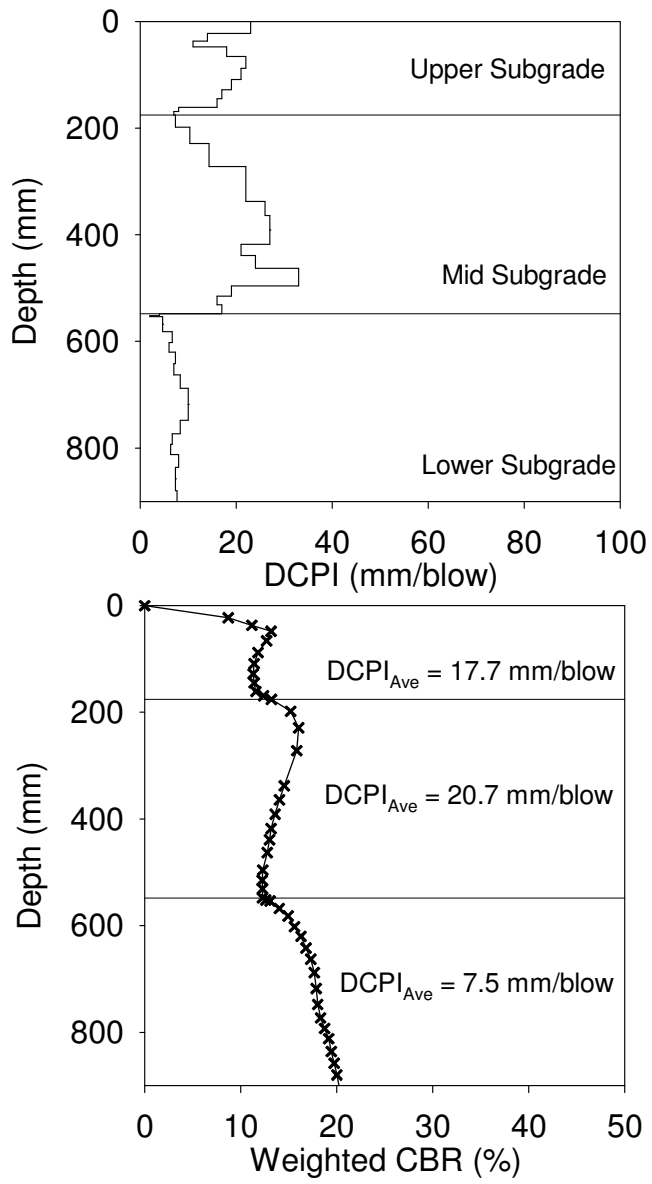
Figure 49. Wisconsin US-10 Test Bed 2 Point E4 DCPI determination for each layer
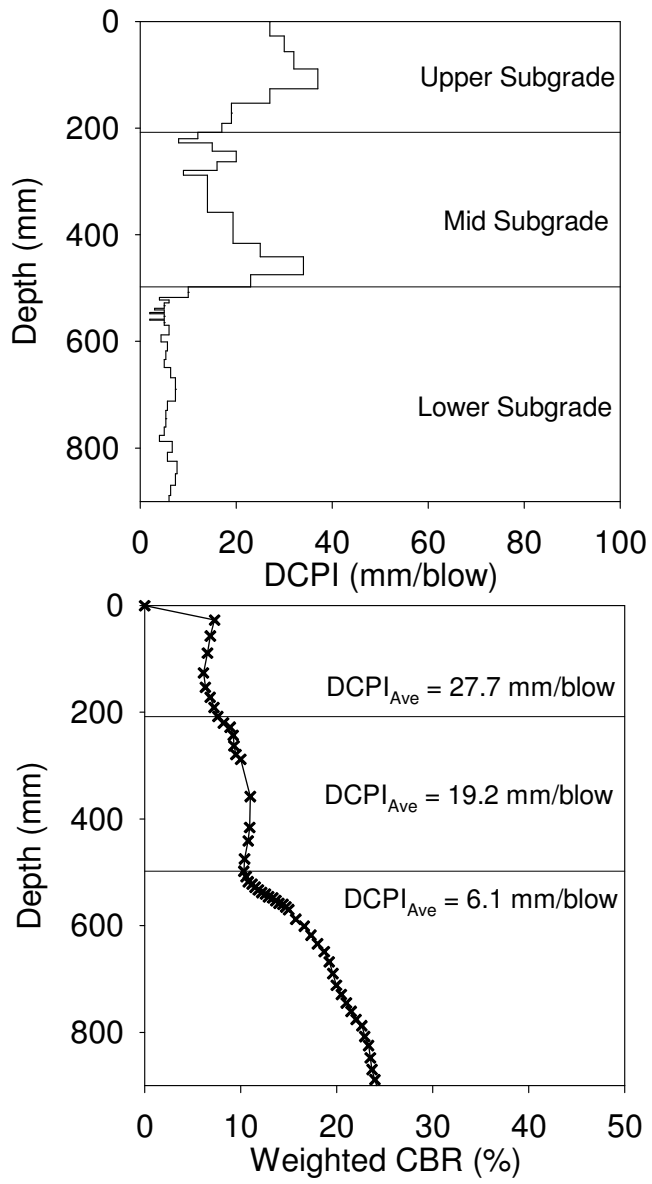
Figure 50. Wisconsin US-10 Test Bed 2 Point E6 DCPI determination for each layer
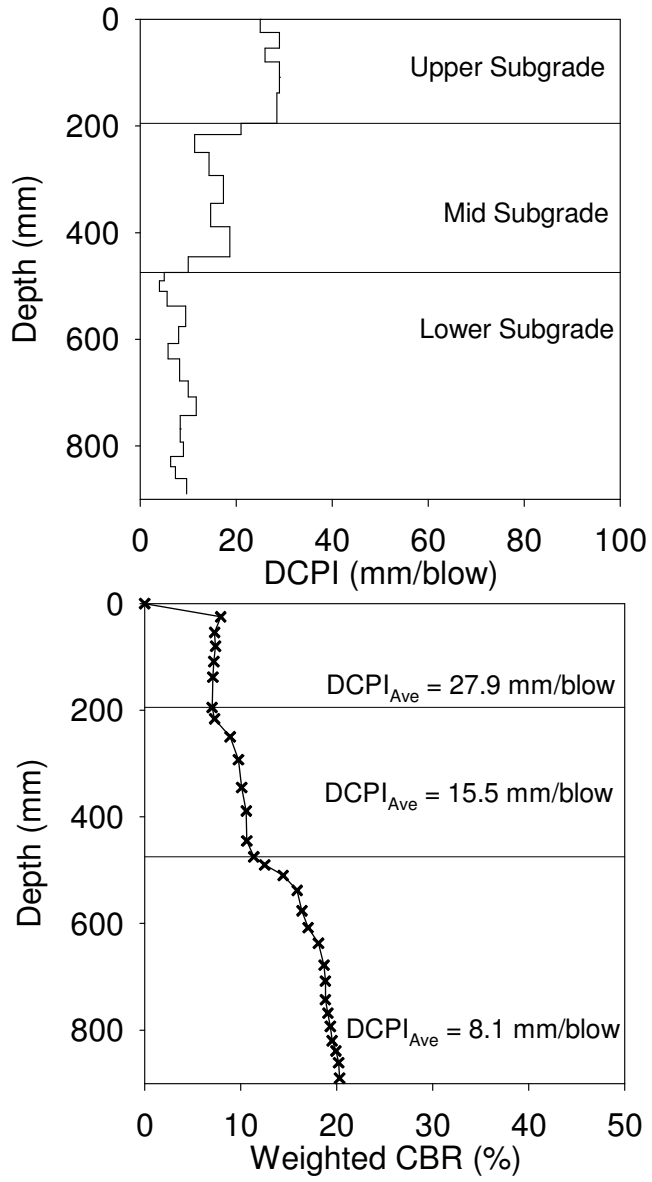
Figure 51. Wisconsin US-10 Test Bed 2 Point F7 DCPI determination for each layer
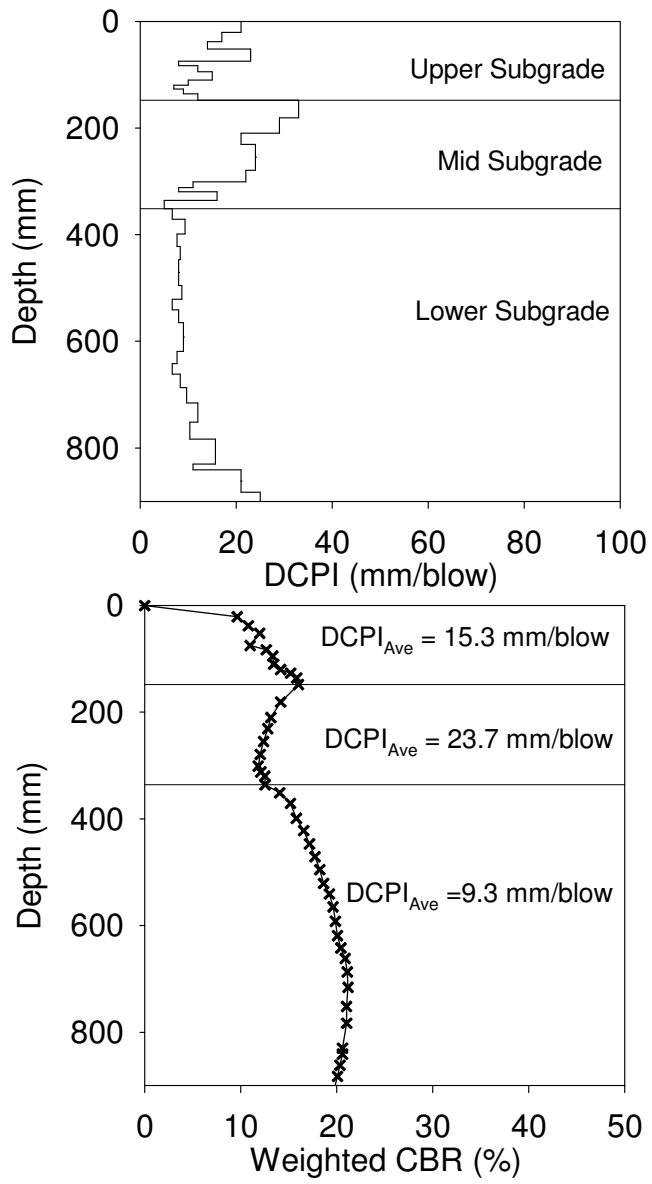
Figure 52. Wisconsin US-10 Test Bed 2 Point G9 DCPI determination for each layer

APPENDIX F. SUMMARY OF RESILIENT MODULUS TEST DATA

The following tables present the sample data for all laboratory tests.

Table 7. Michigan I-94 laboratory moduli data

Site	Project	Description	γ_d (kN/m³)	w (%)	k_1	k_2	k_3	$R^2_{(Adj)}$	$s_{u5\%}$ (kPa)	$s_{u1\%}$ (kPa)	$M_{r(T307)}$ (MPa)	$E^*_{s(T307)}$ (MPa)	$E_{s(T307)}$ (MPa)
MI	I-94	Shelby Tube	16.96	18.1	2277.37	0.60	-0.40	0.284	—	—	241.1	237.5	438.4
MI	I-94	Shelby Tube	17.07	23.4	2678.31	0.02	-1.88	0.474	—	—	195.0	190.0	1077.6
MI	I-94	Shelby Tube	17.09	16.6	996.02	0.64	-9.36	0.832	53.9	28.45	26.7	26.8	1.4
MI	I-94	Shelby Tube	17.17	19.1	1476.89	-0.13	-8.72	0.887	83.35	37.85	41.1	41.1	11.3
MI	I-94	Shelby Tube	16.78	20.5	770.53	0.57	-6.67	0.856	84.85	44.4	29.7	29.8	4.1
MI	I-94	Shelby Tube	16.85	21.4	961.34	0.39	-1.79	0.689	111.3	59.6	75.9	76.1	17.0
MI	I-94	Shelby Tube	16.93	19.0	924.82	0.33	-5.56	0.803	90.35	44.4	40.2	39.6	4.8
MI	I-94	Shelby Tube	16.70	22.2	666.92	0.39	-7.56	0.849	66.45	36.05	22.3	22.3	2.0
MI	I-94	Shelby Tube	17.07	21.4	935.12	-0.09	-1.96	0.638	132.8	63.6	66.9	66.8	21.1
MI	I-94	Shelby Tube	16.54	21.9	1777.32	0.71	-3.78	0.620	122.7	65.8	107.4	108.4	27.8
MI	I-94	Shelby Tube	16.54	21.5	1025.12	-0.07	-5.17	0.743	79.75	42.6	45.1	45.1	5.5
MI	I-94	Shelby Tube	16.82	20.2	825.32	0.20	-2.14	0.543	92.95	53.1	59.6	59.8	14.3
MI	I-94	Shelby Tube	16.65	21.3	944.20	0.27	-1.84	0.526	140.35	66.15	72.3	72.5	14.1
MI	I-94	Shelby Tube	16.45	22.2	1291.84	-0.56	-3.98	0.699	104.35	47.65	66.9	67.5	10.3
MI	I-94	Shelby Tube	16.65	21.0	1401.40	0.30	-3.12	0.603	130.8	73.75	86.6	86.8	60.0
MI	I-94	Subgrade	17.58	18.4	1491.94	0.43	-3.05	0.695	170.05	91.15	96.6	96.5	31.4
MI	I-94	Subgrade	18.30	9.2	1376.80	0.44	-0.11	0.448	533.55	337.65	147.7	146.9	92.0
MI	I-94	Subgrade	18.95	13.8	2287.39	-0.21	-0.61	0.198	540.95	245.1	203.0	202.5	142.7
MI	I-94	TB-2 Sand	16.85	13.8	460.43	1.05	-0.61	0.968	82.85	81.4	121.1	121.0	26.3
MI	I-94	TB-2 Sand	19.28	12.5	655.25	0.80	-0.26	0.978	75.95	75	146.7	146.3	36.5
MI	I-94	TB-3 Base	15.72	0.9	1244.07	0.68	0.15	0.935	262.35	261.25	288.1	288.3	306.0
MI	I-94	TB-3 Base	13.63	0.9	916.27	0.51	0.85	0.955	138.5	121.85	238.6	237.5	54.1
MI	I-94	TB-3 Base	16.45	1.3	852.44	0.78	0.06	0.979	146.15	118.1	214.7	214.4	73.6
MI	I-94	TB-3 Base	17.93	1.4	1564.65	0.78	-0.69	0.845	216.8	196.9	281.1	281.5	214.4
MI	I-94	TB-3 Base BS	16.21	4.7	555.08	0.95	-0.20	0.978	220.4	202.85	154.9	154.7	128.3
MI	I-94	Base/ Subgrade	16.65 17.37	1.8 15.6	1084.62	0.43	-0.78	0.76	179.1	154.1	125.8	126.0	37.5

BS = Back saturated sample; $s_{u5\%}$ = undrained shear strength at failure or 5% vertical strain; $s_{u1\%}$ = undrained shear strength at 1% vertical strain

Table 8. Michigan I-96 laboratory moduli data

Site	Project	Description	γ_d (kN/m³)	w (%)	k_1	k_2	k_3	$R^2_{(Adj)}$	$s_{u5\%}$ (kPa)	$s_{u1\%}$ (kPa)	$M_{r(T307)}$ (MPa)	$E^*_{s(T307)}$ (MPa)	$E_{s(T307)}$ (MPa)
MI	I-96	Subgrade	19.54	12.7	240.68	0.06	1.79	0.579	—	—	32.6	32.0	0.4
MI	I-96	Subgrade	19.91	11.0	251.93	0.09	2.23	0.764	104.5	55.2	36.6	36.2	0.9
MI	I-96	Subgrade	20.15	7.6	1206.94	0.26	-1.32	0.296	231.65	160	101.2	101.2	45.3
MI	I-96	Subgrade	19.38	6.8	1194.76	0.40	-1.99	0.212	173.15	141.6	91.2	90.7	35.5
MI	I-96	Subgrade	19.45	9.7	543.85	0.49	-0.45	0.710	98.85	82.95	54.9	54.9	9.5
MI	I-96	Subgrade	19.84	8.9	1001.80	0.57	-2.37	0.766	140.4	106.4	75.0	75.1	13.0
MI	I-96	Shelby Tube	18.03	17.2	633.46	0.33	-5.69	0.752	77.15	42.75	29.1	28.8	1.4
MI	I-96	Shelby Tube	18.52	16.2	734.01	-0.01	-5.54	0.771	89.75	39.35	33.1	33.0	1.8
MI	I-96	Sand Subbase	19.18	7.1	607.86	0.65	0.25	0.958	105	101.4	141.9	141.3	51.1
MI	I-96	Sand Subbase	20.92	4.4	989.98	0.87	-0.34	0.927	210.3	208.5	232.6	232.5	200.1
MI	I-96	Sand Subbase	20.02	7.8	554.51	1.11	-0.84	0.924	99.1	97.25	143.3	142.2	12.1
MI	I-96	Sand Subbase	20.63	7.3	532.19	1.04	-0.48	0.982	125.15	125.65	146.9	146.8	41.8
MI	I-96	Sand Subbase	19.96	6.2	827.38	0.51	0.71	0.925	138.3	137.4	200.5	200.3	157.6
MI	I-96	Sand/ Subgrade	19.98 19.78	6.1 9.0	690.29	0.86	-0.32	0.909	129.6	126	163.5	163.2	50.8
MI	I-96	Sand/Geo/ Subgrade	19.19 19.69	6.1 9.0	610.58	0.76	-0.22	0.989	190.4	172.5	131.7	131.6	65.9

$s_{u5\%}$ = undrained shear strength at failure or 5% vertical strain; $s_{u1\%}$ = undrained shear strength at 1% vertical strain

Table 9. Pennsylvania US-22 laboratory moduli data

Site	Project	Description	γ_d (kN/m³)	w (%)	k_1	k_2	k_3	$R^2_{(Adj)}$	$s_{u5\%}$ (kPa)	$s_{u1\%}$ (kPa)	$M_{r(T307)}$ (MPa)	$E^*_{s(T307)}$ (MPa)	$E_{s(T307)}$ (MPa)
PA	US-22	2A Subbase	21.44	7.3	898.80	0.80	-0.28	0.948	—	—	198.4	198.0	111.8
PA	US-22	2A Subbase BS	21.48	6.4	892.19	0.58	0.32	0.942	217.3	174.45	196.2	196.0	130.3
PA	US-22	2A BS-Closed	21.52	6.9	862.50	0.63	-0.09	0.963	295.6	150.75	168.3	167.9	56.0
PA	US-22	CTB/Geo/2A	22.07	5.5	748.66	0.91	-0.04	0.919	346.05	259.75	213.8	213.6	119.9
PA	US-22	ATB/2A	21.39	6.3	1224.92	0.73	-0.01	0.877	272.1	229.4	281.8	281.4	158.7
PA	US-22	CTB/2A	21.58	5.7	1117.65	0.68	0.27	0.919	639.1	473.1	272.0	271.5	168.2
PA	US-22	CTB/2A	21.58	6.1	908.92	0.78	0.00	0.974	318.05	253.5	224.0	224.1	187.2
PA	US-22	CTB/2A	21.55	6.2	1601.19	0.36	0.55	0.868	460.95	379.05	302.2	300.9	281.6
PA	US-22	2A/Subgrade	22.14 / 17.77	5.9 / 15.1	1040.66	0.47	-0.83	0.648	149.55	124.15	123.4	122.9	15.1
PA	US-22	2A/Subgrade BS	22.03 / 17.30	7.5 / 20.7	632.53	0.15	-2.73	0.603	58.5	41.85	42.5	42.0	0.6
PA	US-22	2A/Geo/Subgrade	22.00 / 17.09	7.4 / 20.1	445.54	0.81	-1.15	0.616	—	—	60.1	58.7	1.6
PA	US-22	2A/Geo/Subgrade BS	22.22 / 17.36	6.9 / 20.1	628.86	0.04	-3.00	0.291	58.5	41.85	40.2	39.7	0.5
PA	US-22	TB2 Natural	17.55	21.6	618.14	-0.07	-6.21	0.643	NA	NA	28.4	28.1	0.5
PA	US-22	TB2 Natural	17.42	20.1	727.79	0.21	-7.02	0.752	118.1	53.55	30.8	30.8	6.7
PA	US-22	TB2 Natural	17.10	18.6	626.85	0.52	-3.27	0.766	75.5	55.55	40.5	40.3	4.0
PA	US-22	TB2 Natural	18.00	15.9	986.48	0.66	-6.52	0.726	96.85	54.55	41.6	41.5	2.7
PA	US-22	Subgrade	18.30	16.4	1390.00	0.20	-4.98	0.703	115.2	55.55	68.3	68.0	6.2
PA	US-22	Subgrade	18.33	18.6	396.47	0.00	-3.39	0.429	77.55	44.7	23.8	23.7	1.1
PA	US-22	Subgrade	17.88	16.3	788.64	0.06	0.92	0.135	186.7	111.75	93.8	93.8	47.1
PA	US-22	Subgrade	18.08	16.5	450.59	-0.28	-4.14	0.383	64.4	39.9	24.3	24.2	0.7
PA	US-22	Subgrade	18.41	15.3	963.32	0.62	-2.20	0.583	171.4	80.65	73.8	73.8	11.5
PA	US-22	Subgrade BS	17.72	19.2	583.23	0.04	-5.14	0.653	58.7	38.75	27.6	27.6	0.8

BS = Back saturated sample; $s_{u5\%}$ = undrained shear strength at failure or 5% vertical strain; $s_{u1\%}$ = undrained shear strength at 1% vertical strain

Table 10. Pennsylvania US-22 laboratory moduli data (con't)

Site	Project	Description	γ_d (kN/m³)	w (%)	k_1	k_2	k_3	$R^2_{(Adj)}$	$s_{u5\%}$ (kPa)	$s_{u1\%}$ (kPa)	$M_{r(T307)}$ (MPa)	$E^*_{s(T307)}$ (MPa)	$E_{s(T307)}$ (MPa)
PA	US-22	Cement Subgrade	17.71	17.7	3781.75	1.05	-2.88	0.247	712.71	648.85	284.2	294.5	57.4
PA	US-22	2A/Cement Subgrade #1	21.43 / 17.46	5.4 / 18.0	1319.77	0.35	0.55	0.748	369.2	257.8	247.6	247.3	201.3
PA	US-22	2A/Cement Subgrade #2	21.27 / 17.66	5.4 / 17.3	1488.41	0.55	-0.12	0.848	355.4	253.5	262.0	262.7	183.8

$s_{u5\%}$ = undrained shear strength at failure or 5% vertical strain; $s_{u1\%}$ = undrained shear strength at 1% vertical strain

Table 11. Pennsylvania US-422 laboratory moduli data

Site	Project	Description	γ_d (kN/m³)	w (%)	k_1	k_2	k_3	$R^2_{(Adj)}$	$s_{u5\%}$ (kPa)	$s_{u1\%}$ (kPa)	$M_{r(T307)}$ (MPa)	$E^*_{s(T307)}$ (MPa)	$E_{s(T307)}$ (MPa)
PA	US-422	Foam Sample	1.44	—	287.07	0.20	-0.21	0.947	502.75	69.3	32.8	32.8	39.0
PA	US-422	Foam+OGS	14.92	—	773.06	0.61	0.12	0.946	685.15	289.05	162.8	162.8	154.8
PA	US-422	OGS	18.54	0.2	968.40	0.84	-0.35	0.958	201.85	159.3	219.1	219.2	143.8

$s_{u5\%}$ = undrained shear strength at failure or 5% vertical strain; $s_{u1\%}$ = undrained shear strength at 1% vertical strain

286

Table 12. Iowa I-29 laboratory moduli data

Site	Project	Description	γ_d (kN/m³)	w (%)	k_1	k_2	k_3	$R^2_{(Adj)}$	$s_{u5\%}$ (kPa)	$s_{u1\%}$ (kPa)	$M_{r(T307)}$ (MPa)	$E^*_{s(T307)}$ (MPa)	$E_{s(T307)}$ (MPa)
IA	I-29	Subgrade	17.90	15.3	771.96	0.71	-3.03	0.698	210.6	50.05	53.6	53.5	7.0
IA	I-29	Subgrade	16.57	19.0	102.71	0.05	1.67	0.651	—	—	14.1	14.1	0.7
IA	I-29	Subgrade	17.69	16.7	220.32	0.52	-1.73	0.439	123.5	41.95	18.2	18.2	1.8
IA	I-29	Select Backfill	20.61	3.9	863.61	0.86	-0.25	0.852	161.45	159.8	212.2	211.7	148.0
IA	I-29	Select Backfill	21.87	3.6	1612.60	0.60	-0.20	0.826	336.95	330.85	289.1	288.8	221.8
IA	I-29	Select Backfill	21.89	9.9	675.42	0.96	-0.35	0.960	—	—	182.0	181.9	81.3
IA	I-29	Select Backfill	22.49	7.0	1040.43	1.05	-0.67	0.822	219.85	211.45	271.8	271.0	120.5
IA	I-29	Select Backfill	20.75	4.3	947.20	0.80	-0.32	0.974	209.4	198.7	206.8	206.6	182.0
IA	I-29	Select Backfill	20.86	3.7	1022.11	0.79	-0.08	0.868	232.85	214.05	243.6	242.9	152.7
IA	I-29	Select Backfill	21.98	7.1	959.41	0.76	-0.16	0.840	209.3	206.15	211.1	211.1	136.6
IA	I-29	Select Backfill	22.04	6.8	698.40	0.98	-0.16	0.947	216.3	215.05	206.2	206.4	111.7
IA	I-29	RPCC	15.86	5.3	1148.64	0.61	0.09	0.916	236.25	175	246.7	246.6	164.5
IA	I-29	RPCC	16.85	8.0	830.79	0.93	-0.10	0.951	292.7	229.4	238.4	238.2	92.5
IA	I-29	RPCC	16.85	5.2	1090.27	0.91	-0.30	0.907	297.35	256.4	274.4	274.8	197.2
IA	I-29	RPCC	17.00	5.0	912.97	0.57	0.83	0.879	303.3	305.3	251.1	250.9	257.3
IA	I-29	RPCC	16.66	10.2	1044.60	0.92	-0.22	0.919	428.05	428.25	274.9	274.3	262.0
IA	I-29	RPCC BS	16.81	13.2	1451.77	0.57	-0.36	0.634	159	159.6	234.8	234.2	169.9

BS = Back saturated sample; $s_{u5\%}$ = undrained shear strength at failure or 5% vertical strain; $s_{u1\%}$ = undrained shear strength at 1% vertical strain

Table 13. Iowa I-29 laboratory moduli data (con't)

Site	Project	Description	γ_d (kN/m³)	w (%)	k_1	k_2	k_3	$R^2_{(Adj)}$	$s_{u5\%}$ (kPa)	$s_{u1\%}$ (kPa)	$M_{r(T307)}$ (MPa)	$E^*_{s(T307)}$ (MPa)	$E_{s(T307)}$ (MPa)
IA	I-29	RAP	17.80	0.5	1355.23	0.72	-0.16	0.846	152.45	112.6	281.9	279.7	57.4
IA	I-29	RAP	20.07	0.5	1325.61	0.58	0.28	0.851	248.8	217.45	286.8	286.8	149.3
IA	I-29	RAP	17.34	7.0	1218.85	0.59	-0.10	0.942	103.4	94.5	226.0	223.6	31.7
IA	I-29	RAP	19.82	7.0	1413.83	0.73	-0.03	0.966	260.25	248.2	327.4	326.4	201.9
IA	I-29	RAP	17.34	9.8	1472.30	0.70	-0.41	0.874	140.1	125.15	270.3	269.6	83.5
IA	I-29	RAP	19.33	9.8	1608.26	0.89	-0.48	0.833	185.05	160.8	363.4	362.6	106.9
IA	I-29	Existing Sand Subbase	18.83	6.4	824.99	0.68	-0.26	0.970	91.9	91	163.2	162.7	35.4
IA	I-29	Existing Sand Subbase	19.82	6.4	839.28	0.55	0.17	0.957	111.15	110.55	167.0	166.8	83.5
IA	I-29	Existing Sand Subbase	17.84	0.0	1047.12	0.56	-0.04	0.847	136.5	128.95	192.6	192.3	87.2
IA	I-29	Existing Sand Subbase	19.33	0.0	936.43	0.68	0.03	0.988	191.45	187.7	205.4	205.4	145.6
IA	I-29	Existing Sand Subbase	21.00	9.4	511.88	1.03	-0.35	0.936	133.7	134.05	149.0	148.6	40.1
IA	I-29	Existing Sand Subbase	21.54	8.4	592.90	0.94	-0.21	0.952	140.45	141.5	163.2	162.8	51.5
IA	I-29	RPCC/ Select Backfill	16.90 / 20.41	5.8 / 4.9	1148.57	0.49	0.44	0.933	263.95	262.1	239.0	238.6	228.4
IA	I-29	RPCC/ Select Backfill	15.67 / 21.35	5.7 / 5.2	947.65	0.51	0.66	0.977	196.25	180.05	223.6	223.0	140.4
IA	I-29	RPCC/ Select Backfill	15.73 / 20.41	5.3 / 5.0	1087.97	0.69	-0.10	0.951	160.85	154.3	229.6	229.7	172.6
IA	I-29	RPCC/ Select Backfill	16.92 / 21.41	5.7 / 4.9	840.16	0.44	0.90	0.943	245.65	214.4	202.7	202.8	233.4

$s_{u5\%}$=undrained shear strength at failure or 5% vertical strain; $s_{u1\%}$=undrained shear strength at 1% vertical strain

Table 14. Iowa I-29 laboratory moduli data (con't)

Site	Project	Description	γ_d (kN/m³)	w (%)	k_1	k_2	k_3	$R^2_{(Adj)}$	$s_{u5\%}$ (kPa)	$s_{u1\%}$ (kPa)	$M_{r(T307)}$ (MPa)	$E^*_{s(T307)}$ (MPa)	$E_{s(T307)}$ (MPa)
IA	I-29	RPCC/RAP	16.93 / 19.94	4.9 / 7.3	1328.24	0.72	-0.07	0.906	244.3	214.4	292.9	292.5	226.6
IA	I-29	RPCC/RAP	15.75 / 19.86	4.5 / 7.7	1083.03	0.71	-0.04	0.910	175.15	140.7	239.5	239.1	123.6
IA	I-29	RPCC/RAP	15.67 / 18.12	5.0 / 6.3	1110.86	0.72	-0.31	0.884	143.25	122.3	219.9	219.2	83.7
IA	I-29	RPCC/RAP	16.93 / 18.29	4.9 / 5.3	1057.72	0.54	0.30	0.949	171.25	158.3	220.6	220.2	144.0
IA	I-29	Select Backfill/ Subgrade	21.13 / 17.39	8.1 / 16.3	453.29	0.81	-0.45	0.969	106.55	100.5	95.0	94.9	22.2
IA	I-29	RAP/ Subgrade	18.82 / 17.29	8.3 / 16.6	697.90	0.65	-0.38	0.937	114.0	111.0	124.2	123.7	31.9
IA	I-29	Sand/ Subgrade	20.46 / 16.95	6.6 / 16.5	571.42	0.68	-0.34	0.975	117.4	112.3	106.2	106.1	46.5
IA	I-29	Sand/ Subgrade	21.85 / 16.80	5.7 / 19.1	267.79	0.86	-0.23	0.995	NA	NA	64.8	64.0	5.4
IA	I-29	FA Subgrade	17.41	17.3	854.95	0.46	1.55	0.621	838.8	245.1	125.3	125.2	46.1
IA	I-29	RPCC/FA Subgrade #1	16.29 / 17.10	8.2 / 17.5	1108.43	0.41	0.20	0.878	241.1	226.1	166.7	166.7	87.9
IA	I-29	RPCC/FA Subgrade #2	16.29 / 17.07	8.2 / 17.6	886.40	0.54	0.07	0.912	234.2	208.6	190.1	189.4	104.2

$s_{u5\%}$=undrained shear strength at failure or 5% vertical strain; $s_{u1\%}$=undrained shear strength at 1% vertical strain; FA=fly ash treated subgrade

Table 15. Wisconsin US-10 laboratory moduli data

Site	Project	Description	γ_d (kN/m³)	w (%)	k_1	k_2	k_3	$R^2_{(Adj)}$	$s_{u5\%}$ (kPa)	$s_{u1\%}$ (kPa)	$M_{r(T307)}$ (MPa)	$E^*_{s(T307)}$ (MPa)	$E_{s(T307)}$ (MPa)
WI	US-10	Subgrade	19.34	7.0	769.46	0.15	-2.09	0.745	117.3	64.55	55.8	55.8	10.0
WI	US-10	Subgrade	19.34	14.1	769.46	0.15	-2.09	0.745	117.3	64.55	55.8	55.8	10.0
WI	US-10	Subgrade	20.63	6.9	1835.49	0.49	-1.63	0.486	546.05	370.65	150.8	150.5	261.9
WI	US-10	Subgrade	19.06	15.5	1068.68	0.18	-4.37	0.751	102.65	60.6	56.8	56.8	7.2
WI	US-10	Subgrade	20.21	12.1	1400.77	0.19	-1.37	0.113	311.6	163.5	115.5	115.4	63.7
WI	US-10	Subbase Sand	15.72	3.2	655.50	0.79	-0.35	0.944	NA	NA	139.0	137.5	9.7
WI	US-10	Subbase Sand	17.15	11.6	686.10	0.92	-0.34	0.993	75.05	75.1	172.7	172.7	91.9
WI	US-10	Subbase Sand	17.26	2.7	797.33	0.52	0.28	0.881	76.95	77.2	171.1	164.6	110.5
WI	US-10	Subbase Sand	17.25	6.2	1057.42	0.61	-0.32	0.919	74.05	74.35	183.3	183.3	149.2
WI	US-10	Subbase Sand	17.81	10.4	1083.58	0.70	-0.44	0.934	83.65	83.45	198.3	197.9	147.7
WI	US-10	Sand/Geo/ Subgrade	17.04 19.60	8.3 11.2	750.95	0.63	-0.70	0.934	108.28	106.75	112.9	113.0	49.5
WI	US-10	Sand/ Subgrade	17.04 19.60	8.2 11.3	873.14	0.54	-0.68	0.959	96.25	94.15	119.8	119.7	47.3

$s_{u5\%}$ = undrained shear strength at failure or 5% vertical strain; $s_{u1\%}$ = undrained shear strength at 1% vertical strain

APPENDIX G. RESILIENT MODULUS TEST ANALYSIS

RESILIENT MODULUS VERSUS BULK STRESS

Granular (i.e., base and subbase materials) and composite samples are summarized in the following figures using resilient modulus versus bulk stress graphs.
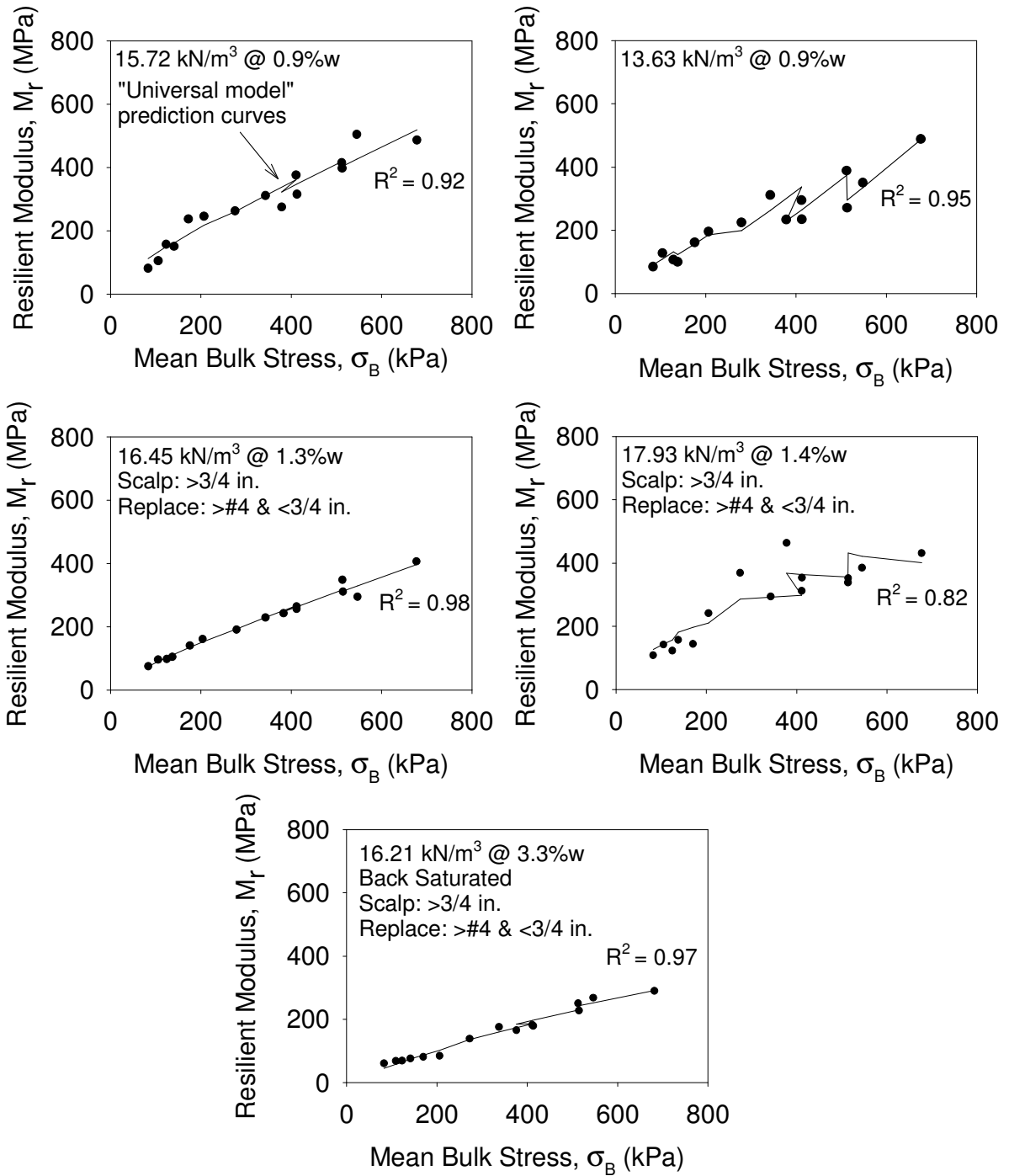
Figure 53. Summary of σ_B and M_r for Michigan I-94 untrimmed base samples
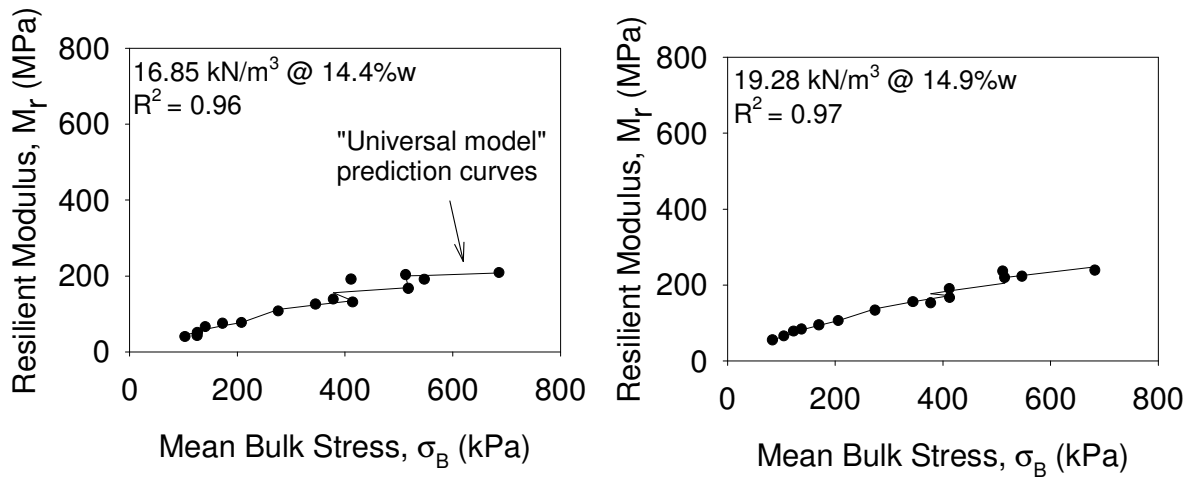
Figure 54. Summary of σ_B and M_r for Michigan I-94 existing sand subbase samples
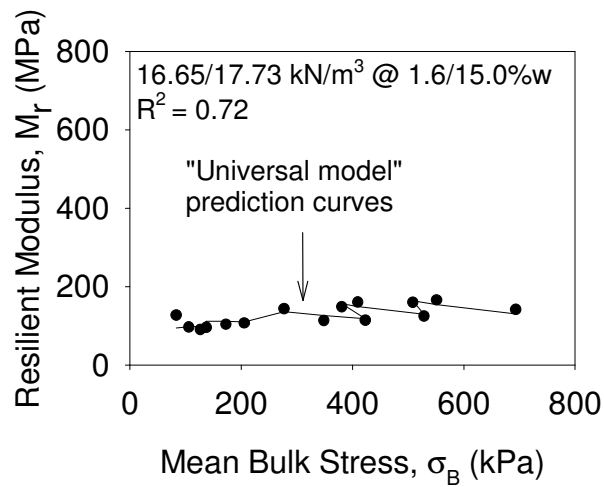
Figure 55. Summary of σ_B and M_r for Michigan I-94 untrimmed base over subgrade
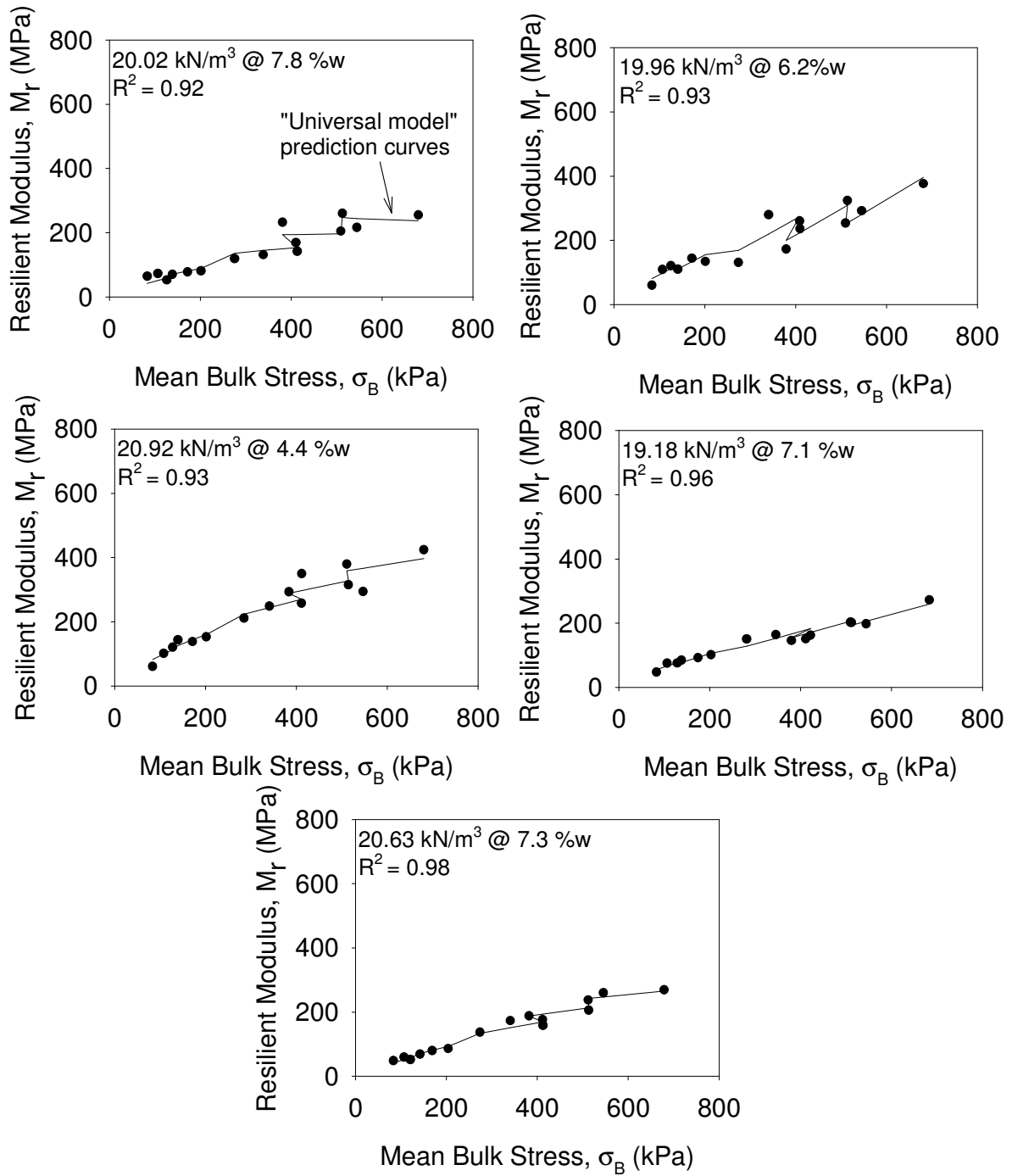
composite sample

Figure 56. Summary of σ_B and M_r for Michigan I-96 sand subbase samples
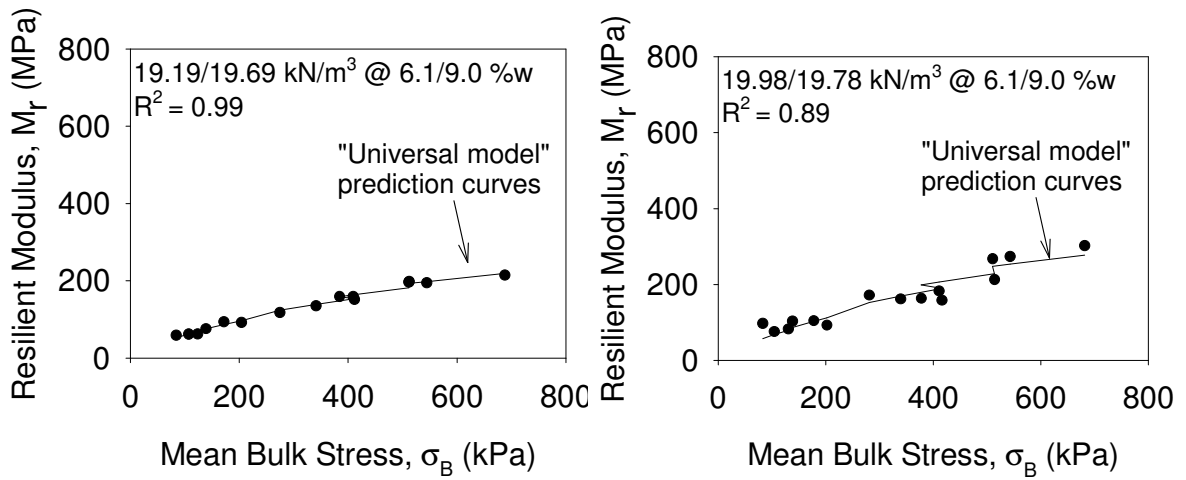
Figure 57. Summary of σ_B and M_r for Michigan I-96 sand subbase over subgrade composite sample with (left) and without geosynthetic (right)
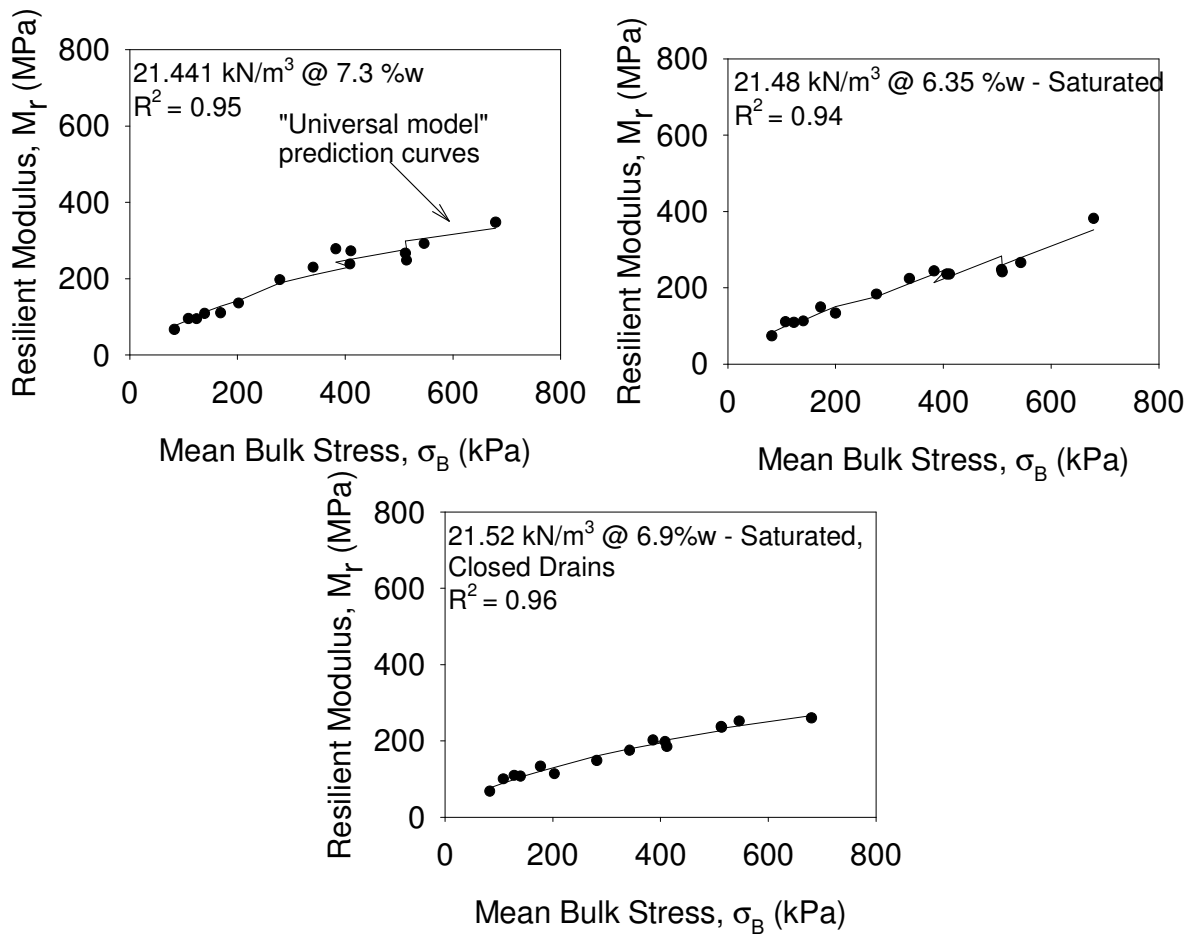
Figure 58. Summary of σ_B and M_r for Pennsylvania US-22 saturated and partially saturated Class 2A subbase material samples
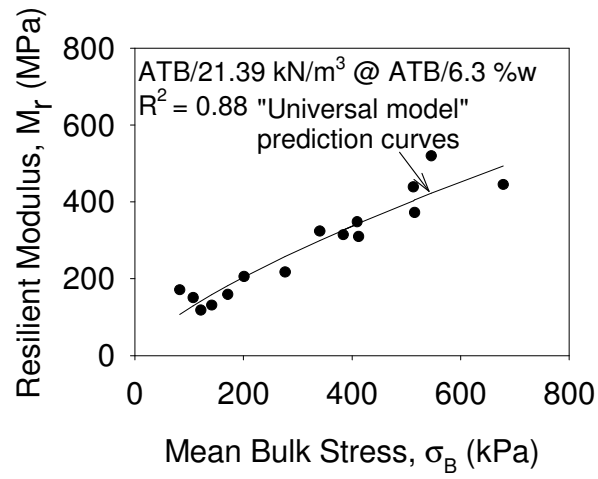
Figure 59. Summary of σ_B and M_r for Pennsylvania US-22 ATB over Class 2A subbase

material composite sample
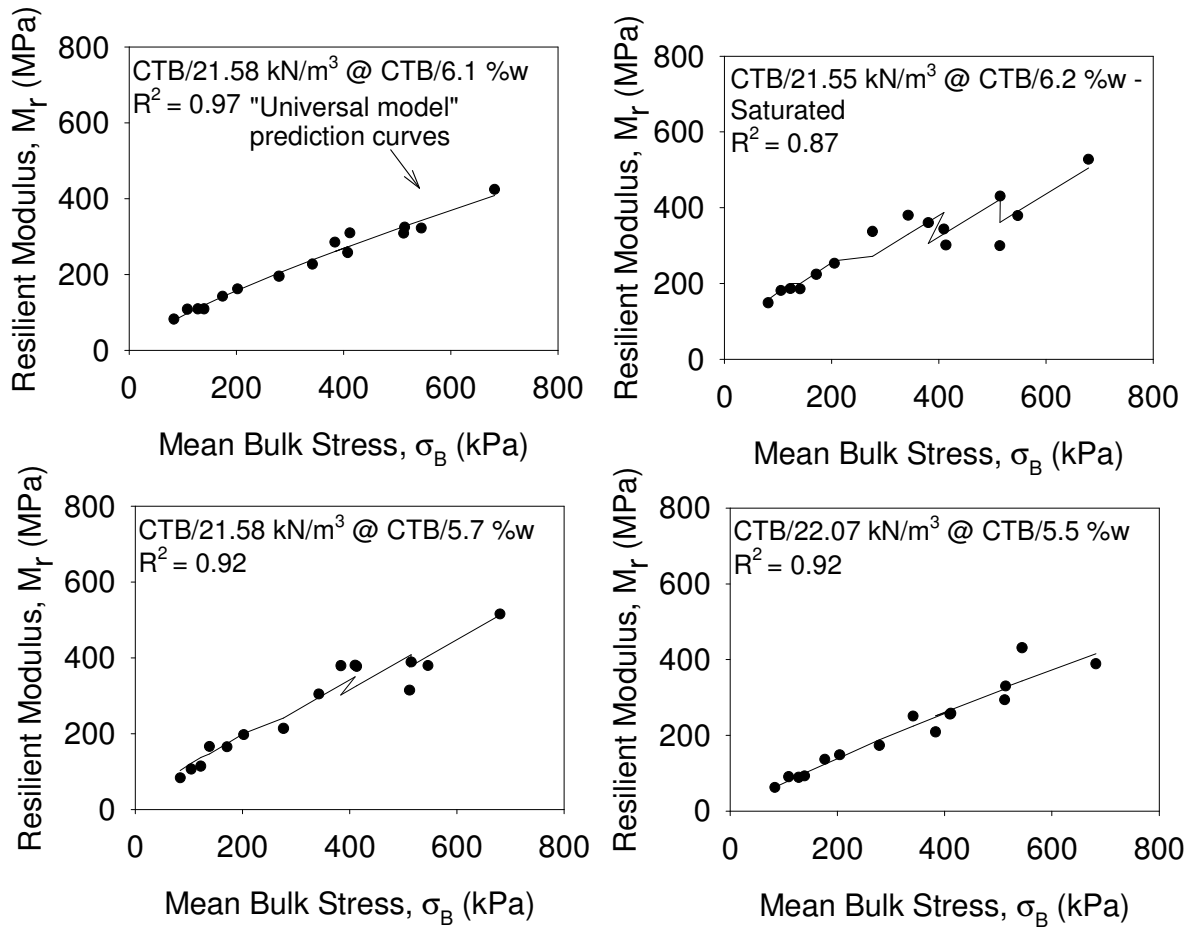
Figure 60. Summary of σ_B and M_r for Pennsylvania US-22 saturated and partially saturated CTB over Class 2A subbase material composite samples
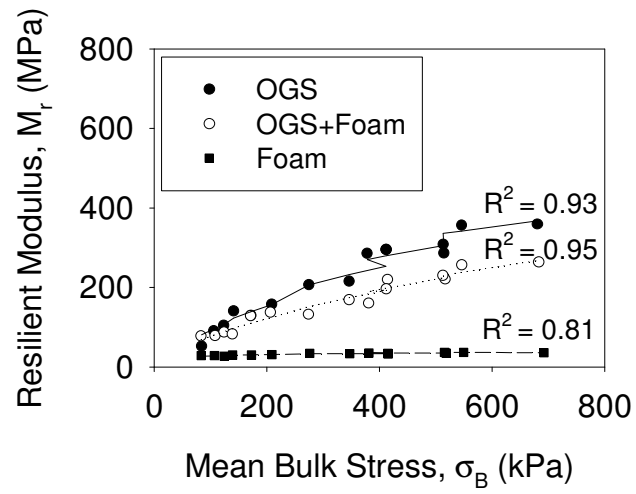
Figure 61. Summary of σ_B and M_r for Pennsylvania US-422 samples
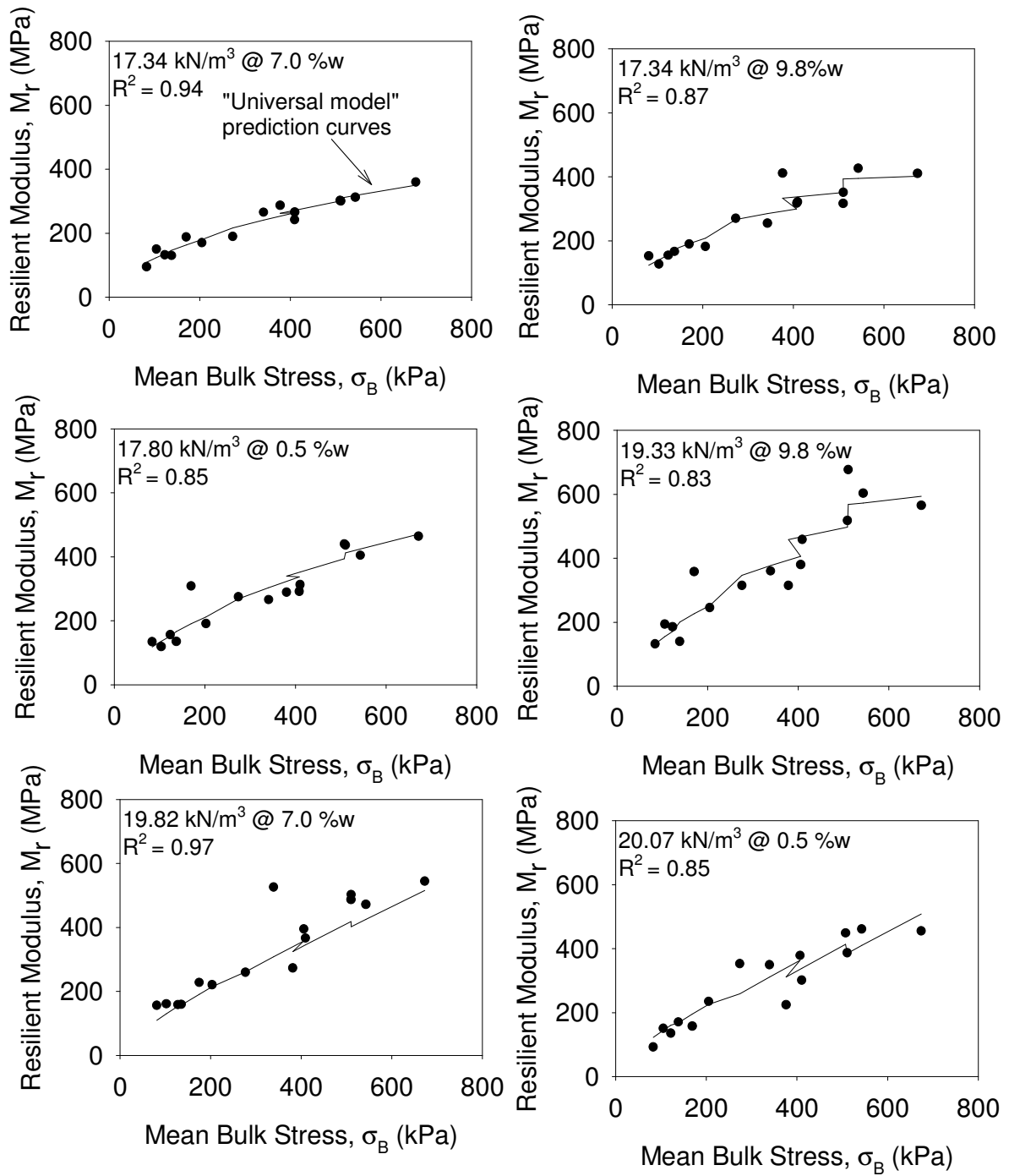
Figure 62. Summary of σ_B and M_r for Iowa I-29 RAP subbase samples
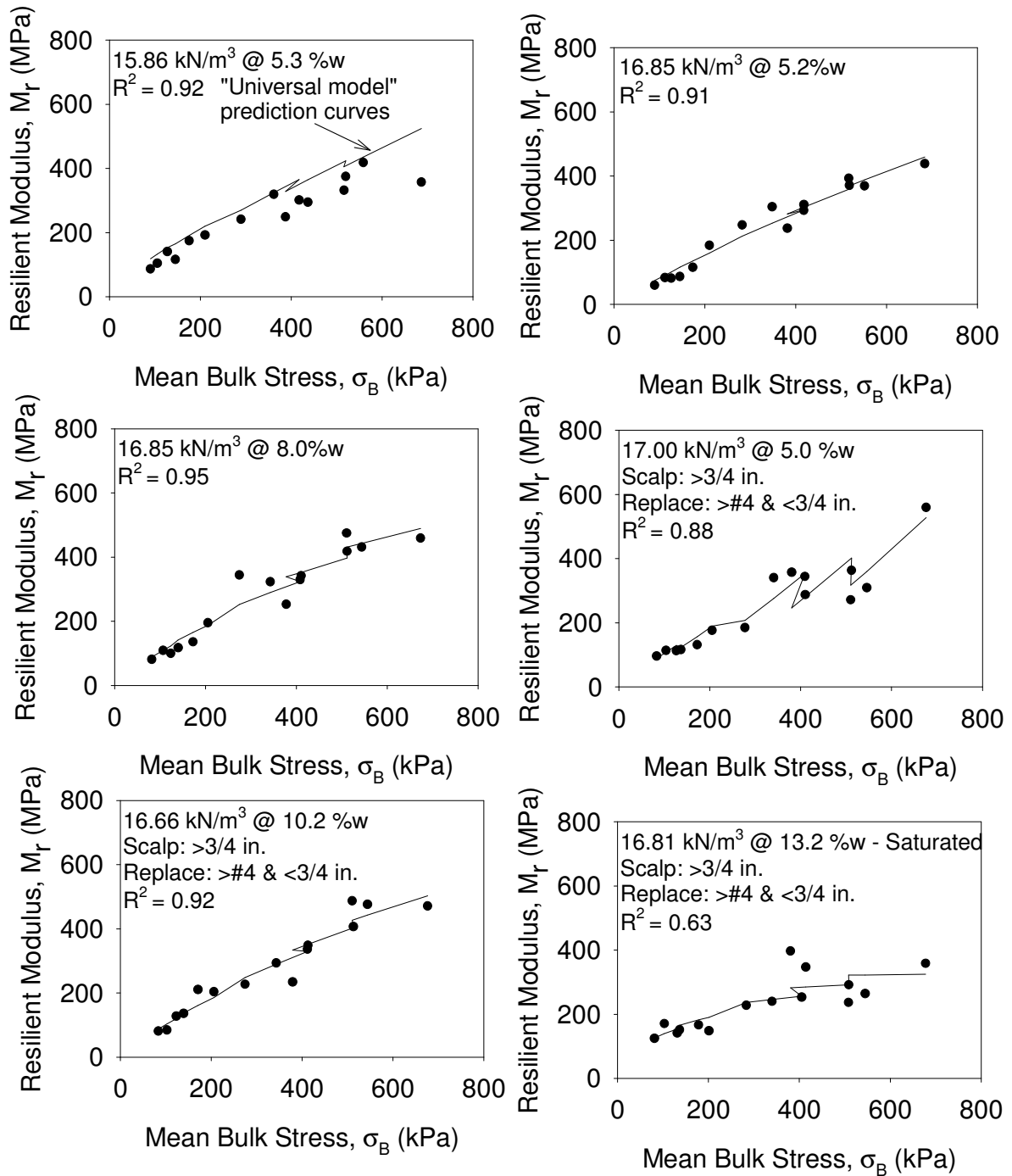
Figure 63. Summary of σ_B and M_r for Iowa I-29 RPCC base samples
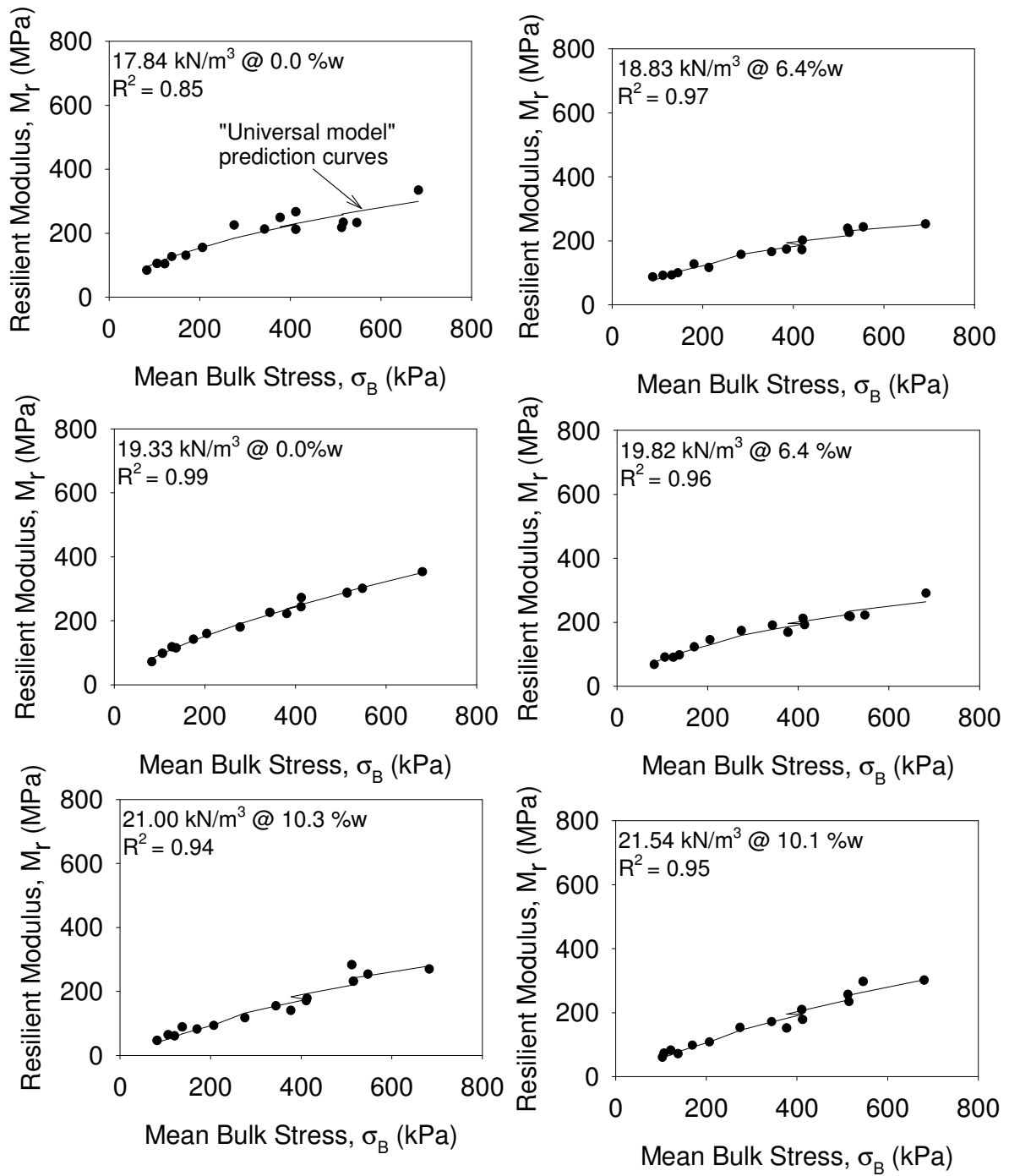
Figure 64. Summary of σ_B and M_r for Iowa I-29 existing sand subbase samples
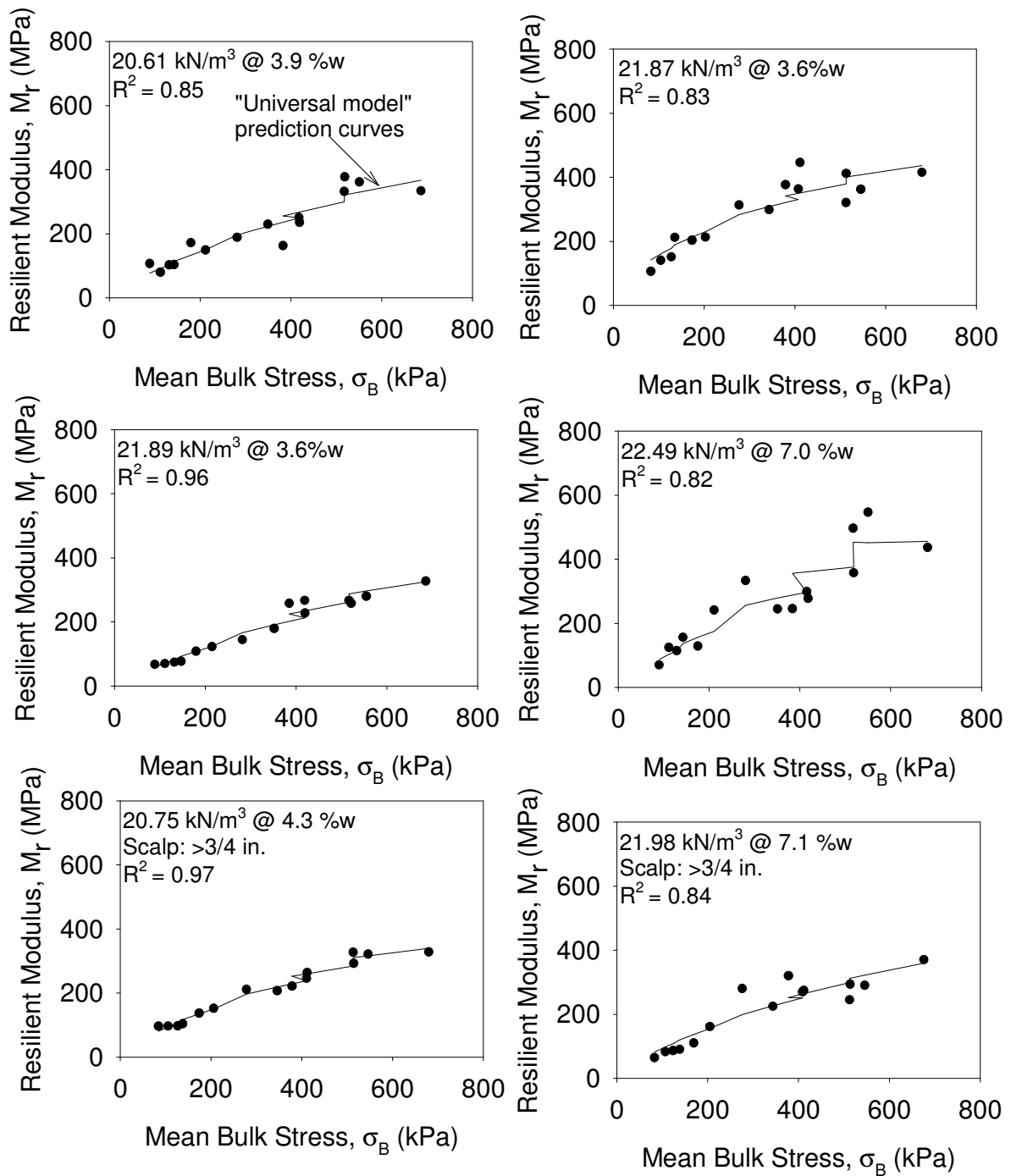
Figure 65. Summary of σ_B and M_r for Iowa I-29 special backfill subbase samples

(Part 1)
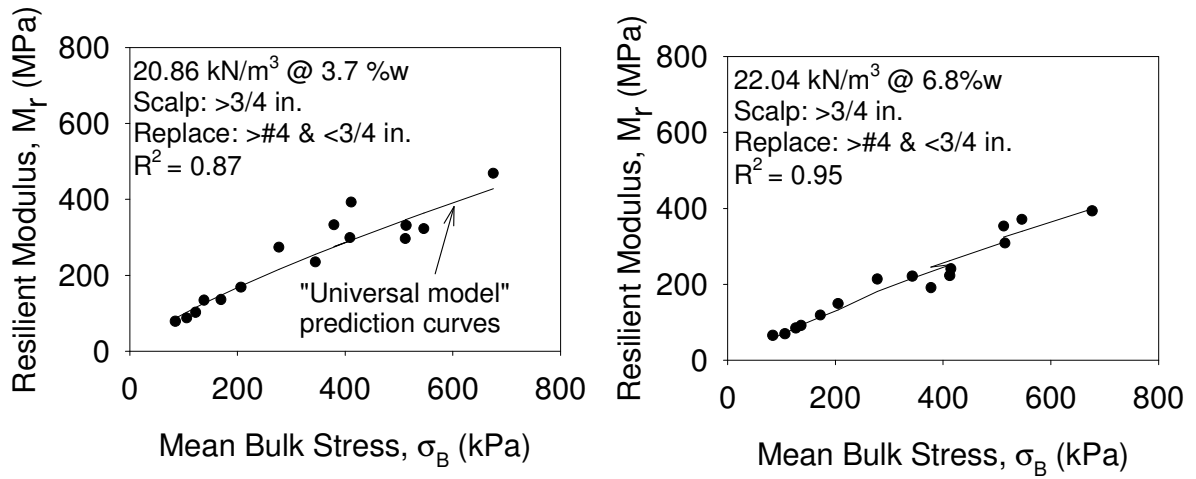
Figure 66. Summary of σ_B and M_r for Iowa I-29 special backfill subbase samples

(Part 2)
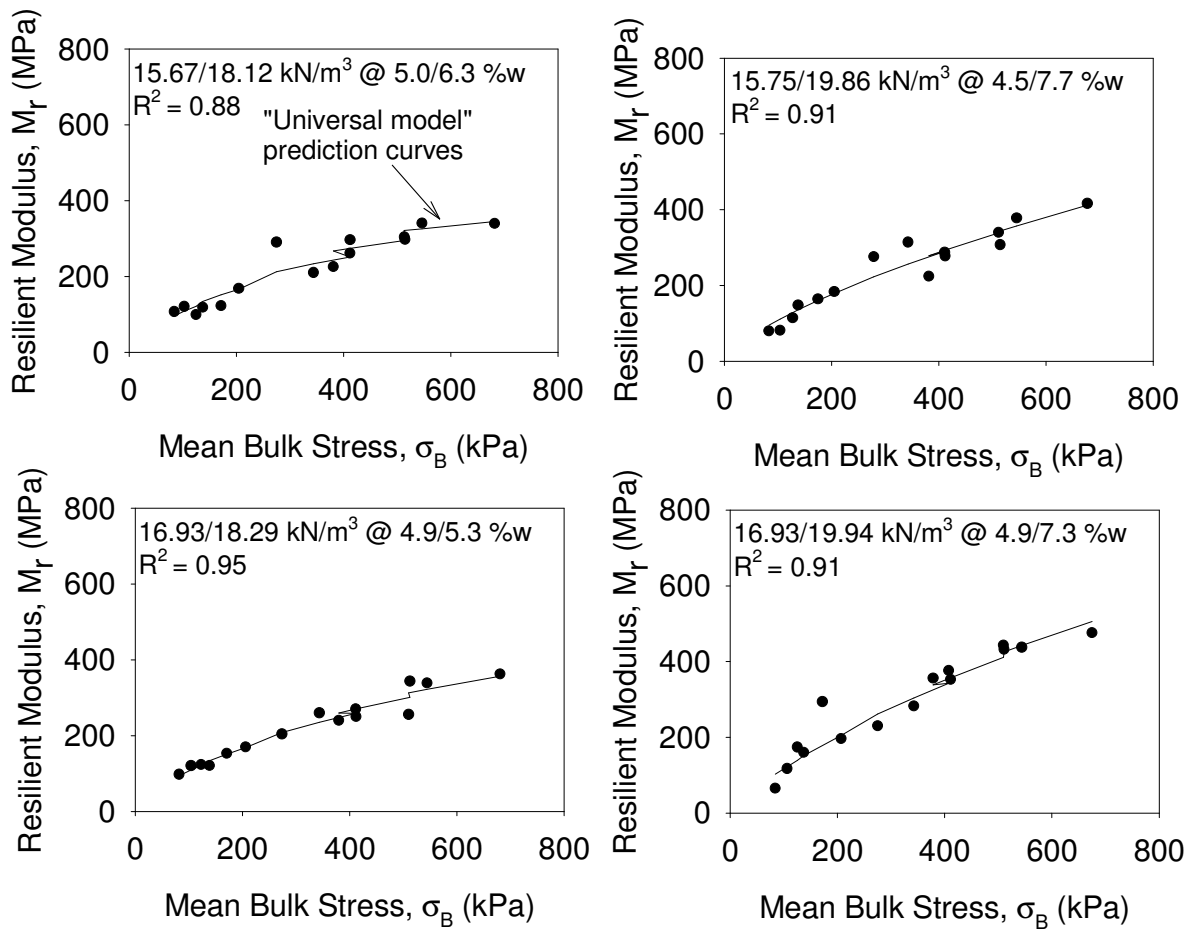
Figure 67. Summary of σ_B and M_r for Iowa I-29 RPCC base over RAP subbase material composite samples
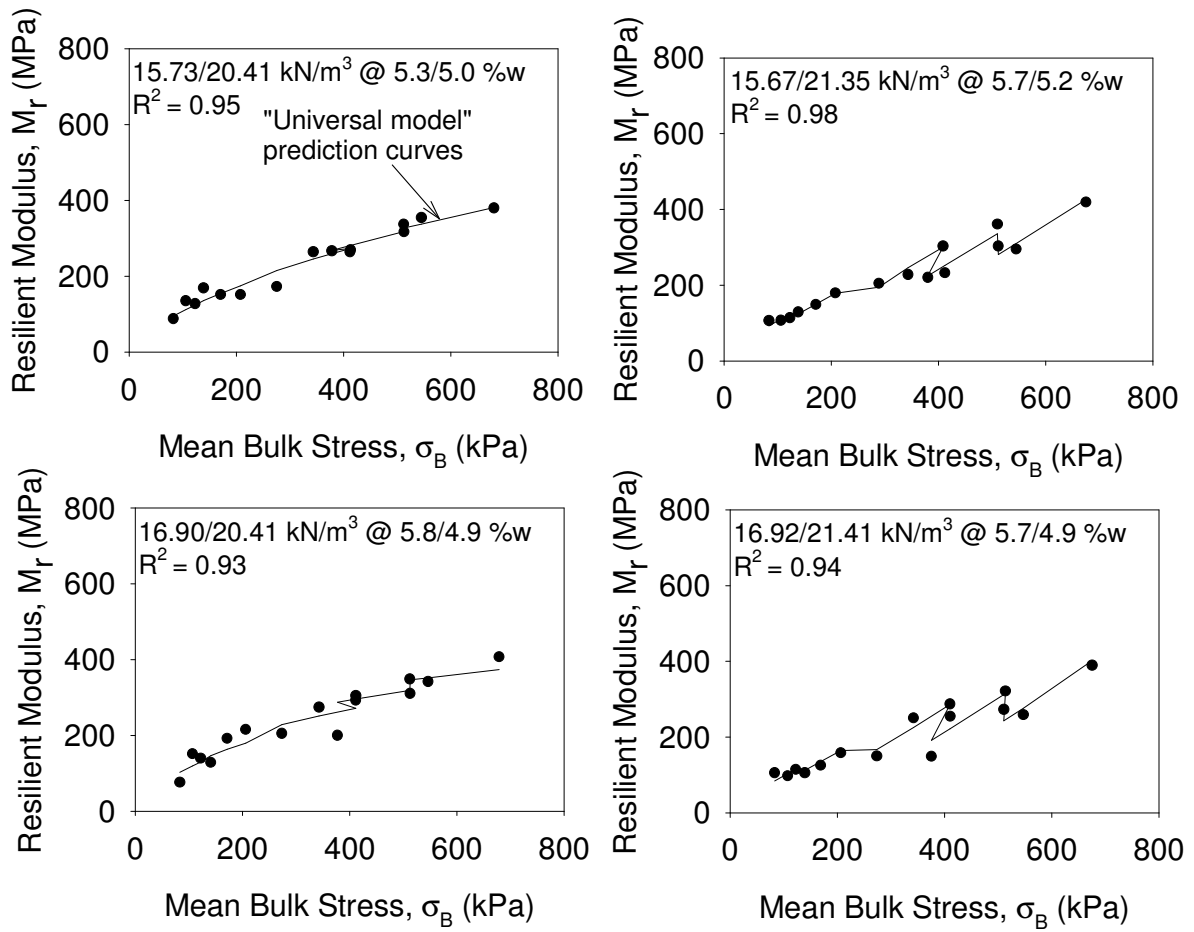
Figure 68. Summary of σ_B and M_r for Iowa I-29 RPCC base over select backfill subbase

material composite samples
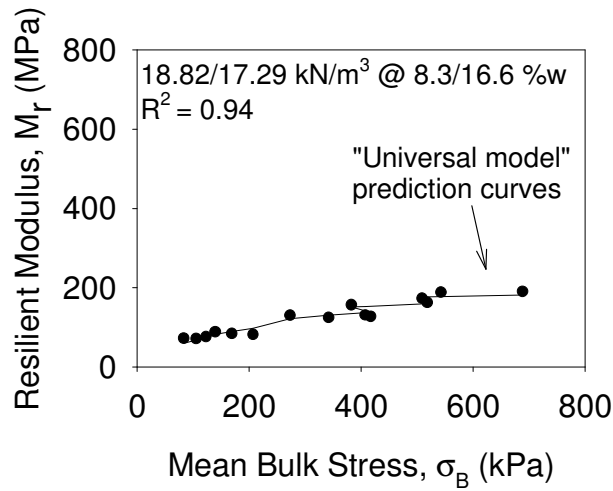
Figure 69. Summary of σ_B and M_r for Iowa I-29 RAP subbase over subgrade material
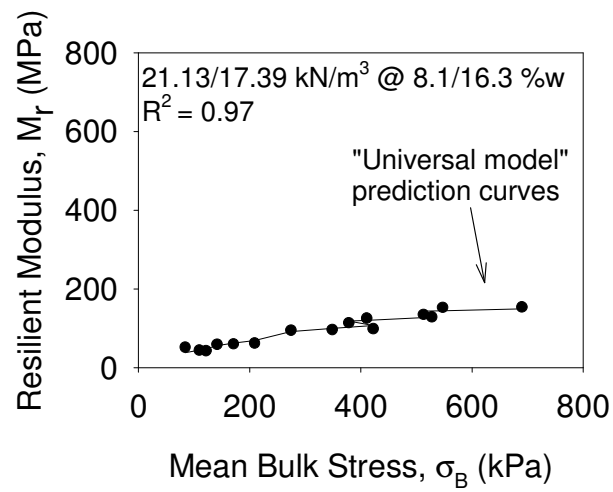
composite sample

Figure 70. Summary of σ_B and M_r for Iowa I-29 select backfill subbase over subgrade

material composite sample
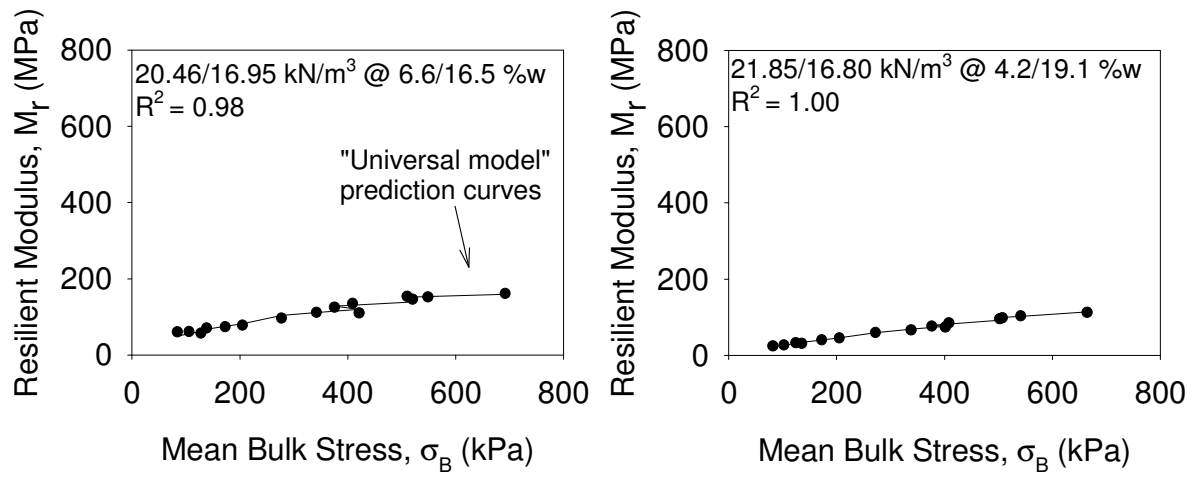
Figure 71. Summary of σ_B and M_r for Iowa I-29 existing sand subbase over subgrade material composite samples
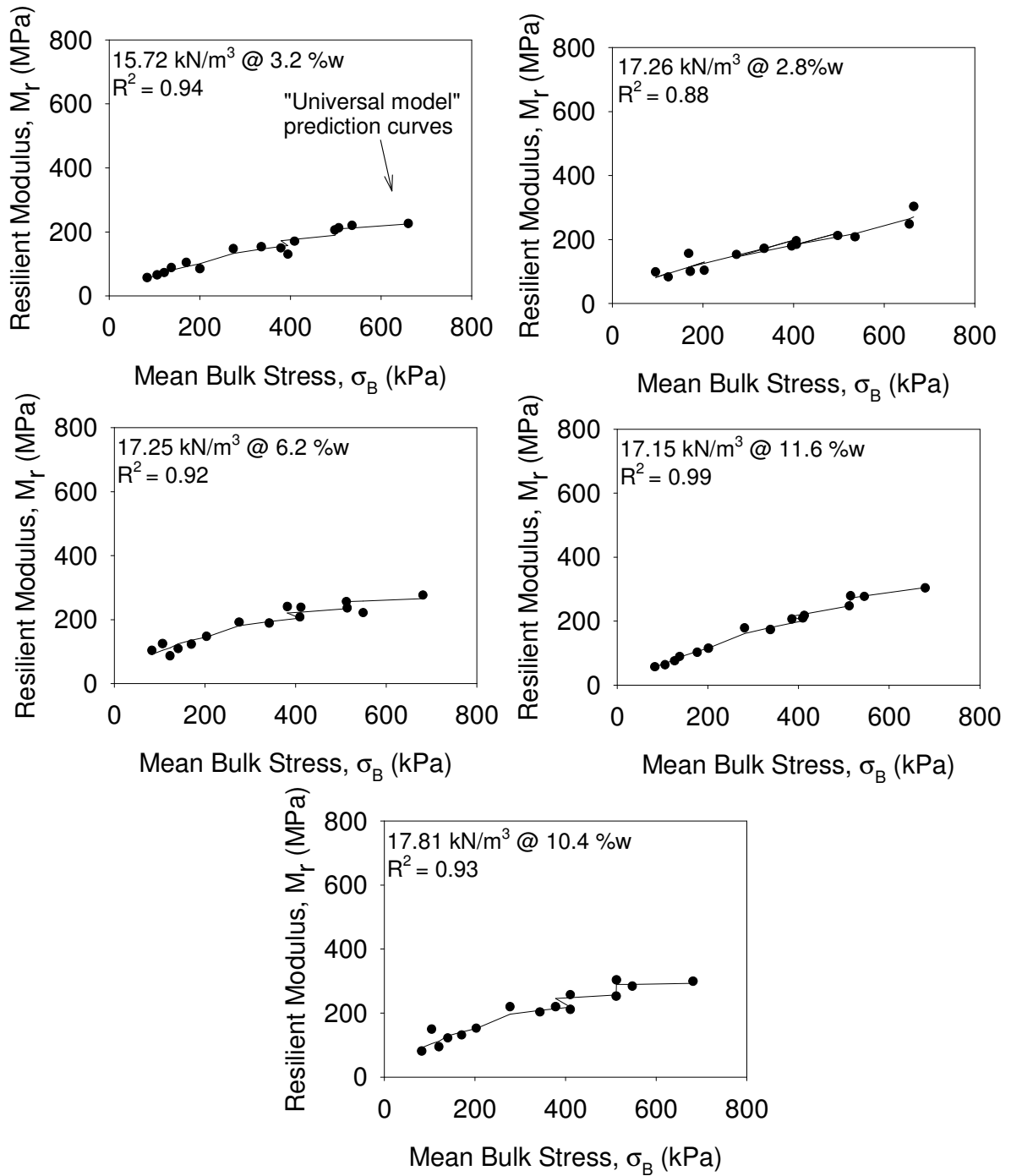
Figure 72. Summary of σ_B and M_r for Wisconsin US-10 sand subbase samples
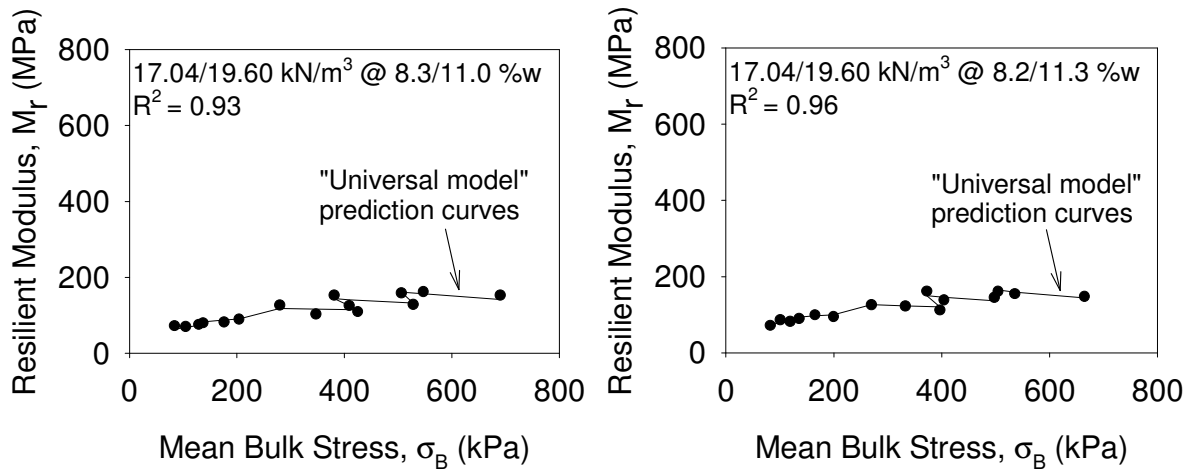
Figure 73. Summary of σ_B and M_r for Wisconsin US-10 sand subbase over subgrade composite sample with (left) and without geosynthetic (right)

RESILIENT MODULUS VERSUS DEVIATOR STRESS

Subgrade and Shelby tube samples are summarized in the following figures using resilient modulus versus deviator stress graphs.
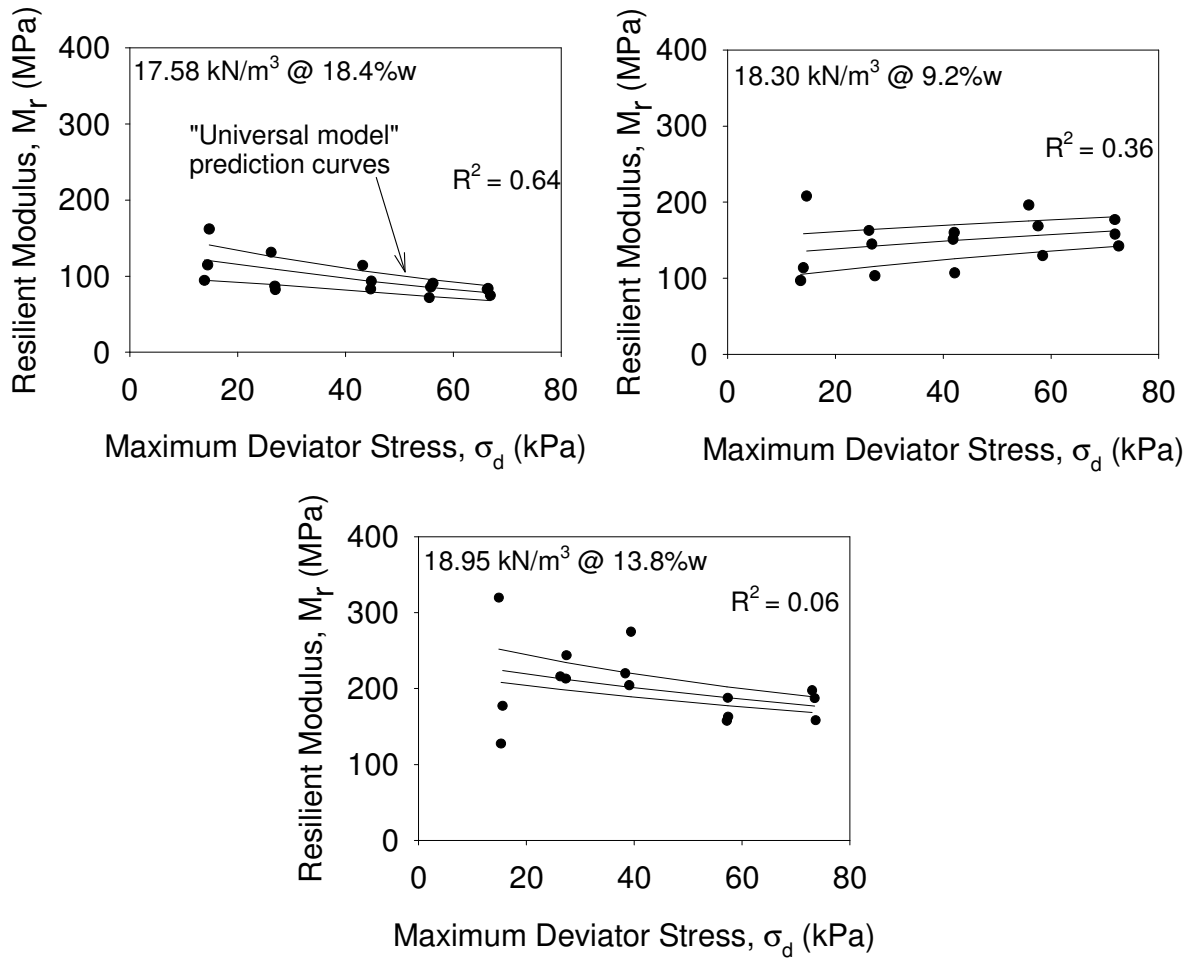
Figure 74. Summary of σ_d and M_r for Michigan I-94 subgrade samples
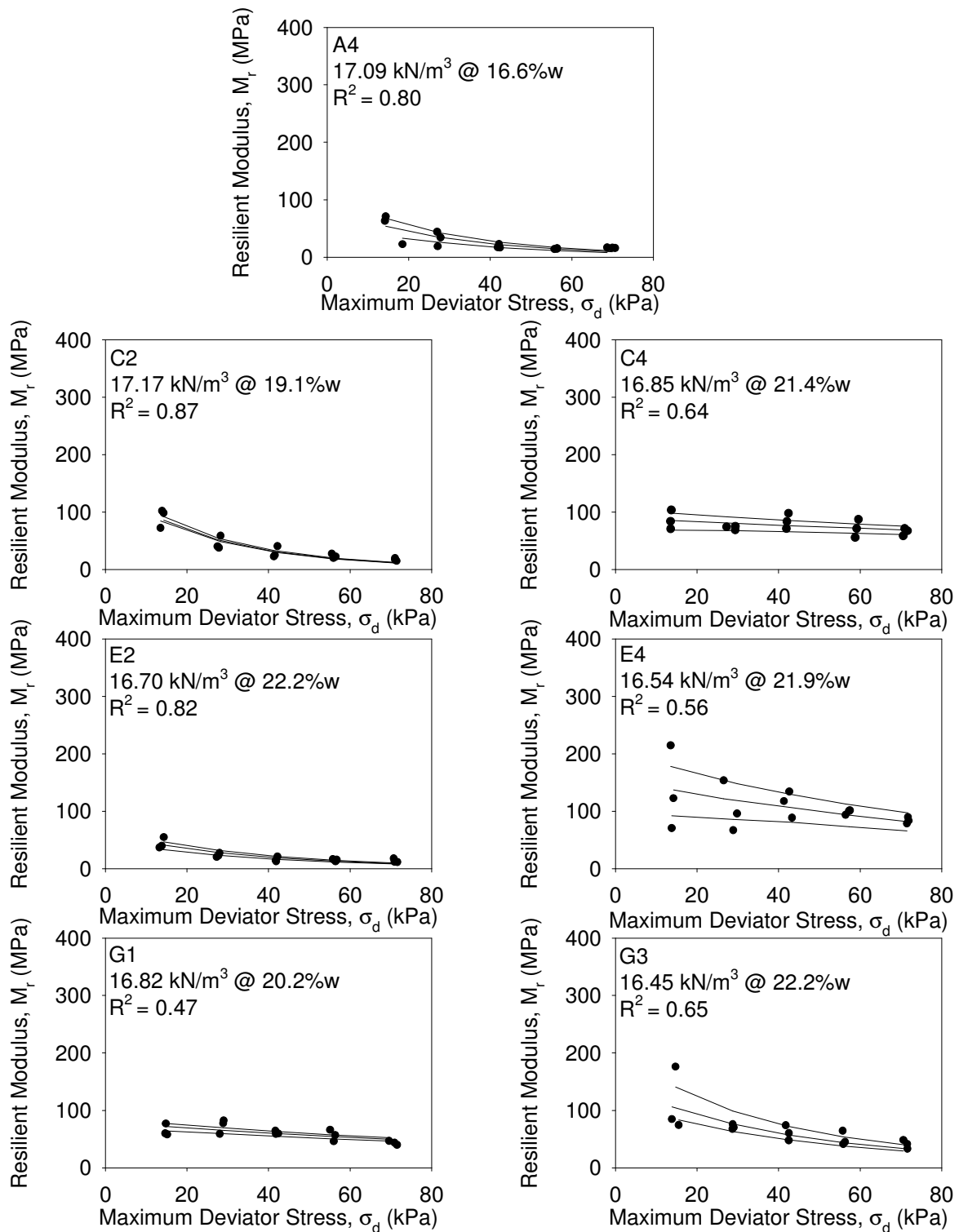
Figure 75. Summary of σ_d and M_r for Michigan I-94 Shelby tube samples (0.4–1.0 m depths)
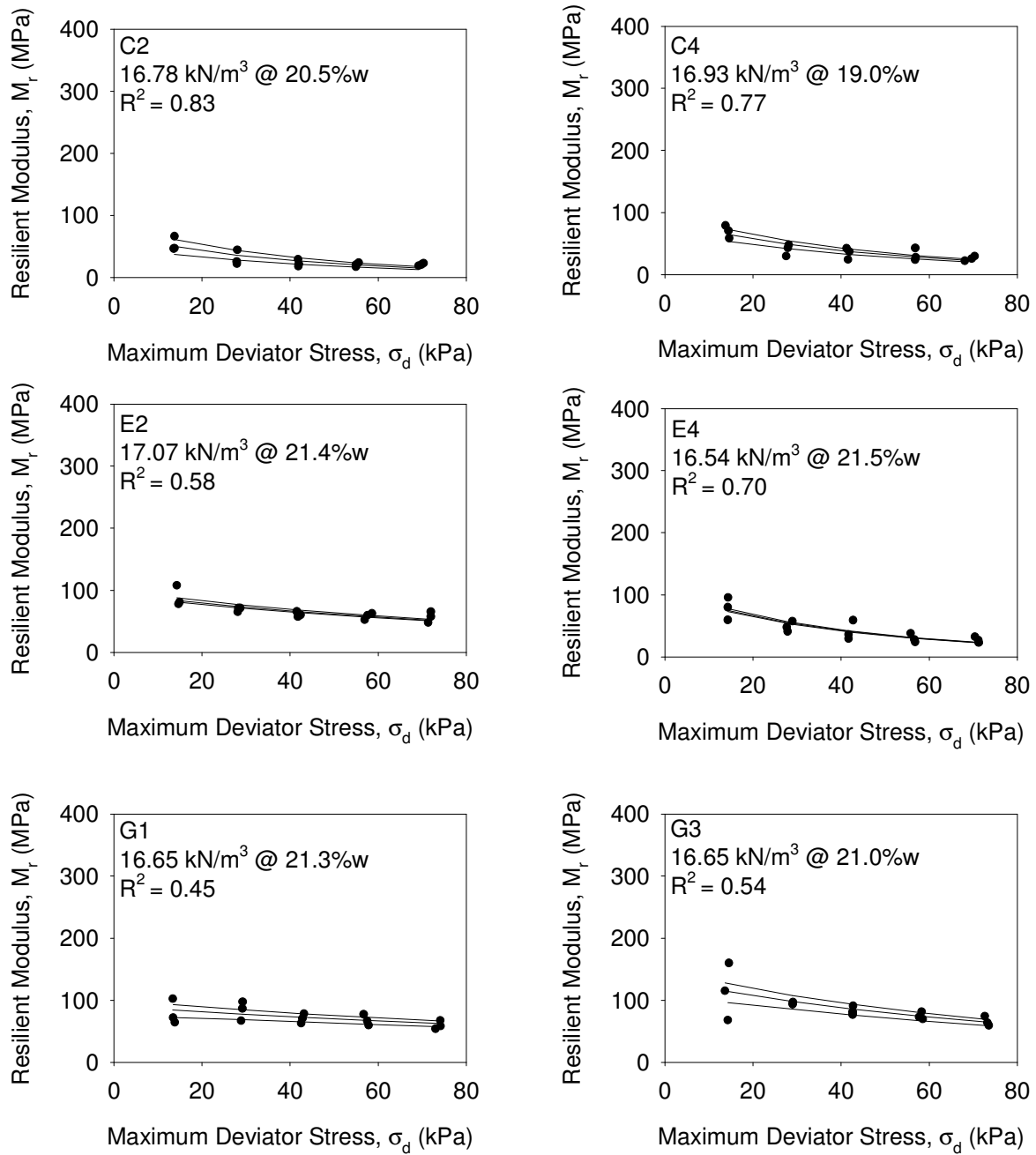
Figure 76. Summary of σ_d and M_r for Michigan I-94 Shelby tube samples (1.0–1.7 m depths)
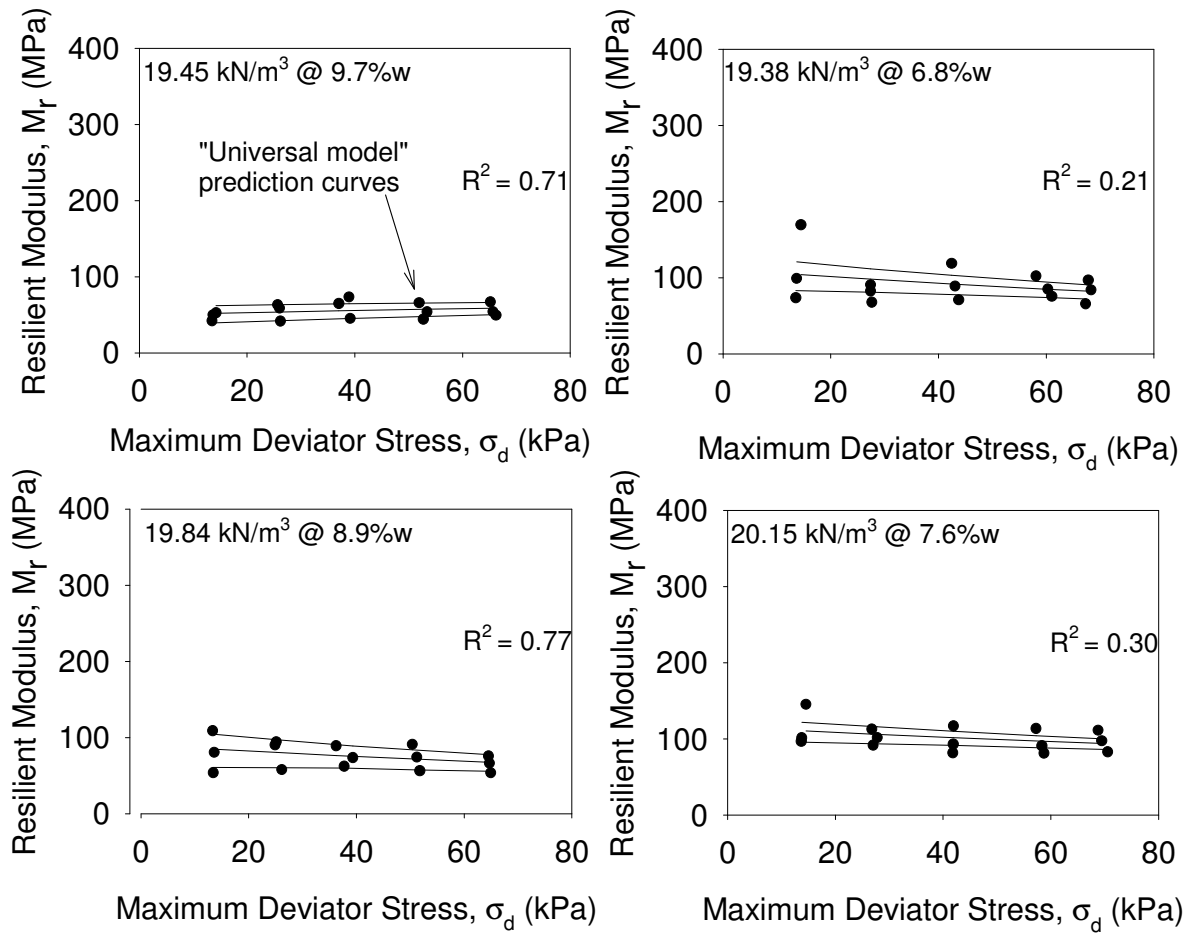
Figure 77. Summary of σ_d and M_r for Michigan I-96 subgrade samples (Part 1)
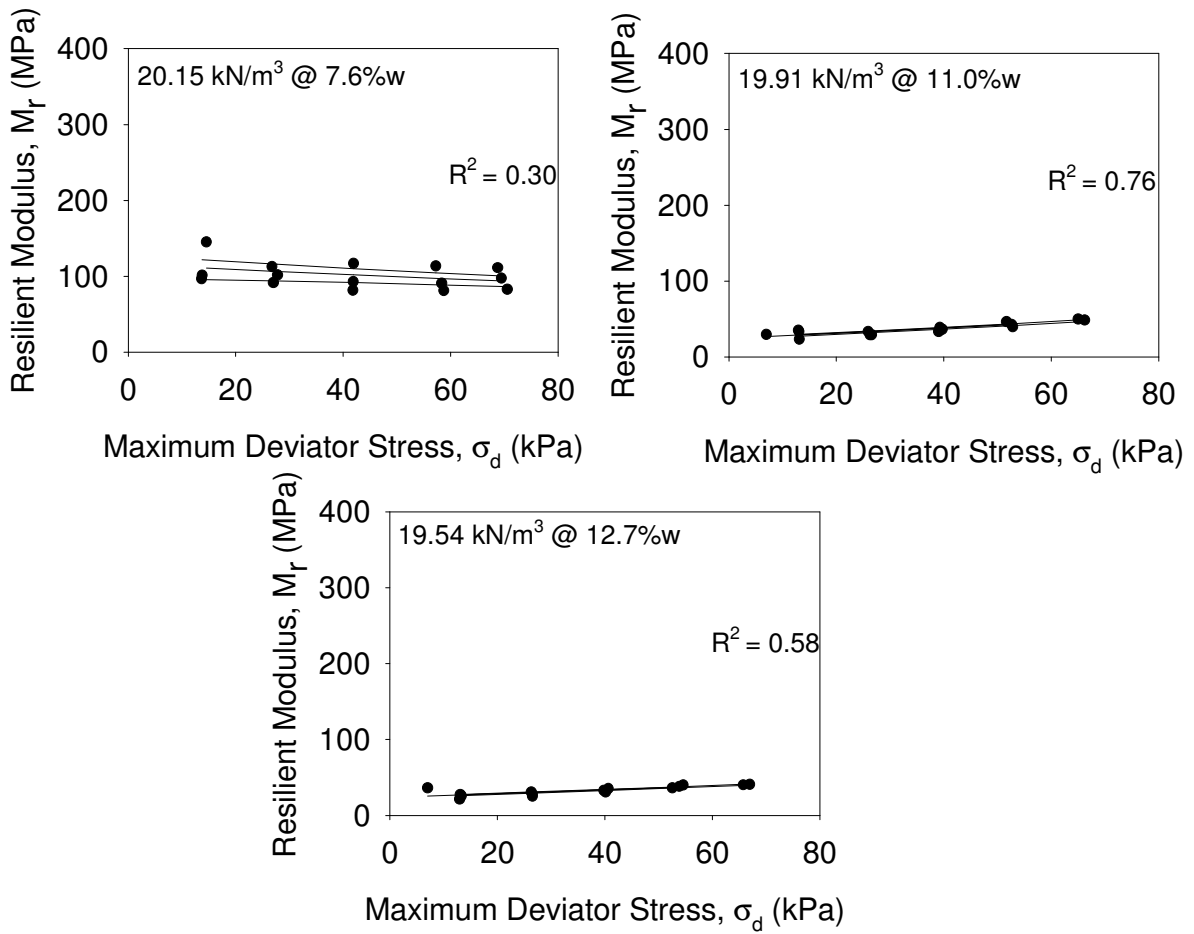
Figure 78. Summary of σ_d and M_r for Michigan I-96 subgrade samples (Part 2)
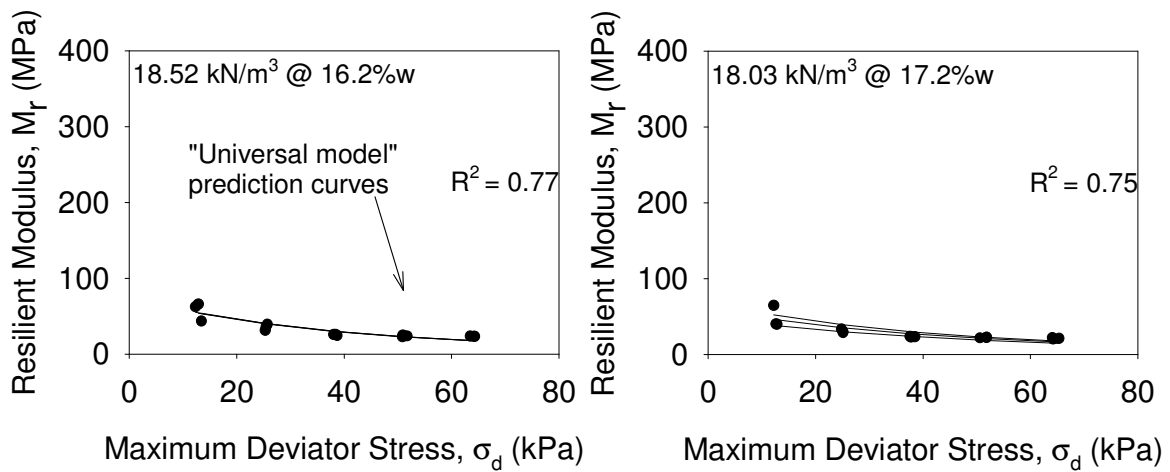
Figure 79. Summary of σ_d and M_r for Michigan I-96 Shelby tube samples (0.4–1.0 m depths)
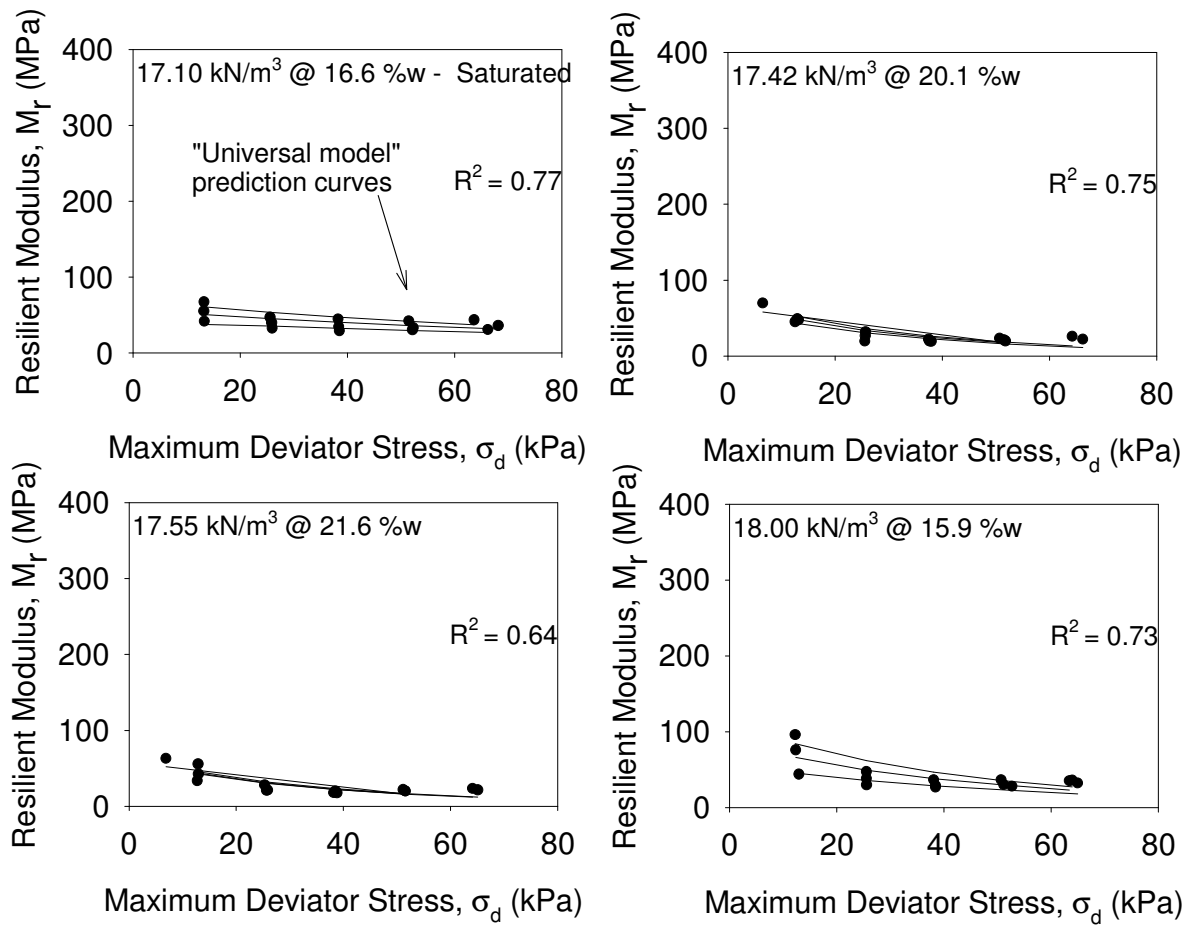
Figure 80. Summary of σ_B and M_r for Pennsylvania US-22 TB-2 subgrade samples
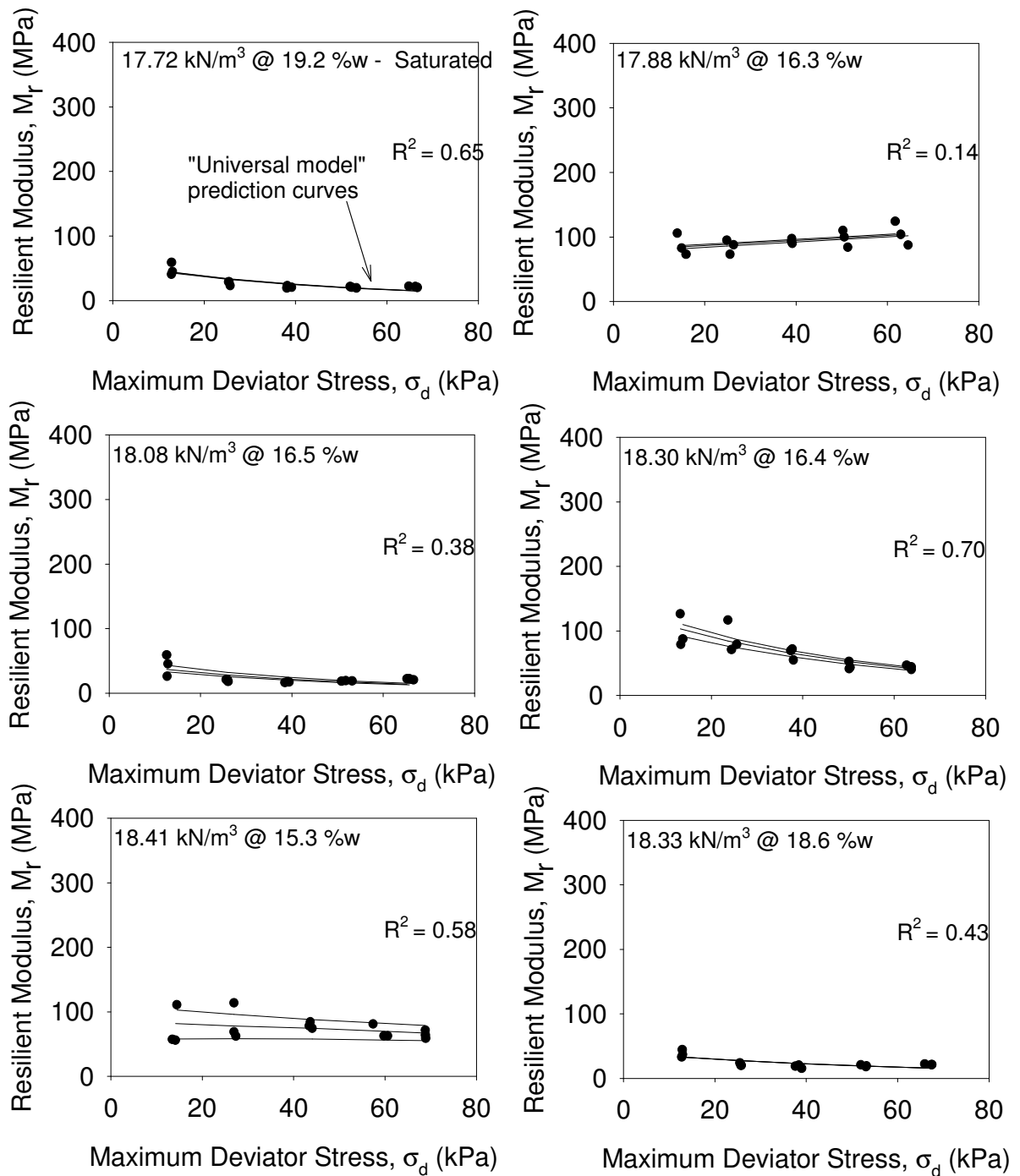
Figure 81. Summary of σ_B and M_r for Pennsylvania US-22 TB-6 subgrade samples
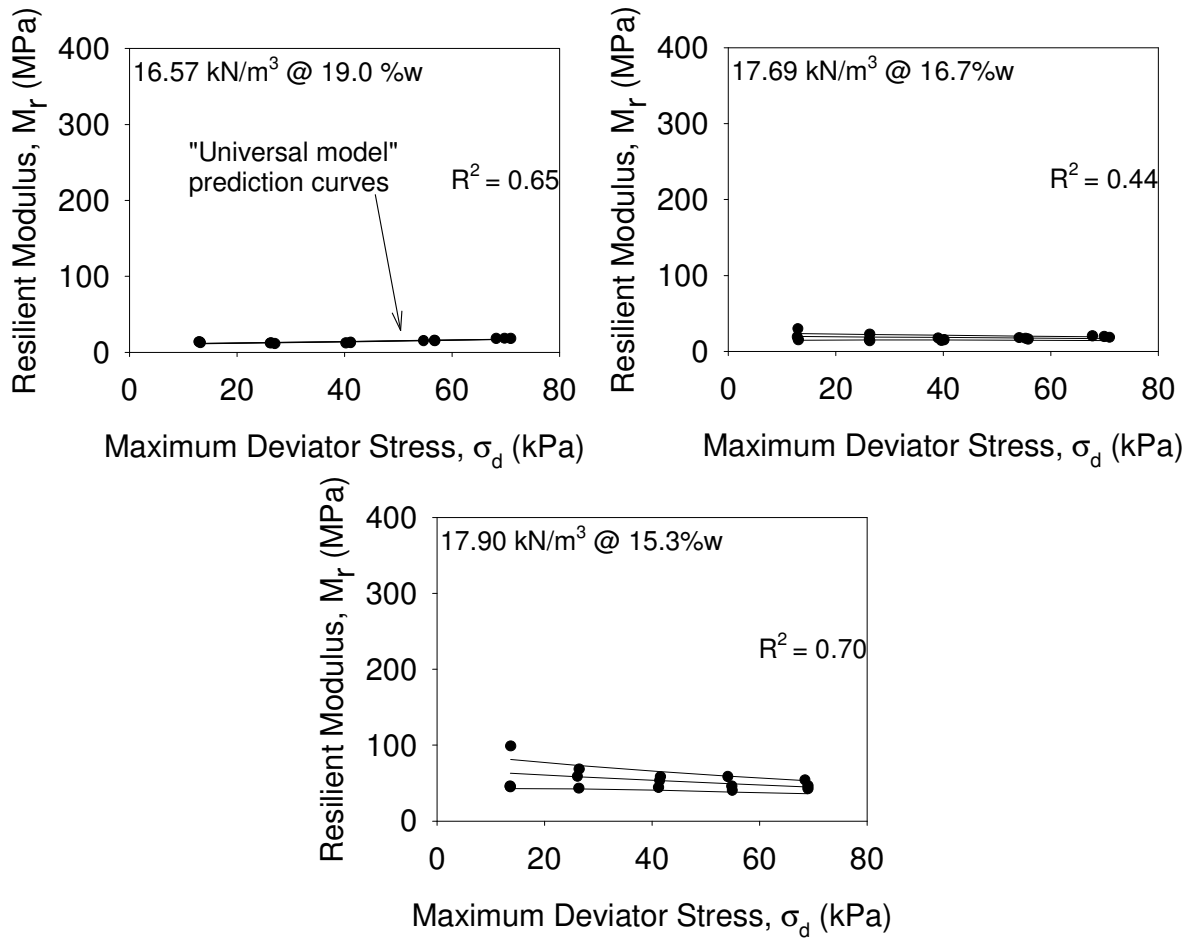
Figure 82. Summary of σ_B and M_r for Iowa I-29 subgrade samples
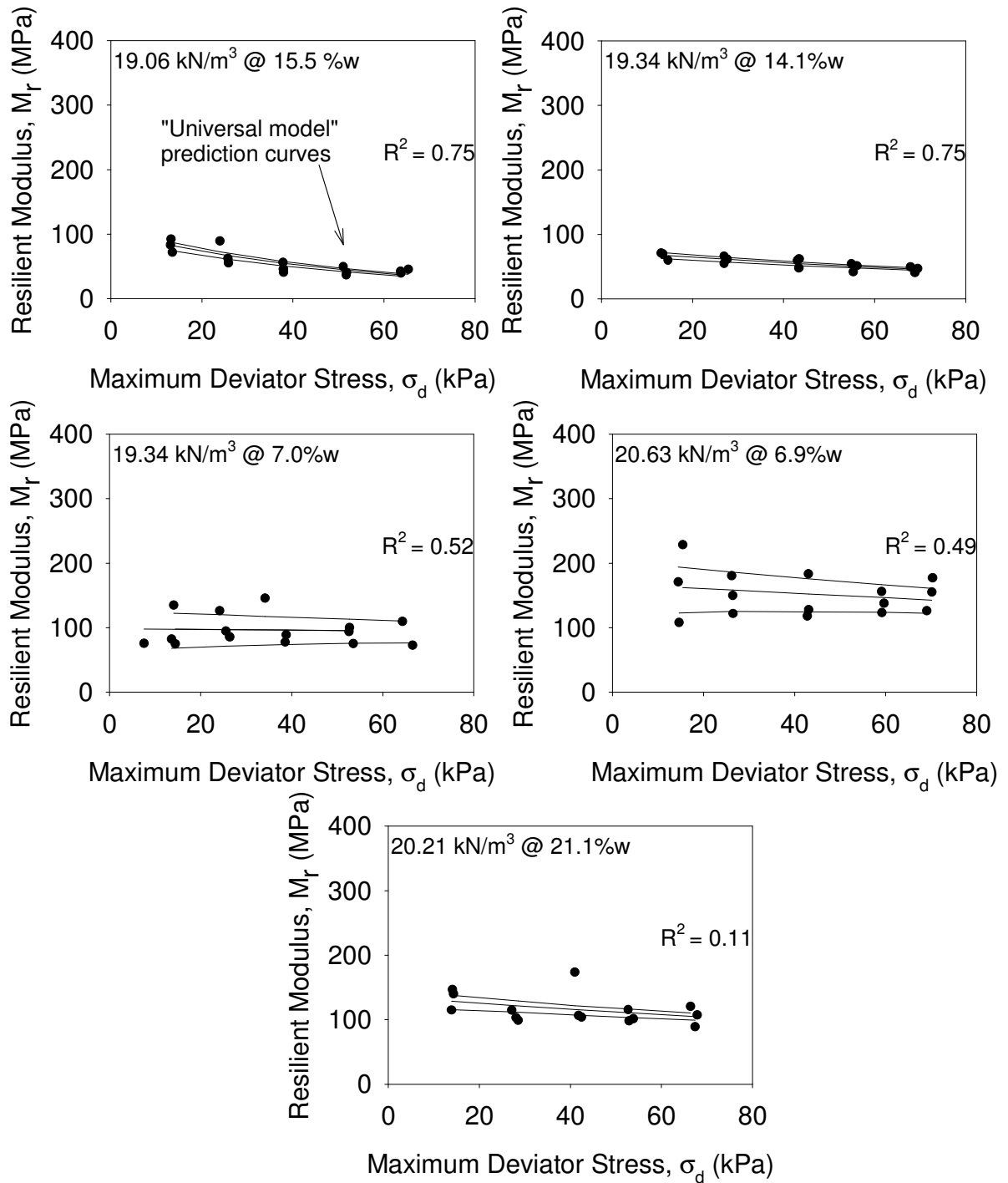
Figure 83. Summary of σ_B and M_r for Wisconsin US-10 subgrade samples

APPENDIX H. PROCTOR AND KNEADING COMPACTION COMPARISON TESTS

To analyze the difference between proctor compaction and kneading compaction, tests were performed on a loess material sampled from western Iowa. The dry density-moisture relationships for each compaction method are compared in Figure 84. The different parameters for each compaction method are summarized in Table 16. As expected, increasing the compaction energy increases the optimum dry density and decreases the optimum moisture content. By adjusting the blow pressure and blows per layer, it is possible for the kneading compaction method to obtain optimum density and moisture values that are close to the values determined by Proctor methods.
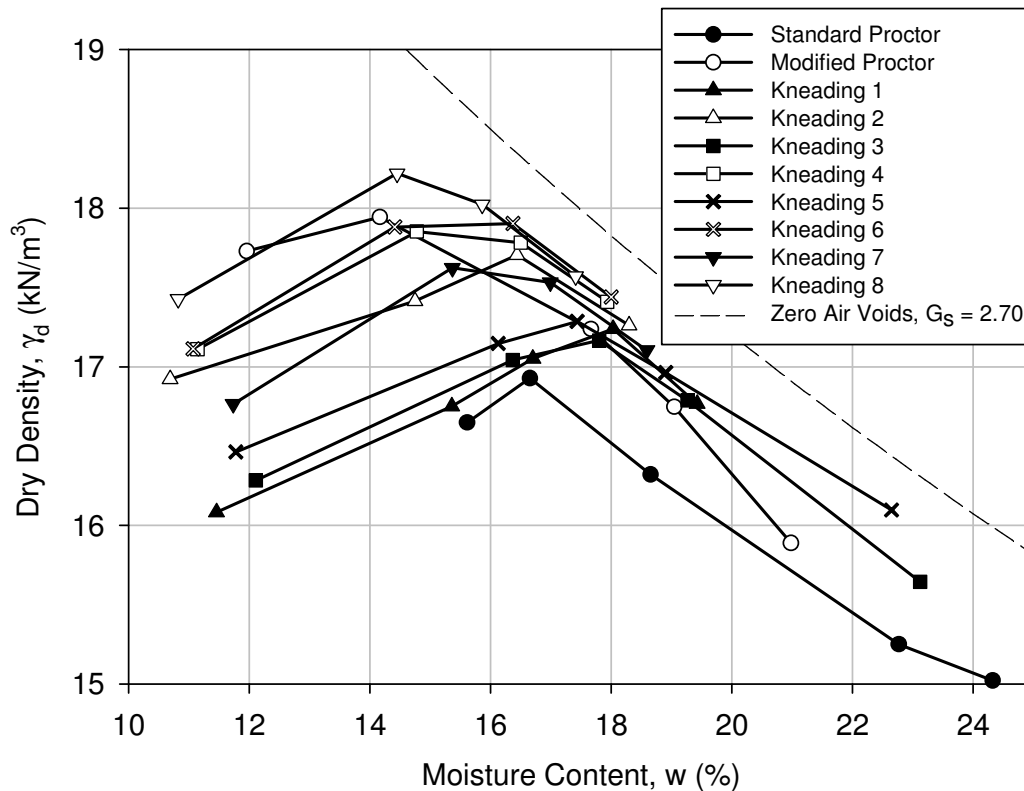
Figure 84. Comparison of Proctor and kneading compaction tests for western Iowa

loess

Table 16. Summary of differences in parameters for Proctor and kneading compaction tests

Test	# of Layers	Area of Tamper (cm^2)	Volume of Sample (cm^3)	Blows per Layer	Pressure per Blow (KPa)	Compaction Energy Applied to Sample (kN-m/m^3)
Std. Proctor	3	20.3	943.9	25	12.1	593
Mod. Proctor	5	20.3	943.9	25	21.9	2693
Kneading 1	6	20.7	1647.5	10	1379	2586
Kneading 2	6	20.7	1647.5	10	2413	4525
Kneading 3	10	20.7	1647.5	10	1379	4309
Kneading 4	10	20.7	1647.5	10	2413	7541
Kneading 5	6	20.7	1647.5	25	1379	6464
Kneading 6	6	20.7	1647.5	25	2413	11312
Kneading 7	10	20.7	1647.5	25	1379	10773
Kneading 8	10	20.7	1647.5	25	2413	18853

ACKNOWLEDGEMENTS